THE STRUCTURAL RESPONSE OF BURIED SUBSEA PIPELINES TO ICE GOUGING

by

©Alireza Ghorbanzadeh

A Thesis Submitted to the

School of Graduate Studies

in partial fulfillment of the requirements for the degree of

Doctor of Philosophy

Faculty of Engineering and Applied Science

Memorial University of Newfoundland

August 2024

St. John's Newfoundland Canada

ABSTRACT

Ice gouging significantly threatens the integrity of subsea pipelines in Arctic regions. While burial offers protection from direct ice contact, the shear resistance of seabed soil and resulting subgouge deformations can still threaten the stability of buried pipelines. Determining an optimal burial depth that balances safety and economic considerations presents a complex engineering challenge and necessitates a comprehensive understanding of the factors involved in the ice gouging process.

Conventional design approaches often simplify the seabed as a uniform material domain, neglecting the potential complexities introduced by natural and human-made non-uniformities. Trenching and backfilling the pipeline creates such non-uniformities, as the backfill material typically possesses stiffness characteristics different from those of the native soil. These pipeline-backfill-trench wall interaction can significantly affect failure mechanisms around the pipe and, consequently, pipeline response. Additionally, layered seabeds, common in many Arctic regions, are often simplified to uniform medium, potentially leading to inaccurate predictions.

This study simulated ice gouge events in cohesive soils under various non-uniform conditions using the Coupled Eulerian-Lagrangian (CEL) framework within Abaqus/Explicit. Unlike conventional models that idealize seabed soil as elastic, perfectly plastic, this work incorporated the strain-rate dependency and strain-softening effects of cohesive soils through a VUSDFLD user subroutine to improve prediction accuracy. Following mesh sensitivity analysis and model validation against published data, a comprehensive set of scenarios explored the impact of trenching/backfilling, backfill

stiffness and type, trenching methods and trench geometry, and layered soil configurations on keel reaction forces, soil failure mechanisms, and pipeline response (deformations, stresses, axial strains, and ovalization).

The results demonstrated that trenching and backfilling significantly influence seabed failure mechanisms around the pipe. Through careful backfill selection and trench design, pipeline safety can be enhanced. Furthermore, the study revealed that simplifying a layered seabed can lead to misleading predictions. Interactive mechanisms between soil layers can substantially alter soil failure patterns near the ice keel and along the soil layers interface, and it could cause unexpectedly large pipeline deformations at deeper burial depths. The findings of this research offer valuable practical insights for pipeline design in the Arctic, leading to several recommendations for improving the safety and integrity of subsea pipelines in these challenging environments.

STATEMENT OF AUTHORSHIP

I, Alireza Ghorbanzadeh, hereby declare that I have been the first author and the main contributor to the work that was conducted and presented in this doctoral dissertation. I undertook various tasks throughout this research process, including numerical modeling, data analysis, post-processing, visualization, and manuscript preparation. I received significant guidance and support throughout this research process from Dr. Hodjat Shiri (Supervisor), who provided direction on research topics and methodology and gave advice on results. Dr Shiri also reviewed and edited paper drafts. Dr. Xiaoyu Dong (Co-supervisor) contributed by providing modeling advice, and reviewing and editing drafts.

The list of papers and manuscripts extracted from the conducted research work is shown below:

• Ghorbanzadeh, A., Dong, X., Shiri, H., 2024. The influence of pipeline-backfill-trench interaction on pipeline response to ice gouging: a numerical investigation (Under review).

• Ghorbanzadeh, A., Shiri, H., Dong, X., 2024. Effect of Backfilling Stiffness and Configuration on Seabed Failure Mechanisms and Pipeline Response to Ice Gouging (Under review).

• Ghorbanzadeh, A., Shiri, H., Dong, X., 2024. Subsea Pipeline Design against Ice Gouging: Influence of Trenching and Backfilling Techniques (Under review).

• Ghorbanzadeh, A., Dong, X., & Shiri, H. (2024). Layered seabed effects on buried pipeline response to ice gouging. Ocean Engineering, 311, 118955. (Published).

• Ghorbanzadeh, Alireza, Dong, Xiaoyu, and Hodjat Shiri. "The Response of Buried Pipelines to Ice Gouging in the Uniform and Trenched/backfilled Seabed." Paper presented at the 33rd International Ocean and Polar Engineering Conference, Ottawa, Canada, June 2023.

ACKNOWLEDGMENT

I would like to express my deepest gratitude for the unwavering support, insightful guidance, and infinite patience of my supervisor, Dr. Hodjat Shiri. His meticulous supervision and invaluable advice were instrumental in the successful completion of this research. I extend my sincere appreciation to my co-supervisor, Dr. Xiaoyu Dong, whose expertise and guidance were invaluable throughout this journey. I would also like to acknowledge the valuable contributions and support of Dr. Mike Paulin, member of my supervisory committee, whose insights and feedback greatly enriched this research.

I would also like to acknowledge the financial support of the Wood Group, through their Research Chair program at Memorial University of Newfoundland. Additionally, I am grateful for the funding provided by the Natural Science and Engineering Research Council of Canada (NSERC) and the Newfoundland Research and Development Corporation (RDC) (now DIET) through their Collaborative Research and Developments Grants (CRD). I also thank Memorial University for providing exceptional research resources.

I am grateful for the companionship and intellectual exchange with my colleagues at the office, particularly Dr. Hossein Janbazi and Dr. Eduardo Malta, who provided me with valuable insights. My deepest gratitude goes to my siblings and friends, whose unconditional love and support were my emotional bedrock throughout this challenging endeavour. I could not have accomplished this without them.

Mom and Dad, your love continue to inspire me every day. This thesis is dedicated to your memory.

Contents

List of Figures

List of Tables

List of Abbreviations and Symbols

Abbreviations

ALE	Arbitrary Lagrangian–Eulerian
ALA	American Lifelines Alliance
API	American Petroleum Institute
ASCE	American Society of Civil Engineers
CEL	Coupled Eulerian-Lagrangian
CRD	Collaborative Research and Development
CSA	Canadian Standards Association
DNV	Det Norske Veritas
EVF	Eulerian Volume Fraction
FE	Finite Element
FEA	Finite Element Analysis
Max.	Maximum
M-C	Mohr-Coulomb
NSERC	Natural Science and Engineering Research Council of Canada
OCR	Over-Consolidation Ratio
PEEQVAVG	Equivalent Plastic Strain, Computed as a Volume Fraction Weighted Average of All Materials in The Element.
PRCI	Pipeline Research Council International
PRISE	Pressure Ridge Ice Scour Experiment
RDC	Newfoundland Research and Development Corporation
RITTS	Re-Meshing and Interpolation Technique with Small Strain

TSA	Total Stress Analysis
VUSDFLD	User-Defined Field Variables Subroutine in Abaqus

Symbols

Chapter 2

B	Gouge width
D	Gouge depth
s_u	Undrained shear strength of soil
$u(0,0,0)$	Maximum lateral subgouge soil deformation at a coordinate corresponding to the gouge centerline
$u(0,0,z)$	Vertical subgouge attenuation function
z	Depth below the ice keel

Chapter 3, Chapter 4, Chapter 6, Chapter 7, and Appendix

E	Young's modulus of elasticity
D	Nominal pipeline outer diameter
D_{max}	Maximum measured outer diameter of the pipe
D_{min}	Minimum measured outer diameter of the pipe
S_t	Soil sensitivity
W	Ice keel width (half-model)
t	Pipeline wall thickness
p_i	Maximum internal pressure
p_e	Maximum external pressure
f_y	Effective specified yield strength
ε_{max}	The maximum compressive strain
ε_c^{crit}	The critical compressive strain value
s_{ui}	In-situ undrained shear strength at the reference shear strain rate
μ	Increase rate of the shear strength per log cycle
$\dot{\gamma_{ref}}$	Reference shear strain rate
δ_{rem}	The ratio of fully remolded to initial shear strength or the inverse of the sensitivity

$\xi 95$	Relative ductility of the soil or the value of accumulated absolute plastic shear strain resulting in a 95% reduction in the remolded shear strength
ξ	Current cumulative absolute plastic shear strain
φ	Friction angles

Chapter 5

E	Young's modulus of elasticity
D	Nominal pipeline outer diameter
D_{max}	Maximum measured outer diameter of the pipe
D_{min}	Minimum measured outer diameter of the pipe
S_t	Soil sensitivity
W	Trench bottom width
Y	Ice keel width (half-model)
t	Pipeline wall thickness
p_i	Maximum internal pressure
p_e	Maximum external pressure
f_y	Effective specified yield strength
α	Trench wall angle
ε_{max}	The maximum compressive strain
ε_c^{crit}	The critical compressive strain value
s_{ui}	In-situ undrained shear strength at the reference shear strain rate
μ	Increase rate of the shear strength per log cycle
$\dot{\gamma_{ref}}$	Reference shear strain rate
δ_{rem}	The ratio of fully remolded to initial shear strength or the inverse of the sensitivity
$\xi 95$	Relative ductility of the soil or the value of accumulated absolute plastic shear strain resulting in a 95% reduction in the remolded shear strength

ξ	Current cumulative absolute plastic shear strain
φ	Friction angles

CHAPTER 1

Introduction

1.1 Overview

The Earth's polar regions, particularly the Arctic and northern latitudes, have captivated the imagination of explorers and scientists for centuries. However, a new wave of interest has emerged in recent decades – the exploration and development of oil and gas resources. Driven by advancements in drilling technology and a growing global demand for energy, vast reserves of hydrocarbons trapped beneath the Arctic seabed have become increasingly attractive to commercial ventures (Gautier et al., 2009). Extracting oil and gas from these remote regions presents unique challenges (Abdalla et al., 2008). Transportation infrastructure plays a critical role, and pipelines are the primary means for transmitting these resources to distant markets. Pipelines offer a cost-effective and efficient solution for oil and gas transportation over long distances, particularly compared to alternative methods like tankers. While pipelines offer a reliable solution for transport, the harsh offshore environment presents a multitude of geohazards that threaten their integrity- subsea landslides, seafloor instability, fault lines and seismic activity, and extreme weather events, to name a few.

Among these geohazards, ice gouging presents a particularly significant threat in the Arctic. Ice gouging occurs when moving ice sheets or keels (the underwater ridge of a glacier) scrape along the seabed, scouring deep grooves and potentially damaging pipelines buried beneath the seafloor (Barrette et al., 2009). Figure 1-1 illustrates the furrows carved into

the seabed due to ice gouging activity. The unpredictable nature of ice movement and the abrasive force of ice keels make ice gouging a major concern for pipeline integrity and safety in the Arctic and northern environments (Palmer et al., 1990; Paulin et al., 2008).

Ice gouging triggers a complex interaction of forces within the seabed, leading to various failure mechanisms. The tremendous force exerted by the ice keel can induce shear failure in the soil. As soil slides along defined failure planes, this results in forming side berms and a frontal mound on the seabed surface. The scraping action of the ice causes extensive deformation in the soil directly beneath the gouge. This subgouge deformation has significant consequences for buried pipelines. As the soil deforms in multiple directions, it can cause the pipeline to shift and experience significant strains, potentially leading to buckling, bending, or even rupture. Figure 1-2 depicts a cross-sectional view of the seabed and pipeline, presenting the seabed displacement mechanisms triggered by ice gouging and some important parameters.

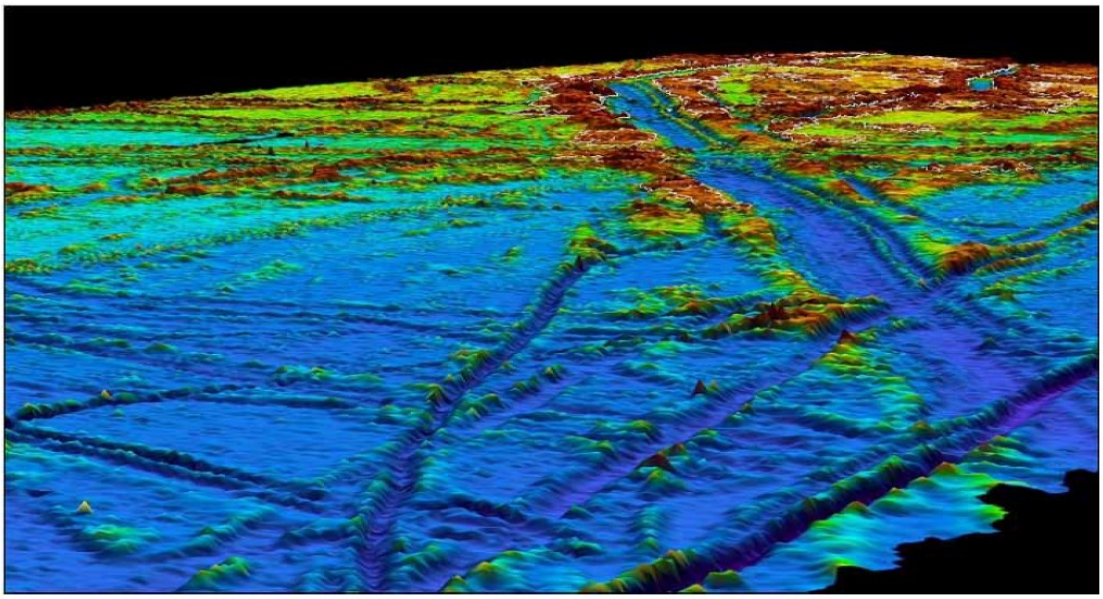

Figure 1-1. The ice scours on the Canadian Beaufort Sea (Blasco et al., 2006)

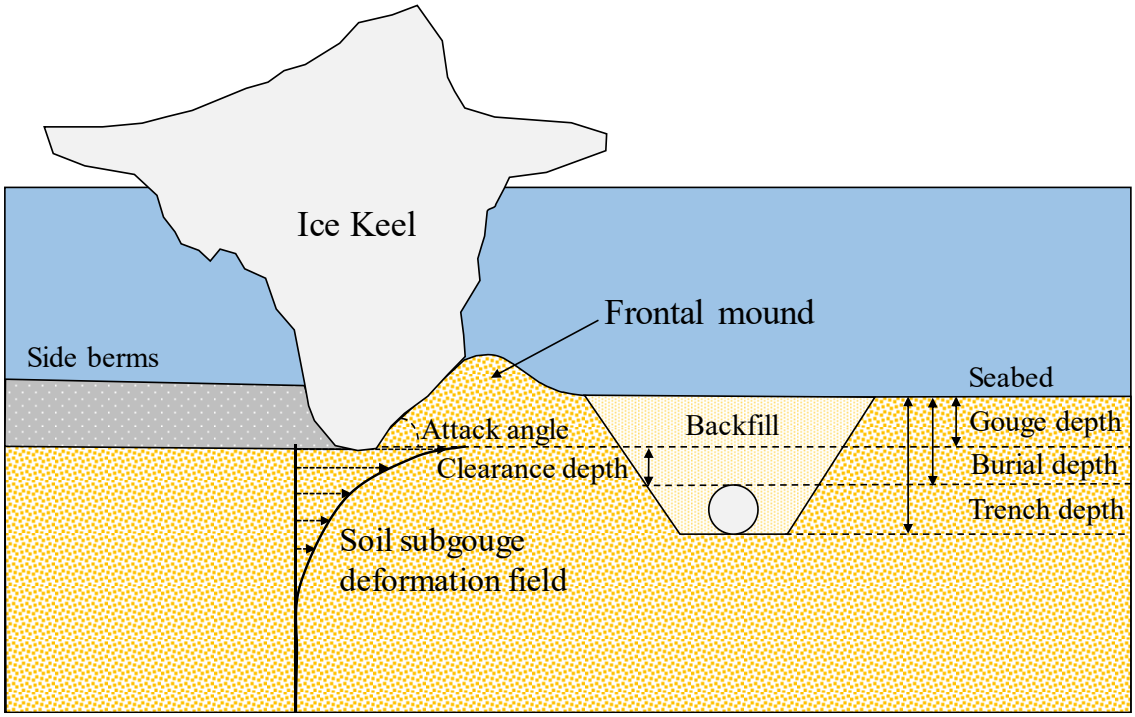

Figure 1-2. Cross-section of the seabed and the pipeline (not to scale)

Burying pipelines beneath the seafloor is a widely adopted strategy to shield them from the destructive forces of ice gouging (Nematzadeh & Shiri, 2020). However, more than simply burying a pipeline below a region's maximum observed ice gouge depth may be required for its protection (Pike, 2016). While burial provides protection for pipelines, the subsea trenching and backfilling process introduces additional complexities that must be carefully considered. Excavating the trench and then backfilling it with the same material inevitably changes the soil's properties. This remolded backfill often exhibits a much lower shear strength than the undisturbed native seabed, ranging from essentially no strength to a value-approaching native soil (Kianian et al., 2021). This variability in strength significantly impacts pipeline response under ice gouging loads. The softer backfill alters the failure mechanisms of the surrounding soil, potentially leading to unexpected deformations and

stresses on the pipeline Kianian et al. (2018). Moreover, different trenching methods (e.g., mechanical cutting vs. jetting) produce distinct trench shapes (Jukes et al., 2011). The geometry of the trench, including its slope and width, further affects how the soil interacts with the pipeline during large soil deformations (Paulin, 1998).

On the other hand, untouched real-world seabeds are rarely uniform in composition. They are often characterized by distinct strata, or layers, with varying geotechnical properties such as strength, stiffness, and permeability. These variations in soil properties across different layers can significantly influence how pipelines respond to ice gouging events (Shiri and Hashemi, 2023). Studies conducted in various Arctic regions have documented the prevalence of layered seabed configurations. Understanding these interactions is crucial for accurately determining safe and cost-effective burial depths.

Conventional pipeline design practices for buried pipelines subjected to lateral movements, such as those caused by ice gouging, rely on simplified idealizations of the pipe-soil interaction. A combination of specialized beam and spring elements represents the complex interaction between the pipe and the surrounding soil. Beam elements simulate the structural behavior of the pipe itself, typically using the actual pipe cross-section. Spring elements represent the soil's resistance to pipe movement in various directions (axial, lateral, vertical uplift, and vertical bearing). These springs exhibit a non-linear relationship between force and displacement. Established guidelines, such as those from ALA (2001), ASCE (1984), and PRCI (2009), provide recommendations on soil resistance characteristics for clayey soils under total stress conditions. These recommendations translate into the force-displacement behavior of the spring elements in the model. To

account for the impact of subgouge soil deformations caused by ice gouging on the buried pipe, these models incorporate the horizontal subgouge soil deformations as input to the lateral soil springs. The deformation values applied at the pipe's burial depth depend on the ice gouge dimensions (keel width and gouge depth). The subgouge soil deformation field variations, particularly for clay soils, are primarily derived from the Pressure Ridge Ice Scour Experiments (PRISE) conducted during the 1990s (Woodworth-Lynes et al., 1996). These experiments utilized centrifuge testing and resulted in empirical relationships for subgouge deformations. It is important to note that these relationships were based on tests with shallow keel attack angles and generally provide conservative estimates compared to the complete experimental data set.

While the conventional beam-and-spring approach offers a simplified and practical method for initial pipeline design, recent research has highlighted its limitations in capturing the complexities of ice gouging events. Studies by Abdalla et al. (2009), Konuk et al. (2006), and Peek & Nobahar (2012) suggest that the method is better suited for scenarios with simple loading conditions (operational loads, minor soil displacements) and can be overly conservative for ice gouging analysis. Peek and Nobahar (2012) pinpoint the issue of structural model superposition error as a critical limitation. This error arises from the method's inability to account for the complex interactions between the soil, ice keel, and pipe during gouging events. Other limitations identified by recent physical and computational modeling include the structural model's inability to represent the soil springs' coupled interaction behavior (Pike, 2016). This limitation is particularly significant for large deformation events with oblique loading conditions. Also, the Winkler-type model

assumes the soil to be uniform and ignores the effects of trenching and backfilling. It also does not account for soil nonlinearity, such as strain rate and strain-softening effects (Hashemi & Shiri, 2022a).

Advancements in computational power and software development have paved the way for 3D continuum FE tools as a valuable alternative for simulating complex geomechanics problems involving buried infrastructure. Researchers like Abdalla et al. (2009), Eskandari (2014), Panico et al. (2012), Phillips et al. (2010), and Pike & Kenny (2012) have successfully developed and partially validated 3D continuum FE tools for ice/soil and pipe/soil interaction analysis in different soil types (clay and sand).

This study investigates ice gouging events in non-uniform seabed using the Coupled Eulerian-Lagrangian (CEL) method within Abaqus/Explicit to simulate the complex interactions between the ice keel, soil, and pipeline. This model was utilized to investigate the effects of trenching, backfilling, and layered seabed compositions on ice gouging forces, soil failure mechanisms, and the resulting response of the buried pipeline. A key advantage of CEL is its ability to handle the large deformations characteristic of these scenarios. A VUSDFLD user subroutine, based on the equation proposed by Einav & Randolph (2005), is incorporated to accurately model the influence of strain-rate dependency and strain-softening on the behavior of the seabed soil.

The core principles and implementation of this method remain consistent across all chapters; they are detailed in Section 3.2. However, specific modifications and adaptations are made to the numerical model to address the unique characteristics of each investigated scenario. For instance, in chapters exploring layered soil conditions or varying trench

dimensions, adjustments are made primarily from a modeling perspective to accurately capture the distinct physical phenomena associated with these cases.

Under the combined loads of operational conditions and ice gouging, the pipeline can undergo both elastic and plastic deformation and may experience both tensile and compressive strains. These loads can lead to pipeline buckling and potential failure in severe cases. This study emphasizes the importance of understanding the interaction between pipeline-backfill-trench walls and the interaction of seabed layers in order to effectively mitigate the risks associated with ice gouging on buried pipelines.

The developed model provides a practical and effective tool for engineering the design of Arctic pipelines, leading to enhanced safety, efficiency, and cost-effectiveness.

1.2 Motivation

Despite the acknowledged importance of non-uniform seabed conditions, research on ice gouging in trenching/backfilling and layered soil strata remains limited. Only a few experimental and numerical studies have partially explored this area, leaving a significant knowledge gap. Traditional pipeline safety assessments often rely on simplified models that treat the seabed as a uniform material domain (Hashemi et al., 2022). This approach fails to capture the complexities introduced by real-world scenarios. These complexities include:

- Variations in soil properties due to trenching and backfilling processes, where the backfill material can exhibit significantly different strengths than the native seabed.
- Layered soil strata, with distinct soil types and strengths, exist at different depths.

Ignoring these non-uniformities can lead to inaccurate predictions of pipeline response under ice gouging loads.

This thesis investigates the impact of these seabed non-uniformities on pipeline response during ice gouging events. The variations induced by trenching/backfilling and the presence of layered soil strata influence the interaction between ice, soil, and the buried pipeline will be examined. Understanding these complex interactions and the resulting stresses and deformations on the pipeline enables researchers and engineers to move beyond simplified models. This research aims to develop more accurate and robust pipeline safety assessments specifically tailored to the unique challenges of the Arctic offshore environment.

1.3 Research Objectives

To achieve a comprehensive understanding of this complex problem, the following specific objectives have been defined:

i. Enhance the understanding of the critical factors affecting pipeline design in the Arctic, such as the interaction of pipeline-backfill-trench wall and the interaction of seabed layers. This will be achieved by developing a comprehensive model combining continuum and beam-spring approaches, which incorporates soil strain softening and strain rate effects to analyze buried pipe response to ice gouging.

ii. Investigate the influence of various trench shapes and backfill characteristics on pipeline performance during ice gouging events. This objective aims to identify how different trench geometries and backfill stiffnesses can be customized for improved pipeline response under specific ice gouging conditions.

iii. Provide insights for the best trenching and backfilling practice for the subsea pipelines in the Arctic and neighboring areas.

iv. Conduct a comprehensive analysis of different layered seabed configurations, including soft over stiff clay and stiff over soft clay. This objective aims to understand the variations in geotechnical properties across distinct strata and their implications on buried pipeline performance during ice gouging events.

This research's ultimate objective is to improve safety, structural integrity, and cost-effective design practices for buried pipelines in the challenging Arctic offshore environment.

1.4 Organization of the Thesis

This doctoral thesis comprises seven chapters and an appendix organized as a paper-based dissertation. The research is presented in a format focused on four journal manuscripts, with targeted supporting literature reviews and a relevant conference paper in the appendix. Chapter 1 provides the background, motivation, and significance of the research problem. It outlines the challenges of ice gouging in the Arctic environment, the importance of pipelines, the complexities of seabed conditions, and the need for accurate modeling of non-uniform seabed, defining the research objectives and scope. Chapter 2 presents a literature review of existing numerical and experimental studies on ice gouging, pipeline-trench interactions, and recent advancements in modeling techniques. Additional targeted literature reviews are included within specific chapters for greater context. Chapter 3 aims to investigate the influence of trenching/backfilling and burial depth on pipeline response to ice gouging by developing and validating a Coupled Eulerian-Lagrangian (CEL) model

for Large Deformation Finite Element (LDFE) analysis. It investigates the influence of pipeline-backfill-trench wall interactions on soil failure mechanisms and pipeline response for shallow and deep pipeline burial configurations. Chapter 4 investigates the effect of backfill stiffness and material and focuses on how variations in backfill materials and stiffness affect seabed failure mechanisms and pipeline response. A range of backfill scenarios, including dense and loose sand and clays of varying strengths, are examined. Chapter 5 explores the impact of different trenching methods and their associated geometries on pipeline response and seabed behavior during ice gouging. It employs the CEL algorithm to model complex soil behavior, including strain-rate dependency and strain softening. Chapter 6 investigates layered seabed analysis and pipeline response in distinct layered seabed configurations commonly found in the Arctic, including soft over stiff clay, stiff over soft clay, and uniform soft and stiff clays. Chapter 7 summarizes the key findings of this comprehensive research, highlights practical implications, and proposes recommendations for future studies to advance the field further. Appendix A includes a peer-reviewed conference paper presenting the initial results and motivations discussed in Chapter 3.

1.5 Thesis outcomes

This doctoral thesis has made a remarkable contribution to offshore pipeline safety in the Arctic by addressing the complexities of ice gouging in the non-uniform seabed. The research has significantly expanded the knowledge of how different seabed characteristics, trenching techniques, and backfill properties influence soil failure mechanisms and pipeline behavior during ice gouging events. The findings provide valuable guidance for engineers

in designing optimized subsea pipelines for Arctic conditions. The research has resulted in several publications:

- Ghorbanzadeh, A., Dong, X., Shiri, H., 2024. The influence of pipeline-backfill-trench interaction on pipeline response to ice gouging: a numerical investigation (Under review).
- Ghorbanzadeh, A., Shiri, H., Dong, X., 2024. Effect of Backfilling Stiffness and Type on Seabed Failure Mechanisms and Pipeline Response during Ice Gouging Events (Under review).
- Ghorbanzadeh, A., Shiri, H., Dong, X., 2024. Subsea Pipeline Design against Ice Gouging: Influence of Trenching and Backfilling Techniques (Under review).
- Ghorbanzadeh, A., Dong, X, Shiri, H., 2024. Layered Seabed Effects on Buried Pipeline Response to Ice Gouging (Under review).
- Ghorbanzadeh, Alireza, Dong, Xiaoyu, and Hodjat Shiri. "The Response of Buried Pipelines to Ice Gouging in the Uniform and Trenched/backfilled Seabed." Paper presented at the The 33rd International Ocean and Polar Engineering Conference, Ottawa, Canada, June 2023.

References

Abdalla, B., Jukes, P., Eltaher, A., & Duron, B. (2008). The technical challenges of designing oil and gas pipelines in the arctic. *OCEANS 2008*, 1–11.

Abdalla, B., Pike, K., Eltaher, A., Jukes, P., & Duron, B. (2009). Development and validation of a coupled Eulerian Lagrangian finite element ice scour model. *International Conference on Offshore Mechanics and Arctic Engineering*, *43451*, 87–95.

ALA. (2001). Guidelines for the design of buried steel pipe. *American Society of Civil Engineers*.

ASCE. (1984). *Guidelines for the Seismic Design of Oil and Gas Pipeline Systems*. Amer Society of Civil Engineers.

Barrette, P., Marquardt, J., & Timco, G. (2009). Test data from scour simulations with rigid indentors and real ice rubble. *CHC-NRC Technical Report CHC-CTR-103*.

Einav, I., & Randolph, M. F. (2005). Combining upper bound and strain path methods for evaluating penetration resistance. *International Journal for Numerical Methods in Engineering*, *63*(14), 1991–2016.

Eskandari, F. (2014). *Buried pipeline response to ice gouging*. Memorial University of Newfoundland.

Gautier, D. L., Bird, K. J., Charpentier, R. R., Grantz, A., Houseknecht, D. W., Klett, T. R., Moore, T. E., Pitman, J. K., Schenk, C. J., & Schuenemeyer, J. H. (2009). Assessment of undiscovered oil and gas in the Arctic. *Science*, *324*(5931), 1175–1179.

Hashemi, S., & Shiri, H. (2022). Numerical Modeling of Ice–Seabed Interaction in Clay by Incorporation of the Strain Rate and Strain-Softening Effects. *Journal of Offshore Mechanics and Arctic Engineering*, *144*(4), 42101.

Hashemi, S., Shiri, H., & Dong, X. (2022). The influence of layered soil on ice-seabed interaction: Soft over stiff clay. *Applied Ocean Research*, *120*, 103033.

Jukes, P., Kenny, S., Panapitiya, U., Jafri, S., & Eltaher, A. (2011). Arctic and harsh environment pipeline trenching technologies and challenges. *OTC Arctic Technology Conference*.

Kianian, M, Esmaeilzadeh, M., & Shiri, H. (2018). Lateral Response of Trenched Pipelines to Large Deformations in Clay. In *Offshore Technology Conference* (p. D032S092R009). https://doi.org/10.4043/28842-MS

Kianian, Morteza, Esmaeilzadeh, M., & Shiri, H. (2021). The Effect of Backfilling Stiffness on the Lateral Response of Deeply Buried Pipelines: an Experimental Study. *Journal of Marine Science and Application*, *20*(1), 21–33.

Konuk, I., Yu, S., & Fredj, A. (2006). Do Winkler models work: A case study for ice scour problem. *International Conference on Offshore Mechanics and Arctic Engineering*, *47497*, 197–203.

Nematzadeh, A., & Shiri, H. (2020). The influence of non-linear stress-strain behavior of dense sand on seabed response to ice gouging. *Cold Regions Science and Technology*, *170*, 102929.

Palmer, A. C., Konuk, I., Comfort, G., & Been, K. (1990). Ice gouging and the safety of marine pipelines. *Offshore Technology Conference*.

Panico, M., Lele, S. P., Hamilton, J. M., Arslan, H., & Cheng, W. (2012). Advanced ice gouging continuum models: comparison with centrifuge test results. *ISOPE International Ocean and Polar Engineering Conference*, ISOPE-I.

Paulin, M. J. (1998). *An investigation into pipelines subjected to lateral soil loading*. Memorial University of Newfoundland.

Paulin, M. J., Kenny, S. P., Palmer, A. C., Been, K., & Caines, J. V. M. (2008). Offshore Pipelines in Cold Regions-Environmental Loadings and Geotechnical Considerations. *SNAME 8th International Conference and Exhibition on Performance of Ships and Structures in Ice*.

Peek, R., & Nobahar, A. (2012). Ice gouging over a buried pipeline: Superposition error of simple beam-and-spring models. *International Journal of Geomechanics*, *12*(4), 508–516.

Phillips, R., Barrett, J., & Al-Showaiter, A. (2010). Ice keel-seabed interaction: Numerical modelling validation. *Offshore Technology Conference*, *20696*.

Pike, K. P. (2016). *Physical and numerical modelling of pipe/soil interaction events for large deformation geohazards*. Memorial University of Newfoundland.

Pike, K. P., & Kenny, S. P. (2012). Advanced continuum modeling of the ice gouge process: Assessment of keel shape effect and geotechnical data. *ISOPE International Ocean and Polar Engineering Conference*, ISOPE-I.

PRCI. (2009). *Guidelines for Constructing Natural Gas and Liquid Hydrocarbon Pipelines through Areas Prone to Landslide and Subsidence Hazards*, *Pipeline Research Council International*.

Woodworth-Lynes, C., Nixon, D., Phillips, R., & Palmer, A. (1996). Subgouge deformations and the security of Arctic marine pipelines. *Offshore Technology Conference*.

CHAPTER 2

Literature Review

2.1 Overview

This chapter provides a comprehensive review of the existing literature on ice gouging, particularly on seabed failure mechanisms, pipeline response, and the impacts of trenching and backfilling on pipeline behavior under large deformations. This review lays the groundwork for the new research objectives presented in this thesis by understanding the mechanisms, governing parameters, and modeling techniques.

The review begins with analyzing foundational physical ice gouging experiments, providing insights into the fundamental processes involved. It then examines the evolution of numerical modeling techniques, highlighting their advantages and growing popularity for investigating complex ice-seabed-pipeline interactions. While acknowledging the potential of the Coupled Eulerian-Lagrangian (CEL) method selected for this thesis, the review also discusses known limitations. Then, a review of the latest applications of artificial intelligence and machine learning methods in the study of ice gouging is presented. Finally, it briefly reviews experimental and numerical studies on trenched and backfilled pipelines subjected to large soil deformations.

2.2 Physical Model Testing of Ice Gouging

Physical model testing plays a crucial role in understanding the complex mechanics of ice gouging. These tests provide insights into gouging processes, soil behavior, and forces acting on buried structures like pipelines. This section reviews key studies conducted under normal gravity conditions and the influence of centrifugal forces.

Chari (1979) is a pioneering study conducted on a comprehensive geotechnical analysis of gouging processes. Chari's findings revealed that failure surfaces could extend below the maximum gouge depth, implying that simply burying a pipeline deeper than the gouge depth may not be sufficient to ensure its safety (Figure 2-1). Large subgouge soil deformations were identified as a potential threat to pipeline integrity, although displacement magnitudes were not explicitly quantified.

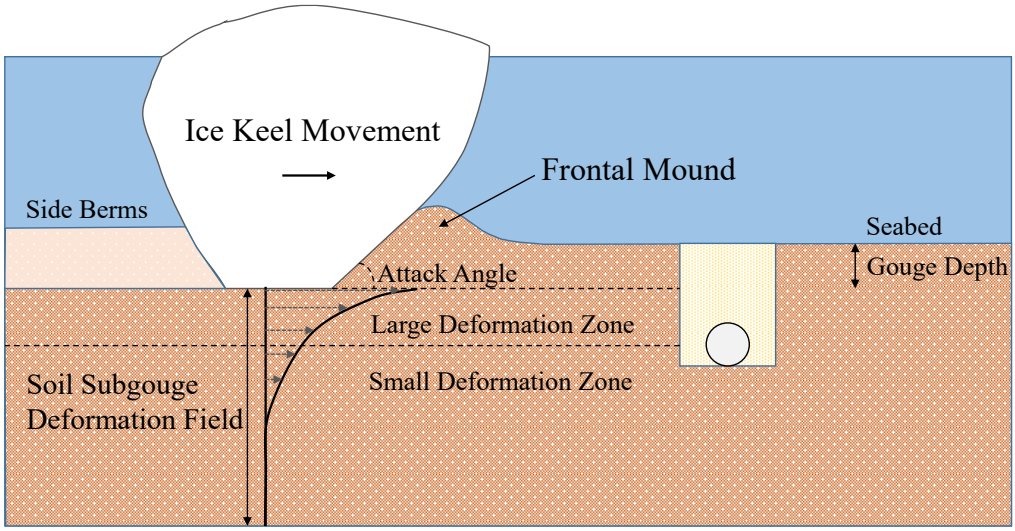

Figure 2-1. Seabed failure mechanisms in ice gouging events in non-layered seabed (not to scale)

Building upon Chari's research, Green et al. (1983) focused on measuring resistance pressures and the impact of varying keel shapes and sizes on these forces. Their instrumented pipeline model buried within the testbed allowed for direct measurement of pressures and forces acting on both the keel and the pipeline. The study investigated the effects of various parameters using different model sizes and keel configurations. Poorooshasb et al. (1989) explored the work of C-CORE (Centre for Cold Ocean Resources Engineering) on small-scale modeling of ice gouges in saturated silt and dry sand. Poorooshasb et al. conducted a series of tests investigating the size and characteristics of the deformation zone below a scouring iceberg model. Their study also explored the influence of width and attack angle on subgouge deformation, identifying soil density and attack angle as significant factors affecting its magnitude.

Initial investigations by Paulin focused on quantifying reaction forces and deformations during ice gouging in sand and clay (Paulin, 1991). A key finding was that the dominant reaction force (vertical or horizontal) depends on the ice keel's angle of attack. Additionally, Paulin observed that while the ice scouring mechanism was similar in submerged and dry sand, submerged conditions resulted in lower loads and reaction forces (Paulin, 1992).

Barker and Timco (2002, 2003) conducted an experimental program to investigate the forces and seabed responses associated with ice block gouging relevant to oil exploration in the Jeanne d'Arc Basin. Their setup employed fixed and free-moving ice blocks in a test tank, simulating 35 configurations with varied seabed types. Interestingly, the ice eroded rather than failing in shear. This erosion and the resulting sliding behavior significantly reduced overall scouring forces, increased vertical seabed loading due to loss of buoyancy, and likely made bearing capacity a more influential factor than previously assumed.

Vikse et al. (2007) performed small-scale laboratory tests to investigate pressure distribution and soil deformation around a buried pipe segment in sand and sandy silt. Vikse et al. observed that the maximum pipe displacement decreased significantly with increasing burial depth. Additionally, the study highlighted the influence of the naturally formed soil mound in front of the keel on vertical pipeline displacements and the larger horizontal movements at lower ice keel attack angles.

Stava et al. (2008) performed small-scale ice gouging experiments in a soft sandy silt-filled tank. They focused on understanding how gouges form, measuring soil deformations and mound characteristics, and investigating the effects on buried pipelines. Been et al. (2008) focused on failure mechanisms within clay during ice scouring. They found that higher undrained shear

strengths led to greater deformations, indicating a strong relationship between scour depth and clay soil properties.

Barrette et al. (2008,2009) conducted full-scale laboratory experiments to investigate how grounded ice and rubble slide on sand and clay seabeds. Their goal was to understand the factors influencing the sliding resistance. Instrumentation in the test flume measured stress distributions, seabed deformation, and ice dynamics. During the full-scale test, the following sequential stages of the ice scouring process were observed: 1) Initial seabed penetration by the ice keel; 2) A transitional period for the ice movement; 3) Stabilization of the ice scour path, becoming parallel to the seabed. Importantly, results showed that friction between the ice and seabed was the primary control for sliding resistance. In clay, this resistance is related to the effective shear response. Their study also found that ice rubble, compared to level ice, promoted clay consolidation, potentially increasing shear resistance over the pipeline's lifespan. The clay's undrained shear strength in all tests exceeded the sliding resistance. Finally, they proposed a method to estimate sliding resistance based on clay's effective internal friction angle, pore water pressure, and effective normal stresses. Barrette (2011), also, documented incidents of pipeline damage caused by this phenomenon. Notable cases include damage to a water intake pipeline in the Great Slave Lake and extensive damage to gas pipelines in Lake Erie. Additionally, iceberg-induced rupturing of communication cables offshore Labrador (Canada) between 1960 and 1970 underscores the potential risks associated with ice-related hazards in offshore environments

Sancio et al. (2011) conducted a large-scale ice gouging test program involving 17 cases using a composite steel and concrete indenter simulating an ice keel. They gouged beds of compacted clay or sand, outfitting a buried 40 ft. pipe with extensive strain gauges. Instrumentation measured keel position, gouging force, keel orientation, and cable inclination. In addition to analyzing the final

gouge shape, they studied soil displacements, pipeline strains, and pore water pressure responses in sand. Interestingly, in the sand, subgouge displacements showed no clear correlation with gouge depth, width, or soil density. Similarly, displacements did not directly relate to undrained shear strength in clay.

Almirall (2017) compared ice-induced sand deformations in saturated and dry conditions using 1g laboratory tests. The effects of velocity, scour geometry, and soil conditions were examined, revealing that subgouge deformations are smaller in 1g tests than in centrifuge models.

While normal gravity physical model testing offers valuable insights, replicating real-world ice gouging events presents challenges due to the non-linear mechanical behavior of geotechnical materials. These non-linearities are influenced by factors like effective confining stress and the material's stress history. To address these limitations, centrifuge-based experiments have emerged as a powerful tool for simulating ice gouging at scales that more closely represent real-world conditions. Centrifuge modeling allows researchers to account for the in-situ stresses in actual seabed conditions by subjecting the model to a carefully controlled g-force environment. This enables the simulation of ice gouging events with more realism than normal gravity testing.

Lach (1996) conducted nine centrifuge model tests at 100 times the force of gravity (100g). Lach's primary objective was to analyze the influence of various factors on the gouging process, including:

- Initial soil stress conditions (representing stress history)
- Model attack angle (ranging from 15° to 25°)
- Keel width
- Vertical keel stiffness

With extensive instrumentation, Lach measured stress and deformation fields within the soil, observed qualitative effects on pipeline segments, and determined resultant forces on the model ice feature. This work set a benchmark for subsequent numerical studies. In this study, model pipeline segments at approximate prototype depths of 1.5 and 0.6 m beneath the scour base did not exhibit any measurable plastic deformation. While Lach's (1996) work provides valuable insights, it lacks a quantitative assessment of the impact of ice gouging on buried pipelines.

The Pressure Ridge Ice Scour Experiments (PRISE) program expanded upon Lach's work with a series of 20 centrifuge tests (at 75g and 150g) in various soil strata (silty clay, sand, sand over clay, clay over sand) replicating conditions common to frequently gouged offshore regions (Woodworth-Lynes et al., 1996). This study's key findings include test keel horizontal reaction forces increased with gouge depth and width but decreased with increasing attack angle. As expected, greater undrained shear strength within the clay led to higher keel horizontal reaction forces. This dataset formed the basis for semi-empirical equations (PRISE Equation) to predict clay's subgouge soil deformation field (Phillips et al., 2005).

Centrifuge modeling was employed by Hynes (1996) to study ice keel scour in a sandy seabed. This study provided valuable data on scour-induced reaction forces, displacements, and pore pressure changes, highlighting a linear relationship between scour loads and depths.

Schoonbeek & Allersma (2005, 2006) centrifuge testing focused on how measurable soil parameters like undrained shear strength (s_u) influenced subgouge soil deformation. Additional variables included gouge speed, depth, keel angle, and surface roughness. They explored layered seabed (soft overlying overconsolidated soil) and instrumented their model to measure horizontal and vertical loads. Their key findings highlight the sensitivity of soil deformation to changes in

the rate of displacement, keel angle, surface roughness, and, most notably, the undrained shear strength of the clay sample.

Yang (2009) investigated subgouge deformations during simulated ice gouging events through The Pipeline Ice Risk Assessment and Mitigation (PIRAM) project. Conducting seven centrifuge tests, the research explores relationships between gouge geometry (depth, frontal berm), ice keel forces, subgouge deformation patterns, and their vertical extent. The influence of frontal berm height, gouge depth, and gouge rate on the outcomes is a key focus. Particle image velocimetry (PIV) was employed to track subgouge deformation. Findings indicate that the combined depth (gouge + frontal berm) significantly impacts force and deformation. Gouge force increases with depth, while the vertical-to-lateral force ratio appears independent of aspect ratio or attack angle. Maximum horizontal subgouge displacement occurs at the keel base, decreasing with depth. Notably, while the vertical deformation extent depends on the combined depth and soil state, it seems independent of the attack angle. Finally, faster gouge rates may significantly increase gouge forces while reducing horizontal subgouge deformation.

2.3 Numerical Simulation of Ice Gouging

The challenges associated with physical simulations, including scaling and replicating real-world conditions, have made numerical modeling a vital tool for investigating ice gouging phenomena. However, traditional Lagrangian methods face inherent limitations in simulating ice gouging. These limitations, such as node displacement and mesh distortion, arise from the large deformations and complex soil flow characteristic of gouging events (Lach, 1996; Woodworth-Lynes et al., 1996). Two finite element (FE) approaches have proven particularly useful: the Arbitrary Lagrangian-Eulerian Method (ALE) and the Coupled Eulerian-Lagrangian (CEL).

Researchers like Konuk et al. (2005) and Konuk & Yu (2007) have successfully employed ALE for detailed ice gouging investigations using LS-Dyna Explicit FE software. Studies like Konuk and Gracie (2004) revealed a logarithmic relationship between subgouge deformations and ice keel angle, highlighting the greater sensitivity at lower angles. Deformation magnitudes were also shown to increase proportionally with gouge depth. The vertical reaction force on the ice feature appears relatively independent of keel geometry, suggesting minimal buoyancy contributions. Additionally, ice-soil reaction forces exhibit sensitivity to the ice ridge angle, particularly at lower angles.

Konuk et al. (2005) investigated how the gouging performance and forces on the pipeline can be affected by the pipeline trench using the ALE finite element approach. In their model, the pipe's behavior was simplified by assuming it to be a rigid structure fixed in its position. They employed the Cap soil model to simulate two different backfill soil types. Key findings from their study include:

- Importance of trench modeling: Including the trench in their model significantly affected the resulting soil deformations, underscoring the necessity of considering this feature in ice gouging analysis.
- Backfill stiffness and pipeline loads: As expected, stiffer backfill materials increased horizontal and vertical loads on the pipe. However, the absolute load magnitudes were likely overestimated due to the rigid pipe constraint.

This study highlights the importance of considering both the trench and its backfill properties when analyzing the response of buried flexible pipelines to ice gouging loads.

Kenny et al. (2007) used ALE with adaptive meshing to model ice gouging in clay and validated their results against PRISE centrifuge data and empirical functions. Their model employed an elastic-perfectly plastic material with the von Mises criterion. Their numerical model's predictions for subgouge soil deformation generally matched the PRISE centrifuge test data but only for soil particles deeper than one gouge depth from the ice keel base. Additionally, the PRISE engineering model yielded conservative results compared to the actual test measurements. Nobahar et al. (2007) compared coupled ice-soil-pipe interaction with a decoupled Winkler spring approach. Key findings include significant effects of ice attack angle and contact properties on soil failure mechanics. The coupled analysis showed soil failure occurring at lower loads for undrained loading in multiple directions compared to single-directional loading. The coupled model predicted lower stresses and strains on the pipeline than the decoupled Winkler model, with the latter providing reasonably conservative estimates.

Fredj et al. (2008) investigated the factors influencing High Pressure/High Temperature (HP/HT) pipeline design during ice gouging events. They focused on the impact of operating pressure and thermal loads on overall pipeline response. Comparing scenarios with and without these operational factors revealed significant differences: for an operating pipe, maximum displacement, bending moment, and curvature were all significantly higher. This highlights the crucial influence of pressure and thermal-induced axial forces on pipeline stresses and strains. The study also explored the effect of gouge width, finding that maximum displacement increases with width. However, plastic strains did not follow the same pattern. Finally, they compared ALE modeling with two Winkler spring formulations; while all models produced consistent results, the spring models overestimated displacement for narrower gouge widths compared to the continuum model.

Peek and Nobahar (2012) compared coupled (3D continuum soil using ALE) and uncoupled (Winkler spring representation) models for determining pipeline burial depth. The uncoupled model used soil displacements and force/displacement curves derived from coupled simulations. Significantly higher peak strains in the uncoupled structural model were attributed to superposition errors resulting from the inconsistent strain fields between the decoupled model and the 3D coupled model where the pipe obstructs soil flow.

The CEL method has emerged as a valuable tool for simulating ice gouging due to its ability to handle the large deformations characteristic of these events. Abdalla et al. (2009) employed CEL to model ice gouging in clay using a modified Dracker-Prager/Cap constitutive model to account for soil volume dilatancy. Their subgouge soil deformation results generally agreed with PRISE centrifuge test data, particularly for deeper soil layers. They correlated well with findings from Konuk et al. (2005) and Kenny et al. (2007) for shallow keel angles. Phillips et al. (2010) compared CEL with ALE clay ice gouging methods. While all three methods produced consistent results aligned with PRISE data, the authors highlighted limitations in current soil constitutive models. They emphasized the need for models incorporating effective stress behavior, shear-induced dilatancy, and drained/undrained soil response for improved accuracy. Additionally, they pointed out that mesh resolution can significantly impact the ability to capture high-strain gradients near the moving ice keel.

Eskandari et al. (2010, 2011) used the ALE approach in Abaqus/Explicit to simulate free-field ice gouging in sand, with soil behavior defined by the critical state NorSand model. As part of the Pipeline Ice Risk Assessment and Mitigation, PIRAM, Joint Industry Project (JIP), their work emphasized the importance of state parameters and critical stress ratios in modeling subgouge soil deformations.

Banneyake et al. (2011) used the CEL method in Abaqus to model ice gouging in normally consolidated clay using the von Mises material law. They emphasized that an undrained soil response is appropriate due to the rapid loading imposed by ice gouging, making complex effective stress models like Cam Clay unnecessary. Simple pressure-independent plastic models (von Mises, Tresca, or Mohr-Coulomb) with proper strain-hardening behavior were suggested. Their model showed good agreement with PRISE data for horizontal subgouge soil deformation, but there were some discrepancies in the vertical direction.

Lele et al. (2011) employed the CEL approach in Abaqus to model ice gouging in clay with an undrained elastic-plastic soil model obeying the von Mises criterion. They noted the limitations of CEL in representing realistic seabed geometry due to the lack of infinite elements. Their model underestimated subgouge soil deformations compared to the PRISE model, likely due to conservative assumptions in the PRISE equations. The authors emphasized the need to validate their model against large-scale field data.

El-Gebaly et al. (2012) also used Abaqus CEL to simulate ice gouging in soft clay with both an elastic-perfectly plastic model and a Mohr-Coulomb model with softening. The model underestimated reaction forces compared to PRISE data, and soil deformations were smaller when softening was included, highlighting the importance of post-yield soil behavior in simulations.

Eskandari et al. (2012) further explored their numerical model's capabilities in simulating ice gouging in sand, specifically examining subgouge soil deformation, ice keel forces, soil formation behavior, and failure mechanisms. Sand density and gouge depth were identified as critical factors influencing the Critical Stress Ratio's (CSR) role. Additionally, they found that incorporating the state parameter alongside the critical stress ratio significantly improved predictions of subgouge

soil deformation. The researchers also developed an equation for estimating horizontal ice keel reaction forces.

Panico et al. (2012) investigated the impact of sand friction characteristics on ice gouging behavior. They modeled sand with both constant and varying friction properties. Critical state behavior of the sand had a greater impact on outcomes than peak friction angle. While uncertainties existed in test preparation, their continuum model showed good agreement with centrifuge data in predicting keel reaction forces. Additionally, their model accurately predicted pipeline strain demands compared to experimental data and idealized beam-spring models, highlighting its potential for cost-effective analysis.

Rossiter and Kenny (2012) evaluated the validity of ALE and CEL formulations using Abaqus software for modeling ice gouging in clay. CEL may not accurately represent defined shear stress limits at the keel-soil interface, potentially leading to inaccurate predictions of soil clearing, subduction, and ice keel reaction forces. ALE results for horizontal subgouge soil deformation in shallow depths did not fully align with the Lach (1996) test data, suggesting stiffer clay properties might be needed in shallow layers.

Pike and Kenny (2012) used centrifuge test data from Lach (1996) to explore how various factors influence ice gouging. They compared the effects of soil conditions (state), keel angle, width, and buoyant weight of the simulated iceberg. A significant contribution of their work is a method for selecting appropriate soil model parameters based on undrained shear strength, overconsolidation ratio, and basic soil properties. Their method leverages the undrained shear strength profile, overconsolidation ratio profile, and plasticity index to estimate the shear modulus, a key parameter in elastic soil models. They then utilize an elastic-perfectly plastic soil model requiring an elastic

modulus value. Given the assumed undrained conditions, they simplify the calculations to derive the elastic modulus from the undrained shear strength and plasticity index. The researchers agreed with their CEL model predictions and the centrifuge data for horizontal subgouge deformations and ice-soil reaction forces. However, some discrepancies emerged at depths exceeding one gouge depth below the keel base. They attributed this to mesh resolution and element formulation limitations, which struggle to capture the highly localized shear zone and sharp strain gradients near the moving keel. Another identified limitation stemmed from the soil model not accounting for tensile capacity. This resulted in the model overestimating the height of soil berms formed during gouging, potentially influencing the horizontal deformations. Similarly, underestimation of vertical subgouge deformations was observed. The authors suggested this mismatch could be partially due to the assumed elastic model, which cannot simulate soil volume change under vertical keel forces. They highlight the need for further development to address these limitations on vertical gouge behavior. Overall, Pike and Kenny's work demonstrates the effectiveness of their CEL model for ice gouging simulations. Their methodology for selecting soil model parameters and the identified limitations provide valuable insights for further research and model refinement.

Peek et al. (2013) combined large-scale physical ice gouging tests in clay with 3D finite element modeling using Abaqus CEL. Importantly, they allowed the ice keel to move and rotate freely during the simulation, providing a more realistic representation. The clay was modeled as an elastic-perfectly plastic material with von Mises failure criteria, strain hardening, and tension and compression capacity. Discrepancies in predicted pulling force compared to test results highlighted the need to incorporate strain-rate effects in the soil model. The model over-predicted the height of side berms, potentially due to a lack of mechanisms for simulating soil disintegration, cracking, and air entrainment.

Liferov et al. (2014) conducted 3D finite element modeling of ice gouging in clay using Abaqus CEL with a Drucker-Prager/Cap soil model. Hardening assumptions and flow rule considerations were included to address dilatant plastic shear deformations. Their model confirmed the relationship between ice keel attack angle and subgouge soil deformation: steeper angles resulted in smaller deformations. They noted that low ice velocities allowed for a focus on soil behavior without significant inertial effects.

Shin et al. (2019) developed a 3D model capable of simulating ice gouging using CEL. The model's accuracy was enhanced by considering the initial geostatic stress conditions within the soil and realistically representing the interaction between the ice keel and the seabed.

Nematzadeh and Shiri (2019a) conducted in-depth research on the complex phenomenon of ice gouging in sand environments, utilizing advanced numerical modeling techniques. Their simulations employed a 3D numerical approach using the CEL method. A significant focus of their work was developing a Modified Mohr-Coulomb model (MMC) specifically designed to account for the non-linear hardening and softening behavior characteristic of dense sand. Furthermore, they incorporated innovative "smart" self-correcting soil models that automatically adjust shear strength parameters based on the magnitude of plastic strains (Nematzadeh and Shiri, 2019b). Additionally, Nematzadeh and Shiri (2020) allowed for precise simulation of the non-linear hardening, softening, and pressure-dependent behavior exhibited by dense sand under ice gouging loads. Their research underscored the importance of incorporating realistic soil behavior into ice gouging models. These findings have important implications for pipeline design, suggesting that conventional decoupled methods may overestimate subgouge soil deformation. Consequently, these overestimations could lead to unnecessarily deep pipeline burial recommendations.

Hashemi and Shiri (2022) described that the pressure induced by ice keel through the ice gouging process causes the seabed soil to undergo large localized plastic deformation, where the classical Lagrangian method confronts mesh instability challenges. Also, the conventional Mohr-Coulomb soil model cannot account for the strain-rate dependency and strain-softening effects, which are significant in ice gouging events. Free-field ice gouging in clay was simulated using a coupled Eulerian-Lagrangian approach, and they incorporated the strain-rate dependency and strain-softening effects by developing a user-defined subroutine and incremental updating of the undrained shear strength using Einav and Randolph (2005) equation. The primary assumptions of Einav and Randolph (2005) include:

- Steady-State Advancing Mechanism: The model assumes that the penetrometer creates a continuously moving zone of plastic deformation in the soil, maintaining a steady-state shape as it advances. This simplifies the analysis by allowing the use of a stationary upper bound mechanism to represent the soil flow.
- Rigid Perfectly Plastic Soil: The initial upper bound mechanism is optimized for an ideal rigid perfectly plastic soil model (either Tresca or Von Mises). This provides a well-defined velocity field and failure mechanism, serving as a basis for incorporating more complex constitutive models.
- Incompressibility: The soil is assumed to be incompressible, meaning its volume remains constant during deformation. This simplifies the strain calculations and is a reasonable assumption for saturated clays.
- Isotropic Material Behavior: The model assumes the soil's strength and deformation properties are the same in all directions. This simplifies the analysis but may not accurately represent natural soils, which often exhibit anisotropy due to their depositional history and stress state.

- Simplified Strength Degradation Model: The strength degradation model is based solely on the accumulated absolute shear strain, ignoring other factors like rotation and strain orientation. While this simplifies the analysis, it may not capture the full complexity of soil behavior during cyclic loading.
- Neglect of Elastic Effects: The influence of soil elasticity is considered negligible, particularly compared to the effects of strain rate and strength degradation. While this simplifies the analysis, it may not be accurate for soils with high rigidity index (stiffness relative to strength).
- Simplified Treatment of Velocity Discontinuities: The model uses a simplified approach to handle velocity discontinuities (sharp changes in velocity) by assuming a uniform shear strain rate across a finite discontinuity layer. While this allows for the inclusion of strain rate effects, it introduces some inconsistency due to overlapping areas of discontinuity layers and shear zones.

The significant effect of incorporation of the strain-rate dependency and strain-softening effects into the constitutive soil model is elaborated by Hashemi and Shiri (2022). These effects are more visible on the keel reaction forces, subgouge soil deformations, and the dimensions of soil heaves in front and sides of the ice keel. Based on the insights from Hashemi and Shiri (2022), strain-rate dependency and strain-softening effects were incorporated into the present study.

Layered seabed configurations, characterized by distinct strata of varying geotechnical properties, introduce additional considerations that can significantly influence the response of buried pipelines to ice gouging events. These configurations may encompass soft over stiff clay and stiff over soft clay. Such non-uniform soil strata have been extensively documented in offshore Arctic regions, where numerous gouging signatures have been observed. Studies conducted in areas such as the

Chukchi Sea (C-CORE, 2008; Winters and Lee, 1984), the Alaskan Beaufort Shelf (C-CORE, 2008), and the Russian Sakhalin (C-CORE, 1995) have provided substantial evidence of the occurrence of layered seabed configurations in these environments. These observations highlight the significance of considering non-uniform geological strata in analyzing ice gouging interactions, emphasizing the need for comprehensive investigations that account for the complex interaction between moving ice features, seabed compositions, and buried pipeline responses.

A notable contribution to the study of layered seabed configurations in ice gouging analysis was made by Hashemi et al. (2022), Hashemi and Shiri (2022b, 2023), and Shiri and Hashemi (2023). Their work examined the free-field analysis of layered seabed formations, investigating soil failure mechanisms under the influence of ice gouging forces. This research explained the distinct response of layered seabed compositions comprising soft over stiff clay, stiff over soft clay, and loose and dense sand over soft and stiff clay, providing an understanding of the behavior of geological strata when subjected to ice-induced loads. They showed that the interactions between the soil layers with different strengths could significantly override the usual seabed response to ice gouging in uniform soil (as illustrated in Figure 2-1). In the soft over stiff clay, for the gouge depths less than the thickness of the soft layer, the subgouge soil deformation was truncated in the interface of the soil layers. This suggests that the trench depth can be safely limited to the thickness of a soft layer and the pipeline buried in a stiff layer with its crown touching the soft layer. The study revealed that the interaction between the stiff and soft layers in stiff over soft clay could lead to a subgouge soil deformation with a wavy shape, where the peak point is deeper than in a uniform soil. This wavy subgouge deformation profile includes a nadir point near the interface of the soil layers and a peak point deeper in the soft soil layer. While their work provide valuable insights into the behavior of layered seabeds during ice gouging, it does not explicitly address the response

of buried pipelines in such scenarios. The absence of a pipeline in his model limits the ability to directly assess the structural behavior and potential damage to the pipeline under these conditions.

Shin et al. (2024) developed a CEL model to investigate how ice gouging impacts clay slopes on the seabed. They created a user-defined subroutine (VUMAT), allowing the incorporation of strain-softening and strain-rate dependent behavior into a Tresca-based soil model. Model results were validated against data from the PRISE centrifuge experiments. The validated model was then used for parametric studies, investigating the impact of the ice keel's initial kinetic energy and seabed slope angle on soil deformation. Simulations revealed that increased initial kinetic energy of the ice keel and shallower seabed slopes resulted in significantly greater soil displacement and deformation.

In addition to ALE and CEL methods, researchers have explored other numerical approaches for simulating ice gouging events. Sayed & Timco (2009) employed a 2D finite element model with the Particle-In-Cell (PIC) advection method for simulating ice gouging in sand. This approach treated soil as a viscous non-Newtonian fluid, allowing individual particles to move and deform during the analysis. Soil strength behavior adhered to the rigid plastic Mohr-Coulomb model, and sand displacement was assumed to occur at the critical state. Their model aligned with the PRISE engineering equation and highlighted the influence of gouge depth and sand friction angle on mean normal stress.

Fadaifard and Tassoulas (2014) employed 2D finite element analysis within a computational fluid dynamics (CFD) framework to model ice gouging in clay. Soil was represented as a strain-rate dependent fluid utilizing the Herschel-Bulkley model to capture its non-Newtonian behavior. Calibration was performed against the Lach (1996) centrifuge data. Despite the limitations of the

2D approach in representing clearing mechanisms, the model showed good agreement with test data for horizontal subgouge soil deformations and ice keel reaction forces. The absence of clearing mechanisms led to a continuous buildup of the frontal mound during the simulation.

Liu et al. (2015) investigated the ice gouging phenomenon using the Discrete Element Method (DEM) to simulate experiments from the PIRAM and Development of Ice Ridge Keel Strength (DIRKS) projects. This research aimed to understand better ice keel interactions with the seabed and the potential impacts on offshore structures. The ice keels were modeled as bonded spheres using the Cohesive Frictional Model (CFM) within the Yade DEM code. The soil tray, berms, and reaction structures represented steel facets. The DEM model successfully captured essential features observed experimentally, including the initial strength peak, loss of cohesion, and the final load increase as rubble accumulated. Differences between the simulations and experiments were noted and attributed to factors such as water drag, continuing ice keel compression, and the difference between a steel berm and a gravel bed. These observations provide areas for future model refinement.

In recent years, the application of Machine Learning (ML) and Artificial intelligence (AI) has seen a surge across diverse fields. This surge is primarily due to significant advancements in ML, which have made it a powerful tool for simulating complex problems, both linear and non-linear, with high accuracy, speed, and affordability. Ice gouging, a complex phenomenon with profound implications for subsea infrastructure design and operation, has not been immune to this trend.

Kioka et al. (2003, 2004) developed a hybrid approach for approximating subgouge soil depth, combining the power of Neural Networks (NN) with established mechanical modeling techniques. Their research demonstrated the importance of considering both the bottom shape of the ice ridge

and the surrounding ice conditions as they significantly impacted the ice scouring process. The NN-based method achieved a high level of accuracy, leading the authors to suggest that this hybrid approach could outperform traditional nonlinear multiple-regression models for ice scour analysis.

Azimi and Shiri have conducted extensive research on the complex phenomenon of ice-seabed interaction, particularly in the context of Arctic engineering challenges. Their work has focused on developing advanced computational models and leveraging machine learning techniques to improve the understanding of how ice gouging impacts sandy and clay seabed environments.

Initially, they employed dimensional analysis to identify the most influential parameters governing sub-gouge soil deformations during ice gouging events. Seabed soil properties, gouge geometry, and ice keel characteristics were key factors. Building upon this, Azimi and Shiri (2020a) utilized linear regression models to estimate horizontal and vertical sub-gouge deformations in sandy and clay seabed environments. The findings indicated that the shear strength of the seabed soil and the ratio of gouge depth to width is particularly important for accurate modeling.

To address the complex interactions present in sandy environments, the researchers explored the use of Gene Expression Programming (GEP). This approach demonstrated its effectiveness in simulating the complex dynamics of ice-seabed interactions (Azimi & Shiri, 2020b). Furthermore, a sensitivity analysis using Extreme Learning Machines (ELMs) pinpointed the gouge depth ratio and seabed shear strength as the most impactful parameters on ice keel reaction forces and sub-gouge soil deformation in sand (Azimi and Shiri, 2021c). The authors proposed a set of ELM-based equations to approximate the parameters related to ice gouging. The researchers also focused on modeling subgouge sand deformations using a multi-layer perceptron neural network. By leveraging the capabilities of neural networks, particularly the multi-layer perceptron architecture,

Azimi and Shiri (2021d) developed a predictive model capable of accurately representing subgouge sand deformations. Further refining their methods, Azimi and Shiri (2021b) evaluated the ice-seabed interaction mechanism in sand using a self-adaptive evolutionary extreme learning machine. A self-adaptive evolutionary algorithm was employed to optimize the parameters of the extreme learning machine, enhancing its accuracy and robustness. Their findings provided valuable insights into ice-seabed interactions in sandy environments and demonstrated the effectiveness of the proposed approaches.

Azimi and Shiri's work extended to include clay seabeds. They introduced a non-tuned machine learning approach that bypassed the time-consuming parameter tuning process typical of these models (Azimi et al., 2021). This simplified approach successfully simulated ice gouging in clay environments. Further analysis with ELM models highlighted the importance of seabed depth and ice loading parameters for predicting deformations and reaction forces in clay under ice gouging (Azimi and Shiri, 2021a).

The researchers have consistently explored new techniques to enhance modeling accuracy, including the application of evolutionary design to the generalized Group Method of Data Handling (GMDH) for clay environments (Azimi et al., 2022) and tree-based machine learning algorithms for analyzing sub-gouge deformations (Azimi et al., 2022a, 2022b). Azimi et al. (2022b) used three machine learning algorithms - Decision Tree Regression (DTR), Random Forest Regression (RFR), and Extra Tree Regression (ETR) - to simulate the iceberg-seabed interaction process in the sandy seabed. They found that the ETR algorithm performed reasonably well in simulating horizontal and vertical sub-gouge soil deformations in the sand. Azimi et al. (2022a) employed tree-based machine learning algorithms to simulate the complex process of iceberg-seabed interactions in clay seabed. The study highlighted the importance of accurate

iceberg draft appraisal for efficient iceberg management designs and operational integrity of sea bottom-funded infrastructure against iceberg threats.

A specific focus of their research has been the prediction of iceberg drafts, a crucial factor in Arctic engineering and risk mitigation. By developing Linear Regression (LR) models and employing sensitivity analysis, they identified key parameters impacting draft estimation. They found that iceberg length and width ratios were highly influential with minimal complexity (Azimi et al., 2023). The researchers also derived a set of LR-based relationships for practical engineering applications. Further investigations with neural network modeling highlighted the importance of iceberg keel depth and seabed shear strength impacts on the iceberg draft (Azimi et al., 2023b). Most recently, they have explored the use of Decision Tree Regression (DTR), Artificial Neural Networks (ANN), Support Vector Regression (SVR), Random Forest Regression (RFR), Gradient-Boosting Regression, and further refinements of GMDH for predicting iceberg drafts and evaluating iceberg-seabed interaction (Azimiet al., 2023a; Azimi et al., 2023c; Azimi et al., 2024). Azimi and Shiri's development of novel computational models and application of machine learning techniques have improved the ability to simulate and predict ice-seabed interactions. This has direct implications for optimizing the design and operation of subsea pipelines, offshore structures, and iceberg management strategies in the Arctic and other ice-prone regions.

While significant research has focused on the gouging process and the resulting forces on pipelines, less attention has been paid to the influence of the pipeline's burial environment. The design of the pipeline trench (geometry, backfill material) significantly influences how a buried pipeline responds to large deformations caused by events like ice gouging or fault rupture (Dong et al., 2021; Kianian and Shiri, 2021a). For instance, inclined trench walls can mitigate the detrimental effects of limited trench dimensions, which can otherwise lead to significantly

increased soil pressures and pipeline bending strains (Chaloulos et al., 2015, 2017). The pipeline, backfill, and trench interact complexly, influencing lateral soil resistance. Neglecting this interaction can lead to inaccurate assessments of pipeline vulnerability (Aslkhalili et al., 2021; Dong et al., 2021; Kianian et al., 2018). Recent research by (Kianian et al., 2021; Kianian and Shiri, 2021b, 2023) has provided valuable insights for optimizing pipeline design and developing improved predictive models for the lateral response of buried pipelines in geologically active regions. Novel analytical and numerical methods provide insights for optimizing pipeline design and risk assessments, particularly in geohazardous regions (Asgarihajifirouz et al., 2023; Dong et al., 2023).

References

Abdalla, B., Jukes, P., Eltaher, A., & Duron, B. (2008). The technical challenges of designing oil and gas pipelines in the arctic. *OCEANS 2008*, 1–11.

Abdalla, B., Pike, K., Eltaher, A., Jukes, P., & Duron, B. (2009). Development and validation of a coupled Eulerian Lagrangian finite element ice scour model. *International Conference on Offshore Mechanics and Arctic Engineering*, *43451*, 87–95.

ALA. (2001). Guidelines for the design of buried steel pipe. *American Society of Civil Engineers*.

Almirall, S. A. (2017). *Ice Gouging in Sand and the Associated Rate Effects*. University of Aberdeen.

ASCE. (1984). *Guidelines for the Seismic Design of Oil and Gas Pipeline Systems*. Amer Society of Civil Engineers.

Asgarihajifirouz, M., Dong, X., & Shiri, H. (2023). Assessment of the Response of Trenched–Backfilled Pipelines to Strike-Slip Faults: An Analytical Approach. *Geosciences*, *13*(2), 47.

Aslkhalili, A., Shiri, H., & Zendehboudi, S. (2020). Probabilistic Assessment of Lateral Pipeline-Backfill-Trench Interaction. *Reliability Assessment of Drag Embedment Anchors and Laterally Loaded Buried Pipelines*, 96.

Aslkhalili, A., Shiri, H., & Zendehboudi, S. (2021). Probabilistic assessment of lateral pipeline–Backfill–Trench interaction. *Journal of Pipeline Systems Engineering and Practice*, *12*(3), 4021034.

Atangana Njock, P. G., Zheng, Q., Zhang, N., & Xu, Y.-S. (2020). Perspective Review on Subsea Jet Trenching Technology and Modeling. *Journal of Marine Science and Engineering*, *8*(6), 460.

Azimi, H., Mahdianpari, M., & Shiri, H. (2023). Determination of parameters affecting the estimation of iceberg draft. *China Ocean Engineering*, *37*(1), 62–72.

Azimi, H., & Shiri, H. (2020a). Dimensionless groups of parameters governing the ice-seabed interaction process. *Journal of Offshore Mechanics and Arctic Engineering*, *142*(5), 51601.

Azimi, H., & Shiri, H. (2020b). Ice-Seabed interaction analysis in sand using a gene expression programming-based approach. *Applied Ocean Research*, *98*, 102120.

Azimi, H., & Shiri, H. (2021a). Assessment of ice-seabed interaction process in clay using extreme learning machine. *International Journal of Offshore and Polar Engineering*, *31*(04), 411–420.

Azimi, H., & Shiri, H. (2021b). Evaluation of ice-seabed interaction mechanism in sand by using self-adaptive evolutionary extreme learning machine. *Ocean Engineering*, *239*, 109795.

Azimi, H., & Shiri, H. (2021c). Sensitivity analysis of parameters influencing the ice–seabed interaction in sand by using extreme learning machine. *Natural Hazards*, *106*(3), 2307–2335.

Azimi, H., & Shiri, H. (2021d). Modeling subgouge sand deformations by using multi-layer perceptron neural network. *ISOPE International Ocean and Polar Engineering Conference*, ISOPE-I.

Azimi, H., Shiri, H., & Mahdianpari, M. (2022a). Iceberg-seabed interaction evaluation in clay seabed using tree-based machine learning algorithms. *Journal of Pipeline Science and Engineering*, *2*(4), 100075.

Azimi, H., Shiri, H., & Mahdianpari, M. (2023a). Iceberg draft prediction using gradient boosting regression algorithm. *Marine Systems & Ocean Technology*, *18*(3), 151–166.

Azimi, H., Shiri, H., & Mahdianpari, M. (2023b). Sensitivity analysis of parameters governing the iceberg draft through neural network-based models. *Journal of Ocean Engineering and Marine Energy*, *9*(4), 587–602.

Azimi, H., Shiri, H., & Mahdianpari, M. (2024). Generalized Structure of the Group Method of Data Handling for Modeling Iceberg Drafts. *Ocean Modelling*, 102337.

Azimi, H., Shiri, H., & Mahdianpari, M. (2023c). Evaluation of iceberg draft and iceberg-seabed interaction using random forest regression algorithm. *ISOPE International Ocean and Polar Engineering Conference*, ISOPE-I.

Azimi, H., Shiri, H., & Mahdianpari, M. (2022b). Simulation of Subgouge Sand Deformations Using Robust Machine Learning Algorithms. *Offshore Technology Conference*, D021S028R009.

Azimi, H., Shiri, H., & Malta, E. R. (2021). A non-tuned machine learning method to simulate ice-seabed interaction process in clay. *Journal of Pipeline Science and Engineering*, *1*(4), 379–394.

Azimi, H., Shiri, H., & Zendehboudi, S. (2022). Ice-seabed interaction modeling in clay by using evolutionary design of generalized group method of data handling. *Cold Regions Science and Technology*, *193*, 103426.

Bai, Y., & Bai, Q. (2005). *Subsea pipelines and risers*. Elsevier.

Banneyake, R., Hossain, M. K., Eltaher, A., Nguyen, T., & Jukes, P. (2011). Ice-soil-pipeline interactions using coupled eulerian-lagrangian (CEL) ice gouge simulations-extracts from ice pipe JIP. *OTC Arctic Technology Conference*.

Barker, A., & Timco, G. (2002). Laboratory experiments of ice scour processes: rigid ice indentor. *Cold Regions Science and Technology*, *35*(3), 195–206.

Barker, A., & Timco, G. (2003). Laboratory experiments of ice scour processes: buoyant ice model. *Cold Regions Science and Technology*, *36*(1–3), 103–114.

Barrette, P. D., & Timco, G. W. (2008). Ice scouring in a large flume: Test set-up and preliminary observations. *SNAME International Conference and Exhibition on Performance of Ships and Structures in Ice*, D041S015R001.

Barrette, P., Marquardt, J., & Timco, G. (2009). Test data from scour simulations with rigid indentors and real ice rubble. *CHC-NRC Technical Report CHC-CTR-103*.

Barrette, P. (2011). Offshore pipeline protection against seabed gouging by ice: An overview. Cold Regions Science and Technology, 69(1), 3-20.

Been, K., Sancio, R. B., Ahrabian, D., van Kesteren, W., Croasdale, K., & Palmer, A. (2008). Subscour displacement in clays from physical model tests. *2008 7th International Pipeline Conference*, 239–245.

Biscontin, G., & Pestana, J. M. (2001). Influence of peripheral velocity on vane shear strength of an artificial clay. *Geotechnical Testing Journal*, *24*(4).

C-CORE. (1995). *Pressure Ridge Ice Scour Experiment, PRISE: Phase 3-Centrifuge Modelling of Ice Keel Scour: Draft Final Report*.

C-CORE. (2008). *Design Options for Offshore Pipelines in the US Beaufort and Chukchi Seas*.

Chaloulos, Y. K., Bouckovalas, G. D., & Karamitros, D. K. (2017). Trench effects on lateral py relations for pipelines embedded in stiff soils and rocks. *Computers and Geotechnics*, *83*, 52–63.

Chaloulos, Y. K., Bouckovalas, G. D., Zervos, S. D., & Zampas, A. L. (2015). Lateral soil–pipeline interaction in sand backfill: effect of trench dimensions. *Computers and Geotechnics*, *69*, 442–451.

Chari, T. R. (1979). Geotechnical aspects of iceberg scours on ocean floors. *Canadian Geotechnical Journal*, *16*(2), 379–390.

Chen, Xiangyu, Zhang, L., Chen, L., Li, X., & Liu, D. (2019). Slope stability analysis based on the Coupled Eulerian-Lagrangian finite element method. *Bulletin of Engineering Geology and the Environment*, *78*(6), 4451–4463.

Chen, Xuejian, Li, D., Tang, X., & Liu, Y. (2021). A three-dimensional large-deformation random finite-element study of landslide runout considering spatially varying soil. *Landslides*, *18*(9), 3149–3162.

Cheng, X., Huang, R., Xu, L., Ma, C., & Zhu, X. (2021). Parametric study on the trench designing for X80 buried steel pipeline crossing oblique-reverse fault. *Soil Dynamics and Earthquake Engineering*, *150*, 106824.

CSA. (2015). *CSA Z662-15: Oil and gas pipeline systems*.

Dayal, U., & Allen, J. H. (1975). The effect of penetration rate on the strength of remolded clay and sand samples. *Canadian Geotechnical Journal*, *12*(3), 336–348.

DNV GL. (2017). *DNVGL-ST-F101, Submarine pipeline systems*.

Dong, X., Malta, E. R., & Shiri, H. (2023). Deformation of trenched multilayer pipelines during large lateral displacement due to subsea geohazards. *Ocean Engineering*, *278*, 114352.

Dong, X., Shiri, H., Zhang, W., & Randolph, M. F. (2021). The influence of pipeline-backfill-trench interaction on the lateral soil resistance: A numerical investigation. *Computers and Geotechnics*, *137*, 104307.

Einav, I., & Randolph, M. F. (2005). Combining upper bound and strain path methods for evaluating penetration resistance. *International Journal for Numerical Methods in Engineering*, *63*(14), 1991–2016.

El-Gebaly, S., Paulin, M., Lanan, G., & Cooper, P. (2012). Ice gouge interaction with buried pipelines assessment using advanced coupled Eulerian Lagrangian. *OTC Arctic Technology Conference*.

Eskandari, F, Phillips, R., & Hawlader, B. (2012). Finite element analyses of seabed response to ice keel gouging. *Proceedings of the 65th Canadian Geotechnical Conference (GeoManitoba)*.

Eskandari, Farzad. (2014). *Buried pipeline response to ice gouging*. Memorial University of Newfoundland.

Eskandari, Farzad, Phillips, R., & Hawlader, B. (2010). A State Parameter Modified Drucker-Prager Cap Model. *Canadian Geotechnical Conference*.

Eskandari, Farzad, Phillips, R., & Hawlader, B. (2011). Ice gouging analysis using NorSand critical state soil model. *Proceedings of the Pan-Am CGS Geotechnical Conference*, 2–6.

Esmaeilzadeh, M., & Shiri, H. (2019). Trench impact on lateral response of pipeline buried in sand. *Experimental and Numerical Modeling of Lateral Pipeline-Trench Interaction Backfilled with Sand*, 72.

Fadaifard, H., & Tassoulas, J. L. (2014). Numerical modeling of coupled seabed scour and pipe interaction. *International Journal of Solids and Structures*, *51*(19–20), 3449–3460.

FitzMaurice, A., Straneo, F., Cenedese, C., & Andres, M. (2016). Effect of a sheared flow on iceberg motion and melting. *Geophysical Research Letters*, *43*(24), 12–520.

Fredj, A., Comfort, G., & Dinovitzer, A. (2008). A case study of high pressure/high temperature pipeline for ice scour design using 3D continuum modeling. *International Conference on Offshore Mechanics and Arctic Engineering*, *48203*, 563–572.

Gautier, D. L., Bird, K. J., Charpentier, R. R., Grantz, A., Houseknecht, D. W., Klett, T. R., Moore, T. E., Pitman, J. K., Schenk, C. J., & Schuenemeyer, J. H. (2009). Assessment of undiscovered oil and gas in the Arctic. *Science*, *324*(5931), 1175–1179.

Graham, J., Crooks, J. H. A., & Bell, A. L. (1983). Time effects on the stress-strain behaviour of natural soft clays. *Géotechnique*, *33*(3), 327–340.

Green, H. P., Reddy, A. S., & Chari, T. R. (1983). Iceberg scouring and pipeline burial depth. *Proc., POAC'83, 7th Int. Conf. on Port and Oc. Engrg. under Arctic Conditions*, *1*, 280–288.

Hashemi, S., & Shiri, H. (2022a). Numerical Modeling of Ice–Seabed Interaction in Clay by Incorporation of the Strain Rate and Strain-Softening Effects. *Journal of Offshore Mechanics and Arctic Engineering*, *144*(4), 42101.

Hashemi, S., & Shiri, H. (2022b). The response of layered seabed to ice gouging: Sand over clay. *Ocean Engineering*, *266*, 113134. https://doi.org/https://doi.org/10.1016/j.oceaneng.2022.113134

Hashemi, S., & Shiri, H. (2023). Numerical Modeling of Ice-seabed Interaction in Layered Soil: Stiff over Soft Clay. *Canadian Geotechnical Journal*. https://doi.org/10.1139/cgj-2022-0594

Hashemi, S., Shiri, H., & Dong, X. (2022). The influence of layered soil on ice-seabed interaction: Soft over stiff clay. *Applied Ocean Research*, *120*, 103033.

Hynes, F. (1996). *Centrifuge modelling of ice scour in sand*. Memorial University of Newfoundland.

Jan De Nul Group. (2020). *Starfish (Elevated Excavator)*. https://www.jandenul.com/fleet/trenchers

Jukes, P., Kenny, S., Panapitiya, U., Jafri, S., & Eltaher, A. (2011). Arctic and harsh environment pipeline trenching technologies and challenges. *OTC Arctic Technology Conference*.

Kenny, S., Barrett, J., Phillips, R., & Popescu, R. (2007). Integrating geohazard demand and structural capacity modelling within a probabilistic design framework for offshore arctic pipelines. *The Seventeenth International Offshore and Polar Engineering Conference*.

Kianian, M, Esmaeilzadeh, M., & Shiri, H. (2018). Lateral Response of Trenched Pipelines to Large Deformations in Clay. In *Offshore Technology Conference* (p. D032S092R009). https://doi.org/10.4043/28842-MS

Kianian, Morteza, Esmaeilzadeh, M., & Shiri, H. (2021). The Effect of Backfilling Stiffness on the Lateral Response of Deeply Buried Pipelines: an Experimental Study. *Journal of Marine Science and Application*, *20*(1), 21–33.

Kianian, Morteza, & Shiri, H. (2021a). Experimental study of trench effect on lateral failure mechanisms around the pipeline buried in clay. *Journal of Pipeline Science and Engineering*, *1*(2), 198–211.

Kianian, Morteza, & Shiri, H. (2021b). The effect of backfilling stiffness on lateral response of the shallowly trenched-backfilled pipelines in clay. *Marine Georesources & Geotechnology*, *39*(5), 610–622.

Kianian, Morteza, & Shiri, H. (2023). Large Deformation Analysis of Trenched Pipelines Under Lateral Displacements. *Geotechnical and Geological Engineering*, *41*(4), 2537–2552.

Kioka, S. D., Kubouchi, A., & Saeki, H. (2003). Training and generalization of experimental values of ice scour event by a neural-network. *ISOPE International Ocean and Polar Engineering Conference*, ISOPE-I.

Kioka, S., Kubouchi, A., Ishikawa, R., & Saeki, H. (2004). Application of the mechanical model for ice scour to a field site and simulation method of scour depths. *ISOPE International Ocean and Polar Engineering Conference*, ISOPE-I.

Ko, J., Jeong, S., & Lee, J. K. (2016). Large deformation FE analysis of driven steel pipe piles with soil plugging. *Computers and Geotechnics*, *71*, 82–97.

Konuk, I, Yu, S., & Gracie, R. (2005). An ALE FEM model of ice scour. *11th International Conference of the International Association of Computer Models and Advances in Geomechanics, Turin, Italy*.

Konuk, Ibrahim, & Gracie, R. (2004). A 3-dimensional Eulerian finite element model for ice scour. *International Pipeline Conference*, *41766*, 1911–1918.

Konuk, Ibrahim, & Yu, S. (2007). A pipeline case study for ice scour design. *International Conference on Offshore Mechanics and Arctic Engineering*, *42711*, 163–169.

Konuk, Ibrahim, Yu, S., & Fredj, A. (2006). Do Winkler models work: A case study for ice scour problem. *International Conference on Offshore Mechanics and Arctic Engineering*, *47497*, 197–203.

Konuk, Ibrahim, Yu, S., & Gracie, R. (2005). A 3-Dimensional Continuum ALE Model for Ice Scour: Study of Trench Effects. *International Conference on Offshore Mechanics and Arctic Engineering*, *41960*, 945–949.

Lach, P. R. (1996). *Centrifuge modelling of large soil deformation due to ice scour*. Memorial University of Newfoundland. https://research.library.mun.ca/1194/

Lele, S. P., Hamilton, J. M., Panico, M., & Arslan, H. (2011). Advanced continuum modeling to determine pipeline strain demand due to ice-gouging. *The Twenty-First International Offshore and Polar Engineering Conference*.

Liferov, P., & Høyland, K. V. (2004). In-situ ice ridge scour tests: experimental set up and basic results. *Cold Regions Science and Technology*, *40*(1–2), 97–110.

Liferov, P., Nes, H., Asklund, J., Shkhinek, K., & Jilenkov, A. (2014). Ice gouging and its effect on pipelines. *OTC Arctic Technology Conference*, OTC-24605.

Liu, L., Bailey, E., Sarracino, R., Taylor, R., Power, C., & Stanbridge, C. (2015). Numerical simulation of ice ridge gouging. *International Conference on Offshore Mechanics and Arctic Engineering*, *56567*, V008T07A022.

Miller, D. L., & Bruggers, D. E. (1980). Soil and permafrost conditions in the Alaskan Beaufort Sea. *Offshore Technology Conference*, OTC-3887.

Nagula, S. S., & Grabe, J. (2020). Coupled Eulerian Lagrangian based numerical modelling of vibro-compaction with model vibrator. *Computers and Geotechnics*, *123*, 103545.

Nematzadeh, A, & Shiri, H. (2019a). Large deformation analysis of ice scour process in dense sand. *10th Congress on Numerical Methods in Engineering, At Guimaraes, Portugal*.

Nematzadeh, A, & Shiri, H. (2019b). *Self-correcting soil models for numerical simulation of strain rate dependent ice scour in sand*.

Nematzadeh, Afrouz, & Shiri, H. (2020). The influence of non-linear stress-strain behavior of dense sand on seabed response to ice gouging. *Cold Regions Science and Technology*, *170*, 102929.

Neumann Dredging. (n.d.). *Nu Enterprise cutter suction dredge*. https://neumanndredging.com.au/dredging-equipment/nu-enterprise-cutter-suction-dredge

Nobahar, A., Kenny, S., & Phillips, R. (2007). Buried pipelines subject to subgouge deformations. *International Journal of Geomechanics*, *7*(3), 206–216.

Noh, W. F. (1963). *CEL: A time-dependent, two-space-dimensional, coupled Eulerian-Lagrange code*. Lawrence Radiation Lab., Univ. of California, Livermore.

Palmer, A. C., Konuk, I., Comfort, G., & Been, K. (1990). Ice gouging and the safety of marine pipelines. *Offshore Technology Conference*.

Palmer, A., Konuk, I., Love, J., Been, K., & Comfort, G. (1989). Ice Scour Mechanics. *A Research Paper Prepared for Canada Oil and Gas Lands Administration and Gulf Canada Resources Ltd*.

Panico, M., Lele, S. P., Hamilton, J. M., Arslan, H., & Cheng, W. (2012). Advanced ice gouging continuum models: comparison with centrifuge test results. *ISOPE International Ocean and Polar Engineering Conference*, ISOPE-I.

Paulin, M J. (1991). *Preliminary results of physical model tests of ice scour*. Memorial University of Newfoundland, Centre for Cold Ocean Resources Engineering.

Paulin, Michael J. (1992). *Physical model analysis of iceberg scour in dry and submerged sand*. Memorial University of Newfoundland.

Paulin, Michael J. (1998). *An investigation into pipelines subjected to lateral soil loading*. Memorial University of Newfoundland.

Paulin, Michael J, Kenny, S. P., Palmer, A. C., Been, K., & Caines, J. V. M. (2008). Offshore Pipelines in Cold Regions-Environmental Loadings and Geotechnical Considerations. *SNAME 8th International Conference and Exhibition on Performance of Ships and Structures in Ice*.

Peek, R, Been, K., Bouwman, V., Nobahar, A., Sancio, R., & Schalkwijk, R. V. (2013). Buried pipeline response to ice gouging on a clay seabed large scale tests and finite element analysis. *22nd International Conference on Port and Ocean Engineering under Arctic Conditions (POAC)*, 9–13.

Peek, Ralf, & Nobahar, A. (2012). Ice gouging over a buried pipeline: Superposition error of simple beam-and-spring models. *International Journal of Geomechanics*, *12*(4), 508–516.

Phillips, R, Barrett, J., & Al-Showaiter, A. (2010a). Ice keel-seabed interaction: Numerical modeling validation. *Offshore Technology Conference*, *20696*.

Phillips, R, Barrett, J., & Al-Showaiter, A. (2010b). Ice keel-seabed interaction: Numerical modelling validation. *Offshore Technology Conference*, *20696*.

Phillips, R, Clark, J. I., & Kenny, S. (2005). PRISE studies on gouge forces and subgouge deformations. *Proceedings of the International Conference on Port and Ocean Engineering Under Arctic Conditions*.

Phillips, Ryan, Nobahar, A., & Zhou, J. (2004). Trench effects on pipe-soil interaction. *International Pipeline Conference*, *41766*, 321–327.

Pike, K., & Kenny, S. (2016). Offshore pipelines and ice gouge geohazards: comparative performance assessment of decoupled structural and coupled continuum models. *Canadian Geotechnical Journal*, *53*(11), 1866–1881.

Pike, K. P. (2016). *Physical and numerical modelling of pipe/soil interaction events for large deformation geohazards*. Memorial University of Newfoundland.

Pike, K. P., & Kenny, S. P. (2012). Advanced continuum modeling of the ice gouge process: Assessment of keel shape effect and geotechnical data. *ISOPE International Ocean and Polar Engineering Conference*, ISOPE-I.

Poorooshasb, F., Clark, J. I., & Woodworth-Lynas, C. M. (1989). *Small scale modelling of iceberg scouring of the seabed*.

PRCI. (2009). *Guidelines for Constructing Natural Gas and Liquid Hydrocarbon Pipelines through Areas Prone to Landslide and Subsidence Hazards*, *Pipeline Research Council International*.

Qiu, G., Henke, S., & Grabe, J. (2011). Application of a Coupled Eulerian–Lagrangian approach on geomechanical problems involving large deformations. *Computers and Geotechnics*, *38*(1), 30–39.

Raie, M. S., & Tassoulas, J. L. (2009). Installation of torpedo anchors: numerical modeling. *Journal of Geotechnical and Geoenvironmental Engineering*, *135*(12), 1805–1813.

Randolph, M. F. (2004). Characterization of soft sediments for offshore applications. *Proc. ISC-2 on Geotechnical and Geophysical Site Characterization, 2004*.

Rossiter, C., & Kenny, S. P. (2012). Assessment of ice-soil interactions: Continuum modeling in clays. *The Twenty-Second International Offshore and Polar Engineering Conference*.

Roy, K., Hawlader, B., Kenny, S., & Moore, I. (2018). Uplift failure mechanisms of pipes buried in dense sand. *International Journal of Geomechanics*, *18*(8), 4018087.

Sancio, R., Been, K., & Lopez, J. (2011). Large scale indenter test program to measure sub gouge displacements. *Proceedings of the International Conference on Port and Ocean Engineering Under Arctic Conditions*, *POAC11-096*.

Sayed, M., & Timco, G. W. (2009). A numerical model of iceberg scour. *Cold Regions Science and Technology*, *55*(1), 103–110.

Schoonbeek, I. S. S., & Allersma, H. G. B. (2006). Centrifuge modelling of scouring ice keels in clay. *Proceedings, 8th International Conference on Physical Modelling in Geotechnics, ICPMG*, 1291–1296.

Shin, M.-B., Park, D.-S., Park, W.-J., & Seo, Y.-K. (2024). Behavioral analysis of seabed slope subjected to ice gouging. *Cold Regions Science and Technology*, *217*, 104022.

Shin, M.-B., Park, D.-S., & Seo, Y. (2019). Comparative study of ice gouge simulation considering ice keel-seabed interactions. *Journal of Ocean Engineering and Technology*, *33*(6), 556–563.

Shiri, H., & Hashemi, S. (2023). The Impact of Layering Seabed on its Response to Ice Gouging. In *The 33rd International Ocean and Polar Engineering Conference* (p. ISOPE-I-23-205).

Simulia, D. S. (2019). *Abaqus 2019 documentation*. Dassault Systemes Waltham, MA.

Staubach, P., Machaček, J., Skowronek, J., & Wichtmann, T. (2021). Vibratory pile driving in water-saturated sand: Back-analysis of model tests using a hydro-mechanically coupled CEL method. *Soils and Foundations*, *61*(1), 144–159.

Stava, I., Nystrøm, P. R., Vikse, N., Gudmestad, O. T., Liferov, P., & Grønli, J. (2008). Small scale model tests of ice gouge in soft sandy silt. *International Conference on Offshore Mechanics and Arctic Engineering*, *48203*, 891–900.

Tudorache, V.-P., & Antonescu, N.-N. (2020). Challenges of oil and gas exploration in the Arctic. *J. Eng. Sci. Innov*, *5*, 273–286.

van Rhee, C. (2002). Numerical modelling of the flow and settling in a trailing suction hopper dredge. *Proc., 11th Int. Symp. on Transport and Sedimentation of Solid Particles*.

Vikse, N., Gudmestad, O. T., Nystrøm, P. R., & Liferov, P. (2007). Small scale model tests on subgouge soil deformations. *International Conference on Offshore Mechanics and Arctic Engineering*, *42711*, 157–162.

Winters, W. J., & Lee, H. J. (1984). *Geotechnical properties of samples from borings obtained in the Chukchi Sea, Alaska* (Vol. 85, Issue 23). US Geological Survey.

Woodworth-Lynes, C., Nixon, D., Phillips, R., & Palmer, A. (1996). Subgouge deformations and the security of Arctic marine pipelines. *Offshore Technology Conference*.

Yang, W. (2009). *Physical modeling of subgouge deformations in sand*. Memorial University of Newfoundland.

CHAPTER 3

The Influence of Pipeline-Backfill-Trench Interaction on Pipeline Response to Ice Gouging: A Numerical Investigation

Alireza Ghorbanzadeh, Xiaoyu Dong, Hodjat Shiri

Civil Engineering Department, Faculty of Engineering and Applied Science, Memorial University of Newfoundland, A1B 3X5, St. John's, NL, Canada.

This chapter is under review as a journal manuscript.

Abstract

Ice gouging is a destructive incident to subsea pipelines in Arctic regions. Trenching and backfilling is the most efficient and cost-effective way to physically protect the pipeline against ice gouging. Ice gouging imposes a complex combination of stresses and strains through the soil medium, the pipeline, and the interface. Remolded backfill materials with considerably less stiffness than native soil result in more complexity in soil failure mechanisms and pipe trajectories. However, this critical aspect is less explored in the literature on ice gouges. This paper investigated the influences of pipeline-backfill-trench interaction on the soil failure mechanisms and the pipeline responses by coupled Eulerian-Lagrangian (CEL) method. Two model configurations (shallowly buried and deeply buried pipeline) were set up to investigate the influence of trenching/backfilling, as well as pipe burial depth. Incorporation of the strain-rate dependency and strain-softening effects in the soil constitutive model involved the development of a user-defined subroutine and incremental update of the undrained shear strength within the Abaqus software. The research findings indicate that the conventional approach of assuming uniform seabed soil for trenched and backfilled pipelines may not accurately capture the pipeline behavior and soil failure mechanisms. Consequently, it can lead to incorrect pipeline performance design when subjected to ice gouging loads.

Keywords: ice gouging; Coupled Eulerian-Lagrangian (CEL); pipeline-backfill-trench interaction; Arctic pipelines

3.1 Introduction

The Arctic holds significant potential for the oil and gas industry due to its vast, potentially untapped resources. However, extracting these resources presents unique challenges and limitations (Tudorache & Antonescu, 2020). One particularly complex challenge is ice gouging, a process that occurs in shallow areas in the Arctic and other regions where floating ice features, such as icebergs and ice ridges, are driven by wind, water currents, and tides. The process causes significant compressive and shear stresses on the seabed, leading to soil failure mechanisms, including subgouge soil displacements, frontal mounds, and side berms (Figure 3-1). Ice gouging is a serious hazard for pipelines, potentially causing leaks and structural damage. Burying pipelines is the most cost-effective way to mitigate this risk, but it does not eliminate it completely. Subsurface movements and stress transfer can still cause pipe deformations. A primary objective of ice gouging studies is to identify the best burial depth that protects pipelines while minimizing construction costs (Hashemi and Shiri, 2022).

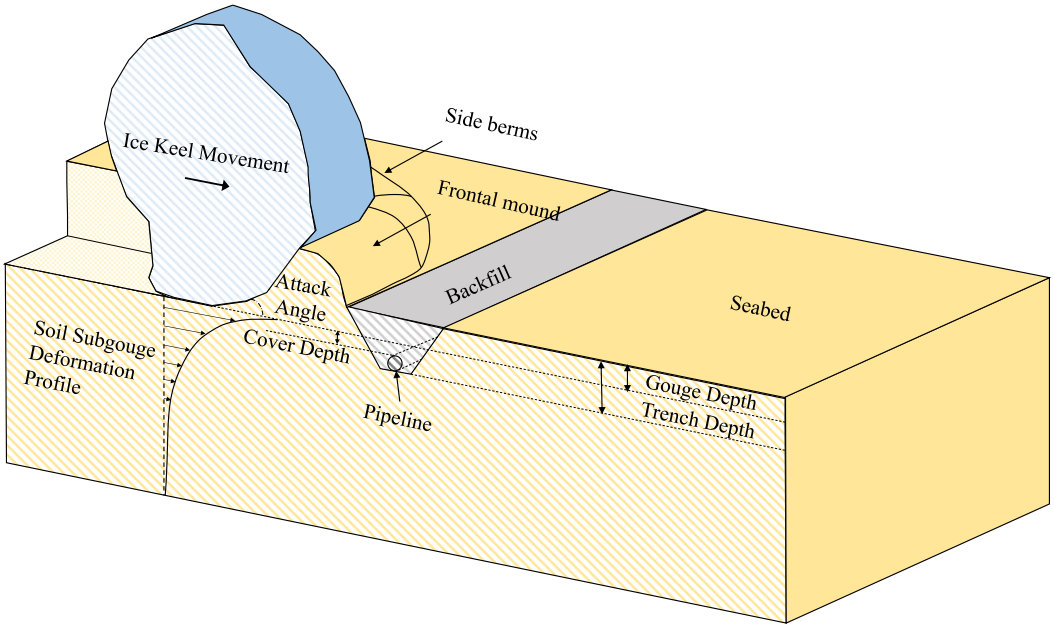

Figure 3-1. Schematic of ice gouging over a buried pipeline (not to scale)

Numerous experimental (e.g., Paulin, 1992, Lach, 1996, Phillips et al., 2005, Schoonbeek & Allersma, 2006) and numerical models (e.g. Nematzadeh & Shiri, 2020; Abdalla et al., 2008, 2009; Banneyake et al., 2011; El-Gebaly et al., 2012; Pike & Kenny, 2016; Phillips et al., 2010) investigated the ice gouging process. However, limited research addressed the specific effects of trenching and backfilling on buried pipelines. Pipelines are often buried in trenches backfilled with excavated soil, but the trenching process reduces the soil's shear strength due to disturbance and mixing with seawater. Research has shown that this stiffness contrast and pipeline-backfill-trench wall interaction significantly affects the soil failure mechanisms and pipeline response to lateral pipeline displacement during events like an ice gouge (Aslkhalili et al., 2020; Dong et al., 2021; Paulin, 1998). The crucial influence of pipeline-backfill-trench wall interaction on pipeline response represents a significant knowledge gap within the field of ice gouging research. Moreover, conventional pipeline design codes (e.g. (ALA, 2001; ASCE, 1984; PRCI, 2009) for ice gouging analysis often rely on the structural beam-spring method (Winkler method). While fast and simple, this method has limitations. Importantly, it assumes uniform soil conditions, neglecting the pipeline-backfill-trench wall interaction. This significant limitation is addressed in the current study.

This study investigates the crucial effects of pipeline-backfill-trench wall interaction on pipeline response to ice gouging. Using Abaqus/Explicit, a Coupled Eulerian-Lagrangian (CEL) numerical model is employed to simulate the complex dynamics of an ice keel interacting with a trenched and backfilled pipeline. To accurately capture soil behavior, a VUSDFLD user subroutine, implementing the equation proposed by Einav and Randolph (2005), accounts for strain rate dependency and strain-softening effects. The model was validated against experimental and numerical data (Lach, 1996; Pike, 2016) to ensure its accuracy.

Key findings revealed that the interaction between the pipeline, softer backfill, and trench walls significantly influences ice keel reaction forces, soil failure mechanisms, and pipeline response. The study further revealed that during ice gouging events, the interaction between the pipeline, backfill material, and trench walls can lead to backfill removal from the trench. This backfill removal, in turn, increases pipeline deformation and the likelihood of failure. This highlights the importance of considering these factors for safe and cost-effective Arctic pipeline design.

3.2 Numerical Modelling Framework

3.2.1 Overview

The Coupled Eulerian-Lagrangian (CEL) method was first introduced by Noh (1963) as a solution to the limitations of the classic Lagrangian finite element method in analyzing large deformations. The CEL method simulates the interaction between fluid and solid phases in various engineering and environmental systems. It has also been used in various geomechanical problems involving large soil displacements, such as pile driving (Ko et al., 2016; Staubach et al., 2021), slope stability, and landslides (Chen et al., 2019; Chen et al., 2021), soil compaction (Nagula & Grabe, 2020), and ship-embankment collisions (Qiu et al., 2011). Currently, CEL is widely considered a powerful tool for evaluating the performance of pipelines in challenging environments and for developing design strategies to protect pipelines from ice gouging and other environmental hazards.

The study utilized the Coupled Eulerian-Lagrangian (CEL) method in Abaqus/Explicit software, which uses an explicit time integration approach (Simulia, 2019). In this method, the soil is modeled as the Eulerian material that can flow through fixed elements, causing the material boundaries and the Eulerian volume fraction (EVF) of the soil in the meshes to change over time. In the Eulerian approach, the fluid and solid phases are treated as continuous media, and the control

volume is divided into discrete grid cells. The EVF represents the fraction of each grid cell occupied by the solid phase; its range is between 0 and 1. Moreover, the CEL method enables simulation of the interaction between the soil, ice keel, and pipeline through a general contact based on a penalty contact approach, allowing for large mesh movements without any mesh distortion, contact issues, or instability.

3.2.2 Model Configuration

The Finite Element Model consists of four different parts. First, the Eulerian media was taken in two parts: soil medium and void (Figure 3-2). This study analyzed the dimensions of the Eulerian medium to reduce computational time and optimize the numerical model. The study considered soil subgouge displacements, the ice keel reaction forces, frontal mound, and side berm height to find the minimum distance required for steady-state ice keel movement. The steady-state condition refers to a situation where the reaction forces and frontal mound remain nearly constant as the ice keel moves. Also, the effect of boundaries on results was investigated. A void domain was implemented to accurately capture the formation of the frontal mound and side berms. The Eulerian media was meshed using Eulerian, three-dimensional, eight-node, reduced integration brick elements (EC3D8R).

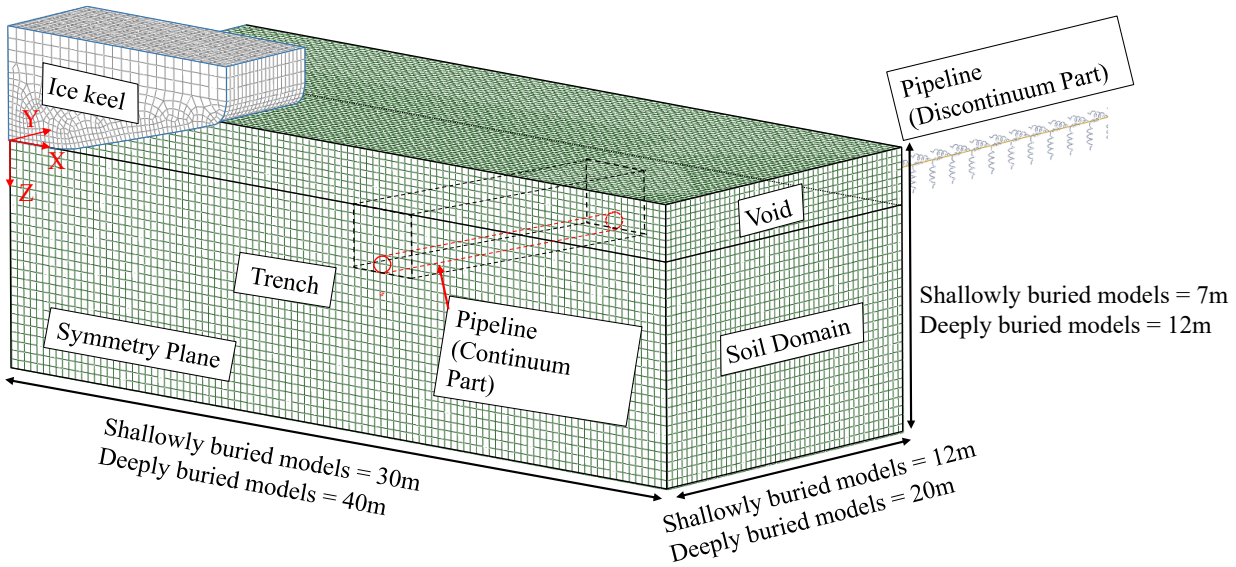

Figure 3-2. Finite element model scheme

This study modeled the ice keel as a rigid indenter using C3D8R elements (Figure 3-2). Previous research by (Blasco et al. 2011) has demonstrated that gouges retain a constant profile over a substantial distance. As a result, the ice keel was assumed to have a steady-state gouge condition and undergo rigid translation, ignoring any hydrostatic terms related to heave, pitch, and rotation.

In the current study, the pipeline was modeled as a two-part assembly, consisting of a continuum part represented by shell elements (S4R in Abaqus) and a discontinuum part (instigated using the Winkler-type method) represented by structural elements (PIPE31H in Abaqus). The continuum part of the pipeline was embedded within the Eulerian medium, and the length of the pipeline was equal to the width of the Eulerian medium. To fully capture the axial effect and reduce computational time, the pipeline was extended beyond the Eulerian environment and modeled as a structural model with a length of 5 km. A kinematic coupling constraint connected the continuum and structural parts. The discontinuum part of the pipeline was modeled by nonlinear spring

elements, SPRINGA, in Abaqus. The soil spring vertical and axial resistance curves were established according to the recommendations of PRCI (2009), while the soil spring lateral resistance curve was generated based on the equation provided by Phillips et al. (2004).

The study implemented a half-symmetrical approach to the model, incorporating half the length of the pipe and ice in this model (with the centerline of the gouge serving as the plane of symmetry). This approach assumes that the boundary conditions at the midsection of the pipe align with the symmetry conditions. Furthermore, the velocity of soil particles perpendicular to the external faces of the soil domain was constrained.

According to Pike and Kenny (2016), a four-step approach was adopted in the coupled analysis of ice-soil-pipeline interaction. The first step involves applying geostatic stress to the soil domain to account for the effect of gravity. In the second step, the ice keel was lowered to the desired gouge depth, and an internal pressure of 12MPa was applied to the shell elements of the pipeline, while an equivalent temperature change was applied to the structural elements due to limitations in the internal software (The internal pressure's impact is not transported to the structural elements through the kinematic coupling constraint.). In the third step, the temperature of both the structural and continuum parts of the pipeline is raised by 50°C. Finally, in the fourth step, the ice keel is moved horizontally over a large displacement domain using a velocity boundary condition, with tracer particles used to monitor subgouge displacements.

3.2.3 Soil Properties and Ice-Soil-Pipeline Interface Behavior

This study modeled the seabed soil as an elastic–perfectly plastic clay obeying the Tresca criterion in a total stress analysis (TSA). Since the ice gouge events are rapid, it can be assumed to be an

undrained loading case; thus, the change in soil volume can be neglected. For this purpose, the soil Poisson's ratio was set at 0.499 (Pike & Kenny, 2016).

The ice keel–soil and pipe–soil interfaces were defined using a Coulomb friction model with friction coefficients of 0.3 and 1.0, respectively. The surface polarity option has been used for the pipe-soil interface (outer pipe surface). There is no relative motion when the equivalent frictional stress on the interface is less than the pre-defined critical stress, which is proportional to the contact pressure. The shear stress limit in these simulations was set to half of the peak undrained shear strength.

3.2.4 Strain Softening and Shear Rate Effects

In soil mechanics, it has been recognized that the conventional Mohr-Coulomb constitutive model is inadequate in simulating the influence of strain rate and soil softening. Research has shown that an increase in strain rate beyond a certain threshold can increase soil resistance by as much as 20%. Given the high-velocity nature of ice gouging and the significant soil displacements that occur, it is crucial to consider the effect of strain rate and soil softening (Hashemi & Shiri, 2022). The consideration of strain rate dependency and strain softening effects were incorporated into the numerical model through the implementation of an empirical equation proposed by Einav and Randolph (2005) into a VUSDFLD user subroutine (equation (3-1)).

$$s_u = \left[1 + \mu \times \log_{10}\left(\frac{\max(|\dot{\gamma_{max}}|,\dot{\gamma_{ref}})}{\dot{\gamma_{ref}}}\right)\right] \times \left[\delta_{rem} + (1-\delta_{rem})e^{-3\xi/\xi_{95}}\right] s_{ui} \qquad (3\text{-}1)$$

Equation (3-4) encompasses the effect of strain-rate dependency in its first portion, while the latter half encompasses the impact of strain-softening, in which μ is the increased rate of the shear strength per log cycle, $\dot{\gamma}_{ref}$ is the reference shear strain rate, δ_{rem} is the ratio of fully remolded to initial shear strength or the inverse of the sensitivity (S_t), ξ_{95} is the relative ductility of the soil or

the value of accumulated absolute plastic shear strain resulting in a 95% reduction in the remolded shear strength, and s_{ui} is the in-situ undrained shear strength at the reference shear strain rate. The parameters relevant to strain rate and strain softening, as selected from the study conducted by Hashemi and Shiri (2022), are listed in Table 3-1.

Table 3-1. Strain softening and shear rate effects parameters for an ice gouging event

Parameters	Value
Rate of shear strength increase, μ	0.1
Reference shear strain rate, $\dot{\gamma_{ref}}$	0.024 s^{-1}
The ratio of fully remolded to initial shear strength for native soil, δ_{rem}	0.77
Accumulated absolute plastic shear strain for 95% reduction in strength due to remolding, $\xi 95$	12

Previous studies such as Dayal & Allen (1975), Graham et al. (1983), and Biscontin & Pestana (2001) recommended the range of 0.05 to 0.2 for μ; therefore, the value of μ was chosen as 0.1. As Raie & Tassoulas (2009) suggested, reference shear strain rate ($\dot{\gamma_{ref}}$) was taken as 0.024. The value of ξ95 for typical soft marine clays was established as 12, falling within the range of 10 to 25, as Randolph (2004) suggested for soils with varying degrees of softening, from rapidly softening to gradually softening. Soil sensitivity of native soil was taken as 1.3, while that of the backfill material was unity. The calculation of δ_{rem} considers the soil sensitivity, which is assumed to be 1.3 for the native soil and unity for the backfill material.

3.3 Calibration of Numerical Model

Because the physical experimental study of a flexible buried pipeline in clayey soils under the impact of ice gouging has not been published, the free-field test (Test 05 in Lach, 1996), the PRISE empirical equation (Phillips et al., 2005), and the numerical model developed by (Pike & Kenny, 2016) that considers the interactions between ice, soil, and pipeline were selected for validation.

Test 05 from Lach's (1996) series of nine centrifuge model tests was selected, with a prototype ice keel gouge depth of 1.21m. The soil properties used were based on Lach's (1996) study and the undrained shear strength (s_u) and overconsolidation ratio (OCR) profiles were reported. Pike & Kenny (2016) provided a method for obtaining the varying elastic modulus with depth, and the variation in undrained shear strength and elastic modulus with depth is shown in Figure 3-3.

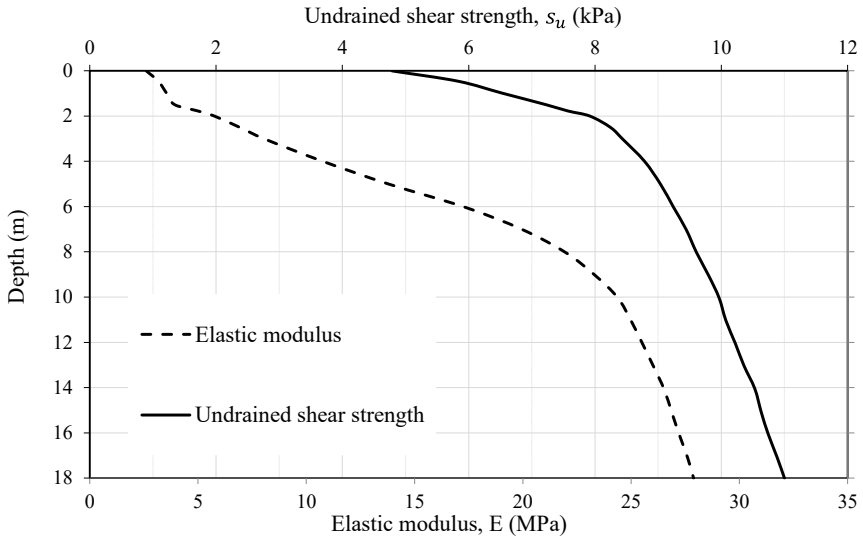

Figure 3-3. In-situ undrained shear strength (s_u) and Elastic modulus profiles extracted from the (Lach, 1996; Pike & Kenny, 2012)

The temperature was used as a dummy variable to define the linear temperature variation with depth in the Abaqus/CAE simulation. Further information on the modeling procedures, including

material properties and boundary conditions, can be found in Pike and Kenny (2016) and Hashemi and Shiri (2022).

3.3.1 Mesh Sensitivity Analysis

Three mesh densities with varying fineness were evaluated - fine (0.25m), medium (0.5m), and coarse (1.0m). Figure 3-4 compares the results from the mesh sensitivity analysis, in terms of the horizontal and vertical keel reaction forces, with the subgouge soil deformation.

Table 3-2 outlines the computational runtime and mesh density. Sensitivity analysis results, as depicted in Figure 3-4(a), demonstrate that the coarse mesh generates more horizontal soil displacement within the subgouge area, whereas the medium and fine meshes provide more converging predictions of horizontal soil displacement. Furthermore, the comparison of keel reaction forces after reaching steady-state conditions, as illustrated in Figure 3-4(b), shows that the coarse mesh generates a significant amount of noise, with predictions higher than those of the medium and fine mesh cases.

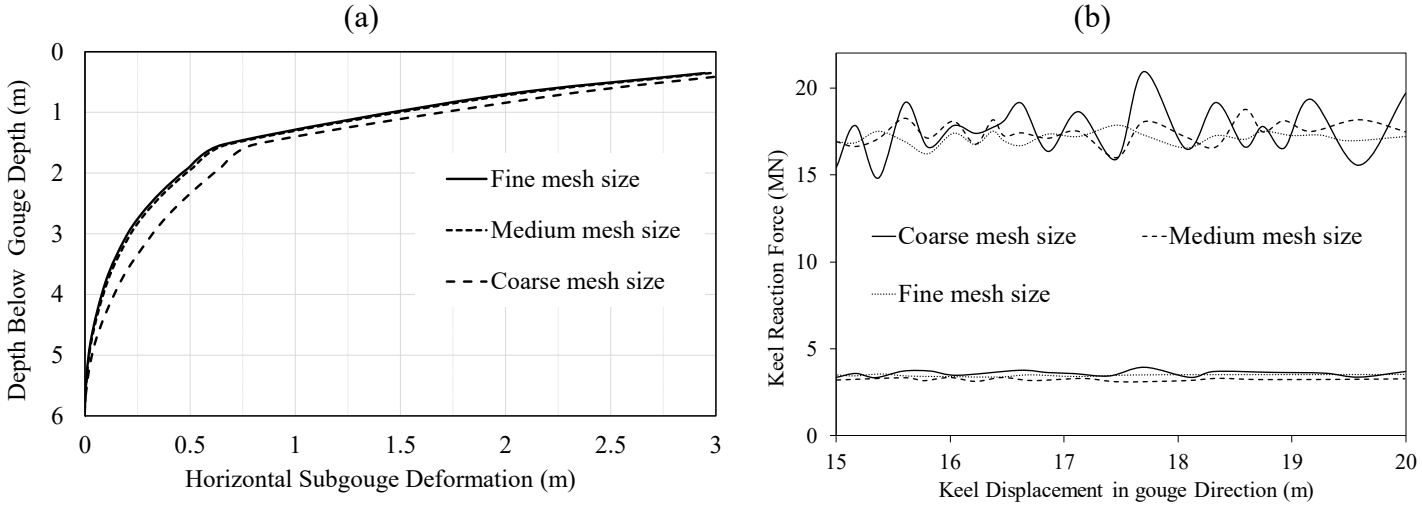

Figure 3-4. Mesh sensitivity analysis results: a) Soil subgouge displacements, b) Ice keel reaction forces

Table 3-2. Mesh sensitivity analysis for simulations of free-field ice gouging

Case	Min. element size (m)	Max. element size (m)	Number of Eulerian elements	Runtime on 76 CPUs
Course Mesh size	1.0	1.0	24,266	2 h 35 min
Medium Mesh size	0.5	1.0	108,192	5 h 45 min
Fine Mesh size	0.25	1.0	331,520	21 h 15 min

A good correlation exists between the predictions of medium and fine mesh cases. Therefore, a medium mesh size was selected for the comprehensive parametric study to balance computational efficiency and solution accuracy.

3.3.2 Validation of the Numerical Model

Figure 3-5 compares horizontal soil subgouge displacement results from the current study, considering and not considering strain rate and strain-softening effects, alongside centrifuge data (Lach 1996) and the PRISE equation (Phillips et al., 2005). The results from the current study, incorporating strain rate and strain-softening effects, demonstrate more realistic horizontal subgouge displacements in contrast to utilizing conventional Mohr-Coulomb and similar studies. Figure 3-5 illustrates a notable inconsistency near the gouge depth without considering these effects, previously observed in studies neglecting them (e.g. (Abdalla et al., 2009)). Moreover, the discrepancy observed in Figure 3-5, where the PRISE equation predicts a 28% greater maximum horizontal subgouge deformation compared to the coupled numerical model incorporating strain softening and shear rate effects, underscores the potential overestimation of structural demands associated with conventional beam-spring approaches. The findings from the horizontal subgouge displacement analysis underscore the significance of accounting for strain softening and strain rate effects in ice gouging analyses.

Table 3-3 also provides the values of the ice keel reaction forces after reaching a steady state, both in the current model and the results from Lach (1996). This free-field validation study highlights the efficacy of the CEL model in predicting horizontal soil subgouge displacement and ice keel reaction forces in ice gouging scenarios.

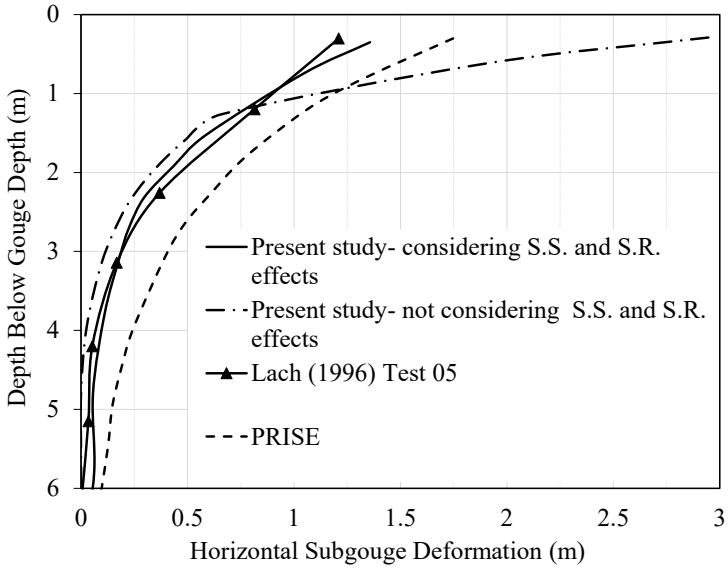

Figure 3-5. The comparison of the soil horizontal subgouge deformations

Table 3-3. The comparison of the vertical and horizontal ice keel-seabed reaction forces

Model	Horizontal ice keel reaction force (MN)	Vertical ice keel reaction force (MN)
Lach (1996) (Centrifuge test)	5.00	16.90
Present Study (CEL model)	4.95	15.50

Pike and Kenny (2016) employed a developed numerical modeling technique to evaluate the efficacy of decoupled structural and coupled continuum models. The coupled continuum case study was performed using the Total Stress Analysis (TSA) method under undrained conditions. The cohesive soil had an elastic modulus of 10 MPa, undrained shear strength of 50 kPa, and a total unit weight of 19kN/m^3, and the chosen parameters align with those presented in the study

by Peek and Nobahar (2012), except the cover depth for the pipeline, which was 0.457 meters. An internal pressure of 12 MPa is imposed on the pipeline, and the temperature of the pipeline is elevated by 50°C to replicate its operating conditions. Additional information on the fully coupled continuum modeling processes (such as contact properties, boundary conditions, and soil springs characteristics) is covered in section 3.2.2.

The maximum pipeline displacement (referred to as "Max.") occurs when the ice keel crosses it, and the term "Rebound" characterizes the elastic unloading state after the ice keel has passed the centreline of the pipe. Figure 3-6 provides a demonstration of substantial agreement between the results of the current study and those presented in Pike and Kenny (2016) regarding pipeline displacements along the pipeline axis in the (a) horizontal (gouge motion), (b) transverse lateral, and (c) transverse vertical directions.

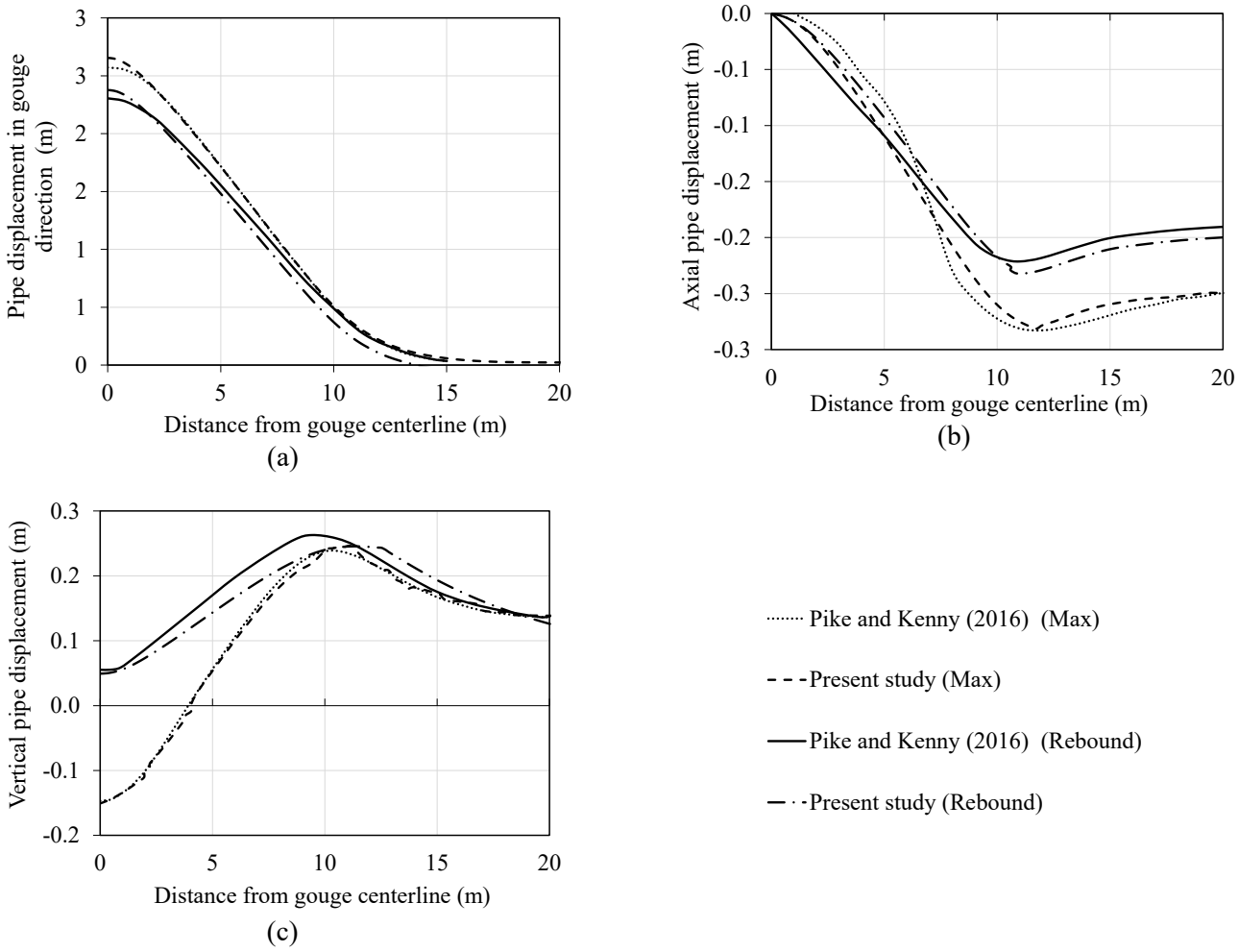

Figure 3-6. Comparison of pipeline displacements along the pipeline axis in the (a) horizontal (gouge movement), (b) transverse lateral (axial), and (c) vertical directions

Additionally, Figure 3-7 compares pipeline logarithmic axial strain trailing and leading edges of the pipeline.

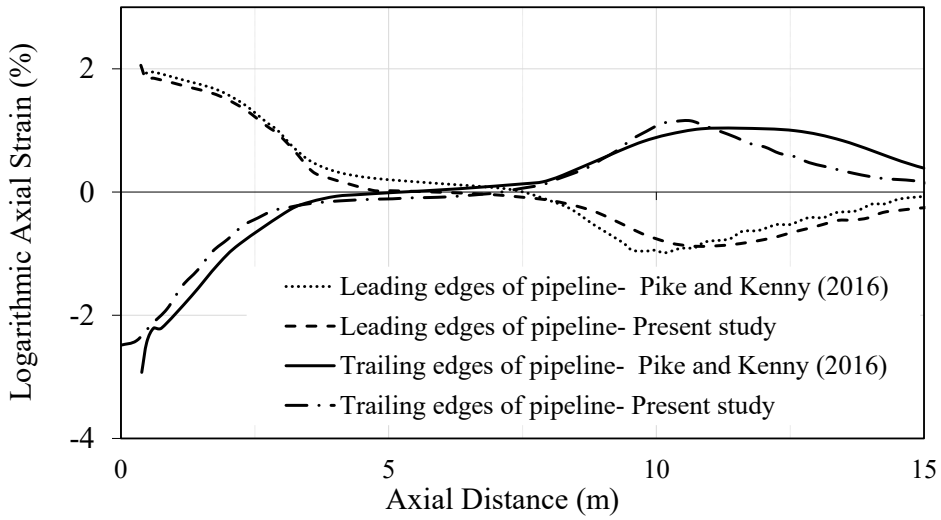

Figure 3-7. Comparison of pipeline axial strain along the pipeline axis

The results of the calibration studies verify the validity of the model employed in the current study for the pipeline responses.

3.4 Criteria for Determining the Failure of Submarine Buried Pipelines

The design of buried pipelines under significant ground deformation must satisfy three criteria as outlined in existing literature and design codes, covering different modes of deformation:

a) *Tensile yielding:* The DNVGL-ST-F101 (DNV, 2017) standard specifies that when designing buried steel gas pipelines, the maximum axial tensile strain allowed in the pipeline during significant soil deformation should not exceed 2.00%.

b) *Local buckling:* Pipeline buckling is defined as a pipeline's lateral or radial deformation resulting from compressive loading. This can occur when the pipeline is subjected to external loads, such as ice gouging or soil pressure, that violate the criteria specified in the design codes, such as CSA Z662-15 (2007). According to CSA Z662-15 (2007), the maximum compressive strain (ε_{max}) must be below the critical compressive strain value (ε_c^{crit}), which is calculated using the equations (3-2) and (3-3).

$$\varepsilon_c^{crit} = 0.5\frac{t}{D} - 0.0025 + 3000\left(\frac{(p_i - p_e)D}{2Et}\right)^2 \quad \text{for } \frac{(p_i - p_e)D}{2tf_y} < 0.4 \tag{3-2}$$

$$\varepsilon_c^{crit} = 0.5\frac{t}{D} - 0.0025 + 3000\left(\frac{0.4f_y}{E}\right)^2 \quad \text{for } \frac{(p_i - p_e)D}{2tf_y} \geq 0.4 \tag{3-3}$$

where p_i and p_e are the maximum internal and external pressure, f_y is the effective specified yield strength, E is Young's modulus of elasticity, D is the pipeline diameter, and t is the pipeline wall thickness.

c) *Local collapse:* Ovalization is another type of failure that can result from ice gouging, which refers to the geometric change in the shape of a pipeline from its original circular cross-section to an elliptical or oblong shape. DNV (2017) defined the ovalization parameter as equation (3-4) (see Figure 3-8). The level of acceptable ovalization is specified as 3% by the submarine pipeline standard (DNV (2017)) standard.

$$f_0 = \frac{D_{max} - D_{min}}{D} \leq 0.03 \tag{3-4}$$

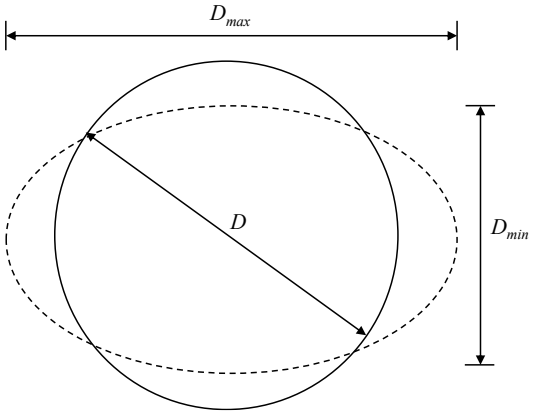

Figure 3-8. Definition of ovalization in a deformed pipeline

Drawing on these three established failure criteria, this section has provided a framework for evaluating pipeline performance under the studied cases of ice gouging.

3.5 Numerical Analysis of Trenched-Backfilled Pipeline

The Coupled Element Method (CEL) was utilized to model two different burial depths of a pipeline (as reported by Paulin (1998)) under ice gouge loading. The simulations were conducted once with a uniform seabed and once with a trenched, backfilled seabed. The numerical analysis incorporated the pipeline parameters, trench geometries, and soil properties obtained from centrifuge tests (T1P1 and T2P1) (Paulin, 1998). The silty clay used in these tests was a mixture of Speswhite kaolin clay (50%) and Sil-Co-Sil silt (50%), pre-consolidated to 400 kPa to achieve a target undrained shear strength of approximately 40 kPa. The backfill soil, composed of the same material but with a different stress history, exhibited an undrained shear strength of about 3.3 to 3.5 kPa. The undrained shear strength was measured using standard laboratory procedures, such as consolidated undrained (CU) and consolidated drained (CD) triaxial tests, on undisturbed soil samples retrieved from the centrifuge model. The cover depths in the various models are consistent; thus, the gouge depths have been altered and selected per the pipeline burial depths reported in previous literature (Lach, 1996; Pike and Kenny, 2016). The shallowly buried pipeline was represented by T1P1 (Case 1), while the deeply buried pipeline was depicted by T2P1 (Case 3). The pipe material properties were consistent with those presented in the study by Peek and Nobahar (2012).

To attain the targeted undrained shear strength of approximately 40 kPa, the silty clay used in the experiments underwent pre-consolidation to 400 kPa through a combination of 50% Speswhite kaolin clay and 50% Sil-Co-Sil silt. The backfill soil was made of the same material as the native soil but with a different stress history, yielding an undrained shear strength of approximately 3.3 to 3.5 kPa. The relevant parameters are listed in Table 3-4, with Cases 1 to 2 representing T1P1 and Cases 3 to 4 representing T2P1. A summary of the constant parameters is provided in Table

3-5. The dimensions of the Eulerian medium for the shallowly buried models were 30 meters in length, 7 meters in depth, and 12 meters in width; for the deeply buried cases, these values were 40, 12, and 20 meters, respectively.

Table 3-4. Parameters of interest in the present study plan.

Study Cases	Gouge Depth (m)	$S_{u\,(n)}$ (kPa)	$S_{u\,(b)}$ (kPa)	Trench Depth (m)	Trench base width (m)	Trench wall angle (degree)	Description
Case 1	0.45	36.2	3.3	1.75	2.5	90	Shallow / backfilled
Case 2	0.45	36.2	N.A	1.75	N.A	N.A	Shallow / uniform
Case 3	2.85	41.2	3.5	4.20	2.5	90	Deep / backfilled
Case 4	2.85	41.2	N.A	4.20	N.A	N.A	Deep / uniform

Table 3-5. Constant Parameters in all case scenarios

Parts		Parameter	Value
Ice keel		Attack angle (degree)	15.0
		Ice keel Width (m) (half model)	4.0
		Ice keel base length (m)	2.5
Pipe Specifications		Pipe Diameter (m)	0.950
		Pipe wall thickness (mm)	12.7
Soil properties	Native soil	Density (kg/m^3)	1950.0
		Young's modulus (kPa)	16480
	Backfill soil	Density (kg/m^3)	1875.0
		Young's modulus (kPa)	1400.0
Steel properties		Density (kg/m^3)	7800
		Young's Modulus (GPa)	205
		Poisson ratio	0.3
		Expansion Coefficient	1.10e-05

In all the cases, the magnitude of the horizontal and vertical ice keel reaction forces, the displacement of soil tracer particles, and the pipeline displacement and strains were analyzed and compared.

3.6 Results and Discussions

3.6.1 Soil Failure Mechanisms

Examining the soil movement mechanisms in Case 1 and Case 2 shows a significant difference. Figure 3-9 depicts the evolution of seabed plastic strain and the position of the soil tracer particles at different stages of ice gouging in Case 2 (shallow burial depth in uniform seabed). The soil failure mechanism in uniform soil media includes the frontal mound and side berms that have reached a steady state before reaching the pipe and the subgouge displacement. As the ice keel approaches the pipe, the frontal mound is distorted since the pipe prevents the free soil subgouge displacement. The pipe reduces soil subgouge displacement around the pipe compared to areas further away. Finally, the frontal mound and side berms return to the steady-state condition after the ice keel passes over the pipe.

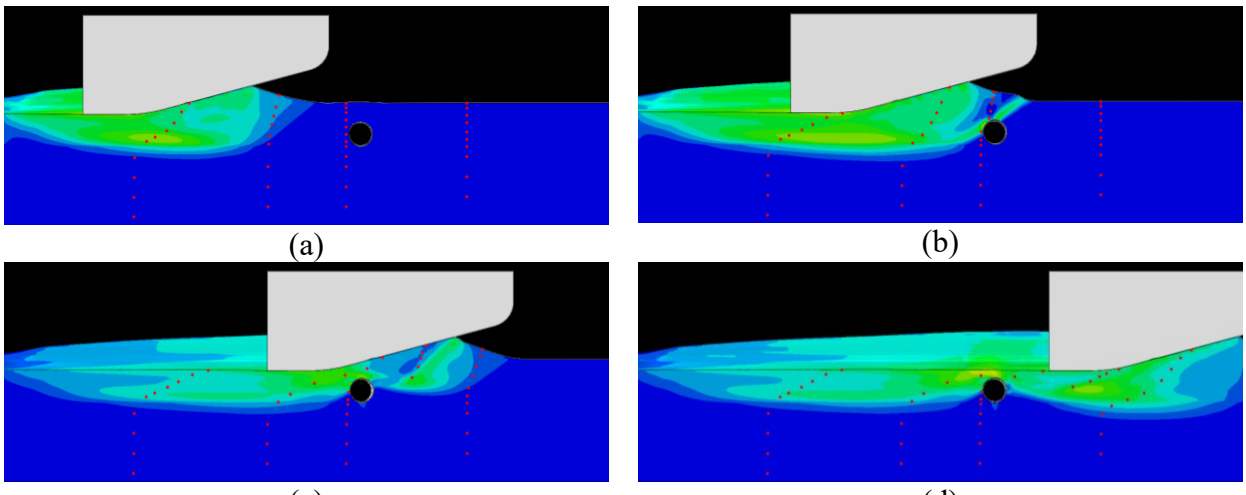

Figure 3-9. Plastic strain contours in the model while the ice keel moves through the uniform seabed soil toward the pipe

However, in the case of the trenched/backfilled pipeline, the seabed soil failure mechanisms get more complicated. Figure 3-10 depicts the interaction of backfill-trench wall effect on the failure mechanism of the seabed in the shallowly buried pipeline configuration. As the ice keel advances, it induces stresses and strains on the seabed soil in various directions, including horizontal subgouge displacements along the gouging path (see the red dots in Figure 3-10 (a)). These stresses, by proximity to the pipeline, cause the native soil to exert pressure upon the trench wall (Figure 3-10 (b)). The backfill's reduced shear strength allows it to be displaced upward under this pressure from both the trench walls and the native soil. Consequently, the front trench wall deforms towards the pipeline, applying additional pressure, while soft backfill can be observed on the pipeline's right side (Figure 3-10 (c)). In the ice gouge symmetry plane, the gradual removal of backfill from the trench allows native soil to replace it. The pipeline's lower half partially obstructs escaping backfill, resulting in some retention within the trench (Figure 3-10 (d)).

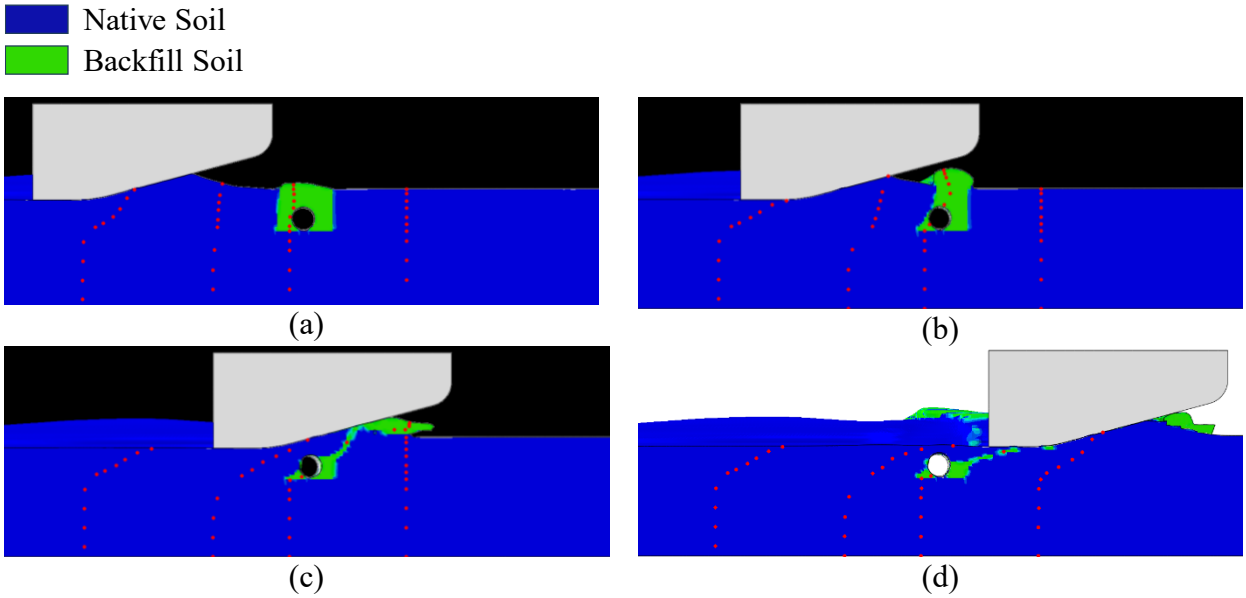

Figure 3-10. Pipe-backfill-trench wall interaction effect in ice gouging (shallowly buried pipe)

Figures 3-11 present backfill removal patterns during ice gouging, providing a back view (half-model). The red dotted line represents the subgouge soil deformation at the front side of the pipeline. This figure shows that beyond the gouge centerline, the removal of backfill soil from the trench decreases and weakens the formation mechanism, with over 90% of the backfill remaining undisturbed after a distance of the ice keel width. Notably, the backfill behind the ice keel remains undisturbed after 1.5 times the width (W) of the ice keel.

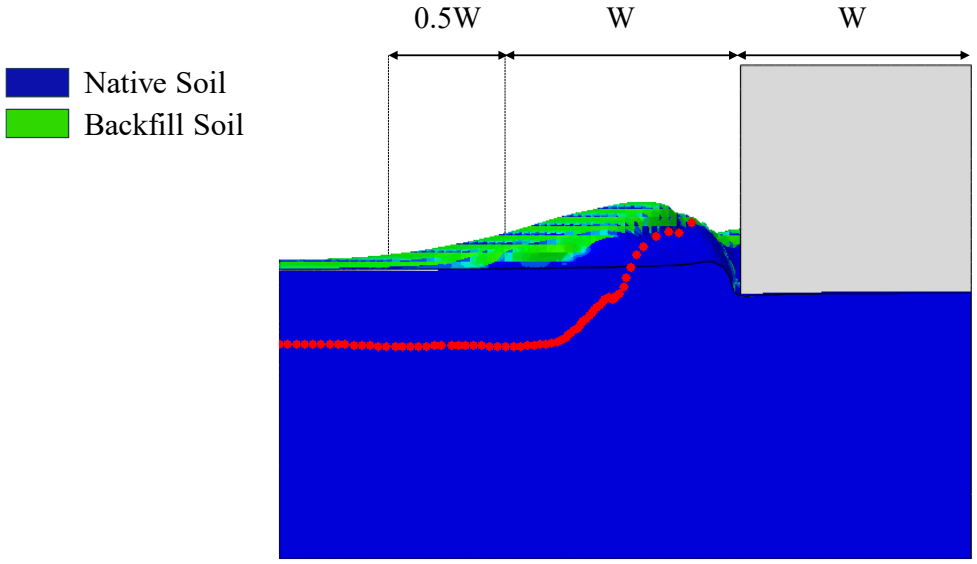

Figure 3-11. A back view of the ice keel after it passes through the trench (half-model)

Finally, the removed part of the backfill is spread on the seabed surface mixed with the frontal mound and side berms (see Figure 3-12). The green zone signifies regions where the Eulerian Volume Fraction (EVF) of the backfill is equal to 1, indicating complete filling. However, in some surface elements, the backfill might not completely occupy the element volume, resulting in an EVF less than 1. The blue lines determine these partially filled elements within the green zone.

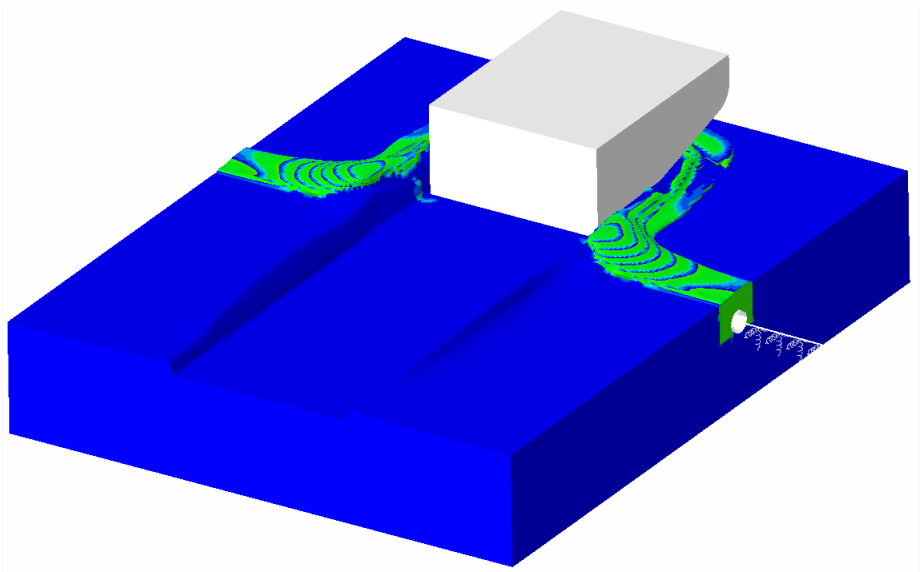

Figure 3-12. The state of the seabed after the ice keel passes through the trench (Full model)

This same pattern is observed when analyzing the deeply buried pipeline case. Figure 3-13 illustrates the influence of the pipeline-backfill-trench wall interaction on seabed behavior during ice gouging in the deeply buried pipeline scenario.

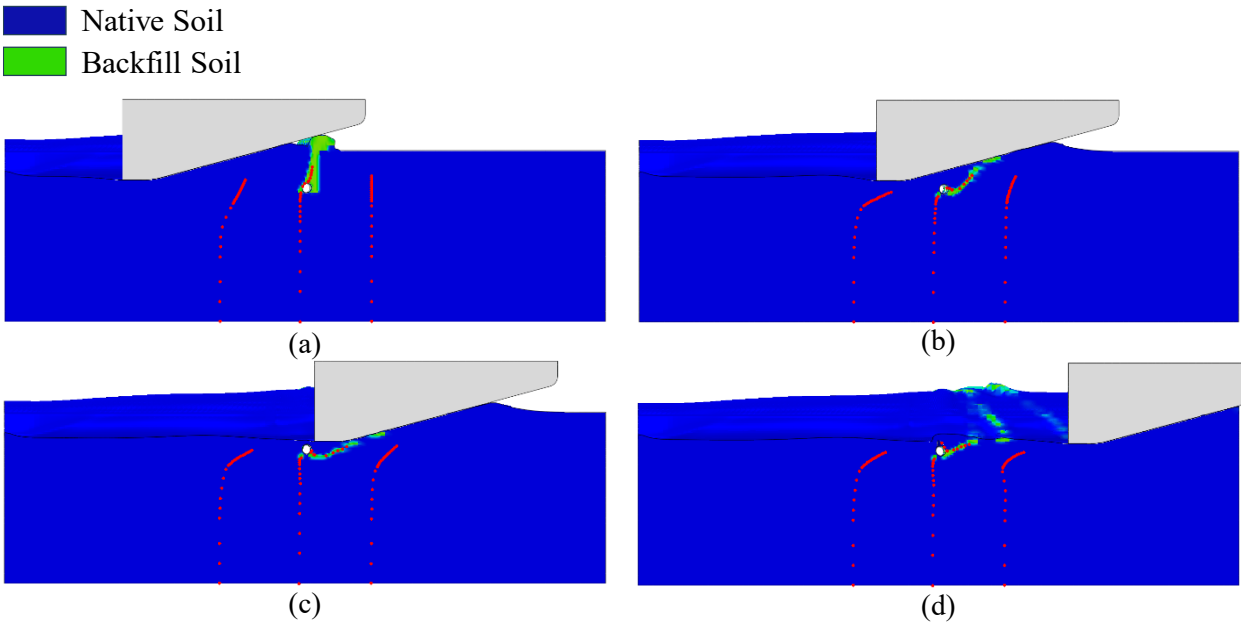

Figure 3-13. Pipe-backfill-trench wall interaction effect in ice gouging (deeply buried pipe)

The interaction of pipeline-backfill-trench wall influences seabed behavior during ice gouging, potentially leading to backfill removal and exerting pressure on the pipeline from the left trench wall.

3.6.2 Ice Keel Reaction Forces

Figure 3-14 shows the horizontal and vertical reaction forces obtained from the case studies. The investigation reveals that the ice keel reaction forces of the trenched model do not significantly differ from those of the untrenched model. The relatively narrow width of the trench, when compared to the distance that the ice keel moves, could result in this convergence.

While the pair cases generally converge, a noticeable drop in both horizontal and vertical reaction forces occurs as the ice keel nears the trench. This drop is closer to the trench in shallow burial scenarios due to the smaller volume of backfill present. The drop initiation coincides with the onset of trench wall-backfill interaction and backfill removal, starting when the ice keel is approximately 7 meters from the trench. A similar drop occurs in deeper burial cases but at a greater distance (18 meters from the trench).

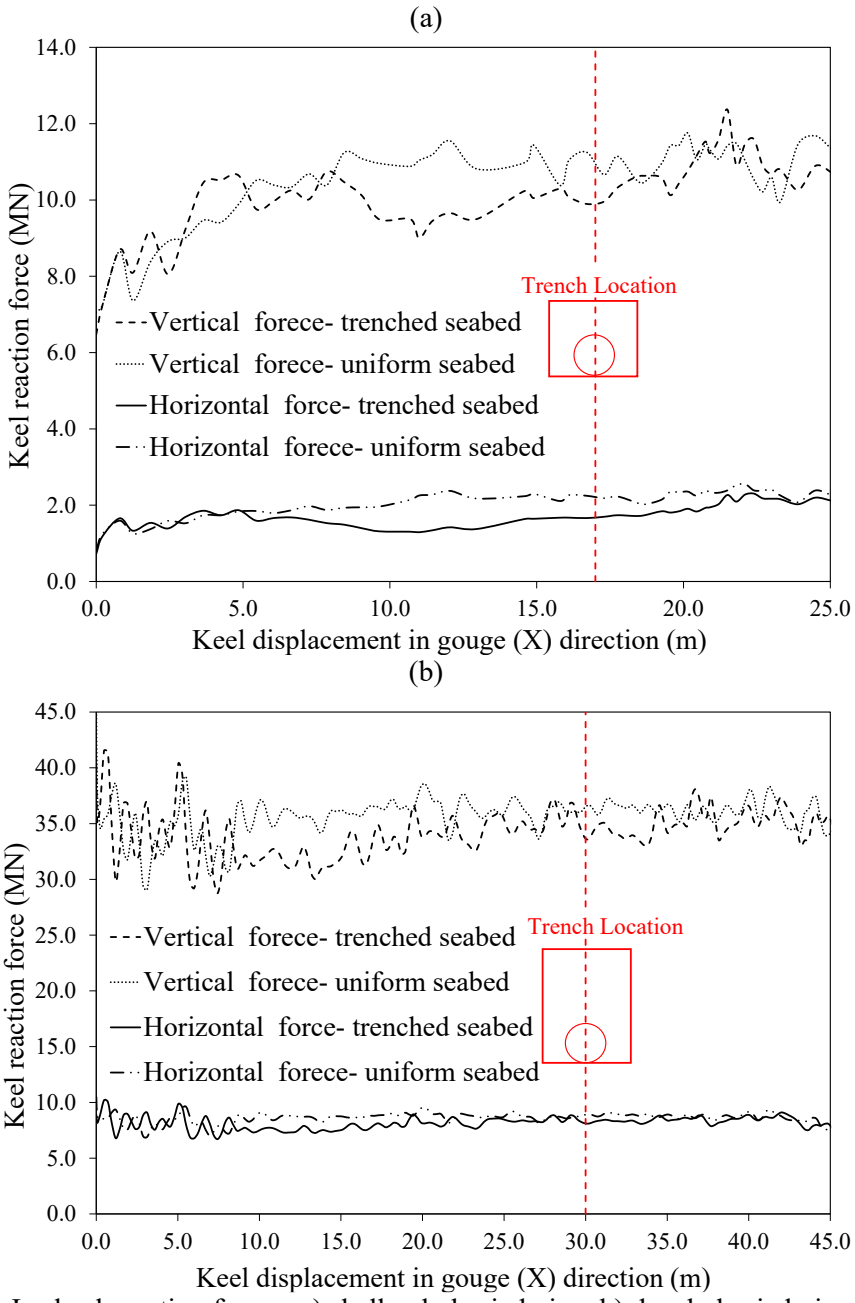

Figure 3-14. Ice keel reaction forces: a) shallowly buried pipe; b) deeply buried pipe (The trench dimensions shown in the graphs do not match the scale of the axes.)

In both configurations, the graphs rapidly converge after the ice keel crosses the trench.

3.6.3 Pipeline Behavior

Figure 3-15 compares the pipeline's trajectory in the vertical plane at the gouge centerline across the case studies. The pipe's horizontal and vertical movement in the mid-plane section exhibits a similar trend in all cases. When the ice keel approaches the pipe, the pipe initially deforms in an upward and gouge direction, and the pipe's maximum displacement (Max. state) occurs when the ice reaches the pipe's top. As the ice keel passes and moves away, some elastic displacement recovers, and the pipe remains stable in the rebound state.

The results demonstrate that the maximum horizontal displacement of the pipeline in backfilled cases is significantly greater than in uniform soil cases. The significant horizontal displacement observed in backfilled cases is attributed to the complex interaction between the pipeline, backfill, and trench walls. Specifically, the deflection of the front trench wall and subsequent removal of backfill exert lateral pressure on the pipeline. The low undrained shear strength and elastic modulus of the backfill soil further exacerbate this displacement.

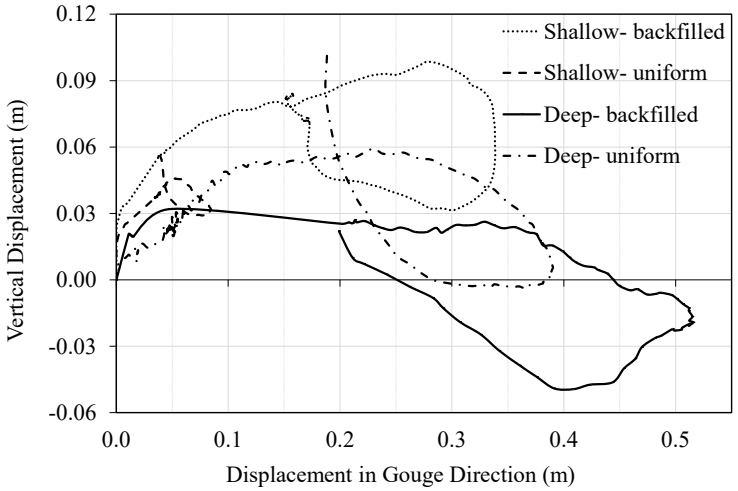

Figure 3-15. Pipe trajectory in the vertical plane at gouge centerline

Figures 3-16 and 3-17 visually present the pipe displacement across all four cases in the horizontal (gouge motion), axial, and vertical directions. The pipe displacement in all three directions,

including maximum and rebound states, is expected to be more significant in the trenched/backfilled models compared to the uniform seabed models. In Figures 3-16 and 3-17 (a) and (b), both the maximum and rebound horizontal displacements of the pipe in both shallow and deep configurations are notably higher in the backfilled cases than the uniform cases. This increased displacement arises due to the pressure from the trench wall, the removal of backfill material, and the backfill's reduced shear resistance. The maximum and rebound axial displacements exhibit a similar behavior. Given the axial symmetry, the axial displacement of the pipe aligns with the zero axis at zero distance.

In Figure 3-16 (c), the shallow pipe moves upward more because of the lighter overburden load, leading to less resistance against uplift. Consequently, in both the maximum and rebound states, the pipe reaches a higher position than its initial level. As a result, the vertical displacement of the shallow pipe is greater in the backfilled cases compared to the uniform cases, a significance evident in Figure 3-15 as well.

In the case of a deeply buried configuration, the scenario differs. The increased burial depth results in a downward vertical force from the ice keel to the soil more than three times that of the shallow cases. This greater force is transmitted to the pipe by soil particles, causing the pipe to experience a downward turning point during the maximum displacement state when the ice passes over the pipe. In the backfilling scenario, the lower elastic modulus allows these stresses to penetrate the pipe more, leading to its downward deflection. After the removal of the ice load, the pipe moves upwards. Comparing the maximum states, the pipe exhibits a greater downward movement in the backfill case. Additionally, substituting native seabed soil for backfill soil almost equals the uplift resistance of the soil. Consequently, in the uniform state, the pipe experiences more vertical displacement in the rebound state compared to the backfill state.

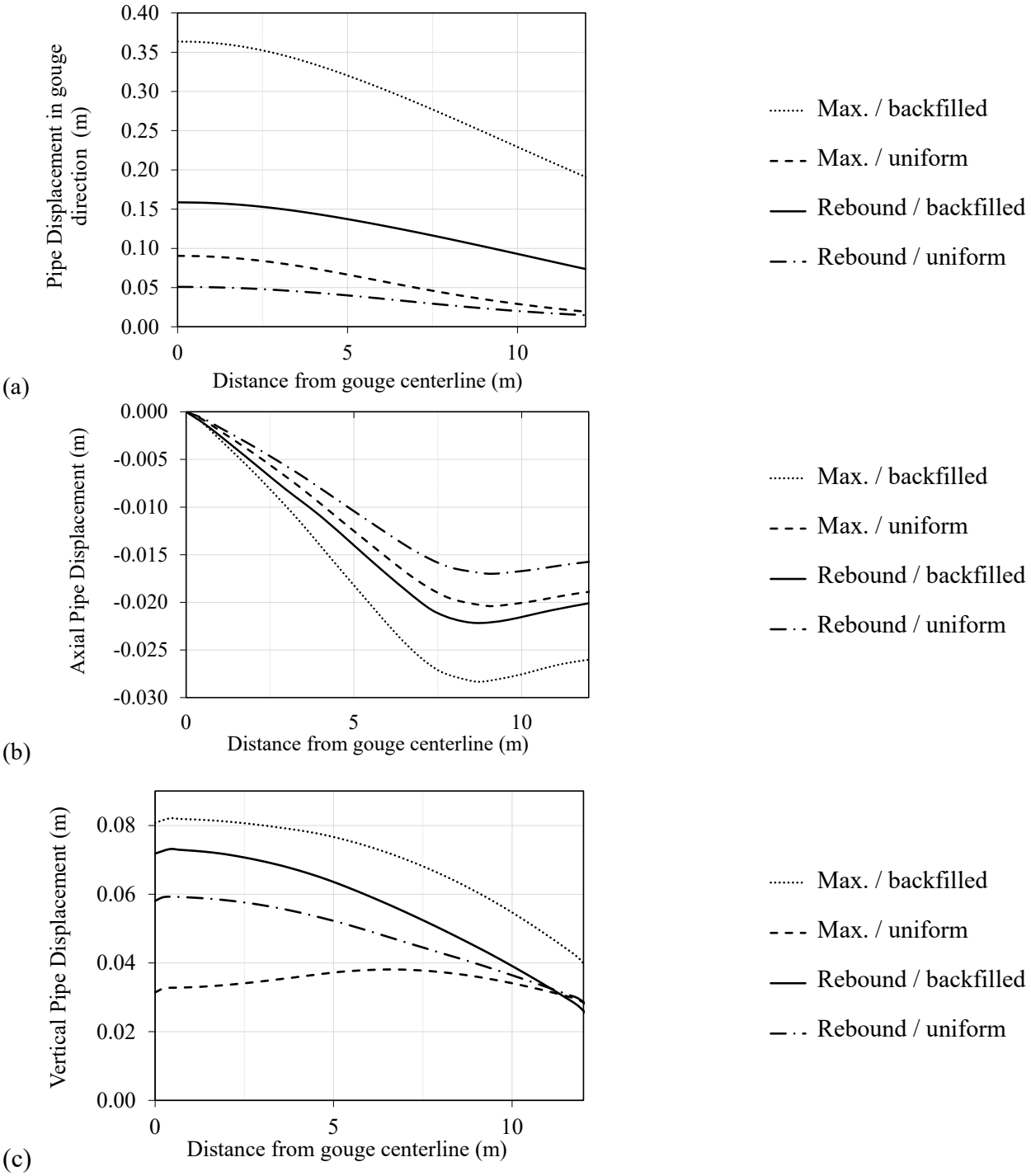

Figure 3-16. Pipe displacement along pipe axis in (a) horizontal (gouge motion), (b) axial, and (c) vertical directions (shallowly buried configurations)

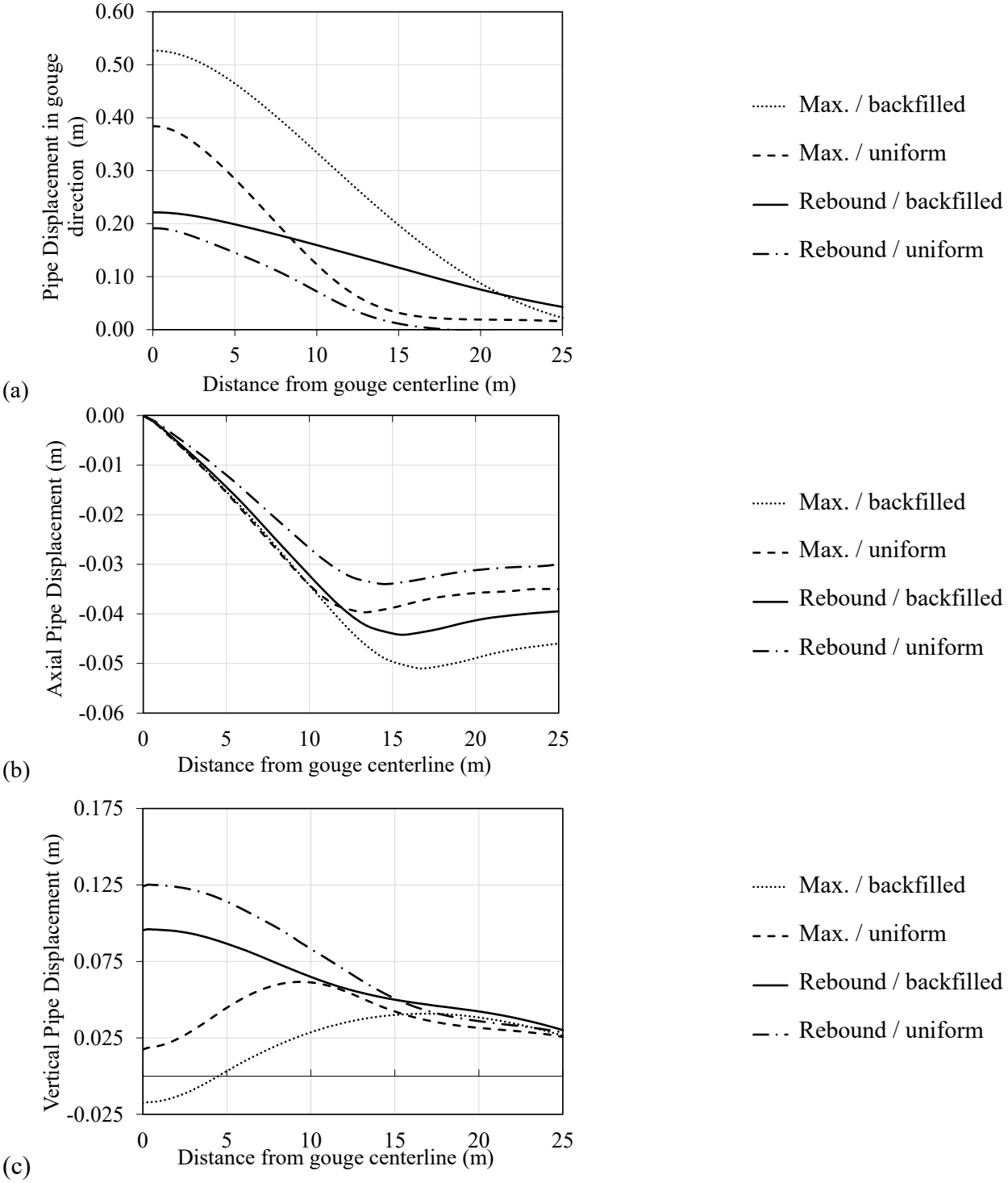

Figure 3-17. Pipe displacement along the pipe axis in (a) horizontal (gouge motion), (b) axial, and (c) vertical directions (deeply buried configurations)

Given the low axial resistance of the pipeline in very soft backfill soil, it is anticipated that the axial strain in the backfilled cases would be higher compared to uniform cases. Figures 3-18 and

3-19 illustrate the peak pipeline axial strains along the pipeline axis caused by ice gouging loading. Results show that the trailing pipe face is subjected to tension, while the leading pipe face is in compression in all cases. Although the backfilled cases display a similar trend to the uniform cases, they show higher values due to greater pipeline displacements. Comparison of the deeply buried pipeline cases with the shallowly buried ones revealed that the former had greater maximum axial strains than the latter, despite having the same cover depths. Furthermore, it was observed that the compressive axial strain approached the critical value (determined by the CSA Z662-15 (2007) equation) in Case 3 (deeply buried backfilled pipeline), potentially resulting in local buckling of the pipeline in the gouge centerline section.

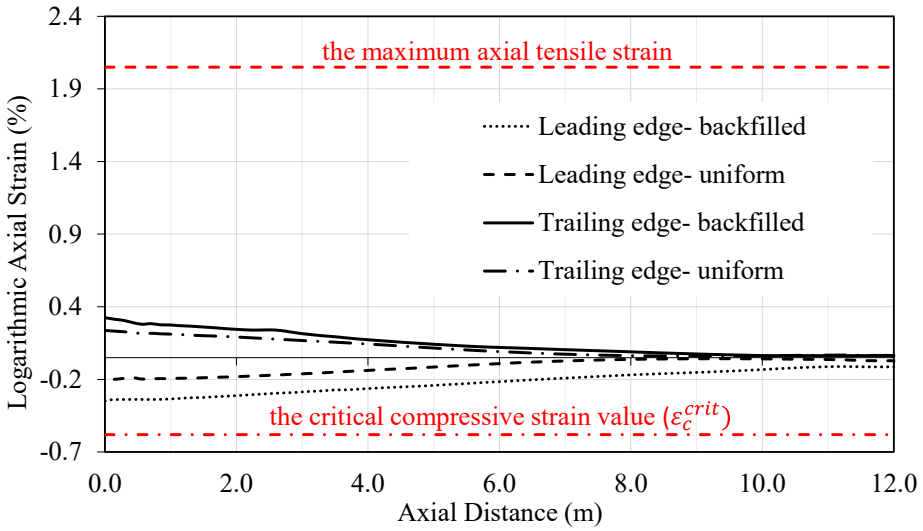

Figure 3-18. Logarithmic axial strain for the trailing and leading edges of the pipeline along the axis (shallowly buried configurations)

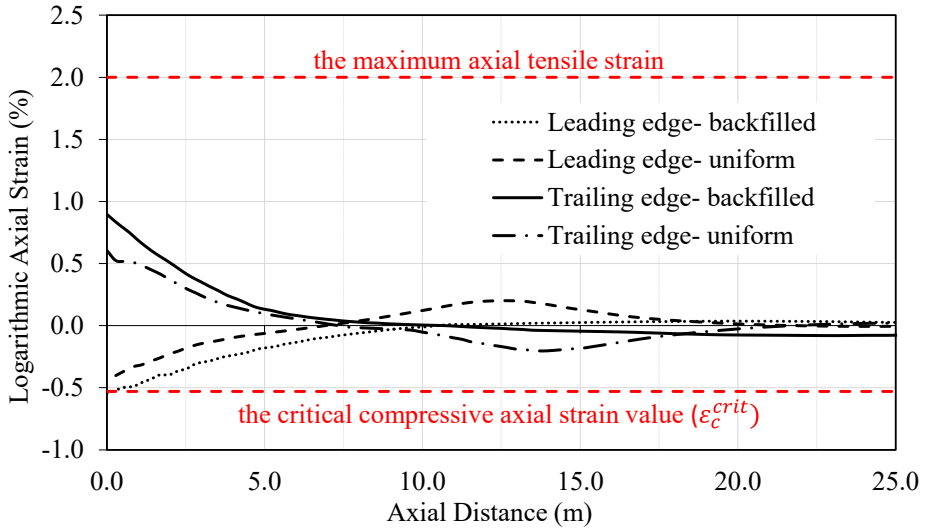

Figure 3-19. Logarithmic axial strain for the trailing and leading edges of the pipeline along the axis (deeply buried configurations)

This study examined pipeline ovalization under various scenarios. Ovalization is attributed to the combined effects of initial internal pressure and temperature, as well as the load exerted by the ice keel passage. Variations in strain magnitude and distribution around the pipeline circumference lead to uneven strain patterns and subsequent ovalization. These strain patterns are further influenced by the surrounding soil characteristics. Figure 3-20 reveals significantly greater ovalization in backfilled models compared to uniform soil cases.

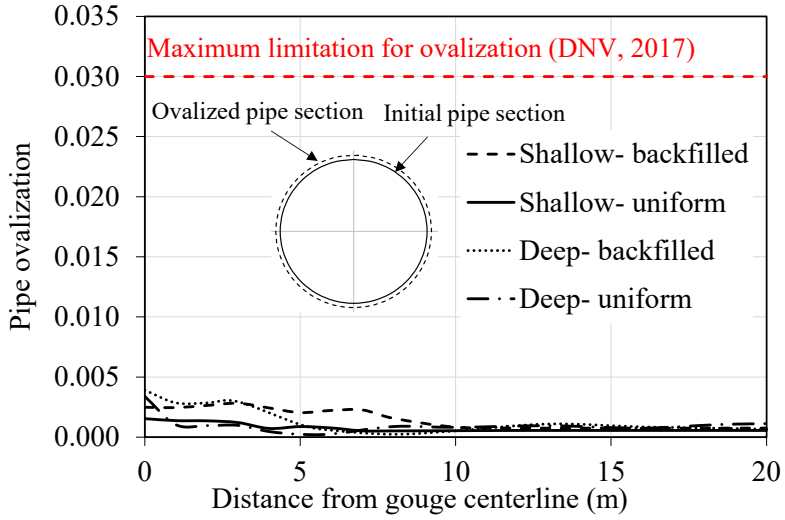

Figure 3-20. Pipeline ovalization along the pipe axis

In uniform soil scenarios, the pipeline is surrounded by consistent native soil with uniform properties. However, the pipeline-backfill-trench wall interaction and backfill removal in backfilled cases create a situation where different pipeline sections experience contact with soils of varying shear strengths and various stresses applied to the pipe from different directions. This disparity contributes to a more pronounced ovalization effect in backfilled pipelines. It is worth noting that the ovalization values obtained in all cases were significantly below the ovalization limit specified by DNV (2017), which is 0.030.

3.7 Conclusions

This study aimed to perform a comprehensive numerical investigation on the effects of pipeline-backfill-trench wall interaction on the pipeline structural response to ice gouging. The Einav and Randolph (2005) relationship was utilized to account for strain softening and shear rate in native and backfill clay soil. The numerical model results of trenched and backfilled pipelines were compared against uniform seabed models. The results indicate the crucial impact of the pipeline-trench-backfill interaction, the backfill's significantly lower elastic modulus and undrained shear strength, and the backfill removal mechanism in driving the observed divergence between outcomes. The key findings of this investigation are as follows:

- The presence of backfill material significantly modifies soil failure mechanisms during ice gouging events. The interaction between the backfill and trench walls results in the expulsion of softer backfill material from the trench due to the lateral pressure exerted by the stiffer trench walls. However, a substantial volume of backfill persists within the trench, extending up to 4 meters from the gouge centerline.

- The presence of backfill within the trench was observed to decrease ice keel/seabed reaction forces by approximately 15%. This reduction is initiated as the ice keel interacts with the backfill and trench walls, but the effect diminishes rapidly as the ice progresses beyond the trench.
- Backfilled scenarios exhibited doubled pipeline displacement due to the pipeline-backfill-trench wall interaction, backfill removal, and reduced backfill shear strength. The deflection of the front trench wall increases lateral pressure on the pipeline as the ice approaches.
- Backfilling increases the pipeline's susceptibility to axial, tensile, and compressive strains, as well as local buckling, due to the lower axial shear strength of the backfill.
- Backfilled pipelines experience increased ovalization compared to those in uniform soil. This is attributed to the pipeline-backfill-trench wall interaction and backfill removal mechanism. Uneven contact with soils of varying shear strengths leads to asymmetrical force distribution and greater ovalization.

These findings underscore the importance of explicitly considering the complex pipeline-backfill-trench wall interactions within ice gouging risk assessments. Neglecting these factors could lead to inaccurate pipeline response predictions and compromise pipeline safety in ice-prone environments.

Acknowledgments

The authors gratefully acknowledge the financial support of the “Wood” through establishing Research Chair program in Arctic and Harsh Environment Engineering at the Memorial University of Newfoundland, the “Natural Science and Engineering Research Council of Canada (NSERC)”

and the “Newfoundland Research and Development Corporation (RDC) (now IET) through “Collaborative Research and Developments Grants (CRD)”. Special thanks are extended to Memorial University for providing excellent resources for conducting this research program.

References

Abdalla, B., Jukes, P., Eltaher, A., & Duron, B. (2008). The technical challenges of designing oil and gas pipelines in the arctic. *OCEANS 2008*, 1–11.

Abdalla, B., Pike, K., Eltaher, A., Jukes, P., & Duron, B. (2009). Development and validation of a coupled Eulerian Lagrangian finite element ice scour model. *International Conference on Offshore Mechanics and Arctic Engineering*, *43451*, 87–95.

ALA. (2001). Guidelines for the design of buried steel pipe. *American Society of Civil Engineers*.

ASCE. (1984). *Guidelines for the Seismic Design of Oil and Gas Pipeline Systems*. Amer Society of Civil Engineers.

Aslkhalili, A., Shiri, H., & Zendehboudi, S. (2020). Probabilistic Assessment of Lateral Pipeline-Backfill-Trench Interaction. *Reliability Assessment of Drag Embedment Anchors and Laterally Loaded Buried Pipelines*, 96.

Banneyake, R., Hossain, M. K., Eltaher, A., Nguyen, T., & Jukes, P. (2011). Ice-soil-pipeline interactions using coupled eulerian-lagrangian (CEL) ice gouge simulations-extracts from ice pipe JIP. *OTC Arctic Technology Conference*.

Chen, Xiangyu, Zhang, L., Chen, L., Li, X., & Liu, D. (2019). Slope stability analysis based on the Coupled Eulerian-Lagrangian finite element method. *Bulletin of Engineering Geology and the Environment*, *78*(6), 4451–4463.

Chen, Xuejian, Li, D., Tang, X., & Liu, Y. (2021). A three-dimensional large-deformation random finite-element study of landslide runout considering spatially varying soil. *Landslides*, *18*(9), 3149–3162.

El-Gebaly, S., Paulin, M., Lanan, G., & Cooper, P. (2012). Ice gouge interaction with buried pipelines assessment using advanced coupled Eulerian Lagrangian. *OTC Arctic Technology Conference*.

Ko, J., Jeong, S., & Lee, J. K. (2016). Large deformation FE analysis of driven steel pipe piles with soil plugging. *Computers and Geotechnics*, *71*, 82–97.

Lach, P. R. (1996). *Centrifuge modelling of large soil deformation due to ice scour*. Memorial University of Newfoundland. https://research.library.mun.ca/1194/

Nagula, S. S., & Grabe, J. (2020). Coupled Eulerian Lagrangian based numerical modelling of vibro-compaction with model vibrator. *Computers and Geotechnics*, *123*, 103545.

Nematzadeh, A., & Shiri, H. (2020). The influence of non-linear stress-strain behavior of dense sand on seabed response to ice gouging. *Cold Regions Science and Technology*, *170*, 102929.

Noh, W. F. (1963). *CEL: A time-dependent, two-space-dimensional, coupled Eulerian-Lagrange code*. Lawrence Radiation Lab., Univ. of California, Livermore.

Paulin, M. J. (1992). *Physical model analysis of iceberg scour in dry and submerged sand*. Memorial University of Newfoundland.

Paulin, M. J. (1998). *An investigation into pipelines subjected to lateral soil loading*. Memorial University of Newfoundland.

Phillips, R, Barrett, J., & Al-Showaiter, A. (2010). Ice keel-seabed interaction: Numerical modeling validation. *Offshore Technology Conference*, *20696*.

Phillips, R, Clark, J. I., & Kenny, S. (2005). PRISE studies on gouge forces and subgouge deformations. *Proceedings of the International Conference on Port and Ocean Engineering Under Arctic Conditions*.

Phillips, Ryan, Nobahar, A., & Zhou, J. (2004). Trench effects on pipe-soil interaction. *International Pipeline Conference*, *41766*, 321–327.

Pike, K., & Kenny, S. (2016). Offshore pipelines and ice gouge geohazards: comparative performance assessment of decoupled structural and coupled continuum models. *Canadian Geotechnical Journal*, *53*(11), 1866–1881.

Pike, K. P. (2016). *Physical and numerical modelling of pipe/soil interaction events for large deformation geohazards*. Memorial University of Newfoundland.

PRCI. (2009). *Guidelines for Constructing Natural Gas and Liquid Hydrocarbon Pipelines through Areas Prone to Landslide and Subsidence Hazards*, *Pipeline Research Council International*.

Qiu, G., Henke, S., & Grabe, J. (2011). Application of a Coupled Eulerian–Lagrangian approach on geomechanical problems involving large deformations. *Computers and Geotechnics*, *38*(1), 30–39.

Schoonbeek, I. S. S., & Allersma, H. G. B. (2006). Centrifuge modelling of scouring ice keels in clay. *Proceedings, 8th International Conference on Physical Modelling in Geotechnics, ICPMG*, 1291–1296.

Simulia, D. S. (2019). *Abaqus 2019 documentation*. Dassault Systemes Waltham, MA.

Staubach, P., Machaček, J., Skowronek, J., & Wichtmann, T. (2021). Vibratory pile driving in water-saturated sand: Back-analysis of model tests using a hydro-mechanically coupled CEL method. *Soils and Foundations*, *61*(1), 144–159.

Tudorache, V.-P., & Antonescu, N.-N. (2020). Challenges of oil and gas exploration in the Arctic. *J. Eng. Sci. Innov*, *5*, 273–286.

CHAPTER 4

Effect of Backfilling Stiffness and Configuration on Seabed Failure Mechanisms and Pipeline Response to Ice Gouging

Alireza Ghorbanzadeh, Hodjat Shiri, Xiaoyu Dong

Civil Engineering Department, Faculty of Engineering and Applied Science, Memorial University of Newfoundland, A1B 3X5, St. John's, NL, Canada.

This chapter is under review as a journal manuscript.

Abstract

Ice gouging is a significant issue for offshore structures in cold environments. Pipelines in Arctic regions are buried in the seabed to prevent the direct contact of pipelines and the impacts of soil displacement from ice gouging. However, choosing the appropriate backfilling material and stiffness to maintain the pipeline's integrity while minimizing construction costs is a complex design consideration. It is crucial to model the interaction between the ice, backfill, trench wall, and pipeline accurately to assess the backfill functionality in a coupled ice gouging analysis. This study comprehensively investigated the effect of backfilling stiffness and configuration on seabed failure mechanisms and pipeline response during ice gouging events on a deeply buried pipeline. The study focused on six different backfill materials, including dense and loose sands and very soft clay to stiff clay. The Coupled Eulerian-Lagrangian (CEL) method was used to simulate the large seabed deformation due to the ice gouging process in a trenched/backfilled seabed in Abaqus/Explicit. Incorporation of the strain-rate dependency and strain-softening effects involved the development of a user-defined subroutine and incremental update of the undrained shear strength within the Abaqus software. Key findings reveal that both overly soft and excessively stiff backfill materials can negatively impact pipeline response during ice gouging. Very soft clay exhibits a distinct "removal" mechanism, leading to increased pipeline displacement, while overly stiff clay and dense sands also result in greater displacement due to efficient force transfer. The results can inform the selection of appropriate backfill materials and backfilling techniques to enhance pipeline protection against ice gouging.

Keywords: backfill stiffness; backfill type; ice gouging; pipeline response; seabed failure mechanisms

4.1 Introduction

Offshore pipelines play a crucial role in the transportation of hydrocarbons from offshore production platforms to onshore facilities. In cold regions such as Arctic regions, these pipelines are exposed to various natural hazards, including ice gouging (Nematzadeh & Shiri, 2020). Ice gouging occurs when huge ice features, such as icebergs, come into contact with the seabed and excavate the sediment, potentially damaging the pipeline.

Ice gouging can cause shear failure, where the forces exerted by the ice cause the soil to slide along a defined failure plane, forming side berms and frontal mounds on the seabed surface. Also, the force of the ice scouring the seabed causes significant deformation in the soil beneath (Hashemi & Shiri, 2022). The subgouge deformation of the soil around the pipeline can have significant implications for the stability of buried pipelines. Figures 4-1 and 4-2 depict the seabed and pipeline during an ice gouging event, with a schematic view (Figures 4-1) and a cross-section highlighting the resulting mechanisms (Figures 4-2).

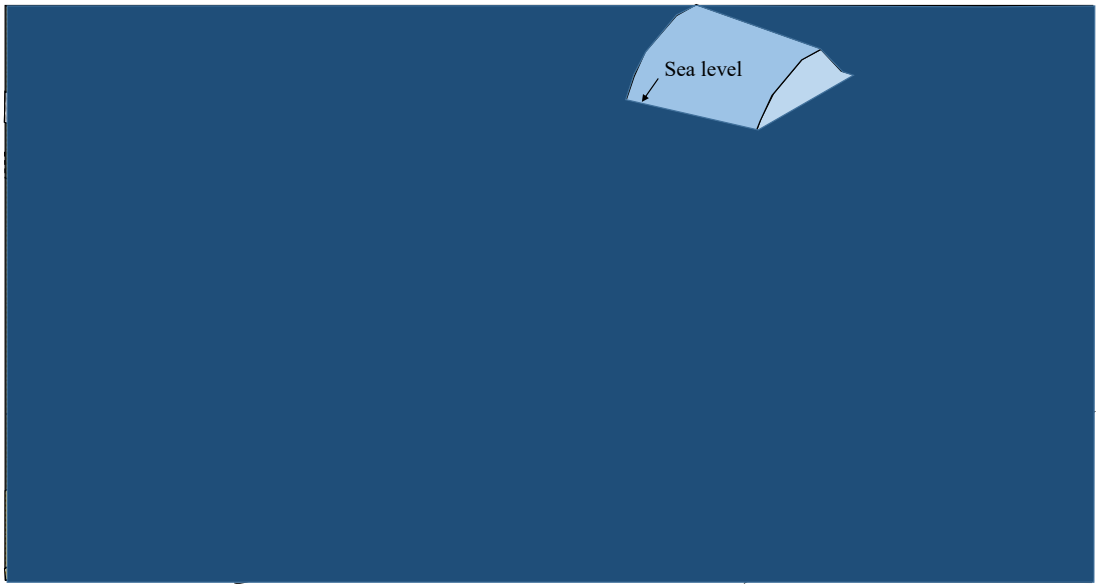

Figure 4-1. Illustration of ice gouging over a buried pipeline (not to scale)

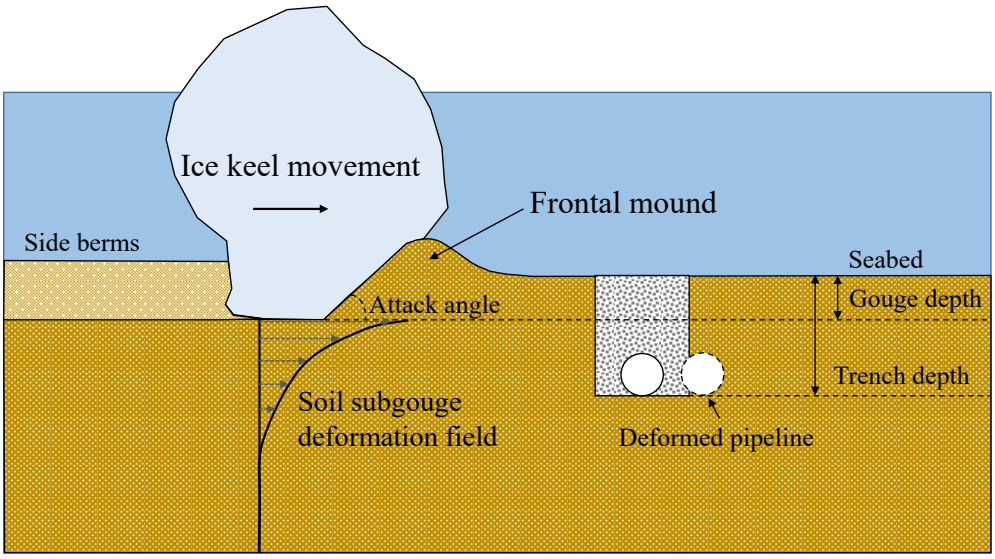

Figure 4-2. Ice gouging process and subgouge deformation (not to scale)

Pre-dredged material is a common backfilling solution to achieve cost-effective protection of pipelines in ice-prone environments. Occasionally, purchased granular materials may also be used to enhance pipeline stability. However, trenching, construction processes, and environmental loads can significantly alter the stiffness of both fine and granular backfill materials, creating a marked contrast with the undisturbed native soil.

Previous research (Aslkhalili et al., 2020; Ghorbanzadeh et al., 2023) demonstrates that this stiffness disparity between backfill and native ground can profoundly impact soil failure mechanisms and pipeline response during ice gouging events. Despite these findings, current pipeline design codes for ice gouging analysis (e.g., PRCI 2009; ALA 2005; ASCE 2014) neglect the crucial interactions between the pipeline, backfill, and trench walls. Due to this knowledge gap, existing design solutions often rely on uniform soil conditions, as found in experimental studies (e.g., Lach, 1996; Yang, 2009) or numerical models (e.g., Pike and Kenny, 2016; Shin et al., 2024).

This study investigates how backfill stiffness and configuration variations influence seabed failure mechanisms and pipeline response during ice gouging. Six distinct backfill materials will be examined: four clay backfills ranging from very soft to stiff, representing scenarios like slurry, disturbed and remolded native clay, and undisturbed seabed material, as well as loose and dense sands, simulating potential purchased backfill. The research will employ the Coupled Eulerian-Lagrangian (CEL) method within Abaqus/Explicit. Strain-rate dependency and strain-softening effects will be incorporated to capture soil behavior accurately. The model's validity was established through comparison of subgouge deformation and ice-soil reaction forces with experimental data conducted by Lach (1996).

The research identified a significant influence of backfill material properties on pipeline response during ice gouging events. Using softer backfill materials reduced passive pressure mobilization, resulting in the formation of full shear bands within the trench wall. This potentially caused trench wall slice movement towards the soil surface and decreased lateral soil resistance, likely contributing to greater pipeline deformation. Conversely, backfill materials with higher shear strength transferred the ice gouge load more directly to the pipeline, potentially increasing the risk of pipeline failure. These findings highlight the importance of considering the impact of trenching and backfilling on pipeline safety during ice gouging events. By carefully selecting backfill material properties and configuration, it may be possible to enhance pipeline response and reduce overall project costs.

4.2 Model Development

4.2.1 Developed CEL Model

This study used the Coupled Eulerian-Lagrangian (CEL) method in Abaqus/Explicit software to model the complex interactions of ice gouging on seabed and pipelines, capturing accurate modeling through a penalty contact approach (Simulia, 2019). CEL allows for large seabed deformations without typical finite element limitations. The Lagrangian approach models ice and pipeline as discrete bodies, while the Eulerian approach models the deforming seabed. Eulerian Volume Fraction (EVF) tracks soil volume in grid cells, aiding stress/strain calculations.

A symmetric finite element (FE) mesh was created to model half of the soil, ice keel, and pipeline domains (see Figure 4-3). The soil was modeled using Eulerian brick elements (EC3D8R) within a 60m x 27m x 17m domain, with a void domain to capture mound and berm formation. The ice keel was modeled as a rigid body using linear brick elements (C3D8R). Mesh sensitivity analysis confirmed that the mesh size (0.2m around the pipeline, 0.5m near gouging, 1m elsewhere) was efficient and sufficient.

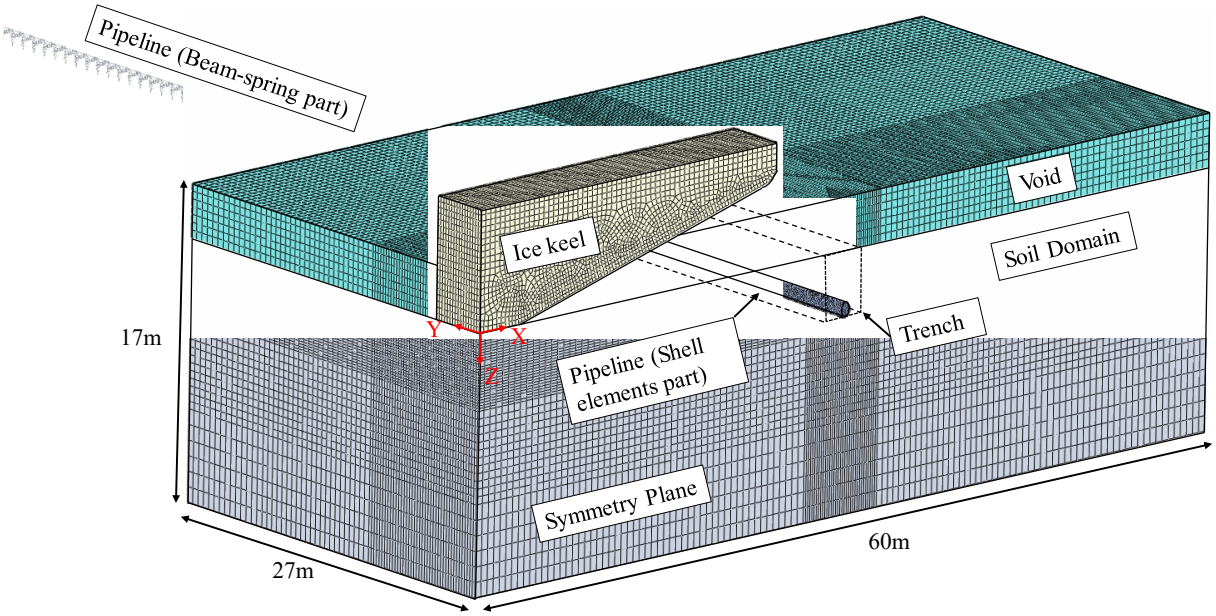

Figure 4-3. Finite element model configuration

Soil particles were constrained from moving perpendicular to domain faces. As confirmed by FE analyses, boundaries were set far enough from the pipeline to avoid boundary effects. The ice keel was moved laterally at 1 m/s without rotation, following Peek and Nobahar's (2012) recommendation.

The pipeline, 0.950 m in diameter and 12.7 mm thick, is buried 3.25 m deep (from the surface to the crown of the pipeline). The continuum part of the pipeline was modeled with 20 S4R shell elements per cross-section, each covering 18°, considering elastoplastic steel with isotropic strain hardening following the von Mises criterion (see Figure 4-4). Young's modulus is 205 GPa, Poisson's ratio is 0.3, and external hydrostatic pore pressure is negligible. The pipeline model extends beyond the soil domain for a distance of 5,000 m using PIPE31H beam elements restrained by SPRINGA Winkler springs. The continuum and discontinuum parts of the pipeline are connected through the kinematic coupling constraint.

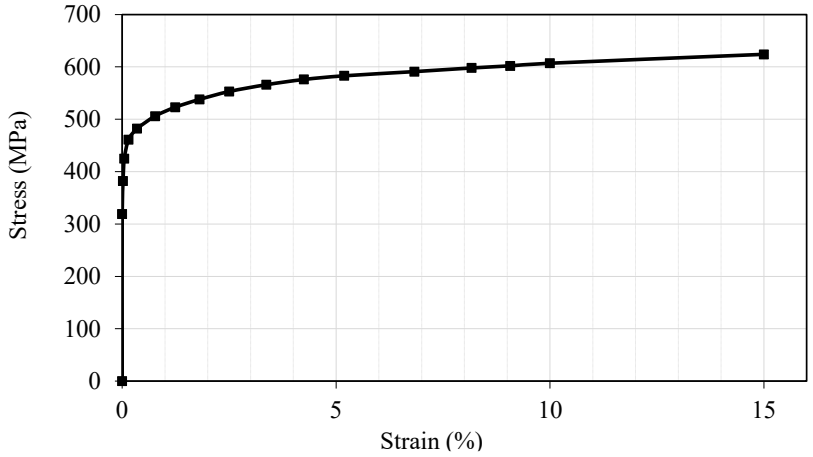

Figure 4-4. The steel stress-strain curve (Ralf Peek & Nobahar, 2012)

Following the Tresca criterion, the seabed soil was modeled as undrained elastic-perfectly plastic clay (Lach, 1996). Friction and dilation angles were assumed to be zero due to above-zero temperatures in the Arctic, where ice gouging often occurs (Hashemi et al., 2022). Soil Young's modulus was assumed to be $400s_{ui,}$ and the Poisson's ratio was set to 0.499.

Contact surfaces in Abaqus/Explicit simulated ice-soil-pipeline interaction. A "hard" normal behavior and Coulomb friction model were used. Native soil-ice and native soil-pipeline friction coefficient values are 0.3 and 1.0, respectively. Surface polarity was used for pipeline-soil, and shear stress was limited to half the peak undrained shear strength.

The analysis comprised four steps: 1) inducing geostatic stress, 2) lowering the ice keel and applying internal pressure by 12MPa to the pipeline (simulated as a temperature change in the structural elements due to software limitations), 3) increasing pipeline temperature by 50°C, and 4) applying a horizontal velocity of 1m/s to the ice keel.

4.2.2 Strain Softening and Shear Rate Effects

Using a VUSDFLD subroutine, the soil model in Abaqus was modified to include strain rate dependency and strain softening effects as per Einav and Randolph (2005) (Equation (4-1)). This

involved incrementally updating the undrained shear strength (s_{ui}) at each time step based on the accumulated plastic shear strain (ξ) and the average maximum shear strain rate ($\dot{\gamma_{max}}$) from the previous step.

$$s_u = \left[1 + \mu \times \log_{10}\left(\frac{\max(|\dot{\gamma_{max}}|, \dot{\gamma_{ref}})}{\dot{\gamma_{ref}}}\right)\right] \times \left[\delta_{rem} + (1 - \delta_{rem})e^{-3\xi/\xi 95}\right] s_{ui} \quad (4\text{-}1)$$

The reference shear strain rate ($\dot{\gamma_{ref}}$) and the increase rate of shear strength per log cycle (μ) are constant, while the maximum shear strain rate ($\dot{\gamma_{max}}$) varies. Similarly, the ratio of fully remolded to initial shear strength (δ_{rem}) and the strain leading to a 95% reduction in remolded strength ($\xi 95$) are also constant. However, the incremental accumulated absolute plastic shear strain (ξ) is variable. The initial undrained shear strength is determined at the reference strain rate. These parameters, chosen from Hashemi and Shiri (2022), are listed in Table 4-1.

Table 4-1. Strain softening and shear rate effects parameters for an ice gouging event

Parameters	Value
μ	0.1
$\dot{\gamma_{ref}}$	0.024 s^{-1}
δ_{rem}	0.77
$\xi 95$	12

Soil sensitivity is considered in the calculation of δ_{rem}, with an assumed value of 1.3 for the native soil and unity (1.0) for the backfill.

4.3 Validation of Numerical Models

To assess the model's accuracy and predictive capabilities, the numerical simulation results were compared with established benchmarks from previous research. Specifically, comparisons were made to both experimental findings from Lach's (1996) Test 05 centrifuge study and predictions based on the PRISE empirical equation (Phillips et al., 2005).

Lach (1996) performed a series of nine small-scale centrifuge tests at 100 gravities, simulating ice gouging in Speswhite kaolin clay under conditions representative of the Canadian Beaufort Sea. Test 05 was chosen for comparison due to its thoroughly documented soil properties, including undrained shear strength and overconsolidation ratio (OCR) profiles, which have been widely cited in the literature (e.g., Pike and Kenny, 2016).

Figure 4-5 compares horizontal soil subgouge displacement results from the current study, considering and not considering strain rate and strain-softening effects, alongside centrifuge data (Lach 1996) and the PRISE equation (Phillips et al., 2005). The results from the current study, incorporating strain rate and strain-softening effects, demonstrate more realistic horizontal subgouge displacements in contrast to utilizing conventional Mohr-Coulomb and similar studies. Figure 4-5 illustrates a discrepancy near the gouge depth without considering these effects, which were previously observed in studies that neglected them. The findings from the horizontal subgouge displacement analysis underscore the significance of accounting for strain softening and strain rate effects in the ice gouging study. The ice keel reaction forces results after reaching a steady state in the current model and Lach (1996) are presented in Table 4-2.

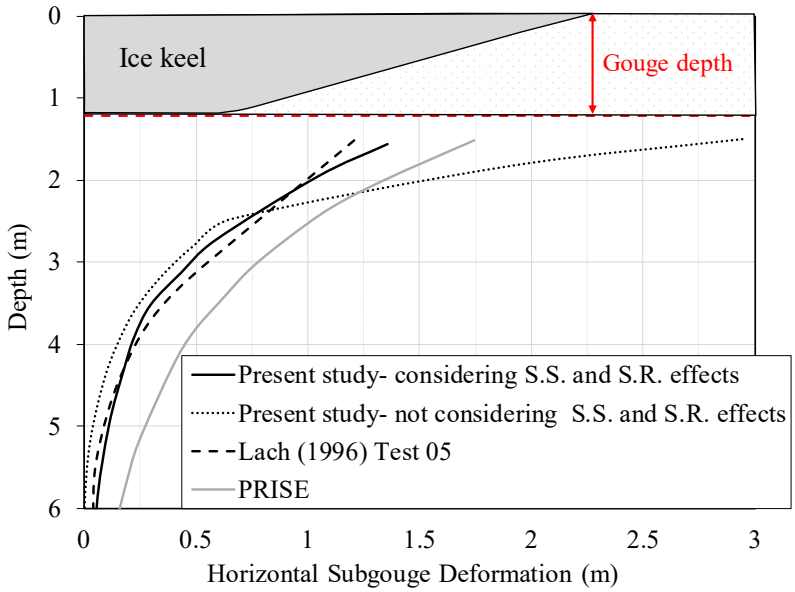

Figure 4-5. The comparison of the soil horizontal subgouge deformations

Table 4-2. The comparison of the vertical and horizontal ice keel-seabed reaction forces

Model	Horizontal ice keel reaction force (MN)	Vertical ice keel reaction force (MN)
Lach (1996) (Centrifuge test)	5.00	16.90
Present Study (CEL model)	4.95	15.50

The validation study demonstrates the success of the CEL model in estimating the horizontal soil subgouge displacement and ice keel reaction forces in ice gouging situations.

4.4 Failure Criteria for Subsea Pipelines

The design of buried pipelines under significant ground deformation must meet three criteria as stipulated in existing literature and design codes to accommodate various deformation modes. These include tensile yielding, local buckling, and local collapse. Tensile yielding is limited to a maximum axial tensile strain of 2.00%, as the DNVGL-ST-F101 (DNV, 2017) standard states. Local buckling is defined as the pipeline's lateral or radial deformation caused by compressive loading. The maximum compressive strain (ε_{max}) should not exceed the critical compressive strain

value (ε_c^{crit}), as specified in design codes such as CSA (2015). ε_c^{crit} is calculated using the equations (4-2) and (4-3).

$$\varepsilon_c^{crit} = 0.5\frac{t}{D} - 0.0025 + 3000\left(\frac{(p_i - p_e)D}{2Et}\right)^2 \qquad \text{for } \frac{(p_i - p_e)D}{2tf_y} < 0.4 \qquad (4\text{-}2)$$

$$\varepsilon_c^{crit} = 0.5\frac{t}{D} - 0.0025 + 3000\left(\frac{0.4f_y}{E}\right)^2 \qquad \text{for } \frac{(p_i - p_e)D}{2tf_y} \geq 0.4 \qquad (4\text{-}3)$$

where p_i and p_e are the maximum internal and external pressure, f_y is the effective specified yield strength, E is Young's modulus of elasticity, and t is the pipeline wall thickness.

Lastly, ovalization failure, which occurs when pipelines are subjected to ice gouging, must be limited to a 3% acceptable ovalization parameter according to the DNV (2017) standard, as increased stress concentrations and reduced stability can increase the risk of pipeline failure. DNV (2017) defined the ovalization parameter as equation (4-4) (see Figure 4-6).

$$f_0 = \frac{D_{max} - D_{min}}{D} \leq 0.03 \qquad (4\text{-}4)$$

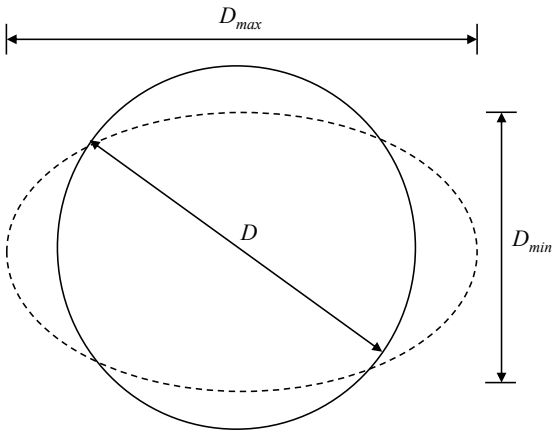

Figure 4-6. Definition of ovalization in a deformed pipeline

The pipeline's response under various backfill conditions was captured and analyzed against established failure criteria, revealing how backfill stiffness and configuration can impact overall pipeline safety during ice gouging.

4.5 Parametric Study

A study was conducted through 6 case studies (CS-1 to CS-6) to investigate the influence of the backfilling stiffness and type under constant trench geometry. The numerical analysis incorporated the pipeline layout and trench geometries obtained from Paulin (1998) T1P1 centrifuge test. Equations 4-5 delineate the profile of native soil in situ undrained shear strength applied in the present case studies (Z is the depth from the seabed). According to this equation, the undrained shear strength at the depth corresponding to the pipeline springline is 40 kPa. Native seabed soil unit weight is 19.12 kN/m^3. Also, gouge depth was assumed to be constant and to be 2.85m in all cases.

$$s_u\ (kPa) = (Z + 9.8) \times 3 \qquad (4\text{-}5)$$

The study used six types of backfills, including four fined-grained and two coarse-grained ones. The backfills used during testing were as follows: CS-1, slurry (represents the natural in-fill or the backfilling by jetting in soft clay (Kianian et al., 2021); CS-2, chunky materials grated native material patted into place (simulate a soft clay after plowing or mechanical backfilling); CS-3, remolded native material pushed into place; CS-4, native seabed material, CS-5, loose fine sand and CS-6, dense fine sand (representing purchased materials). Table 4-3 shows the backfill soil model parameters adopted from the corresponding references for the case analysis in the current study.

Table 4-3. Parametric study map of backfill types for trenched pipeline faced with ice gouging

Case No.	Backfill type	Backfill soil density (kg/m^3)	Undrained shear strength, s_{ub} (kPa)	Angle of internal friction (degree)	Dilation Angle (degree)	Elastic Modulus (MPa)	Poisson Ratio, ν	Refs.
CS-1	slurry	1850	1.8	-	-	400 s_{ub}	0.499	T9P1 test from Paulin (1998)
CS-2	chunk	1850	14.2	-	-	400 s_{ub}	0.499	T9P2 test from Paulin (1998)
CS-3	remoulded	1850	24.7	-	-	400 s_{ub}	0.499	T9P3 test from Paulin (1998)
CS-4	native seabed	1950	41.2	-	-	400 s_{ub}	0.499	Dong et al. (2021)
CS-5	loose fine sand	1480	-	31.0	0.0	5	0.33	Esmaeilzadeh & Shiri (2019)
CS-6	dense fine sand	1721	-	44.0	16.0	$150\sqrt{p'_a \times p'^*}$	0.2	Roy et al. (2018)

*p' is the mean effective stress, p'_a is the atmospheric pressure (=100 kPa)

In all the cases, the magnitude of the horizontal and vertical ice keel reaction forces, the displacement of soil tracer particles, and the pipeline displacement and strains were analyzed and compared.

4.6 Results and Discussions

4.6.1 Soil Displacement Mechanisms

This analysis reveals how the interaction between the pipeline, backfill, and trench walls influences soil movement and pipeline response during ice gouging. Figure 4-7 shows the initial ice keel position, with red tracer particles highlighting subgouge soil positions.

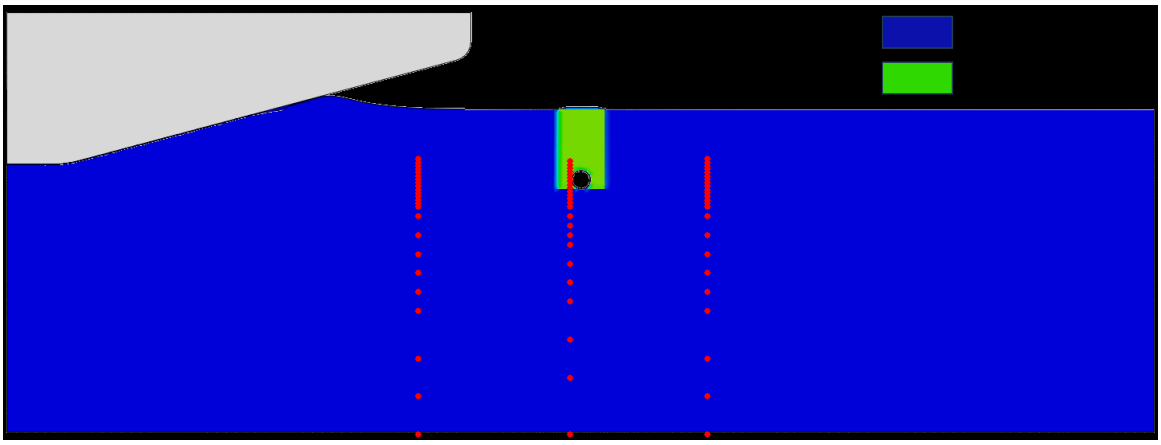

Figure 4-7. Position of soil, pipeline, ice, and tracer particles at the threshold of horizontal movement of the ice keel

Figures 4-8 to 4-11 depict the ice keel's progression towards the pipeline. The initial movement within the uniform native soil induces stresses and strains, including horizontal subgouge displacements. This leads to a steady state with consistent soil features (berms, frontal mounds, etc.) and stable ice keel-soil interaction forces.

However, Figure 4-8 demonstrates how the pipeline-backfill-trench wall interaction disrupts this steady state. As the ice approaches, horizontal stresses and strains cause the native soil to press against the trench wall. This interaction with the softer backfill causes compression and upward displacement, most pronounced in CS-1 (very soft backfill). Here, significant backfill is removed from the trench and replaced by native soil in the ice gouge symmetry plane. The backfill removal mechanism becomes less evident in CS-2 through CS-4 as the shear strength difference between backfill and native soil decreases. Additionally, the pipeline-trench wall interaction begins earlier in cases with softer backfill, allowing the ice load to be transferred more quickly from native soil to the pipeline.

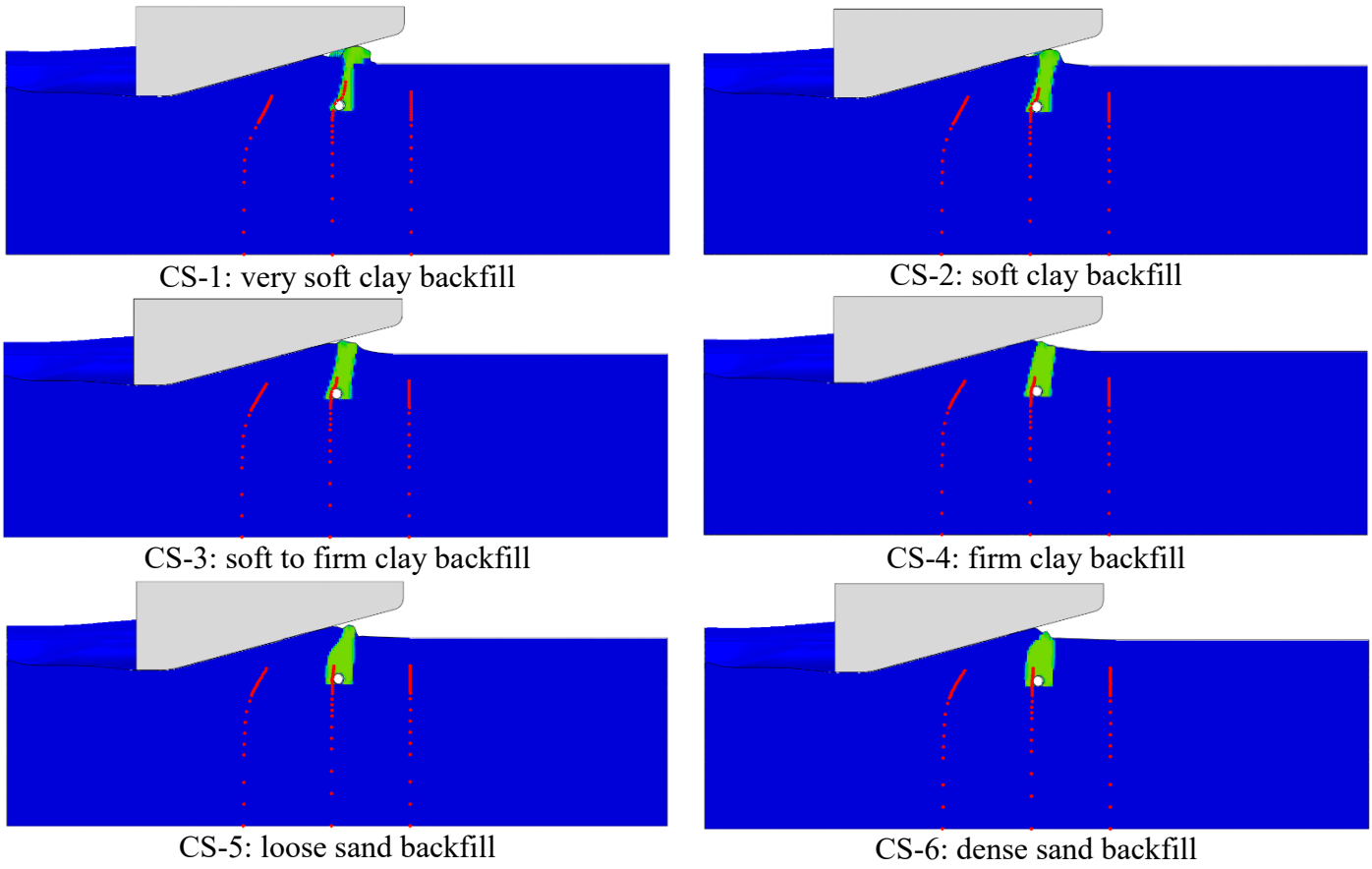

Figure 4-8. Position of soil, pipeline, ice, and tracer particles at time step 12s

The shear strength characteristics of sandy backfill produced distinct responses compared to clayey soils. At the 12-second time step (Figure 4-8), only the upper portion of the left trench wall deforms, and CS-6 exhibits minimal change. This highlights the impact of higher backfill shear strength: it delays trench wall collapse and reduces overall soil deformation, potentially transferring the ice load more directly to the pipeline.

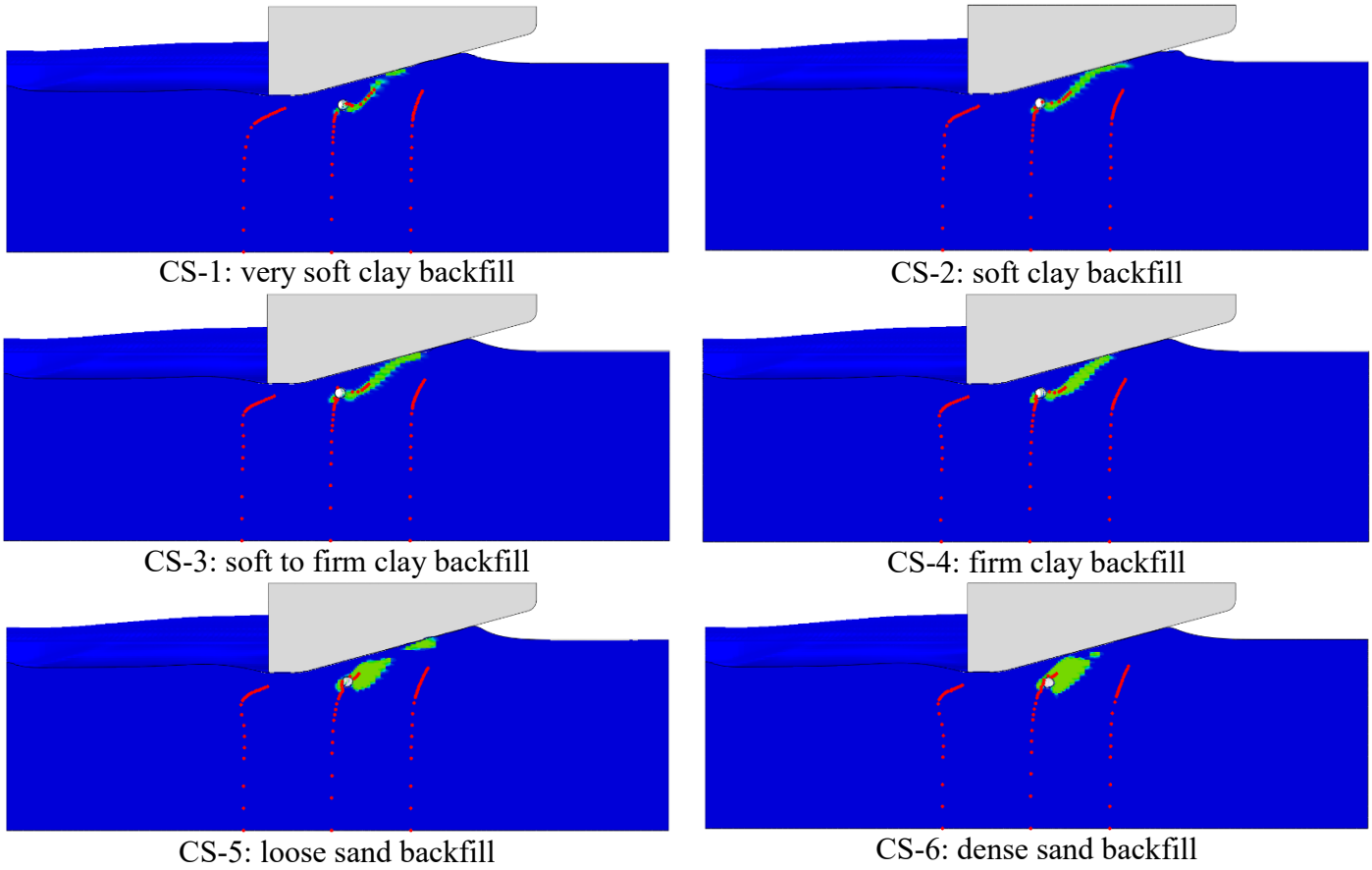

Figure 4-9. Position of soil, pipeline, ice, and tracer particles at time step= 24s

As the ice keel crosses the pipeline, differences based on backfill type become evident. On the leading side, backfill generally slides both over and under the pipeline, exposing it to direct loading from native soil. However, on the trailing side, clayey backfill is primarily displaced by the ice keel's movement. In contrast, sandy backfills undergo compaction due to the ice keel's force, forming a mass on the pipeline's right side (Figures 4-9 and 4-10). This is likely due to the higher internal friction within sandy soils. This compaction pattern near the pipeline suggests a potential for increased stress concentration on the pipeline structure in sandy backfill scenarios.

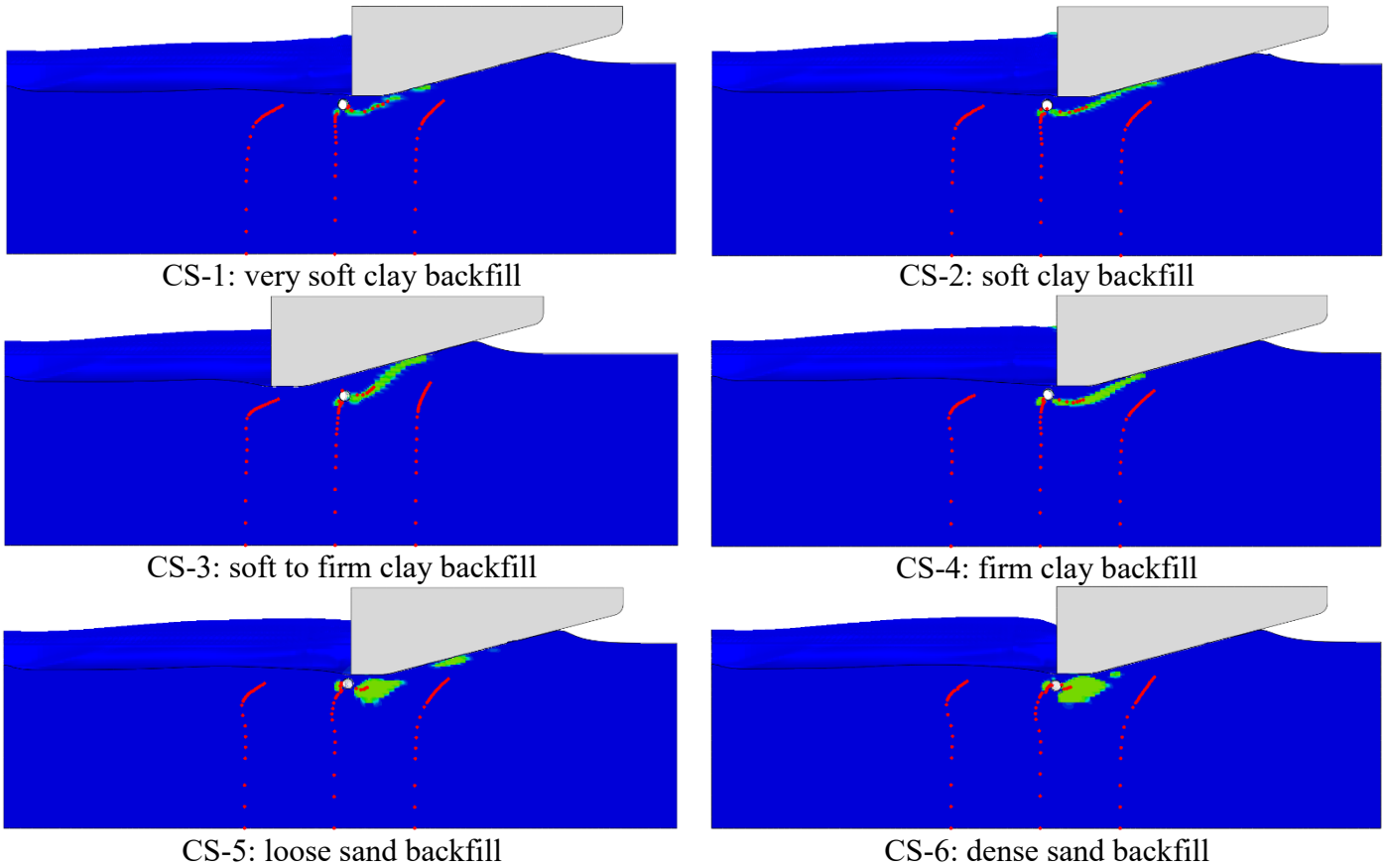

Figure 4-10. Position of soil, pipeline, ice, and tracer particles at time step= 31.2s

Analysis of soil displacement mechanisms across various backfill scenarios reveals the crucial impact of backfill stiffness and configuration on pipeline-backfill-trench wall interaction, ultimately influencing both seabed behavior and pipeline response.

4.6.2 Ice Keel Reaction Forces

Figure 4-11 depicts the horizontal and vertical ice keel-seabed reaction forces. Initial steady-state reaction forces reflect the ice keel's interaction with the undisturbed native soil. As the ice reaches the trench, force profiles begin to diverge. In CS-1 (very soft clay), an early decrease in reaction forces occurs at a displacement of 10m. The pattern of ice-soil reaction forces reflects the interaction between the backfill and trench walls. As observed in the soil failure analysis, this

interaction is most intense and occurs earliest with very soft clay backfill. This explains the significant and early reduction of reaction forces seen in CS-1.

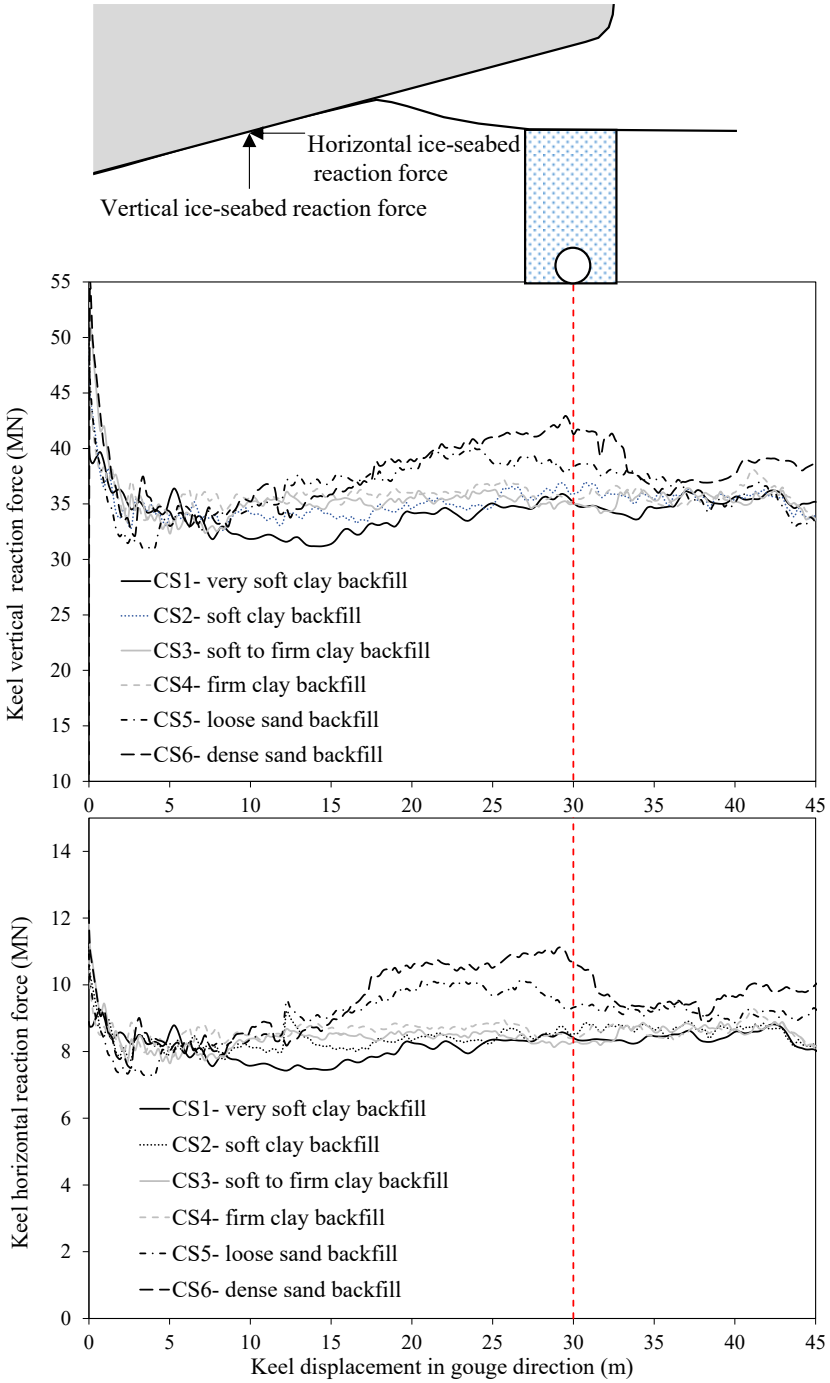

Figure 4-11. Ice keel-seabed reaction forces

Cases CS-2 through CS-4 exhibit differences, which are less pronounced due to the lower shear strength contrast between backfill and native soil and the relatively narrow trench width. Sandy backfills (CS-5 and CS-6) show the most distinct behavior. At a displacement of 15m, forces exceed steady-state values, with CS-6 (dense sand) demonstrating a substantial increase (roughly 15%) in both vertical and horizontal forces. After the ice keel crosses the trench, all scenarios return to the initial steady-state forces.

4.6.3 Pipeline Behavior

All scenarios share a similar pipeline displacement trajectory during ice gouging (see Figure 4-12). As the ice keel approaches (position 1 to 2), the pipeline experiences a combined upward and horizontal displacement (towards the direction of gouging). This reaches a maximum ("Max. State") when the ice reaches the upper part of the pipeline. The upward motion is due to the soil offering less resistance to uplift compared to other directions, while the horizontal displacement is driven directly by the ice movement. After the ice passes over the pipeline (position 2 to 3), a degree of elastic recovery leads to a final, slightly rebounded position ("Rebound State").

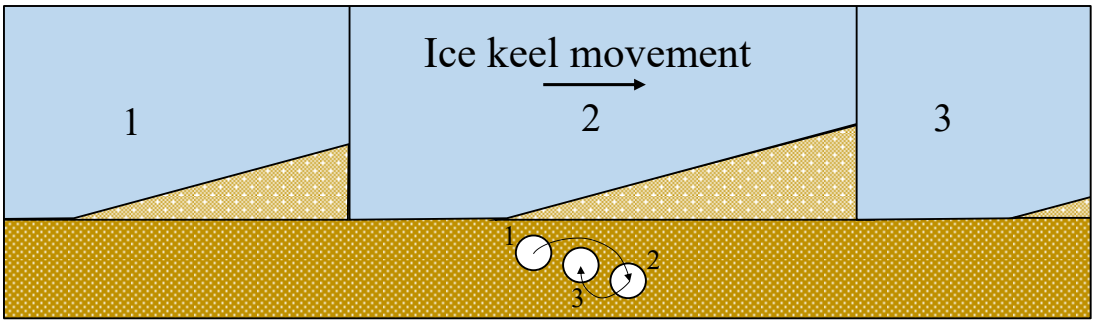

Figure 4-12. Characteristic trajectory of a pipeline during an ice gouging event (not to scale)

Figures 4-13 and 4-14 provide a detailed comparison of pipeline trajectories along the gouge centerline across all backfill case studies.

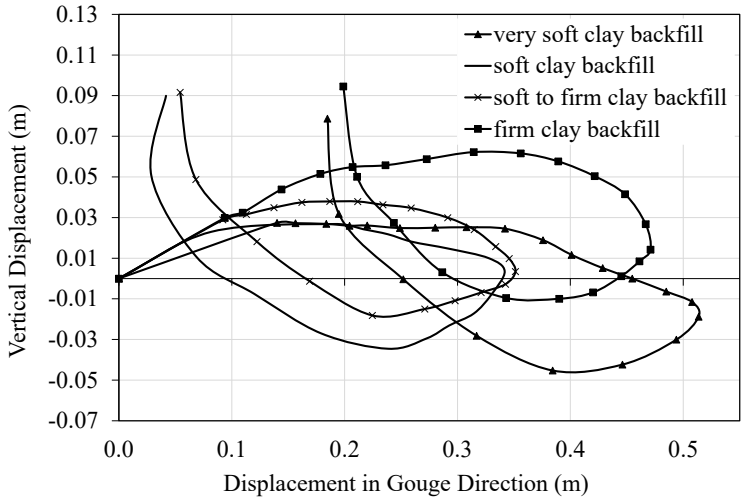

Figure 4-13. Pipeline trajectory in the vertical plane at gouge centerline (clay backfill cases)

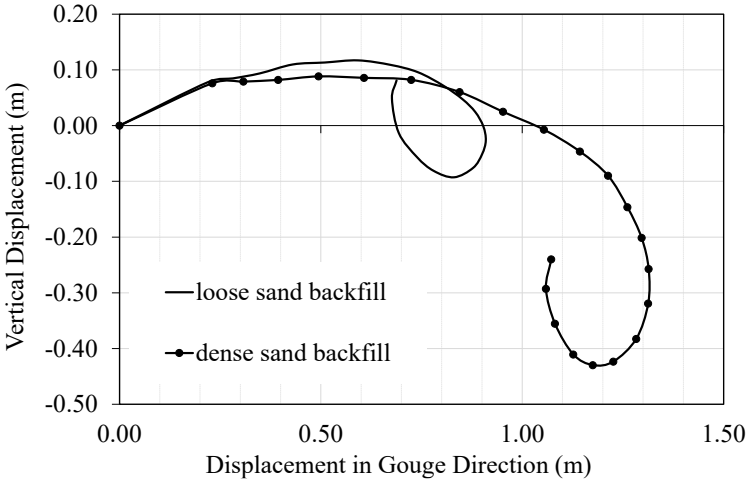

Figure 4-14. Pipeline trajectory in the vertical plane at gouge centerline (sand backfill cases)

In CS-1 (very soft clay), intense backfill-trench wall interaction leads to rapid backfill removal. This weakens passive soil resistance against pipeline displacement while potentially increasing active pressure on the pipeline from the trench wall. In contrast, the higher shear strength of the backfill in CS-4 provides greater lateral resistance, exceeding the vertical uplift resistance. Therefore, the pipeline initially moves vertically with a steeper incline than CS-1, resulting in reduced final lateral displacement. Cases CS-2 and CS-3 exhibit behavior between these extremes.

Sandy backfills demonstrate substantially greater horizontal and vertical displacements compared to clayey backfills. This is attributed to two factors. Unlike clay backfills, where removal is

dominant, sandy backfills resist displacement due to higher internal friction (Figures 4-8 and 4-9). This remaining sand more effectively transmits force from the ice to the pipeline, leading to increased displacement. Moreover, as seen in Figure 4-11, higher horizontal and vertical ice keel-soil reaction forces occur in CS-5 and CS-6, further increasing the vertical force on the pipeline.

Figures 4-15 (maximum state) and 4-16 (rebound state) show the pipeline displacements along the pipeline's longitudinal axis (horizontal, axial, and vertical). Among clay backfill cases, CS-1 (very soft clay) experiences the highest displacement due to the backfill "removal" mechanism and increased active pressure on the pipeline from the trench wall. CS-2 and CS-3 show little difference, as expected from their similar backfill properties. In contrast, CS-4, CS-5, and CS-6 demonstrate increased displacement levels. This aligns with the earlier discussion on the influence of stiffer backfill, which leads to enhanced force transfer to the pipeline.

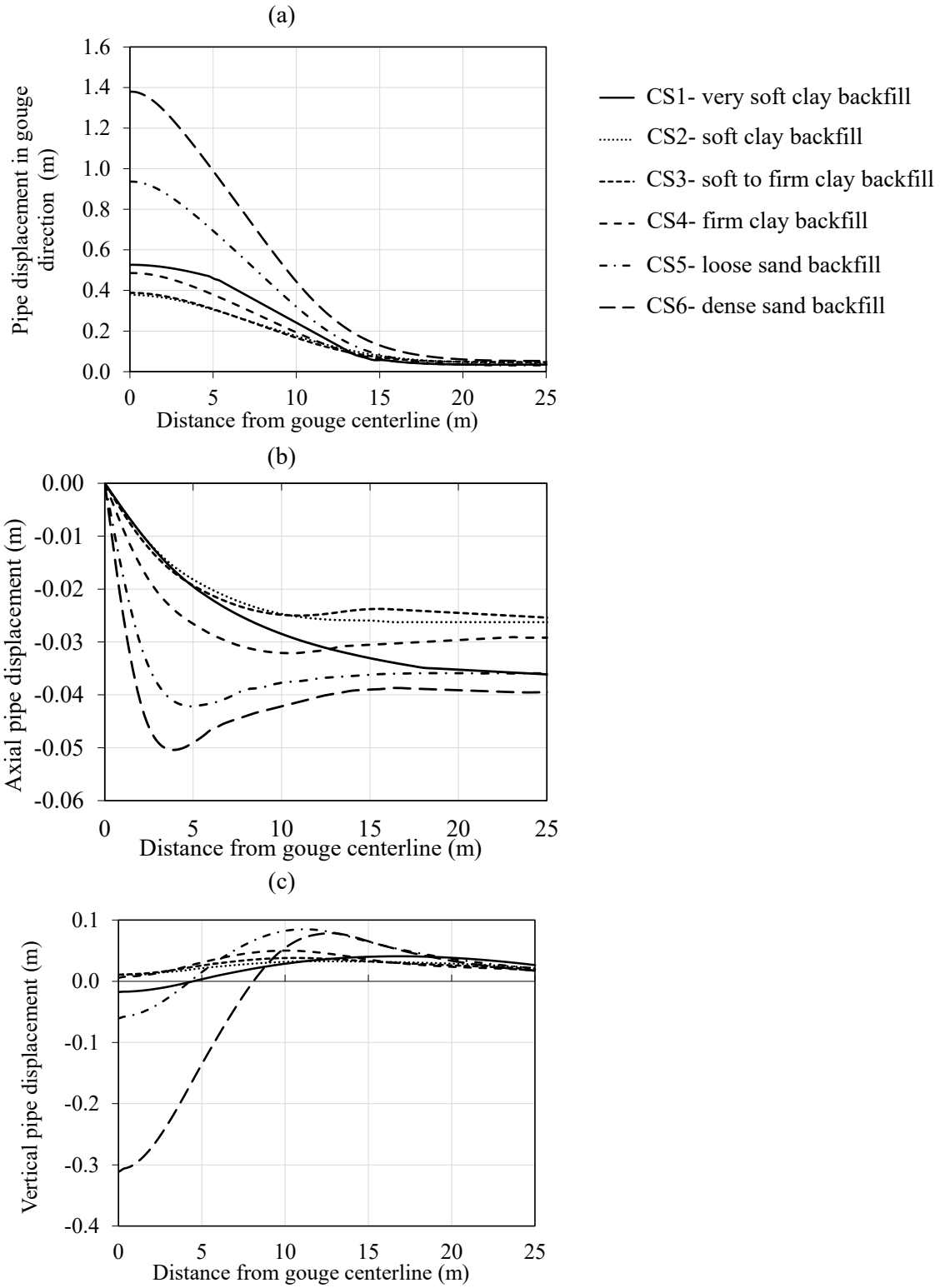

Figure 4-15. Pipeline displacement along the pipeline axis during the maximum displacement state, including (a) horizontal (gouge motion), (b) axial, and (c) vertical directions

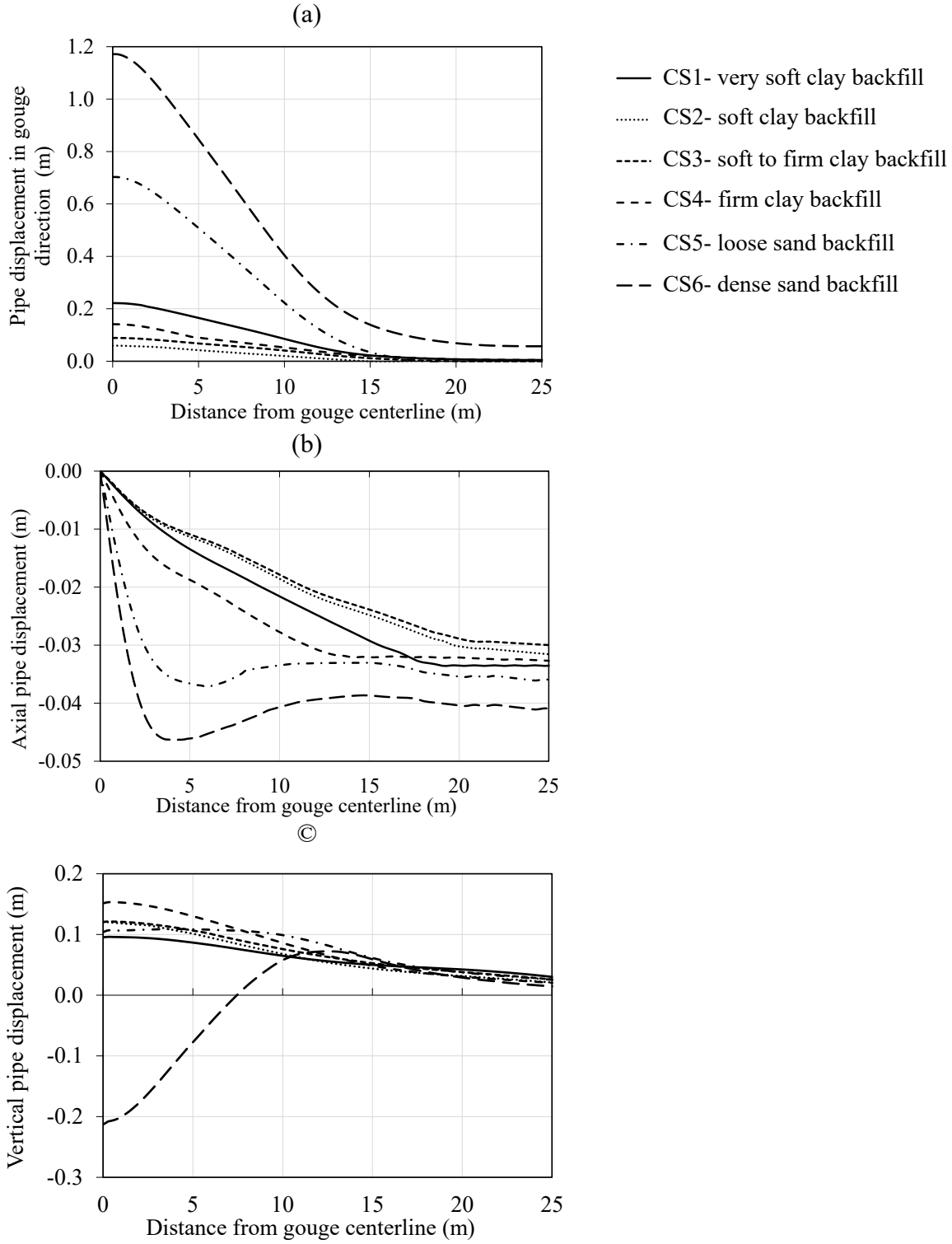

Figure 4-16. Pipeline displacement along the pipeline axis during the rebound displacement state, including (a) horizontal (gouge motion), (b) axial, and (c) vertical directions

Figures 4-17 and 4-18 illustrate the maximum axial strains along the pipeline axis due to ice gouging. The trailing side of the pipeline experiences tensile strain, while the leading side undergoes compression across all cases. These figures highlight the risks associated with both excessively soft and excessively stiff backfill materials. Very soft backfill may lead to high tensile strains, potentially compromising pipeline integrity. On the other hand, excessively stiff backfill increases the likelihood of exceeding critical compressive strain levels. Backfills with intermediate stiffness appear to offer the best protection for maintaining axial strain within safe limits.

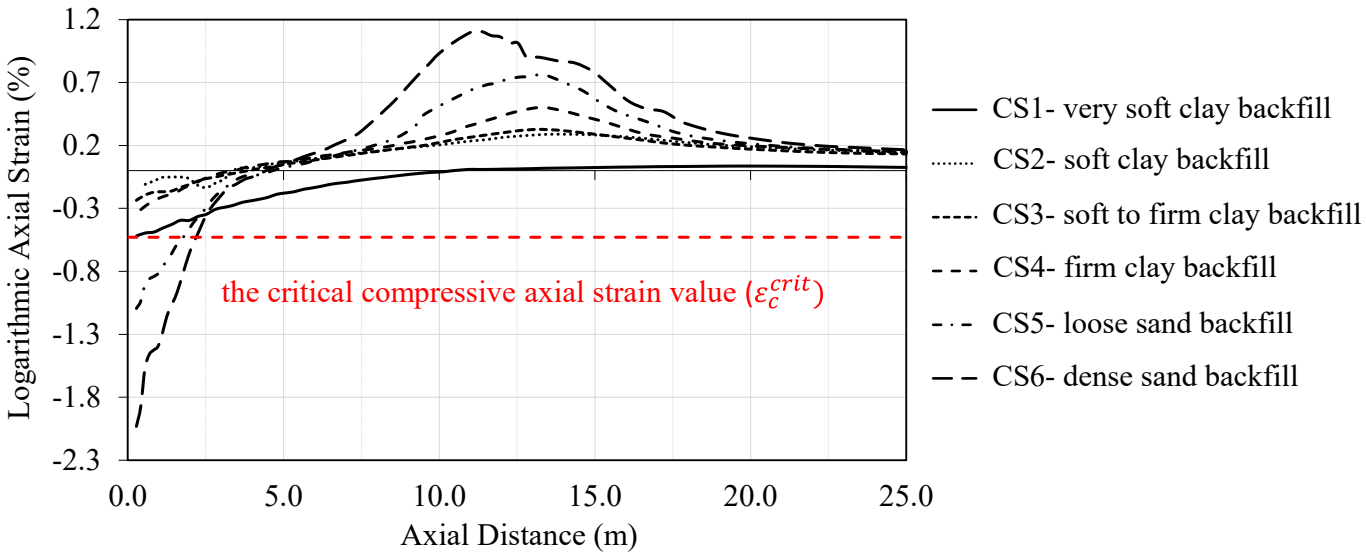

Figure 4-17. Logarithmic axial strain for the leading edge of the pipeline along the axis

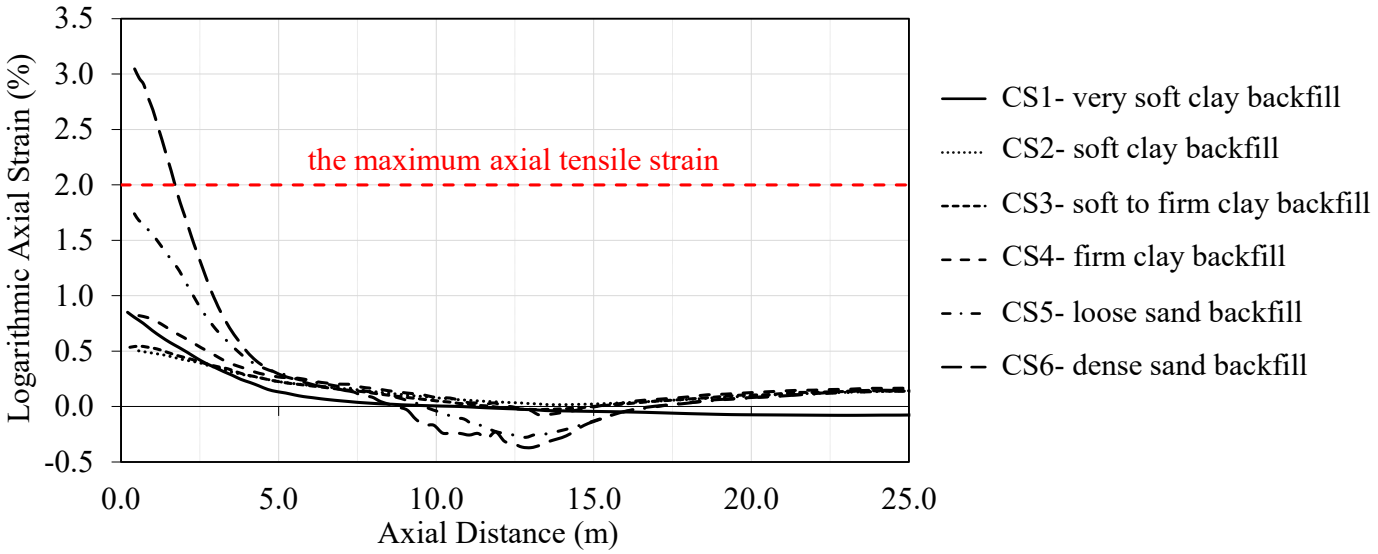

Figure 4-18. Logarithmic axial strain for the trailing edge of the pipeline along the axis

This study examined pipeline ovalization across six scenarios (Figure 4-19). Ovalization is driven by the combined effects of internal pressure, temperature (applied in the initial analysis phase), and the load exerted by the ice gouge.

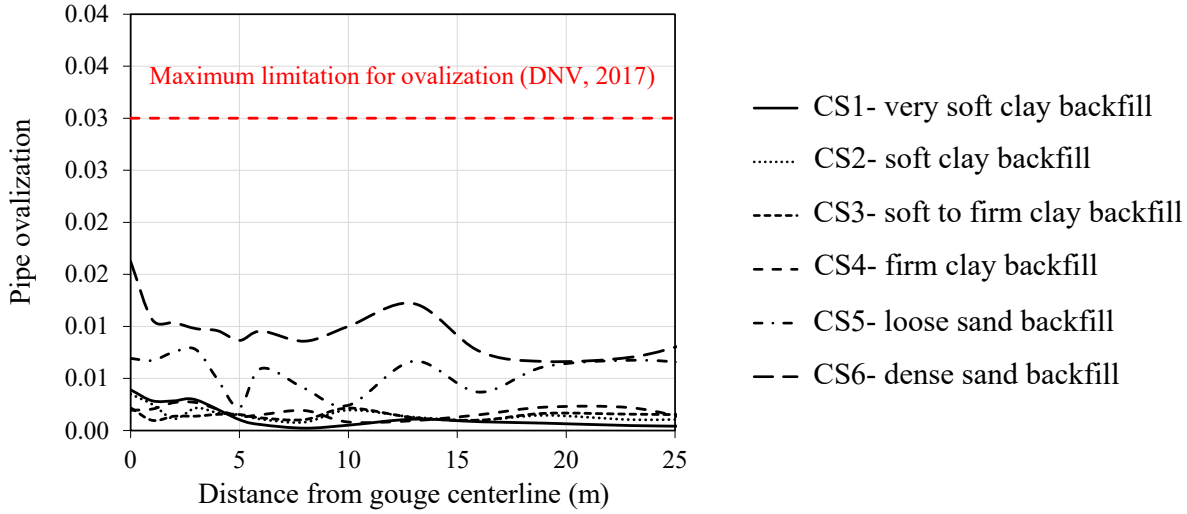

Figure 4-19. Pipeline ovalization along the pipe axis

The pipeline-backfill-trench wall interaction influences the surrounding soil conditions, leading to variations in the magnitude and distribution of strain around the pipeline circumference. This uneven strain distribution results in an irregular ovalization pattern. Figure 4-19 shows that, similar to the pipeline failure analysis, the CS-2 and CS-3 backfills demonstrated the best performance.

Importantly, none of the scenarios resulted in ovalization exceeding the maximum threshold of 0.030 set by DNV (2017).

4.6.4 Discussion

As discussed previously, backfills with intermediate stiffness levels demonstrate superior pipeline performance under ice loading compared to very soft or very stiff materials. This trend is visualized in Figure 4-20, where normalized pipeline displacement (both maximum and rebounded states) is plotted against the normalized stiffness ratio (backfill stiffness divided by native soil stiffness). A third-degree curve was fitted to the data points to determine the ideal backfill shear strength within the clay range (Figure 4-22). Equations 4-5 and 4-6 express the mathematical relationship of these fitted curves.

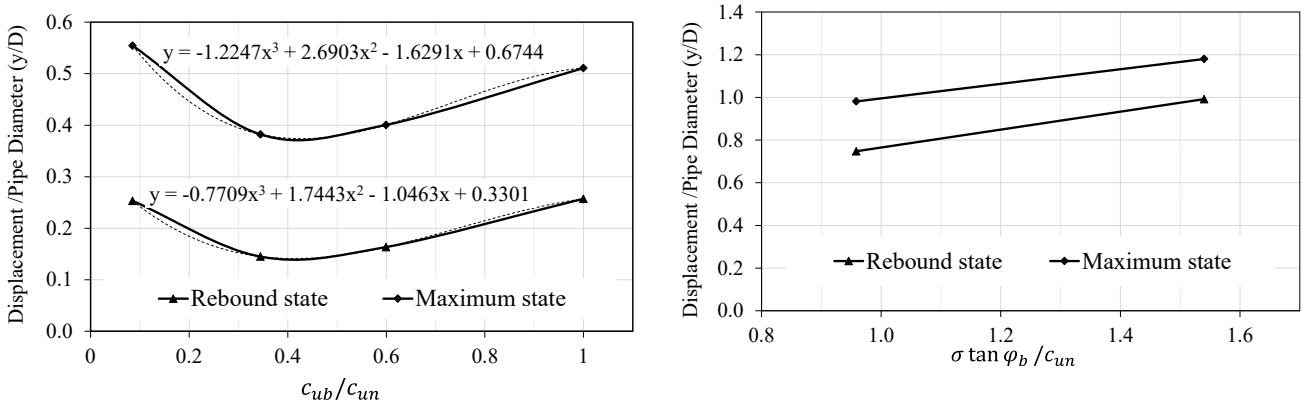

Figure 4-20. Normalized pipeline displacement against backfill stiffness ratio (left, clay backfills; right, sandy backfills)

$$Maximum\ state\text{: } \frac{y}{D} = -1.2247\left(\frac{c_{ub}}{c_{un}}\right)^3 + 2.6903\left(\frac{c_{ub}}{c_{un}}\right)^2 - 1.6291\left(\frac{c_{ub}}{c_{un}}\right) + 0.6744 \quad (4\text{-}5)$$

$$Rebound\ state\text{: } \frac{y}{D} = -0.7709\left(\frac{c_{ub}}{c_{un}}\right)^3 + 1.7443\left(\frac{c_{ub}}{c_{un}}\right)^2 - 1.0463\left(\frac{c_{ub}}{c_{un}}\right) + 0.3301 \quad (4\text{-}6)$$

Through analysis of these equations, it is determined that a stiffness ratio of 0.42 represents the optimal value for maximizing pipeline performance under the given ice-loading conditions. Note that all displacement measurements in this section refer to the symmetry plane cross-section.

4.7 Conclusions

Using continuum finite element modeling, this study investigated the influence of backfill stiffness and configuration on seabed failure mechanisms and pipeline response during ice gouging events. The Einav and Randolph (2005) relationship accounted for strain softening and shear rate in native and backfill clay soil. Through numerical simulations of various trenched and backfilled pipeline configurations, the key findings of the current study are as follows:

- The behavior of backfill material following an ice gouge event is significantly influenced by its type and stiffness, as this impacts the interaction with the trench walls. Clay backfills, due to their lower shear strength, are more prone to removal and dispersion across the seabed. Conversely, sandy backfills, with higher shear strength, tend to aggregate on the trailing side of the pipeline due to their resistance to displacement and the reduced intensity of the removal mechanism.

- Initially, during the steady-state phase before the ice keel reaches the trench, all scenarios exhibit similar horizontal and vertical ice keel-soil reaction forces. However, as the ice keel approaches the trench, these forces diverge. Very soft clay backfills show a decrease in forces, indicating the beginning of backfill-trench wall interaction. Backfills comprised of medium and stiff clay exhibit minimal change in ice keel-soil reaction forces due to the reduced contrast in shear strength between the backfill and the native soil. In contrast, sandy backfills show increased forces, signifying enhanced force transfer through the

stiffer backfill. The timing and magnitude of these changes in ice-soil reaction forces directly reflect the intensity of backfill-trench wall interaction, which is most pronounced when there is a significant difference between backfill and native soil shear strengths.

- The impact of backfill stiffness on pipeline displacement is evident across all scenarios. CS-1 (very soft clay) experiences the highest displacement among the clay backfills. This is due to the combined effects of the intense "removal" mechanism and the strong pipeline-backfill-trench wall interaction. Cases CS-2 and CS-3, with their medium undrained shear strength, exhibit similar and lower displacement levels. Interestingly, CS-4, a stiffer clay backfill, shows higher displacement than CS-2 and CS-3. This can be attributed to the increased resistance provided by the stiffer backfill, which translates to an enormous load being tolerated by the pipeline.

- In contrast, the sandy backfill cases behave differently. The absence of the "removal" mechanism, coupled with the high backfill stiffness and interaction between the pipeline, sandy backfill, and stiff trench wall, allows for efficient transfer of forces from the ice keel to the pipeline. This ultimately leads to substantially larger pipeline displacements in the sandy backfill cases compared to the clay scenarios.

- The trend of higher backfill stiffness leading to higher pipeline displacement holds for CS-4, CS-5, and CS-6 compared to medium-stiffness clays. This is due to the pipeline-backfill-trench wall interaction and the failure mechanism observed in the very soft clay of CS-1. Furthermore, examining the pipeline response in CS-2 and CS-3 reinforces the superior performance of these backfills with medium undrained shear strength. Their behavior

demonstrates that these backfills meet the three critical criteria for maintaining pipeline integrity during ice gouging events.

- This study's analysis reveals that it is possible to determine an undrained shear strength value for backfill clay soil to minimize pipeline displacement. By plotting the pipeline displacement against the backfill's undrained shear strength and fitting a third-degree curve to the data, the point of intersection can reveal the value that leads to the most favorable pipeline response under ice gouging loads.

These findings underscore the critical importance of carefully selecting backfilling stiffness and configuration to improve pipeline performance and safety against ice gouging loads.

Acknowledgments

The authors gratefully acknowledge the financial support of the “Wood” through establishing Research Chair program in Arctic and Harsh Environment Engineering at the Memorial University of Newfoundland, the “Natural Science and Engineering Research Council of Canada (NSERC)” and the “Newfoundland Research and Development Corporation (RDC) (now IET) through “Collaborative Research and Developments Grants (CRD)”. Special thanks are extended to Memorial University for providing excellent resources for conducting this research program.

References

ALA. (2001). Guidelines for the design of buried steel pipe. *American Society of Civil Engineers*.

ASCE. (1984). *Guidelines for the Seismic Design of Oil and Gas Pipeline Systems*. Amer Society of Civil Engineers.

Aslkhalili, A., Shiri, H., & Zendehboudi, S. (2021). Probabilistic assessment of lateral pipeline–Backfill–Trench interaction. *Journal of Pipeline Systems Engineering and Practice*, *12*(3), 4021034.

CSA. (2015). *CSA Z662-15: Oil and gas pipeline systems*.

DNV GL. (2017). *DNVGL-ST-F101, Submarine pipeline systems*.

Dong, X., Shiri, H., Zhang, W., & Randolph, M. F. (2021). The influence of pipeline-backfill-trench interaction on the lateral soil resistance: A numerical investigation. *Computers and Geotechnics*, *137*, 104307.

Einav, I., & Randolph, M. F. (2005). Combining upper bound and strain path methods for evaluating penetration resistance. *International Journal for Numerical Methods in Engineering*, *63*(14), 1991–2016.

Esmaeilzadeh, M., & Shiri, H. (2019). Trench impact on lateral response of pipeline buried in sand. *Experimental and Numerical Modeling of Lateral Pipeline-Trench Interaction Backfilled with Sand*, 72.

Ghorbanzadeh, A., Dong, X., & Shiri, H. (2023). The Response of Buried Pipelines to Ice Gouging in the Uniform and Trenched/backfilled Seabed. *ISOPE International Ocean and Polar Engineering Conference*, ISOPE-I.

Hashemi, S., & Shiri, H. (2022). Numerical Modeling of Ice–Seabed Interaction in Clay by Incorporation of the Strain Rate and Strain-Softening Effects. *Journal of Offshore Mechanics and Arctic Engineering*, *144*(4), 42101.

Hashemi, S., Shiri, H., & Dong, X. (2022). The influence of layered soil on ice-seabed interaction: Soft over stiff clay. *Applied Ocean Research*, *120*, 103033.

Kianian, M., Esmaeilzadeh, M., & Shiri, H. (2021). The Effect of Backfilling Stiffness on the Lateral Response of Deeply Buried Pipelines: an Experimental Study. *Journal of Marine Science and Application*, *20*(1), 21–33.

Lach, P. R. (1996). *Centrifuge modelling of large soil deformation due to ice scour*. Memorial University of Newfoundland. https://research.library.mun.ca/1194/

Nematzadeh, A., & Shiri, H. (2020). The influence of non-linear stress-strain behavior of dense sand on seabed response to ice gouging. *Cold Regions Science and Technology*, *170*, 102929.

Paulin, M. J. (1998). *An investigation into pipelines subjected to lateral soil loading*. Memorial University of Newfoundland.

Peek, R., & Nobahar, A. (2012). Ice gouging over a buried pipeline: Superposition error of simple beam-and-spring models. *International Journal of Geomechanics*, *12*(4), 508–516.

Phillips, R., Clark, J. I., & Kenny, S. (2005). PRISE studies on gouge forces and subgouge deformations. *Proceedings of the International Conference on Port and Ocean Engineering Under Arctic Conditions*.

PRCI. (2009). *Guidelines for Constructing Natural Gas and Liquid Hydrocarbon Pipelines through Areas Prone to Landslide and Subsidence Hazards*, *Pipeline Research Council International*.

Roy, K., Hawlader, B., Kenny, S., & Moore, I. (2018). Uplift failure mechanisms of pipes buried in dense sand. *International Journal of Geomechanics*, *18*(8), 4018087.

Shin, M.-B., Park, D.-S., Park, W.-J., & Seo, Y.-K. (2024). Behavioral analysis of seabed slope subjected to ice gouging. *Cold Regions Science and Technology*, *217*, 104022.

Simulia, D. S. (2019). *Abaqus 2019 documentation*. Dassault Systemes Waltham, MA.

Yang, W. (2009). *Physical modeling of subgouge deformations in sand*. Memorial University of Newfoundland.

.

CHAPTER 5

Subsea Pipeline Design against Ice Gouging: Influence of Trenching Techniques and Trench Geometry

Alireza Ghorbanzadeh, Hodjat Shiri, Xiaoyu Dong

Civil Engineering Department, Faculty of Engineering and Applied Science, Memorial University of Newfoundland, A1B 3X5, St. John's, NL, Canada.

This chapter is under review as a journal manuscript.

Abstract

Subsea pipelines in Arctic environments face the risk of damage from ice gouging, where drifting ice keels scour the seabed. To ensure pipeline integrity, burial using methods like ploughs, mechanical trenchers, jetting, or hydraulic dredging is the conventional protection method. Each method has capabilities and limitations, resulting in different trench profiles and backfill characteristics. This study investigates the influence of these trenching methods and their associated trench geometries on pipeline response and seabed failure mechanisms during ice gouging events. Using advanced large deformation finite element (LDFE) analyses with a Coupled Eulerian-Lagrangian (CEL) algorithm, the complex soil behavior, including strain-rate dependency and strain-softening effects, is modeled. The simulations explicitly incorporate the pipeline, enabling a detailed analysis of its behavior under ice gouging loads. The simulations analyze subgouge soil displacement, pipeline displacement, strains, and ovalization. The findings reveal a direct correlation between increasing trench wall angle and width and the intensification of the backfill removal mechanism. Trench geometry significantly influences the pipeline's horizontal and vertical displacement, while axial displacement and ovalization are less affected. This study emphasizes the crucial role of trenching technique selection and trench shape design in mitigating the risks of ice gouging, highlighting the value of numerical modeling in optimizing pipeline protection strategies in these challenging environments.

Keywords: Subsea pipeline; ice gouging; trenching; finite element analysis; CEL method; Arctic engineering

5.1 Introduction

Ice gouging, or ice scouring, is a prevalent phenomenon near the shores of the world's northern continents. Wind and current forces drive sea ice, often piling it up into pressure ridges. When the submerged keel of an ice feature contacts the seabed, it exerts significant vertical and lateral stresses on the underlying soil. This interaction generates a complex pattern of vertical and lateral soil displacements extending beneath the keel, known as subgouge deformation. Direct contact with pipelines operating in these regions can be detrimental, leading to structural damage and even failure. Pipelines are typically buried beneath the seabed to mitigate this risk. However, even with burial, the subgouge deformation can still impart substantial forces on buried pipelines, potentially causing deformation, structural damage, and even failure (Shiri & Hashemi, 2023). Figure 5-1 provides a simplified visual overview of the seabed and pipeline during ice gouging.

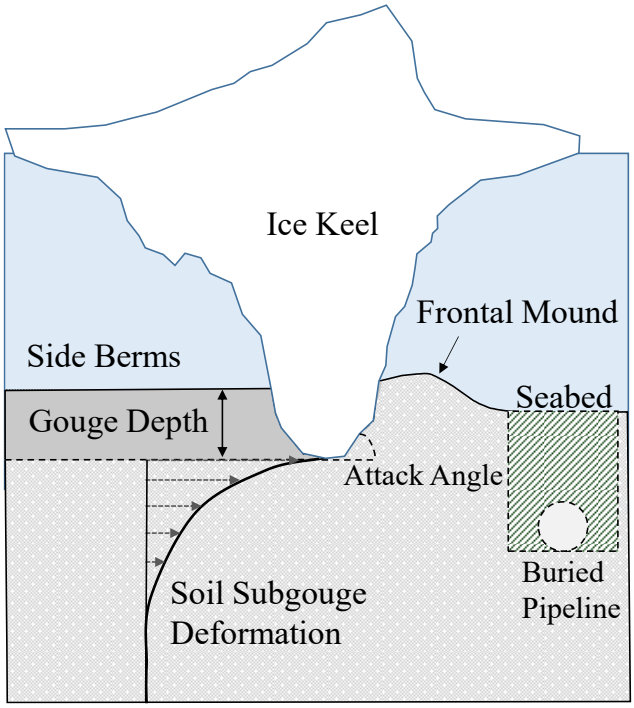

Figure 5-1. Schematic of ice gouging effect on the seabed over a buried pipeline (not to scale)

The design and protection of subsea pipelines in ice-prone environments, such as the Arctic, require a deep understanding of the complex interactions between the pipeline, surrounding soil, and the trench geometry created during burial. Recent research, notably Ghorbanzadeh et al. (2023), has highlighted the significant impact of trenching and backfilling on soil failure mechanisms and pipeline response during ice gouging events. Specifically, the design of the pipeline trench, including slope and width, has been shown to influence the pipeline-backfill-trench wall and its reaction to large soil deformation (Chaloulos et al., 2015, 2017; Jo et al., 2002). However, current design codes (e.g., ALA, 2001; ASCE, 1984; PRCI, 2009) often neglect these critical factors, assuming a uniform soil medium and relying on simplified models or experimental data (e.g., Lach, 1996; Yang, 2009) that may not fully capture the complexities of real-world conditions.

The trench geometry is primarily determined by the trenching method employed during pipeline installation. The five main trenching methods used for burying pipelines are (Paulin et al., 2014):

- Conventional excavation: This traditional method uses excavators or backhoes to dig the trench.
- Hydraulic dredging: It is a widely used method for excavating pipeline trenches, commonly employing cutter suction dredgers (CSD) for harder soils or rock and trailing suction hopper dredgers (TSHD) for softer soils and larger projects.
- Ploughing: A plough-like tool is dragged through the seabed to create a trench.
- Jetting: High-pressure water jets create a fluidized zone in the soil, allowing the pipeline to be lowered into the trench.
- Mechanical trenching: This involves using specialized machines with cutting chains or wheels to excavate the trench.

Figure 5-2 presents a schematic overview of the five trenching methods and their associated equipment. Each of these techniques produces a distinct trench profile, with varying slopes, widths, and depths, which can significantly impact the pipeline's interaction with the surrounding soil and its response to ice gouging loads.

While the impacts of ice gouging on pipelines have been extensively studied (e.g., Nematzadeh & Shiri, 2020; Pike & Kenny, 2016), there remains a knowledge gap regarding the specific influence of trench geometry, determined by the chosen trenching method on pipeline behavior during such events. This study aims to fill this gap by investigating the effects of trench geometry on pipeline response during ice gouging events, analyzing six distinct trench configurations, and simulating realistic scenarios. The Coupled Eulerian-Lagrangian (CEL) method within Abaqus/Explicit is employed to simulate the complex soil behavior during these events. The model will incorporate strain-rate dependency and strain-softening effects for enhanced accuracy. Its validity has been established by comparing simulation results to the experimental data from Lach (1996).

a) Conventional excavation

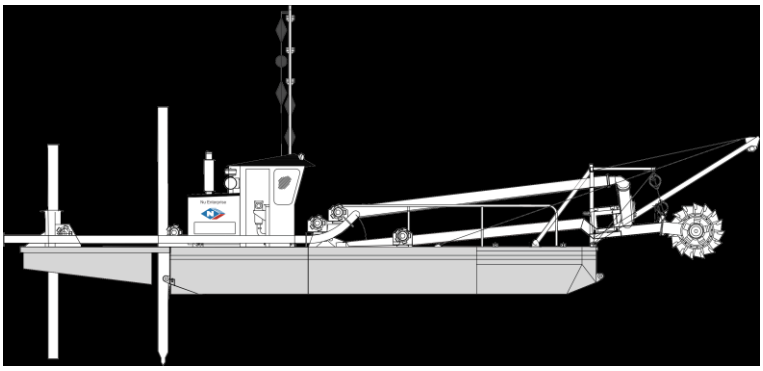

b) CSD

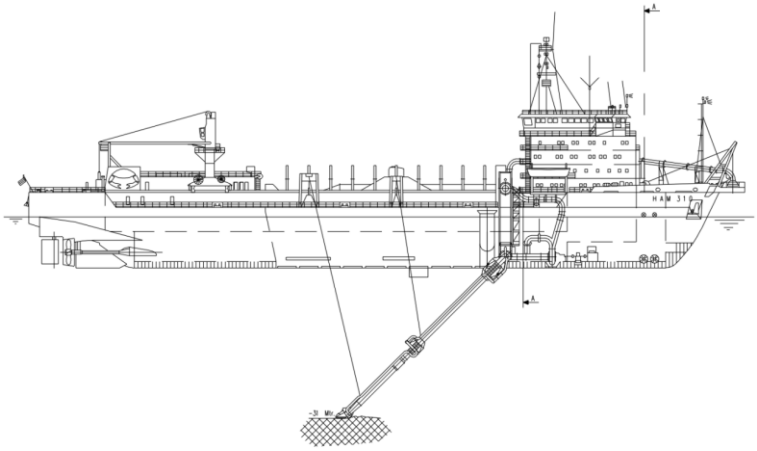

c) TSHD

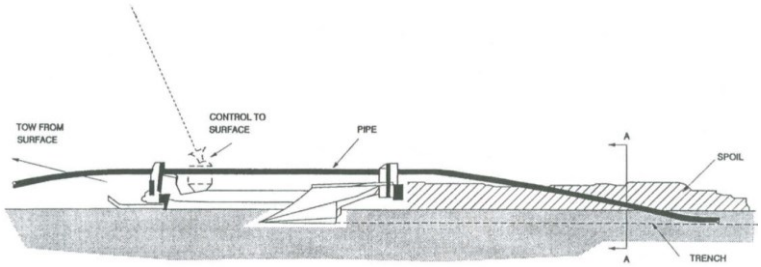

d) Ploughing

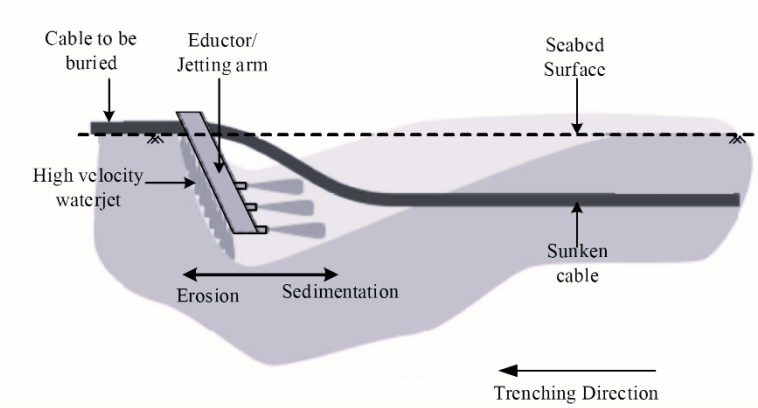

e) Jetting

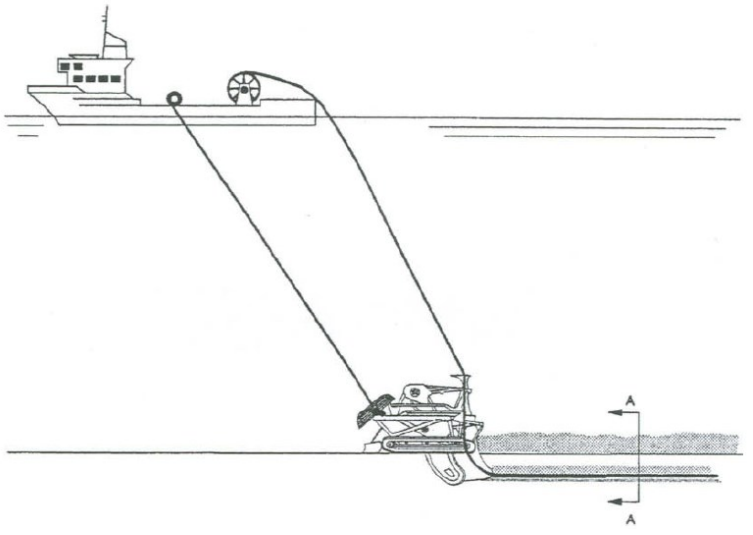

f) Mechanical cutters

Figure 5-2. Trenching methods and their associated equipment; a) Conventional excavation (Jan De Nul Group, 2020); b) CSD (Neumann Dredging, 2024); c) TSHD (van Rhee, 2002); d) Ploughing (Bai & Bai, 2005); e) Jetting (Njock et al., 2020); f) Mechanical cutters (Bai & Bai, 2005)

The study demonstrates a significant impact of the trenching method and geometry on pipeline response during ice gouging. The pipeline, backfill and trench wall interaction plays a crucial role in the pipeline's lateral response against ice gouging. In cases with narrow trenches or zero trench bottom width (as in ploughing), the pipeline interacts with the stiff trench wall earlier, reducing horizontal displacement. However, trenches with shallower wall slopes lead to delayed interaction, increasing pipeline displacement and potentially the risk of damage. These results emphasize the importance of carefully selecting trench configuration to optimize pipeline performance and safety during ice gouging, which could also reduce project costs.

5.2 Numerical Simulation Description

5.2.1 Overview

This study utilizes the Coupled Eulerian-Lagrangian (CEL) method within the Abaqus/Explicit software, employing an explicit time integration approach (Simulia, 2019). The fundamental principle behind CEL is modeling the deforming soil as a Eulerian material. This material can flow through a fixed mesh, allowing the material boundaries and Eulerian volume fraction (EVF, representing the portion of a mesh cell occupied by a material) to change as the simulation progresses. The Eulerian approach views materials (solid and fluid) as continuous media within a control volume divided into discrete grid cells. This contrasts with the Lagrangian approach, which focuses on individual material points, and the mesh distorts their movement. Importantly, using a general penalty-based contact approach, the CEL method enables the simulation of interactions between the soil, ice keel, and pipeline. This allows for significant mesh movements typical of ice gouging events without encountering the mesh distortion, contact problems, or instability issues seen in purely Lagrangian methods.

5.2.2 Utilizing the CEL Method: Model Setup

Ice gouging was simulated using a three-dimensional model with a Coupled Eulerian-Lagrangian (CEL) approach in Abaqus/Explicit. As shown in Figure 5-3, a half-model was utilized to optimize computation. The Eulerian domain, measuring 60 meters in length, 20 meters in half-width, and 17 meters in depth, was discretized using Eulerian elements (EC3D8R). This domain encompassed both the soil medium and a void region, the latter enabling the accurate representation of frontal mound and side berm formation. The ice keel, idealized as a rigid body, was modeled using linear brick elements (C3D8R).

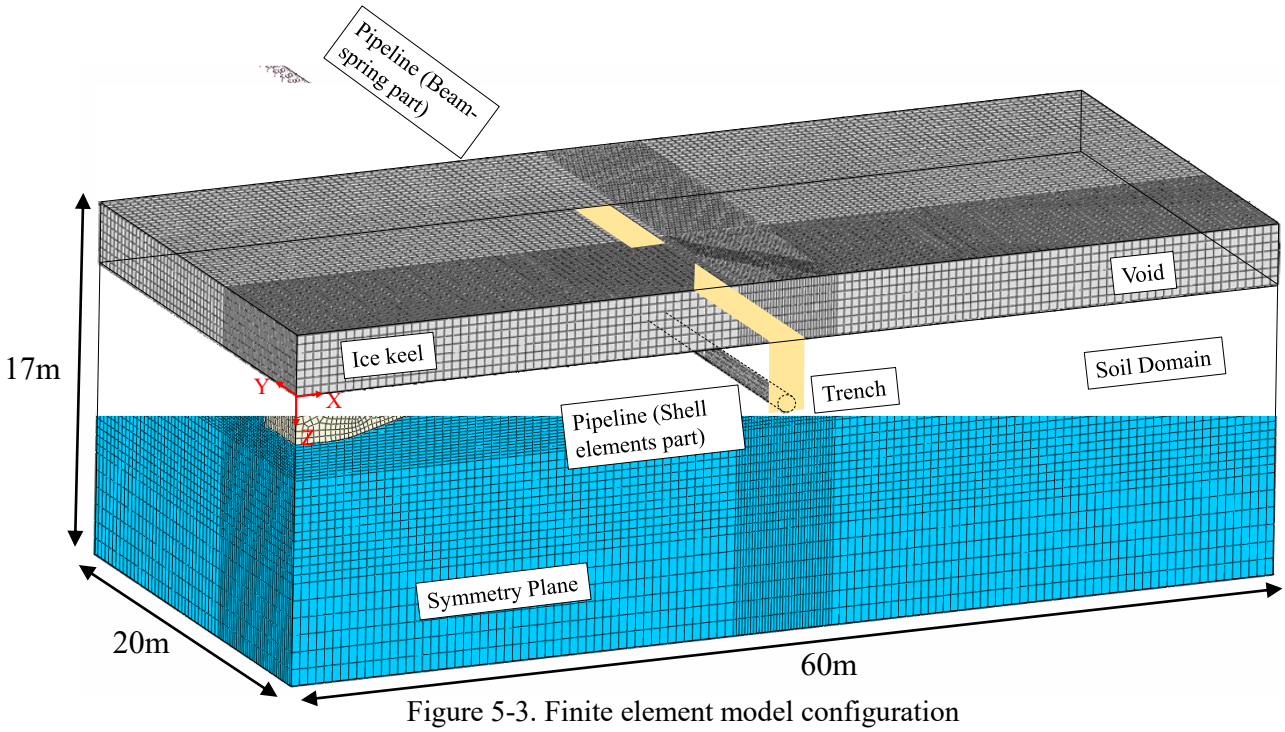

Figure 5-3. Finite element model configuration

A structured finite element mesh, with finer density near the pipeline, was created in Abaqus/CAE (Figure 5-3). Mesh sensitivity analysis determined an optimal size of approximately 0.2m around the pipeline, gradually increasing towards the model boundaries. Boundary conditions were applied to restrict soil movement perpendicular to the domain faces, with boundaries sufficiently far to avoid influencing pipeline response.

The ice keel is modeled to move laterally at 1 m/s without rotation, following Peek and Nobahar (2012) for a balance of computational efficiency and quasi-static behavior. Soil resistance is evaluated from reaction forces at the keel's reference point. The pipeline (0.950 m diameter, 12.7 mm thickness) is buried 3.25 m deep with a 0.35m initial clearance above it. The pipeline is discretized with shell elements (S4R in Abaqus), with 20 elements per cross-section and 0.2m axial length.

The steel pipeline is modeled as an elastoplastic material with isotropic strain hardening (Young's modulus = 205 GPa, Poisson's ratio = 0.3), following the von Mises criterion. The stress-strain relationship is based on Peek and Nobahar (2012). Due to the shallow water conditions, initial hydrostatic pressure and buoyancy are considered negligible. To fully capture the pipeline's axial behavior and account for the effects of axial feed-in, stiffness, and boundary conditions, the pipeline model was extended 5km beyond the soil domain using beam elements (PIPE31H) and Winkler springs (SPRINGA).

The rapid loading associated with an ice gouging event ensures the undrained condition of the soil (Lach, 1996). An elastic-perfectly plastic clay model aligned with the Tresca criterion simulates the seabed soil. Friction and dilation angles are assumed to be zero, and the Poisson's ratio is set to 0.499. Young's modulus is considered constant at $400s_{ui}$ throughout the soil layer.

The contact surface approach within Abaqus/Explicit is used to model the interfaces between the ice, native soil seabed, backfill, and pipeline. A "hard" behavior is defined as normal interaction. The Coulomb friction model simulates the frictional interfaces between the pipeline's outer surface and the soil and between the ice keel and the soil. This study uses friction coefficient values of 0.3 and 1.0 for the soil-ice and soil-pipeline interfaces, respectively. In the case of the pipeline-soil

interface, the surface polarity option is engaged to ensure realistic contact behavior. This means that the pipeline is designated as the "master" surface and the soil as the "slave" surface, preventing soil penetration into the pipeline. Additionally, relative motion at the interface is prevented when the equivalent frictional stress falls below a critical value to account for the potential of sticking behavior between the pipeline and soil. This critical shear stress limit is set to be proportional to the contact pressure and is defined as half of the peak undrained shear strength of the soil.

The analysis is conducted in four steps. The first stage involves inducing geostatic stress. During the second step, the ice keel is lowered to its intended gouge depth, and an internal pressure of 12 MPa is applied to the pipeline's shell elements. However, due to software limitations, an equivalent temperature change is applied to the structural elements instead. In the third step, the temperature of the pipeline's structural and continuum parts is increased by 50°C. Finally, the fourth step involves applying a velocity boundary condition to achieve horizontal displacement of the ice keel.

5.2.3 Strain Softening and Shear Rate Effects

Hashemi and Shiri (2022) highlighted the importance of accounting for these effects when analyzing ice gouging phenomena. To address this in the present study, a specialized user subroutine (VUSDFLD) is utilized within the Abaqus software platform. This subroutine was implemented alongside the empirical Equation proposed by Einav and Randolph (2005).

The VUSDFLD subroutine allowed the model to dynamically modify soil properties based on changing loading rates, resulting in a more realistic representation of soil behavior under the extreme forces caused by ice gouging. To precisely characterize the strain-softening behavior of clay soil, the well-established Equation (5-1) by Einav & Randolph (2005) is utilized, derived from extensive experimental data:

$$s_u = \left[1 + \mu \times \log_{10}\left(\frac{\max(|\dot{\gamma_{max}}|, \dot{\gamma_{ref}})}{\dot{\gamma_{ref}}}\right)\right] \times \left[\delta_{rem} + (1 - \delta_{rem})e^{-3\xi/\xi 95}\right] s_{ui} \quad (5\text{-}1)$$

where:

s_{ui} : The updated undrained shear strength at each time step.

ξ: The current accumulated absolute plastic shear strain.

$\dot{\gamma_{max}}$: Maximum shear strain from the previous time step.

$\dot{\gamma_{ref}}$: The reference shear strain rate (constant).

μ : The rate of shear strength increases per log cycle (constant).

δ_{rem} : Ratio of fully remolded to initial shear strength (constant).

$\xi 95$: The value of accumulated absolute plastic shear strain corresponding to a 95% reduction in the remolded shear strength (constant).

Following recommendations from previous studies (Biscontin & Pestana, 2001; Dayal & Allen, 1975; Graham et al., 1983), 0.1 is selected for the parameter μ. The reference shear strain rate ($\dot{\gamma_{ref}}$) was set to 0.024, aligning with the guidance of Raie and Tassoulas (2009). For typical soft marine clays, a $\xi 95$ value of 12 is determined, falling within the 10-25 range suggested by Randolph (2004) for soils with varying sensitivities. The exact value of $\xi 95$ would depend on the specific soil sensitivity of the seabed.

5.3 Validation of Numerical Models

Validation of the developed model was conducted through comparison with experimental results obtained from geotechnical centrifuge tests performed by Lach (1996). Unlike full-scale tests, centrifuge tests offer the advantage of accurate reproducibility, allowing for a controlled

examination of the effects of subtle design variations (Schoonbeek and Allersma, 2006). Additionally, centrifuge testing enhances the representation of soil behavior under realistic stress conditions due to the increased gravity loading.

In this study, the horizontal subgouge soil displacement and ice keel/soil reaction forces predicted by the CEL model were compared with the PRISE empirical equation (Phillips et al., 2005) and data from Lach's centrifuge tests. Soil parameters, scour dimensions, keel geometry, attack angles, and scour speed were closely matched between the model and the reference data. Elastic modulus were estimated based on reasonable assumptions, aligning with the methodology of Pike and Kenny (2016).

Figure 5-4 compares the subgouge deformation predicted by the CEL model with those measured from PRISE centrifuge tests, while Figure 5-5 compares the ice keel reaction forces from the CEL model and Lach's centrifuge test, demonstrating a strong correlation between the model predictions and experimental data after reaching steady-state conditions

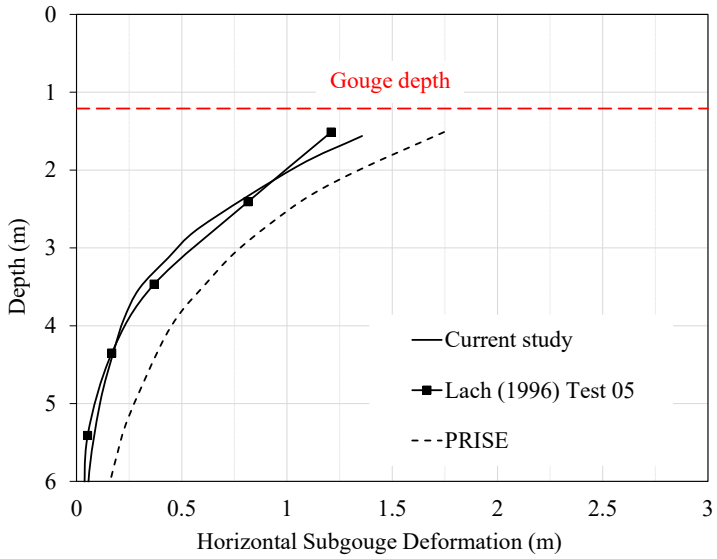

Figure 5-4. The comparison of the soil horizontal subgouge deformations

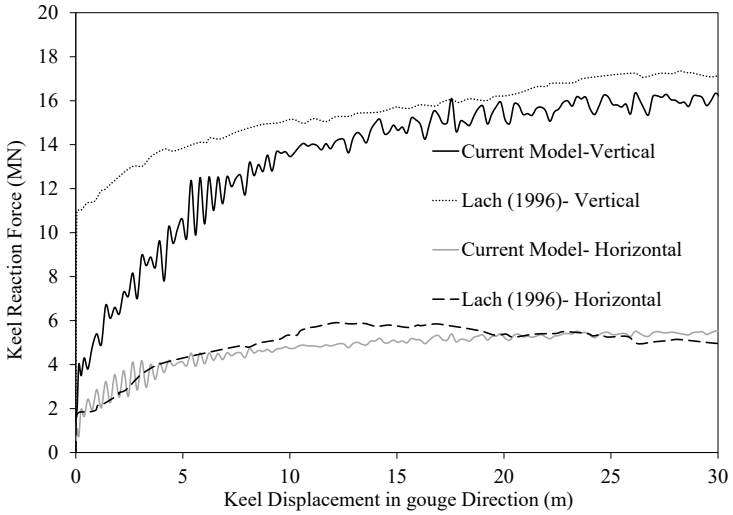

Figure 5-5. The comparison of reaction forces

This validation study demonstrates the CEL model's effectiveness in accurately estimating horizontal soil subgouge displacement and ice keel reaction forces in ice gouging scenarios.

5.4 Critical Limits for Structural Integrity of Buried Pipelines

When buried pipelines experience significant soil deformations associated with ice gouging events, their design must accommodate three primary failure modes to ensure structural integrity. These are tensile yielding, local buckling, and local collapse, as defined within existing literature and design codes.

Tensile Yielding: Excess tensile strain can lead to pipe rupture. To prevent this, the DNVGL-ST-F101 (DNV, 2017) standard specifies a maximum allowable axial tensile strain of 2.00%.

Local Buckling: Compressive loads can cause the pipeline wall to buckle either laterally or radially. To evaluate this risk, the maximum compressive strain must be compared to a critical compressive strain value. Design codes like CSA Z662 (2015) provide formulas to calculate this critical compressive strain (ε_c^{crit}), shown in Equations (5-2) and (5-3).

$$\varepsilon_c^{crit} = 0.5\frac{t}{D} - 0.0025 + 3000\left(\frac{(p_i - p_e)D}{2Et}\right)^2 \quad \text{for } \frac{(p_i - p_e)D}{2tf_y} < 0.4 \quad (5\text{-}2)$$

$$\varepsilon_c^{crit} = 0.5\frac{t}{D} - 0.0025 + 3000\left(\frac{0.4f_y}{E}\right)^2 \quad \text{for } \frac{(p_i - p_e)D}{2tf_y} \geq 0.4 \quad (5\text{-}3)$$

where p_i and p_e are the maximum internal and external pressure, f_y is the effective specified yield strength, E is Young's modulus of elasticity, and t is the pipeline wall thickness.

Ovalization Failure: Ice gouging events can result in ovalization – the deformation of the pipeline's cross-section. The DNV (2017) standard limits acceptable ovalization to 3%, beyond which stress concentrations and instability issues increase the risk of failure. The ovalization parameter is calculated using Equation (5-4).

$$f_0 = \frac{D_{max} - D_{min}}{D_{nominal}} \leq 0.03 \quad (5\text{-}4)$$

where D_{max} is the maximum outer diameter of the pipe, D_{min} is the minimum outer diameter of the pipe, and $D_{nominal}$ denotes the nominal (intended) outer diameter of the pipe. These criteria are essential for designing subsea pipelines that can withstand the extreme forces and deformations associated with ice gouging environments.

5.5 Case Studies

A series of six case studies (Case-1 to Case-6) were conducted to explore the influence of trench geometry, and by extension, trenching technique, on the pipeline response during ice gouging. These analyses held backfill stiffness constant to isolate the effects of trench shape. The numerical models incorporated pipeline layout and backfill properties derived from Paulin's (1998) T2P1 centrifuge test.

Equation (5-5) defined the profile of native soil in-situ undrained shear strength (where Z is the depth from the seabed). Based on this Equation, the undrained shear strength at the pipeline springline depth is 40 kPa. The native seabed soil unit weight was set at 19.12 kN/m3. A constant gouge depth of 2.9m was assumed for all cases.

$$s_u\ (kPa) = (Z + 9.8) \times 3 \qquad (5\text{-}5)$$

Six distinct trench shapes were investigated, including three rectangular profiles, two trapezoidal profiles, and one triangular profile (details in Table 5-1). A schematic representation of these cases is presented in Figure 5-6.

Table 5-1. Parametric study layout

Case No.	Trench wall angle, α (degree)	Trench bottom width, W (m)	Attributed trenching technique
Case 1	90	2.5	Jetting
Case 2	35	0	Ploughing (Jukes et al., 2011)
Case 3	45	2.5	Mechanical Trenching (Cheng et al., 2021)
Case 4	64	2.5	Dredging (Cheng et al., 2021)
Case 5	90	2	Jetting
Case 6	90	3	Jetting

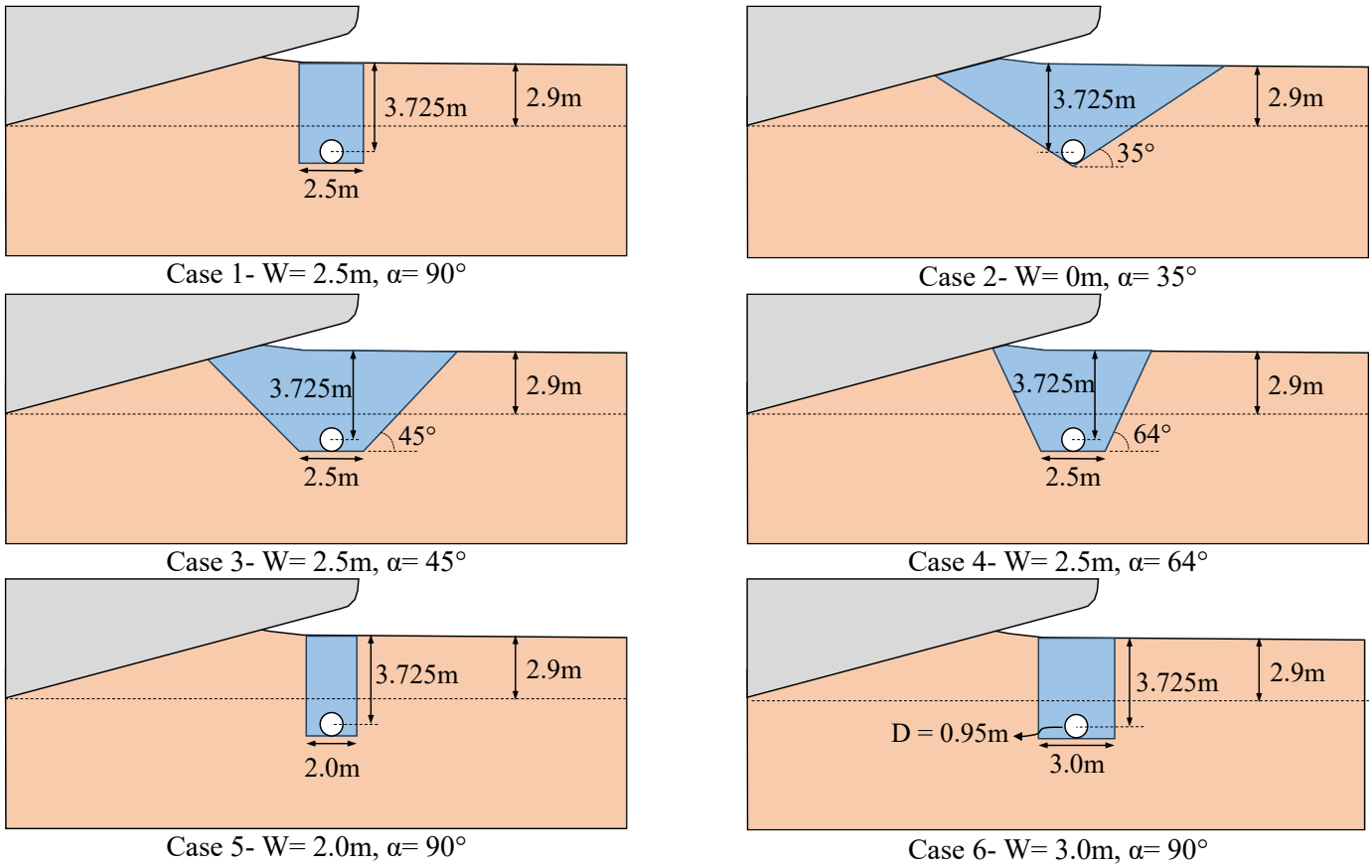

Figure 5-6. Schematics of configurations of Cases 1-6

For each case, the following key parameters were analyzed and compared:

- Soil displacement mechanisms
- Horizontal and vertical ice keel reaction forces
- Pipeline displacement, strains, stresses, and ovalization.

5.6 Results and Discussions

5.6.1 Trench Geometry Effect

Cases 1 to 4 were examined to assess the impact of trench geometry specifically.

5.6.1.1 Soil Displacement Mechanisms

Examining soil movement patterns across all case studies indicates variations in how the seabed and trench geometry responds to ice gouging. These variations consequently influence the

pipeline-backfill-trench wall interaction to this phenomenon. Figure 5-7 presents the initial location of the ice keel at its designated gouge depth. Three sets of tracer particles are employed to visualize the subgouge soil displacements (depicted by the red dots in Figure 5-7). The first set is placed 5 meters ahead of the pipeline centerline, the second set is located directly in front of the pipeline, and the third set is positioned 5 meters behind the pipeline centerline.

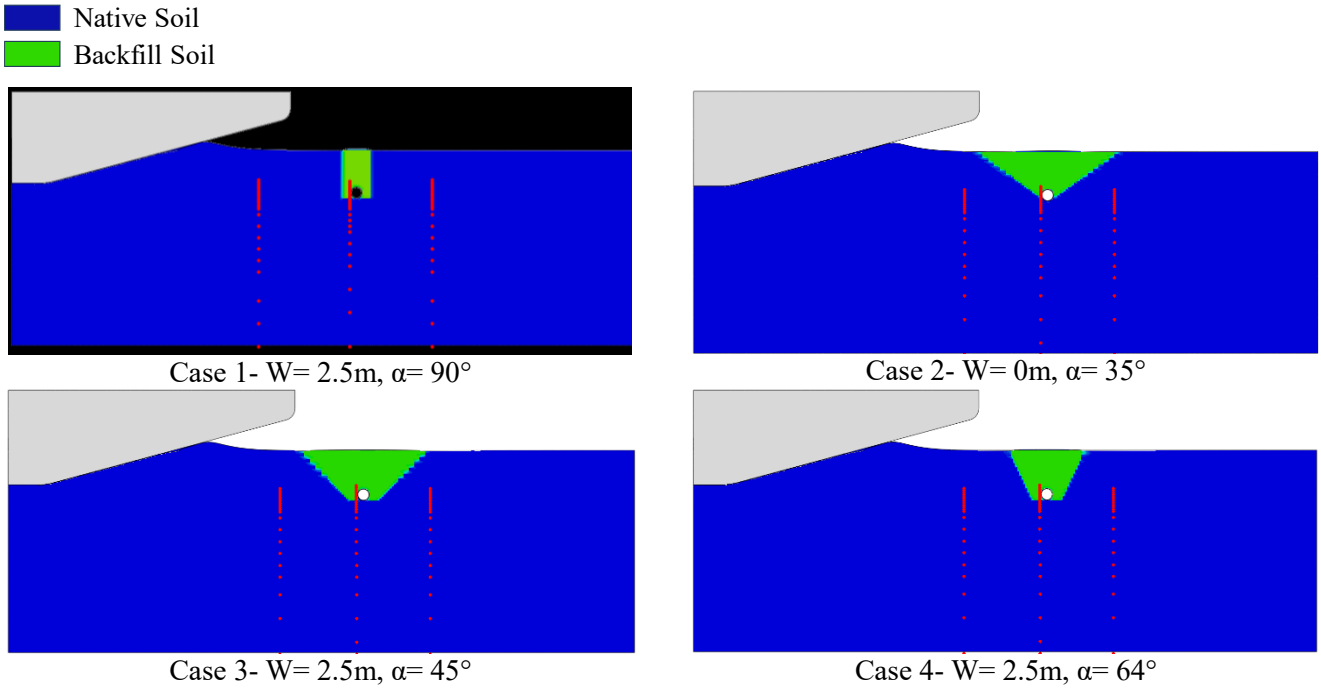

Figure 5-7. Position of soil, pipeline, ice, and tracer particles at the threshold of horizontal movement of the ice keel

Figures 5-8 to 5-10 illustrate the sequential stages of the ice keel's advance towards the pipeline. As the ice keel initiates movement within the native soil, it generates stress and strain in the seabed, causing horizontal subgouge displacements. The model subsequently reaches a steady-state condition characterized by stable soil features, including berms, frontal mounds, and a consistent subgouge soil deformation profile. During this steady state, the forces resulting from ice-soil interaction remain constant. However, Figure 5-8 demonstrates that the presence of backfill material disrupts this steady state. As the ice keel nears the pipeline, the induced horizontal stresses

and strains cause the native soil to exert pressure on the trench walls. The interaction between the soft backfill and stiff trench walls causes the backfill to be compressed and displaced upwards. This effect is most pronounced in cases with high wall angles, such as Case 1 (α= 90°) and Case 4 (α= 64°). As a result, the ice gouge's symmetry plane exhibits a significant replacement of backfill material with native soil. Cases 2 and 3, with moderate wall angles, show a less noticeable occurrence of this mechanism.

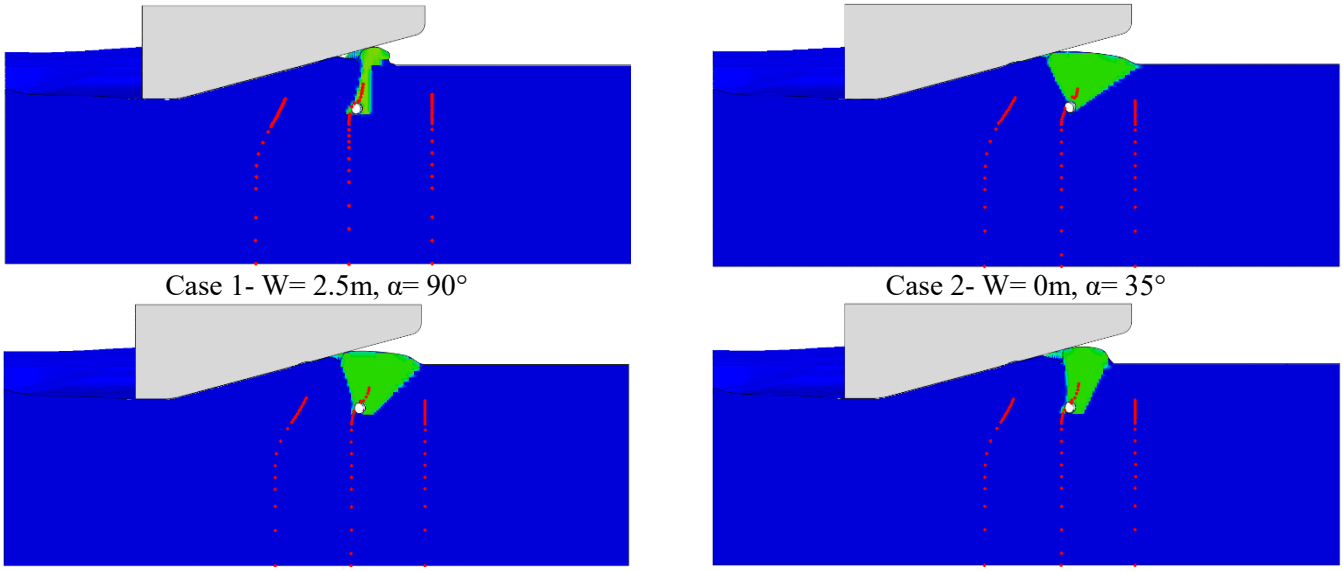

Case 1- W= 2.5m, α= 90°

Case 2- W= 0m, α= 35°

Case 3- W= 2.5m, α= 45°

Case 4- W= 2.5m, α= 64°

Figure 5-8. Position of soil, pipeline, ice, and tracer particles at time step 12s

The interaction between the pipeline, backfill, and trench walls is evident in Figure 5-9, which shows significant deformation of the left trench wall at a simulation time of 17 seconds. The right wall is also impacted in all cases. As the pipeline moves laterally, it interacts with the right trench wall and the native soil, leading to varying degrees of backfill displacement. Notably, in Case 2, lacking a bottom trench width, the pipeline is almost entirely covered by native soil. In contrast, the remaining cases retain some backfill material on the right side.

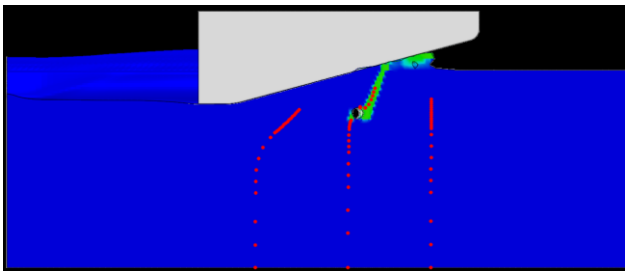

Case 1- W= 2.5m, α= 90°

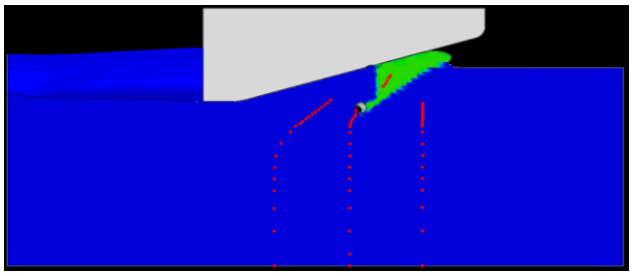

Case 2- W= 0m, α= 35°

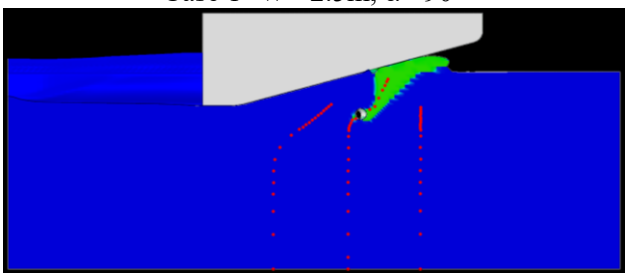

Case 3- W= 2.5m, α= 45°

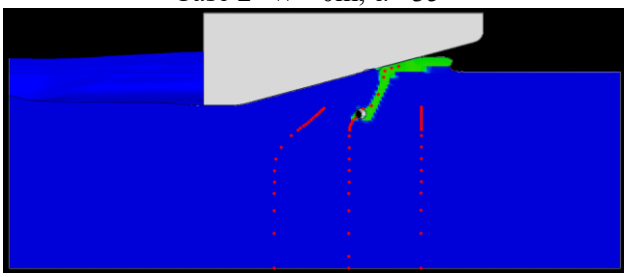

Case 4- W= 2.5m, α= 64°

Figure 5-9. Position of soil, pipeline, ice, and tracer particles at time step 17s

Figures 5-10 depict the progressive removal of backfill material as the ice keel advances over the pipeline. The initial backfill boundaries are significantly depleted, with only a small amount remaining around the pipe's midsection. Consequently, within the ice gouge's symmetry plane, a substantial portion of the backfill is gradually displaced from the trench and replaced by native soil. The lower half of the pipeline acts as a barrier, partially restricting the backfill's complete removal from the trench.

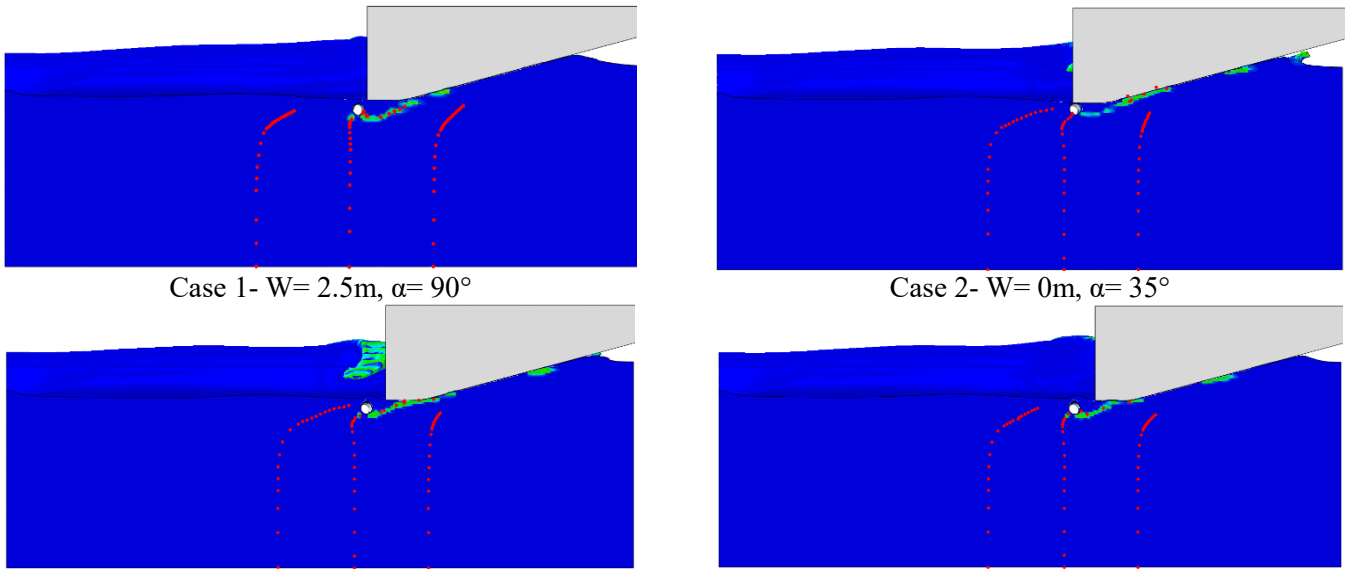

Case 1- W= 2.5m, α= 90°

Case 2- W= 0m, α= 35°

Case 3- W= 2.5m, α= 45°

Case 4- W= 2.5m, α= 64°

Figure 5-10. Position of soil, pipeline, ice, and tracer particles at time step 32s

The backfill soil removal mechanism weakens and diminishes beyond the centerline of the ice gouge (see Figure 5-11). Analysis indicates a direct correlation between increasing trench wall angle and the intensity of the pipeline-backfill-trench wall interaction, leading to more pronounced backfill removal. This results in an increase in the transverse distance of backfill ejected from the trench. This distance ranges from 1.7-2.5 times the ice keel width (Y).

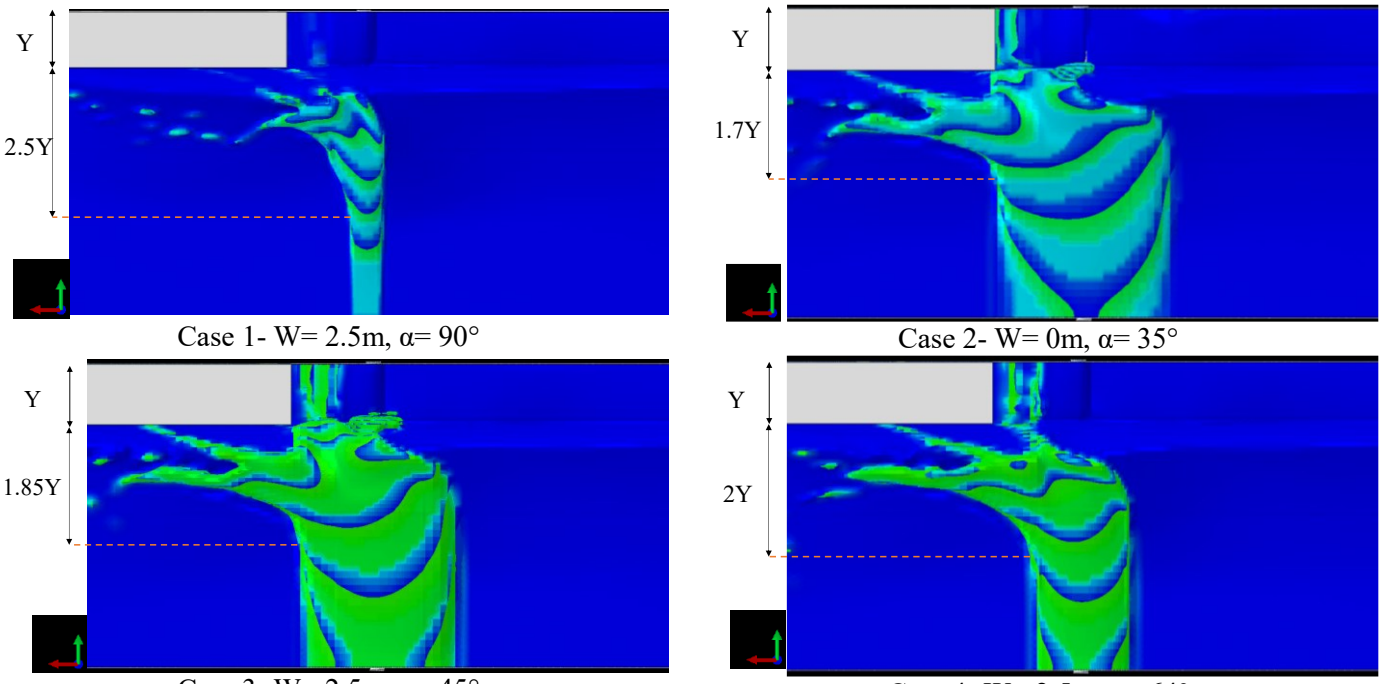

Figure 5-11. A top view of the ice keel after the ice keel passes through the trench (half model)

Figure 5-12 compares the distribution of equivalent plastic shear strains (PEEQVAVG) with developing frontal mounds, side berms, and interactions within the pipeline, backfill and trench. Despite variations in trench configuration, the maximum plastic shear strain pattern remains consistent during the ice gouging process.

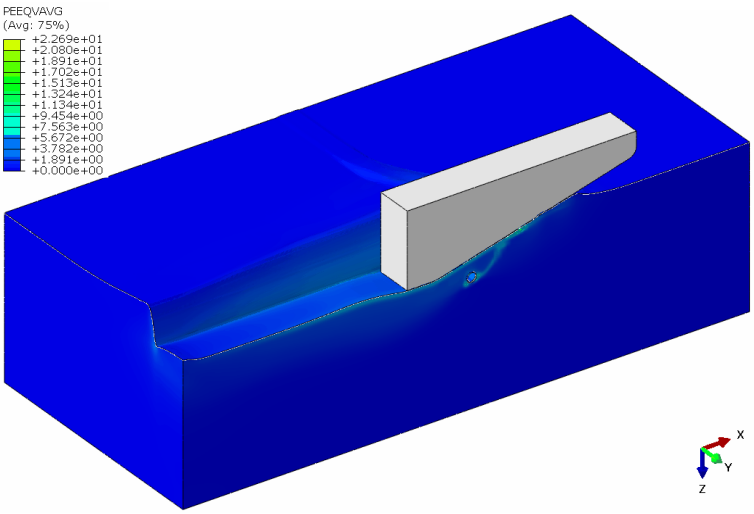

Case 1- W= 2.5m, α= 90°

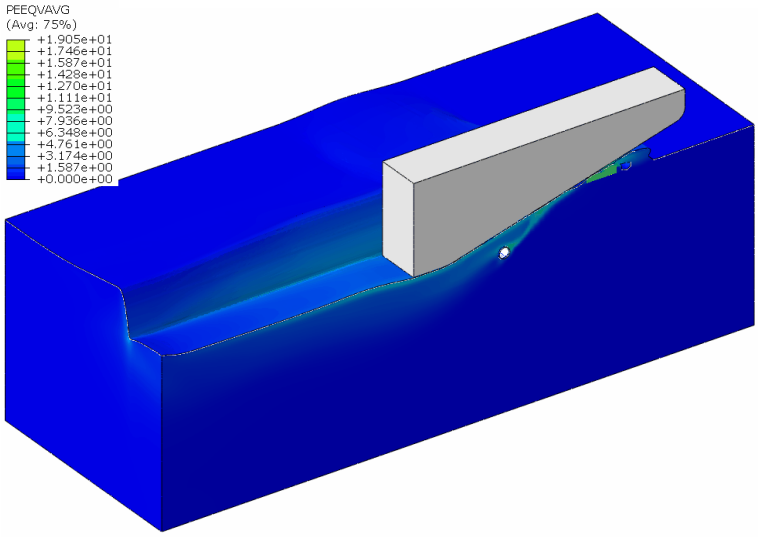

Case 2- W= 0m, α= 35°

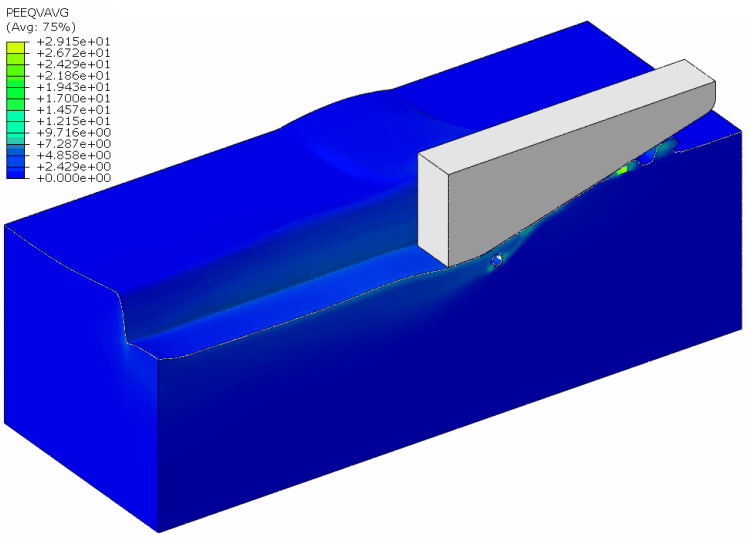

Case 3- W= 2.5m, α= 45°

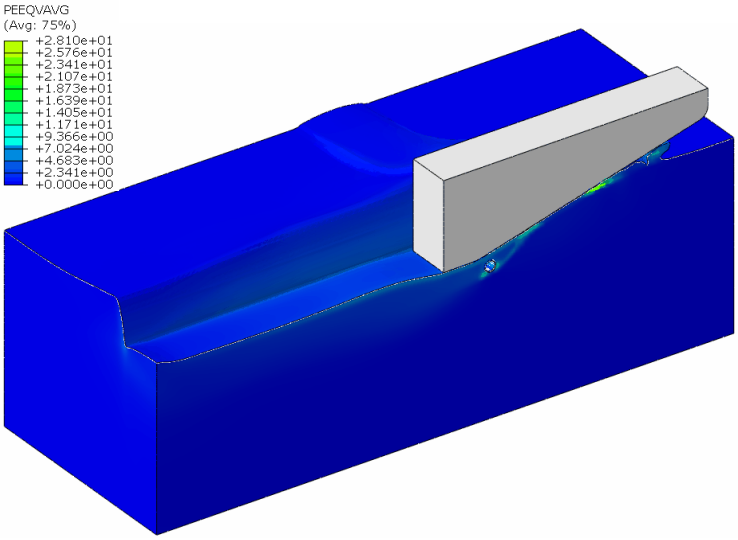

Case 4- W= 2.5m, α= 64°

Figure 5-12. The effect of gouging in different trench configurations on progressive plastic shear strain (time step 26s)

The figures demonstrate a primary concentration of maximum plastic shear strain within the backfill material, the area surrounding the pipeline, contact zones between the ice keel's chest and the frontal mound, and the interface between the keel's base and the underlying soil. An examination of cases 1, 3, and 4 indicates a correlation between increasing trench wall angle (at a fixed width) and a decrease in maximum plastic shear strains.

5.6.1.2 Ice Keel Reaction Forces

Figure 5-13 illustrates the horizontal and vertical reaction forces between the ice keel and the seabed. The ice gouging process exhibits an initial steady-state period where forces primarily result from the ice-native soil interaction. As the ice keel approaches the trench, deviations in the force profiles become apparent. Notably, Case 3 (W=2.5m, α=45°) demonstrates a more noticeable decrease in reaction forces at a displacement of 15m compared to other cases.

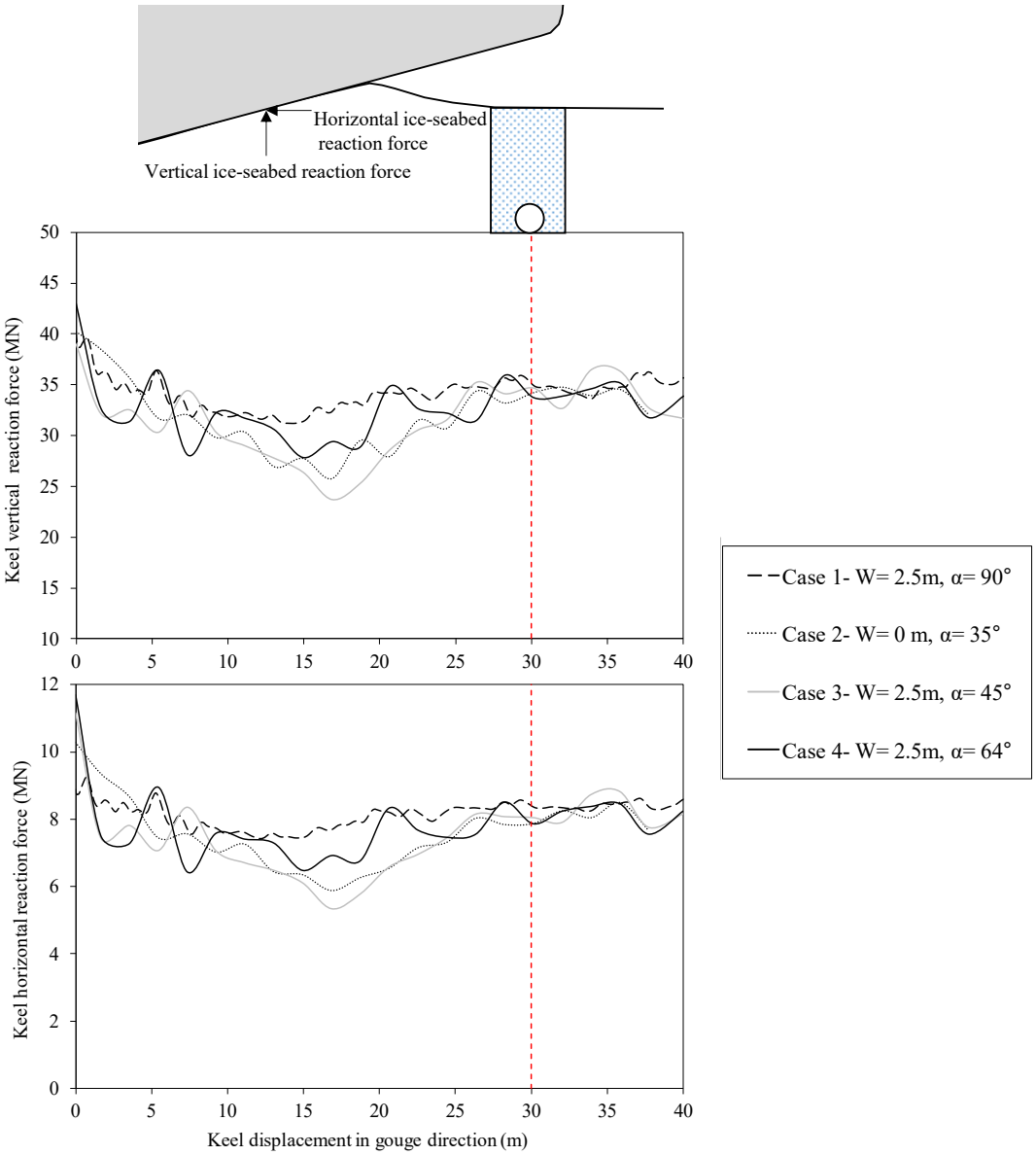

Figure 5-13. Ice keel-seabed reaction forces

This reduction can be ascribed to the larger cross-sectional area in Case 3 and the substantial presence of very soft backfill resulting in this decline. As the trench is filled with displaced native soil, the forces re-establish a steady-state condition. Following the ice keel's passage beyond the trench, all cases converge to the initial steady-state force values.

5.6.1.3 Pipeline Response

Figure 5-14 illustrates the typical pipeline displacement path during ice gouging. Initially, the pipeline moves upward and towards the gouge as the ice keel approaches. This culminates in maximum displacement when the ice reaches the pipeline's top (point 2). This upward movement is due to the soil's lower resistance to uplift, while horizontal movement results from ice-induced stresses. As the ice keel passes, the pipeline partially recovers, settling into a rebound state (point 3).

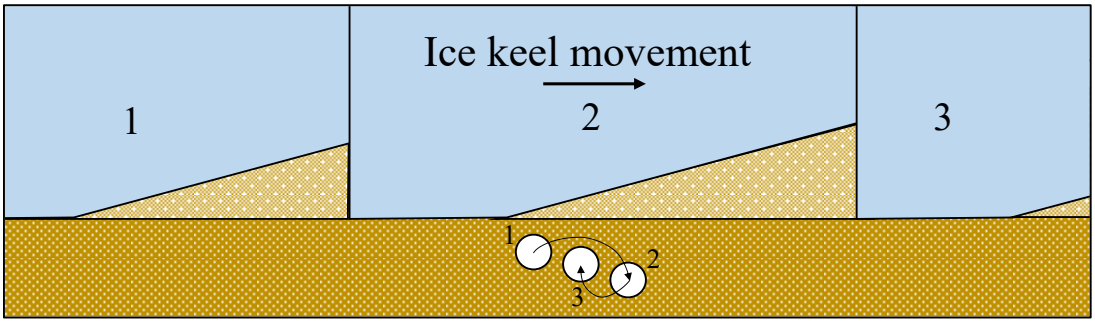

Figure 5-14. Characteristic trajectory of a pipeline during an ice gouging event (not to scale)

Figure 5-15 compares the pipeline trajectories within the vertical plane along the gouge centerline. In Cases 1, 2, and 4, where trench width is constant (W= 2.5m), a decrease in trench wall angle results in a shift towards more significant horizontal and upward pipeline displacement. This is because lower angles increase the proportion of soft backfill material in the pipeline's horizontal path, delaying interaction with the right stiff trench wall. In Cases 1 (W= 2.5m, α= 90°) and 4 (W=

2.5m, α= 64°), the backfill removal mechanism leads to a rapid replacement with native soil above the pipe, restricting its upward movement.

Case 2 (W= 0m, α= 35°) exhibits distinct behavior. The zero-width trench base causes immediate pipeline interaction with the trench wall, limiting horizontal displacement. However, due to the backfill's low uplift resistance, significant upward displacement of the pipeline is observed. Additionally, Figure 5-15 suggests a direct correlation between the downward force exerted by the ice and the resulting upward movement of the pipeline.

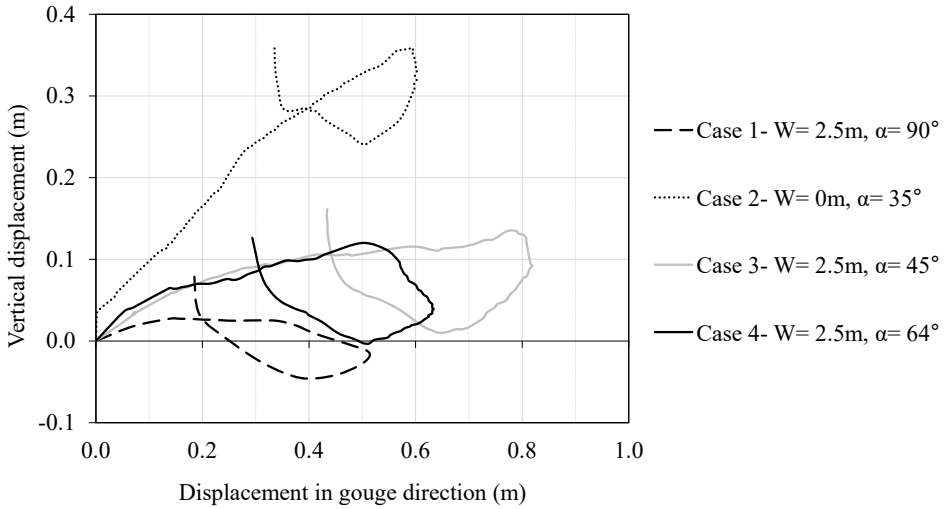

Figure 5-15. Pipeline trajectory in the vertical plane at gouge centerline

The pipeline displacement along the longitudinal axis of the pipeline, including the horizontal, axial, and vertical directions, is illustrated in Figure 5-16 (maximum displacement state). Figure 5-16(a) shows that the maximum displacement, as seen in Figure 5-14, belongs to Case 3 (W= 2.5m, α= 45°). Regarding the pipe horizontal displacement, the interaction between the pipeline, backfill, and trench wall is the main effect. Figure 5-16(b) shows that changing the geometry of the trench has no significant effect on the axial displacement of the pipe. This result seems reasonable since the pipe is in contact with the backfill soil for most of its length. Figure 5-16(c) also shows that the vertical displacement during the maximum displacement of the pipe in the

middle section is not much different in cases with a constant width of 2.5 meters. In Case 2 (W= 0m, α= 35°), the upward displacement is much higher due to the low uplift resistance of the backfill soil. Figure 5-17 depicts the pipeline deflection and displacement vectors in a front view, corresponding to the state of maximum displacement.

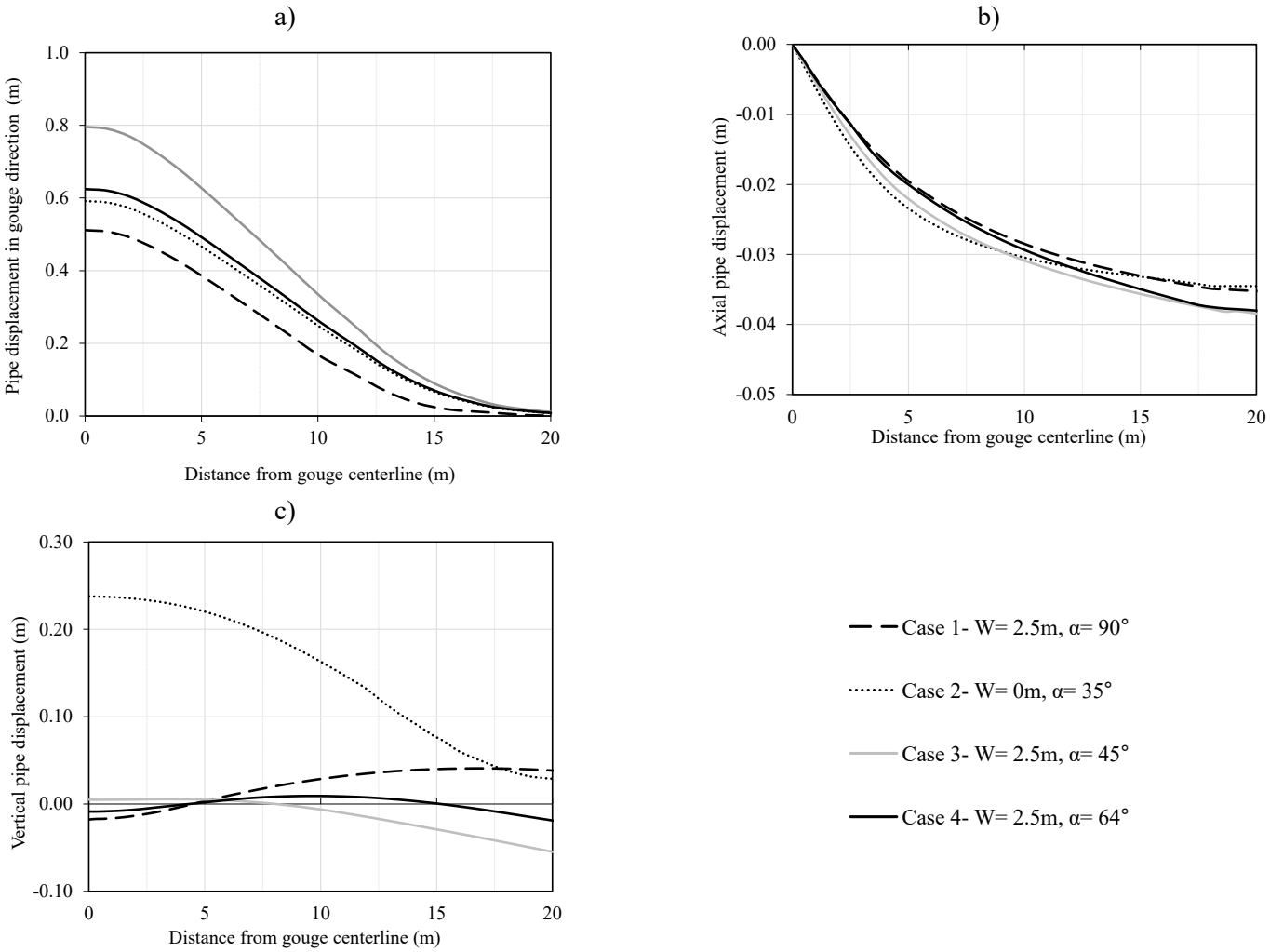

Figure 5-16. Pipeline displacement along the pipeline axis during the maximum displacement state, including (a) horizontal (gouge motion), (b) axial, and (c) vertical directions

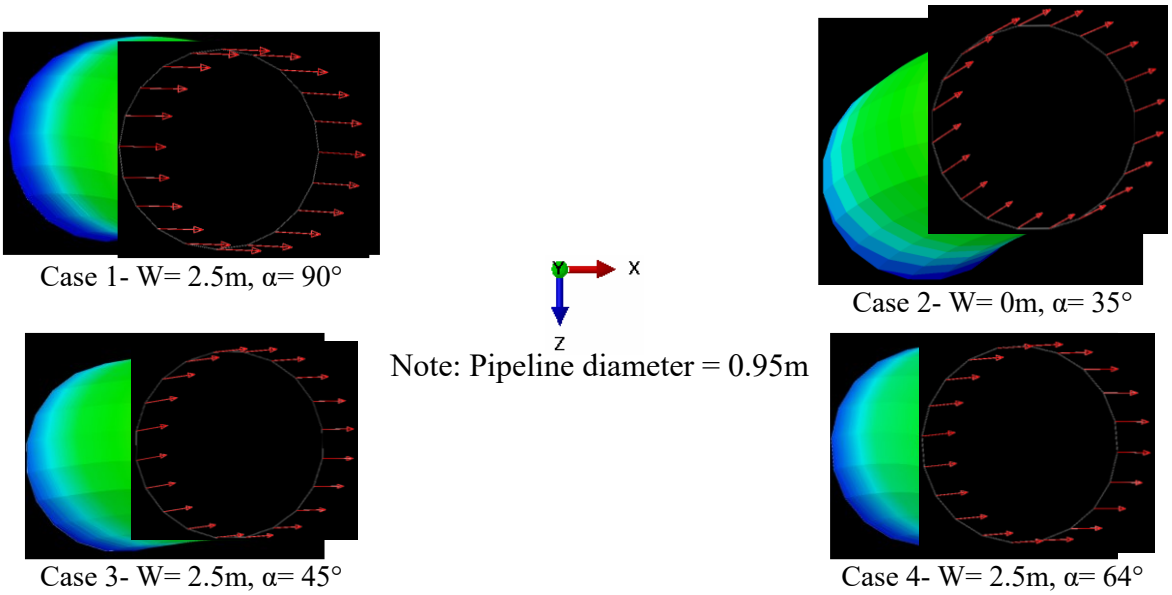

Figure 5-17. Pipeline deflection and displacement vectors at its max. displacement state from the front view

The deformed shape and stress contour of the pipeline under four different trench configurations have been presented in Figure 5-18. Case 2 (W= 0m, α= 35°) experiences stress levels higher than the other cases due to higher pipe deflection and bending stress. In the rest of the cases, there is no significant difference in stress distribution and the maximum value of stress.

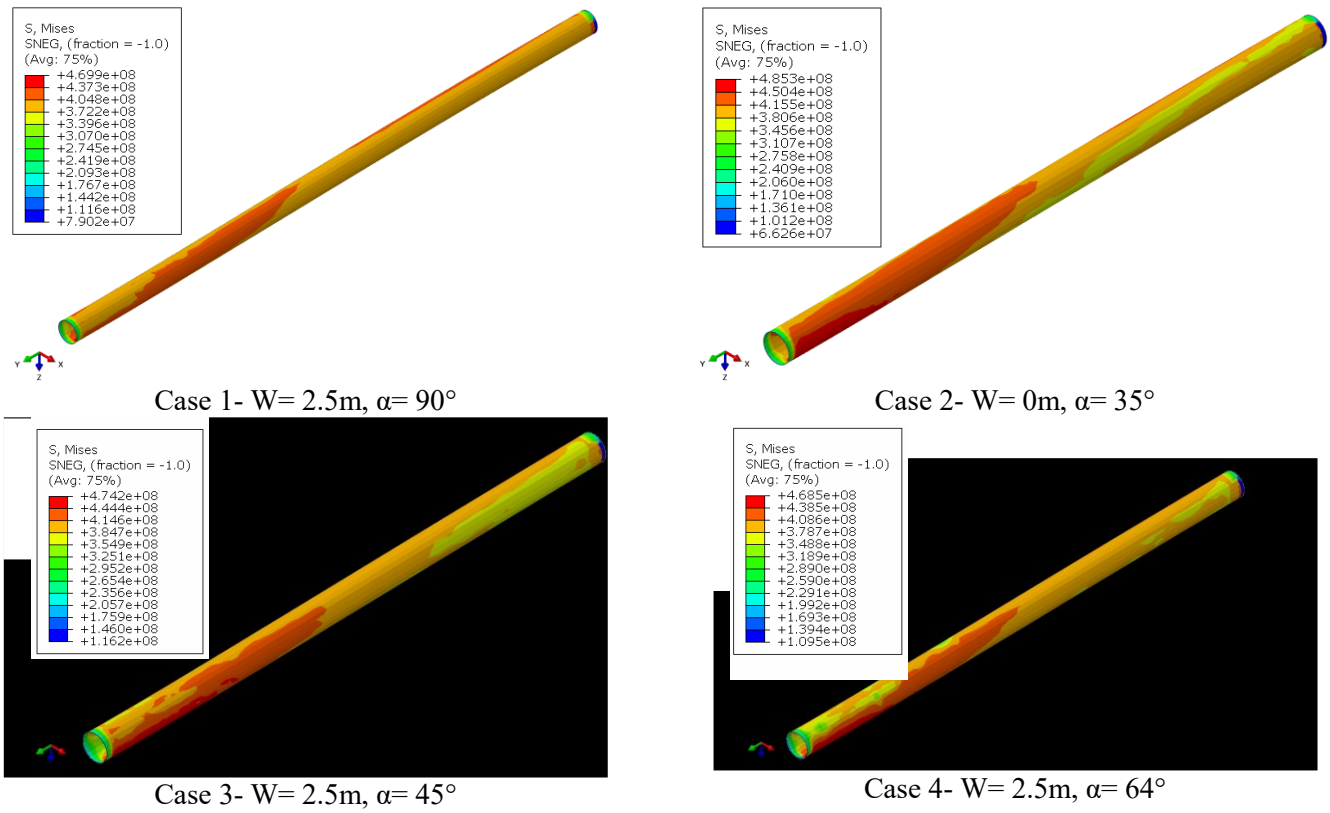

Case 1- W= 2.5m, α= 90°

Case 2- W= 0m, α= 35°

Case 3- W= 2.5m, α= 45°

Case 4- W= 2.5m, α= 64°

Figure 5-18. Stress distribution on deformed shapes of pipeline

Figures 5-19 and 5-20 illustrate the maximum axial strain distribution along the pipeline's axis caused by the ice gouging load. The results demonstrate that the pipeline's trailing face experiences tensile strain. Consistent with the findings related to axial displacement, trench geometry appears to have a negligible effect on the pipeline's axial strain.

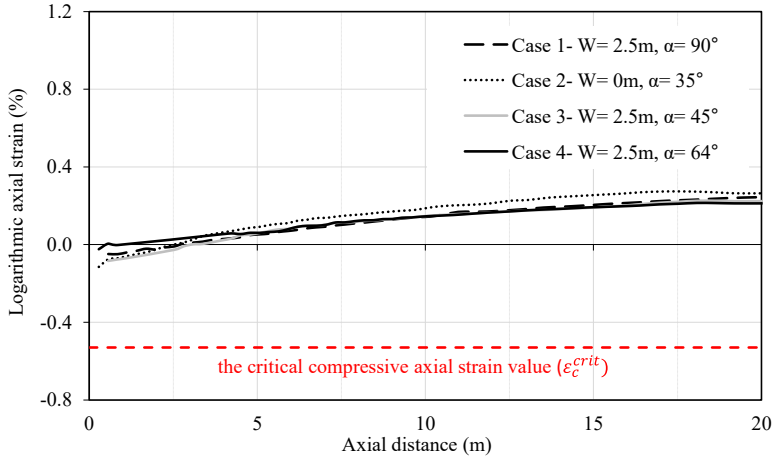

Figure 5-19. Logarithmic axial strain for the leading edge of the pipeline along the axis

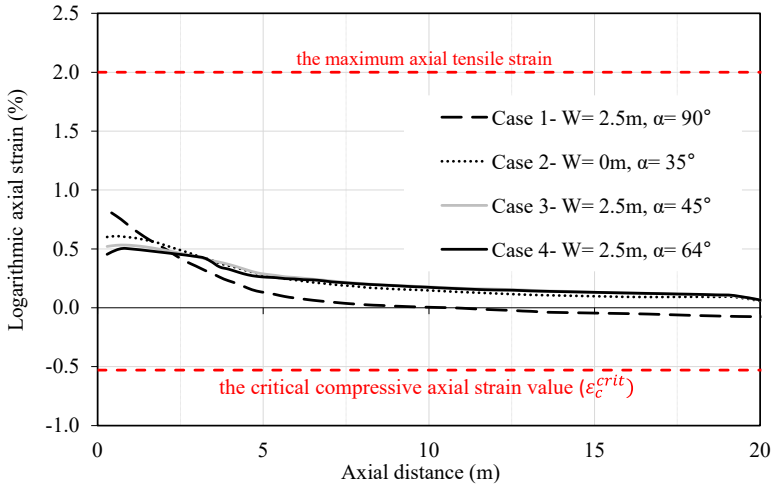

Figure 5-20. Logarithmic axial strain for the trailing edge of the pipeline along the axis

This investigation includes an analysis of pipeline ovalization, as depicted in Figure 5-21. Pipeline ovalization can result from a combination of factors, including internal pressure and temperature during the analysis initialization and external loading exerted by the advancing ice keel. Deviations in the magnitude and distribution of strain across the pipeline's circumference lead to an irregular ovalization pattern. The surrounding soil properties influence the specific distribution of strain. However, as Figure 5-21 presents, trench geometry does not significantly impact pipeline ovalization along its longitudinal axis.

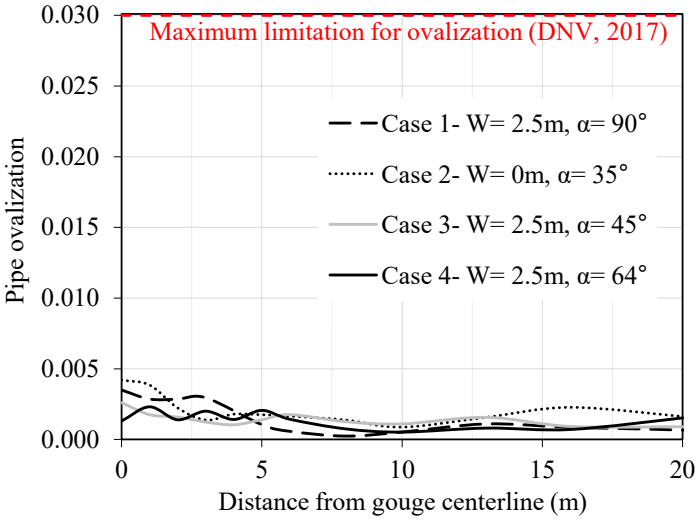

Figure 5-21. Pipeline ovalization along the pipe axis

The observed variations in pipeline displacement, strains, stresses, and ovalization across different trench geometries demonstrate the significant influence of trench design on pipeline response to ice gouging.

5.6.2 Trench Width Effect

Cases 1, 5, and 6 were analyzed to understand the influence of trench width.

5.6.2.1 Soil Displacement Mechanisms

Figure 5-22 illustrates the initial position of the ice keel at its designated gouge depth, along with the tracer particles and the original trench boundaries.

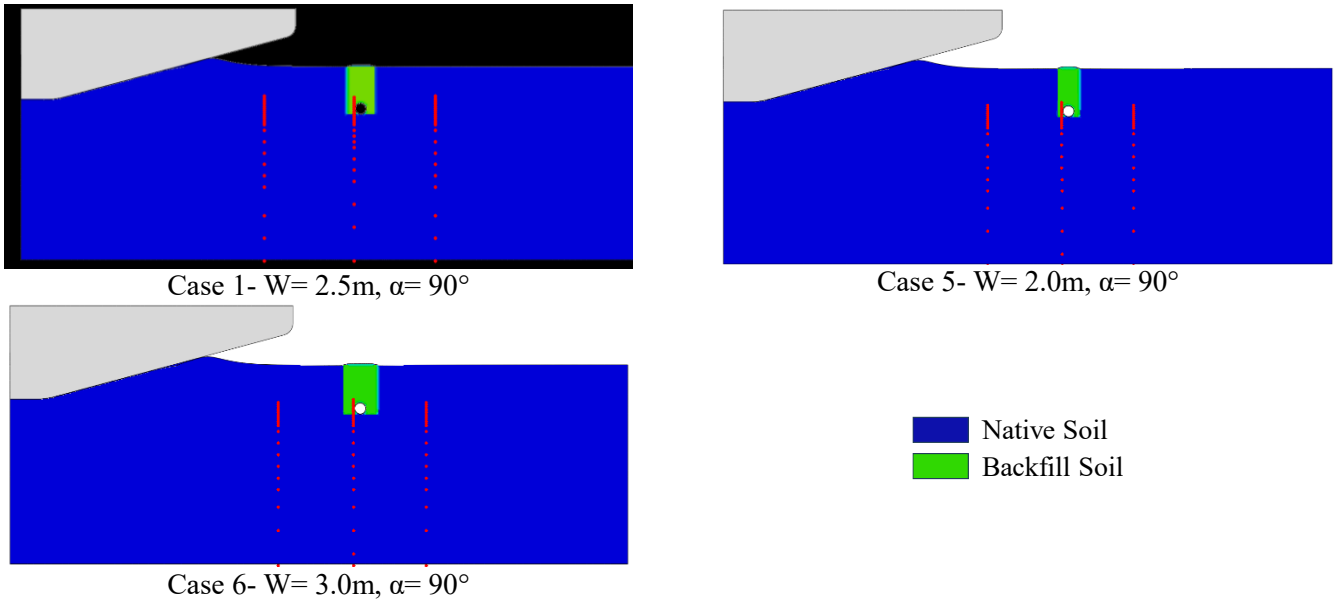

Figure 5-22. Position of soil, pipeline, ice, and tracer particles at the threshold of horizontal movement of the ice keel

The interaction between backfill and trench walls plays a pivotal role in backfill removal as the ice keel approaches the trench. This progressive removal mechanism is evident in all three cases (Figure 5-23). At 16 meters from the pipeline and 12 seconds into the simulation, the left trench wall undergoes complete deformation due to the native soil's pressure, while the right wall remains intact. This interaction results in the observed backfill removal from the trench.

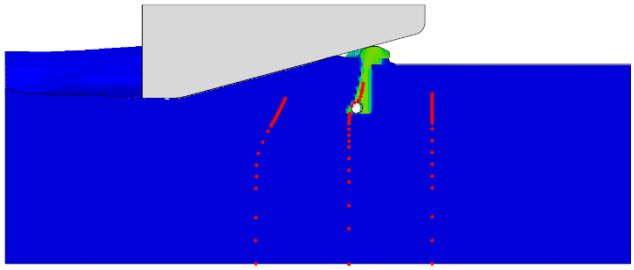

Case 1- W= 2.5m, α= 90°

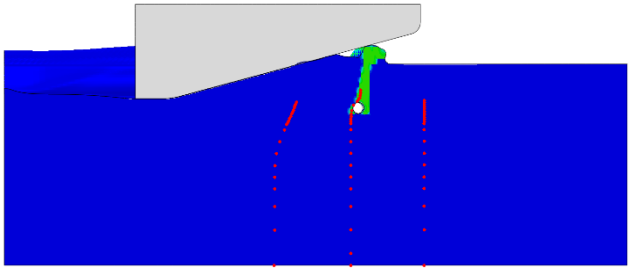

Case 5- W= 2.0m, α= 90°

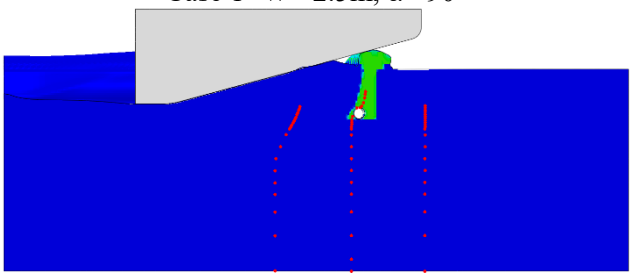

Case 6- W= 3.0m, α= 90°

Figure 5-23. Position of soil, pipeline, ice, and tracer particles at time step 12s

The narrower trench width in Case 5 (W = 2.0m) leads to the earliest onset of right wall degradation (Figure 5-24), causing the pipeline to interact with the trench wall sooner than in wider trench scenarios.

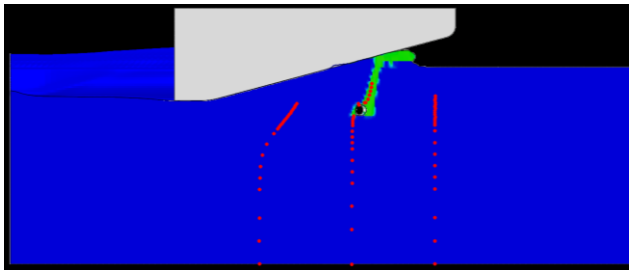

Case 1- W= 2.5m, α= 90°

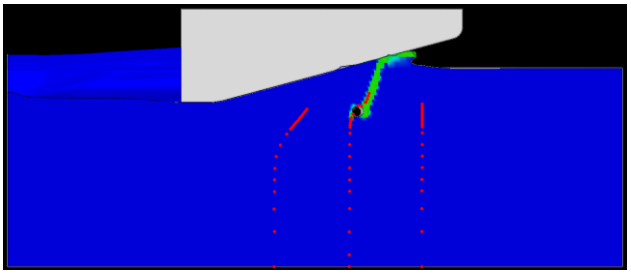

Case 5- W= 2.0m, α= 90°

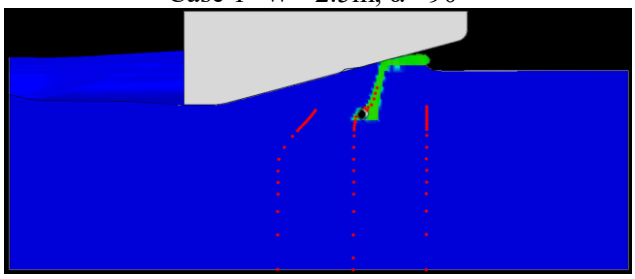

Case 6- W= 3.0m, α= 90°

Figure 5-24.Position of soil, pipeline, ice, and tracer particles at time step 15s

By a time step of 17 seconds (Figure 5-25), Cases 1 (W = 2.5m) and 6 (W = 3.0m) display a replacement of backfill material with native soil at the top and left side of the pipeline. In all three

cases, the right trench wall deflects, and backfill is only present on the right side of the pipe. At this point, the pipeline interacts with both backfill and native soil.

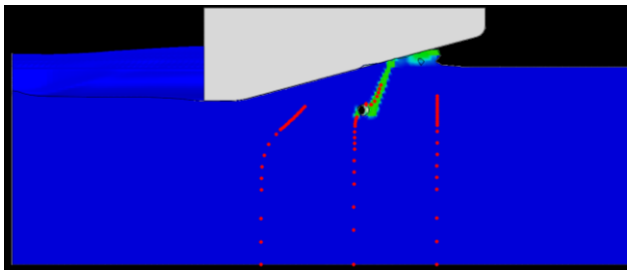

Case 1- W= 2.5m, α= 90°

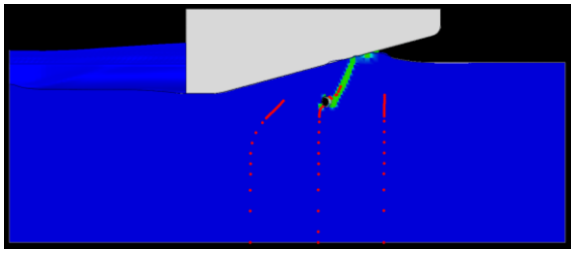

Case 5- W= 2.0m, α= 90°

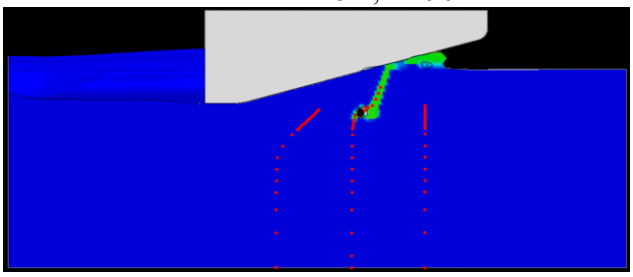

Case 6- W= 3.0m, α= 90°

Figure 5-25. Position of soil, pipeline, ice, and tracer particles at time step 17s

Finally, upon the ice keel's complete passage beyond the initial trench location, all backfill material exits the trench, and the pipe becomes surrounded by native soil (Figure 5-26).

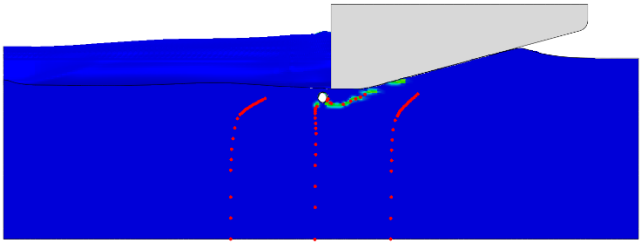

Case 1- W= 2.5m, α= 90°

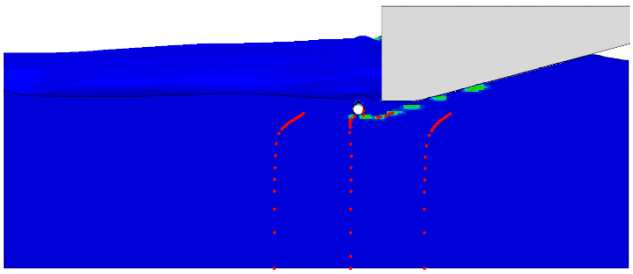

Case 5- W= 2.0m, α= 90°

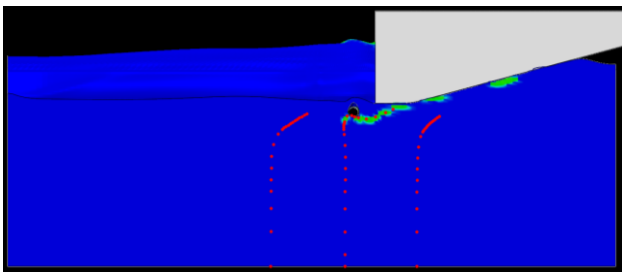

Case 6- W= 3.0m, α= 90°

Figure 5-26. Position of soil, pipeline, ice, and tracer particles at time step 32**s**

Beyond the ice gouge centerline, the backfill-trench wall interaction lessens, decreasing the intensity and extent of the soil removal mechanism. A top view of the ice keel is presented in Figure 5-27. An analysis of the cases reveals that a greater trench width is associated with an increased transverse distance of backfill removed from the trench. This distance ranges from 2.4 times the ice keel width (Y) to 3 times the ice keel width.

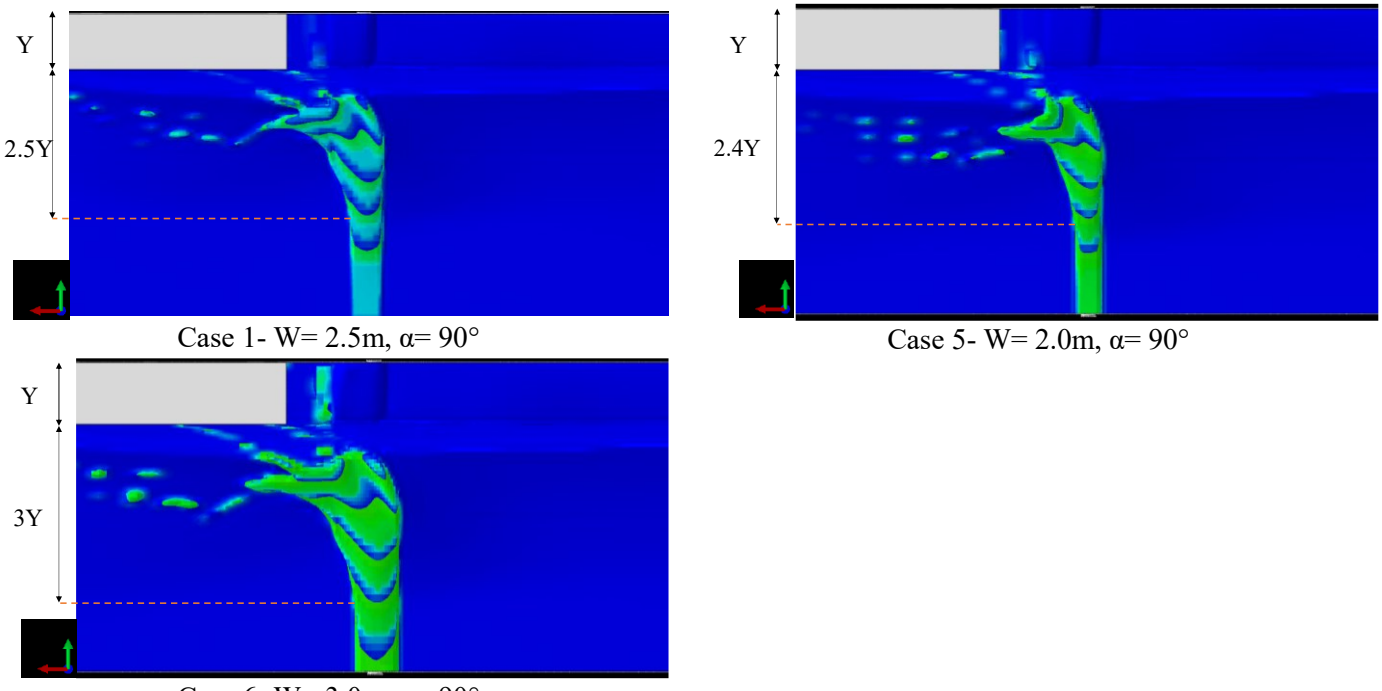

Figure 5-27. A top view of the ice keel after the ice keel passes through the trench (half model)

Figure 5-28 offers a comparative analysis of equivalent plastic shear strains (PEEQVAVG), highlighting the development of the frontal mound, side berms, and pipe-backfill-trench wall interactions. The maximum plastic shear strain distribution demonstrates consistent patterns across the various trench configurations during ice gouging events.

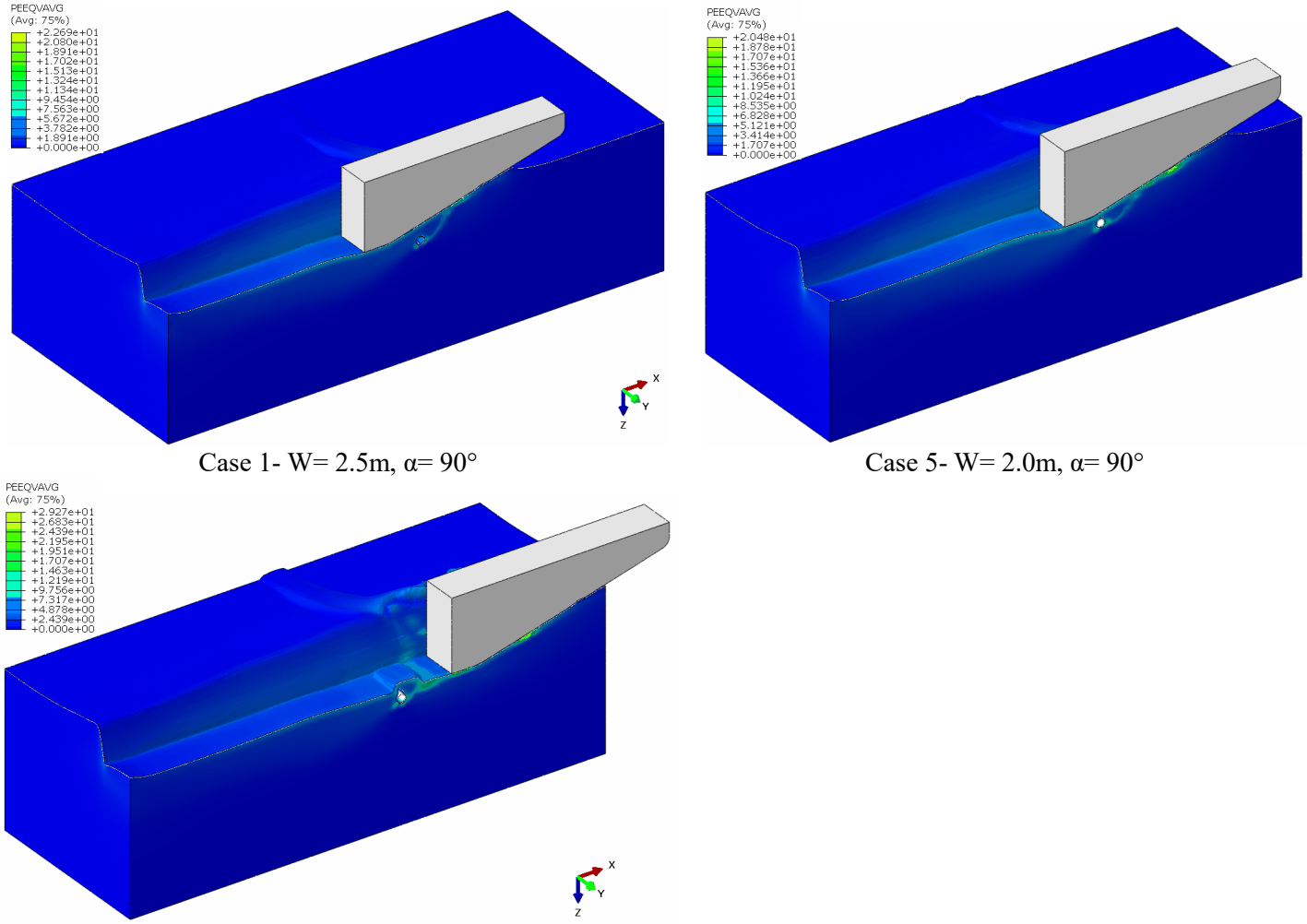

Case 1- W= 2.5m, α= 90°

Case 5- W= 2.0m, α= 90°

Case 6- W= 3.0m, α= 90°

Figure 5-28. The effect of gouging in different trench widths on progressive plastic shear strain

The figures indicate a primary concentration of maximum plastic shear strain within the backfill material surrounding the pipeline, contact zones between the ice keel's chest and frontal mound, and the interface between the keel's base and the underlying soil. Further analysis of Cases 1, 5, and 6 reveals that, with a fixed trench wall angle of 90 degrees, a correlation exists between an increase in trench width and an increase in maximum shear strain.

5.6.2.2 Ice Keel Reaction Forces

Figure 5-29 illustrates the soil's horizontal and vertical reaction forces against the advancing ice keel. As the ice keel approaches the trench, the observed decrease in ice-keel reaction forces across

all cases reflects the onset of interaction between the backfill and the trench wall, as depicted in Figure 5-23. Unsurprisingly, this reduction is less pronounced in Case 5 (W = 2.0m) due to the smaller trench width.

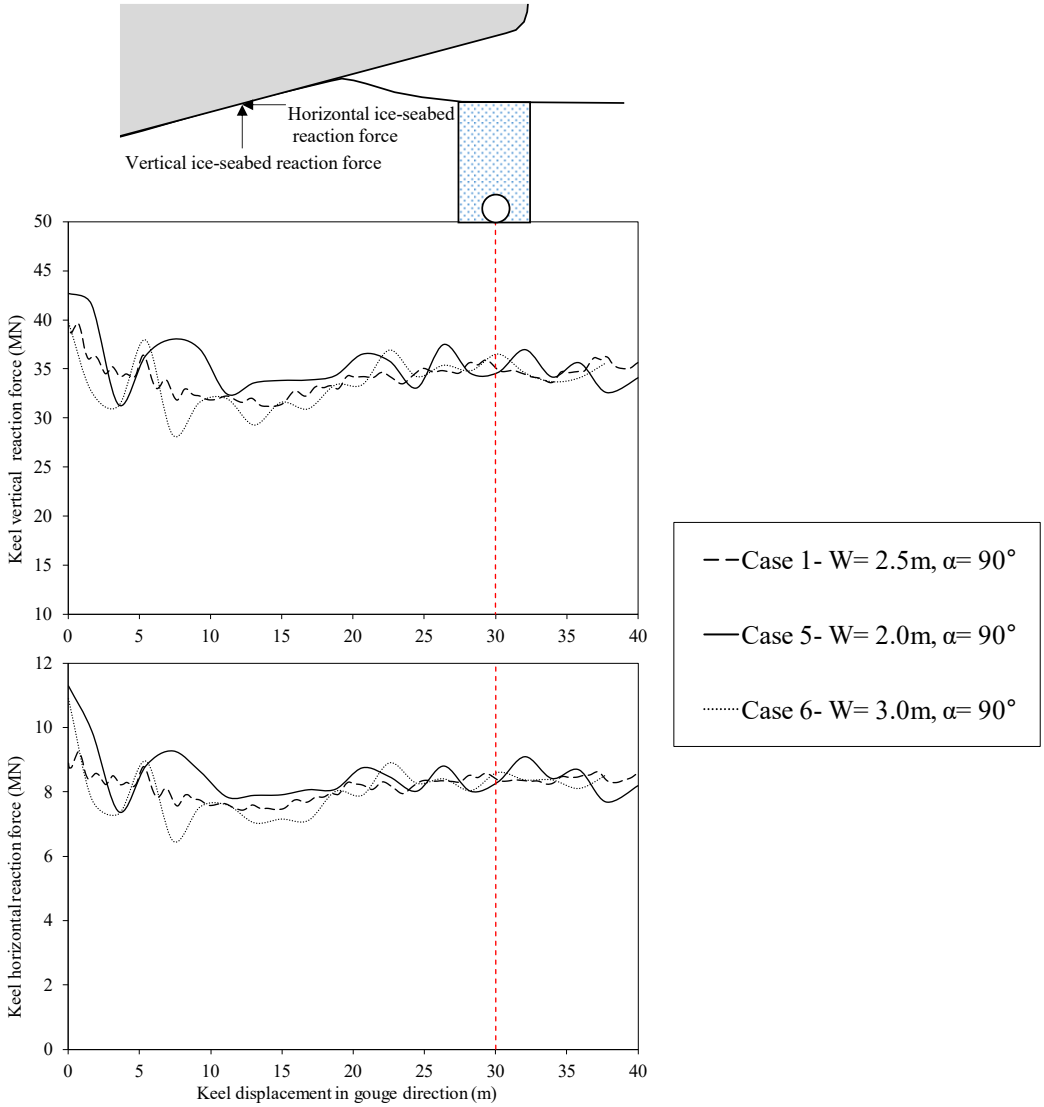

Figure 5-29. Ice keel-seabed reaction forces

A more significant decrease is evident in the case with a width of 3 meters, attributable to the larger volume of soft backfill material. Following the ice keel's passage beyond the trench, the force graphs converge again across all configurations.

5.6.2.3 Pipeline Response

Figure 5-30 compares pipeline trajectories within the vertical plane along the gouge centerline. In Case 5 (W=2.0m), the smallest trench width results in an earlier interaction of the pipe with the trench wall and the stiffer native soil, leading to reduced horizontal displacement of the pipeline. The passive lateral resistance from this interaction, combined with the low uplift resistance of the backfill, contributes to a greater upward displacement of the pipeline in Case 5 compared to Case 1 (W=2.5m). Cases 1 (W=2.5m) and 6 (W=3.0m) exhibit a delayed interaction between the pipeline and trench wall, resulting in horizontal displacement primarily within the backfill soil. This observation aligns with the findings of Kianian et al. (2018), which highlight the significance of trench wall interaction in determining lateral pipeline behavior.

Interestingly, Case 1 (W=2.5m) demonstrates a unique response with reduced upward displacement compared to the other cases. This intermediate position leads to less trench wall interaction than Case 5 (W=2.0m), allowing more significant horizontal movement. However, the backfill removal mechanism in Case 1 (W=2.5m) is faster than in Case 6 (W=3.0m), resulting in a swift replacement of backfill with native soil above the pipeline and limiting excessive upward movement.

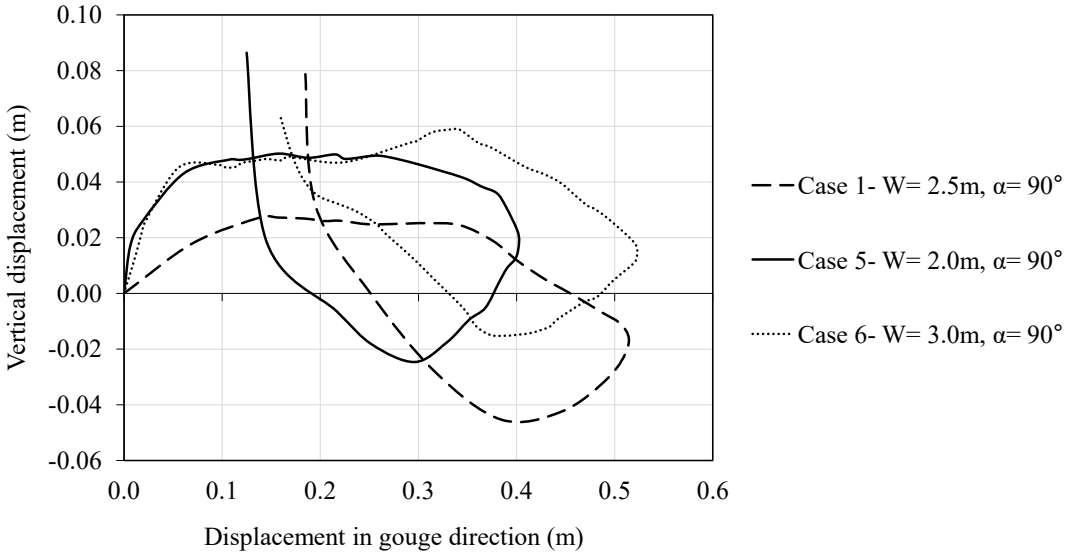

Figure 5-30. Pipeline trajectory in the vertical plane at gouge centerline

Figures 5-31 illustrate pipeline displacement in the maximum displacement state along its longitudinal axis, encompassing horizontal (gouge direction), axial, and vertical components. Figure 5-31(a) demonstrates that Case 5 (W=2.0m) exhibits the smallest horizontal displacement throughout the pipeline's length. This restricted movement is attributed to the narrowness of the trench and the pipeline's interaction with the trench wall. Horizontal displacement in Cases 1 (W=2.5 m) and 6 (W=3.5 m) is broadly similar. Furthermore, Figure 5-31(b) indicates that trench width does not significantly influence axial displacement. This consistency is likely due to the extended contact between the pipeline and backfill material along its length. Figure 5-31(c) confirms the previously discussed findings, showing a more significant downward displacement in Case 1 and a larger upward displacement in Case 5 during the maximum displacement state. Figure 5-32 visually depicts the pipeline deflection and displacement vectors in a front view, corresponding to this maximum displacement state.

a) b)

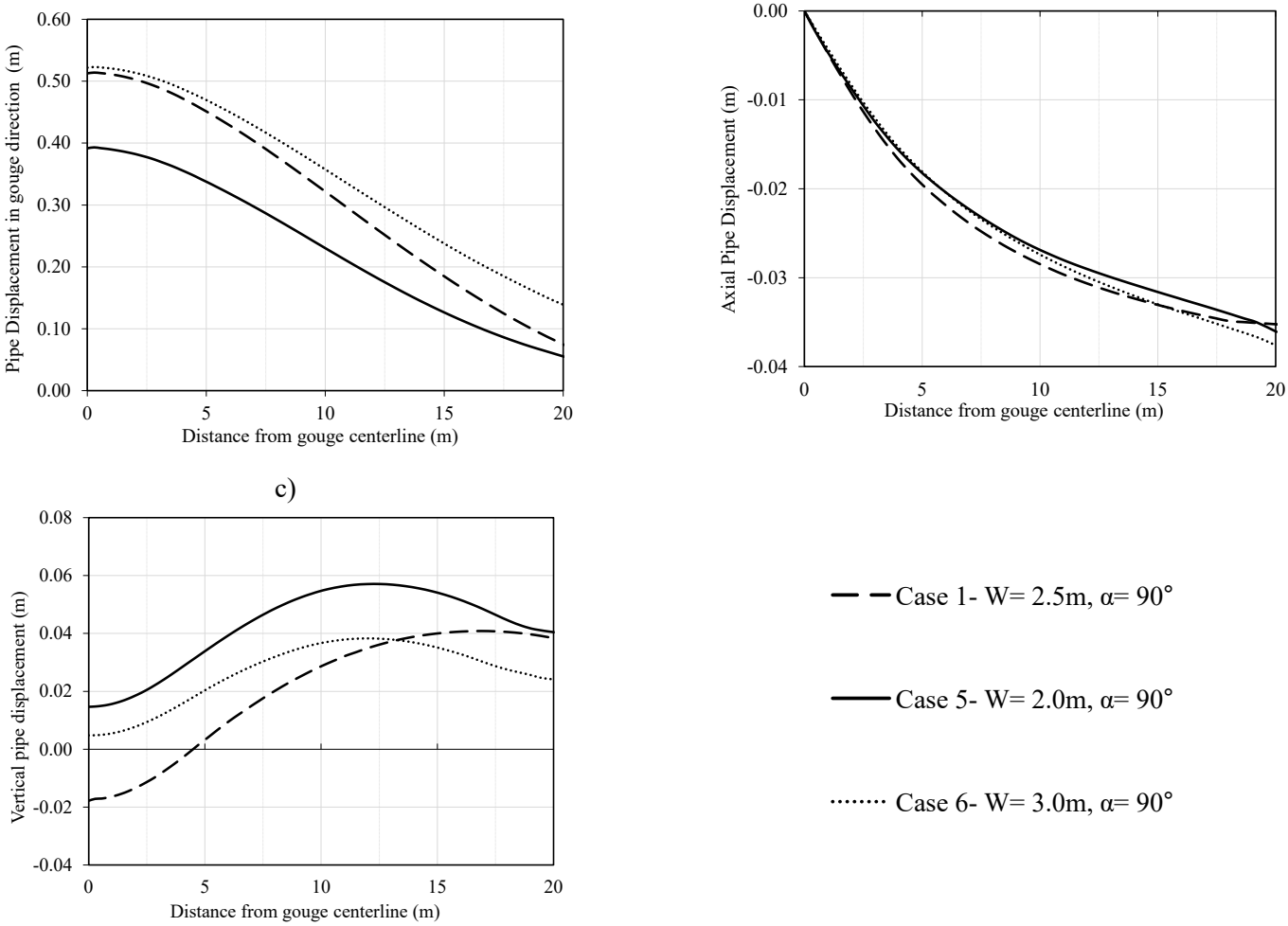

Figure 5-31. Pipeline displacement along the pipeline axis during the maximum displacement state, including (a) horizontal (gouge motion), (b) axial, and (c) vertical directions

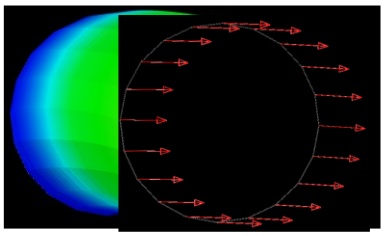

Case 1- W= 2.5m, α= 90°

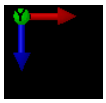

Note: Pipeline diameter = 0.95m

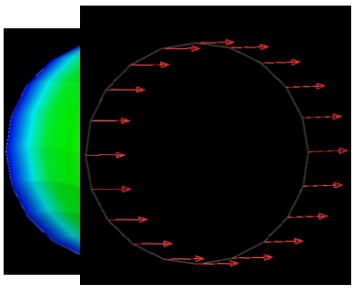

Case 5- W= 2.0m, α= 90°

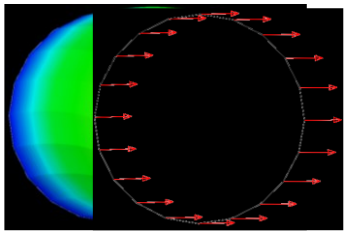

Case 6- W= 3.0m, α= 90°

Figure 5-32. Pipeline deflection and displacement vectors at its maximum displacement state from the front view

Figure 5-33 illustrates the pipeline's deformed shape and stress distribution under four different trench configurations. Case 5 (W = 2.0m), with the narrowest trench, exhibits lower overall stress levels due to reduced pipeline bending. A direct correlation is observed between increasing trench width and increased bending deflection of the pipeline, resulting in a corresponding rise in maximum stress experienced by the pipeline.

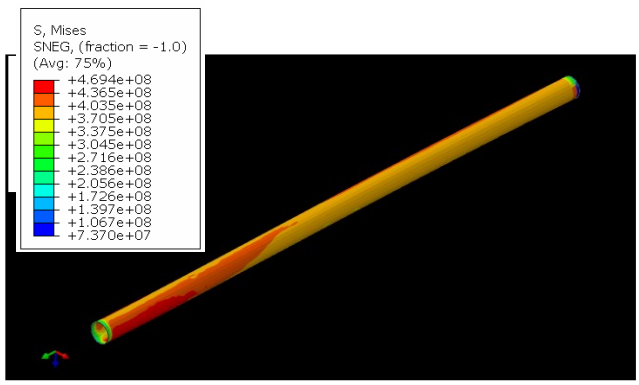

Case 1- W= 2.5m, α= 90°

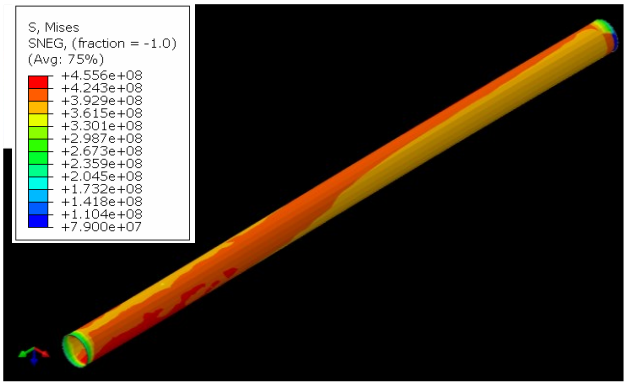

Case 5- W= 2.0m, α= 90°

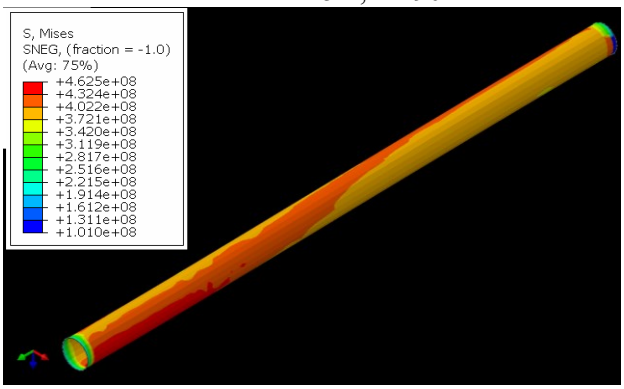

Case 6- W= 3.0m, α= 90°

Figure 5-33. Stress distribution on deformed shapes of pipeline

Figures 5-34 and 5-35 illustrate the distribution of maximum axial strain along the pipeline's axis caused by the ice gouging load. Consistent with the findings related to axial displacement, the width of the trench appears to have a negligible effect on the pipeline's axial strain.

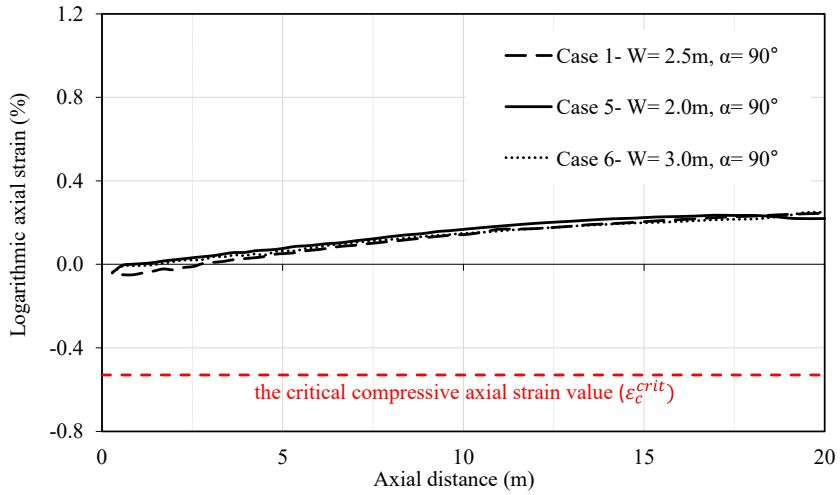

Figure 5-34. Logarithmic axial strain for the leading edge of the pipeline along the axis

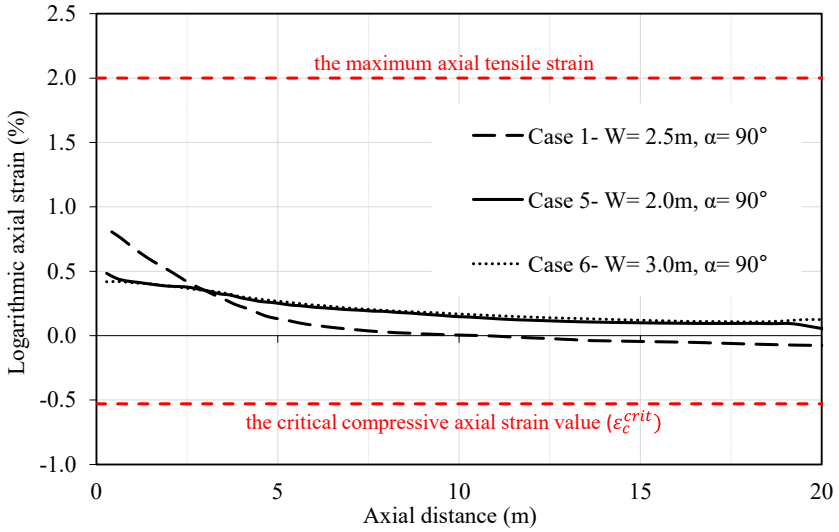

Figure 5-35. Logarithmic axial strain for the trailing edge of the pipeline along the axis

Figure 5-36 presents the pipeline ovalization profile along its longitudinal axis. Figure 5-36 shows that trench width does not significantly influence the pipeline's ovalization along its length.

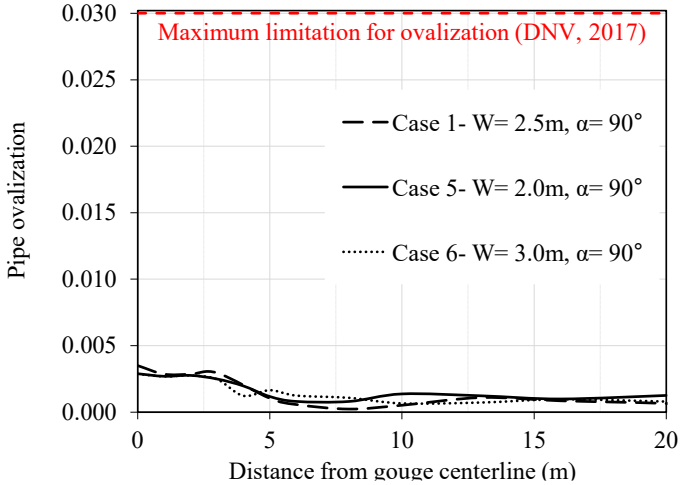

Figure 5-36. Pipeline ovalization along the axis

The analysis of pipeline response to ice gouging under varying trench widths demonstrates that the width of the trench significantly influences the pipeline-backfill-trench wall interaction, leading to distinct displacement patterns and stress, underscoring the importance of this parameter in pipeline design.

5.7 Conclusions

This study examined the pipeline response to ice gouging under a range of trench geometries derived from various trenching methods, including jetting, ploughing, mechanical trenching, and dredging. Additionally, the influence of three distinct trench widths was investigated. Numerical simulations conducted using the Coupled Eulerian-Lagrangian (CEL) method incorporated strain-rate dependency and strain-softening using a user-defined subroutine (VUSDFLD) within the Abaqus/Explicit software. The focus was on analyzing the subgouge soil displacement, pipeline displacement, strains, and ovalization and comparing different trench configurations.

- A key finding was the formation of a characteristic soil displacement pattern as the ice keel interacted with the backfill and trench walls. The removal of backfill material was observed, with the extent of removal directly correlated to increasing trench wall angle and width. The removal mechanism was most pronounced in cases with high wall angles, related to jetting ($\alpha = 90°$) and dredging ($\alpha = 64°$) trenching methods. As a result, the ice gouge's symmetry plane exhibits a significant replacement of backfill material with native soil. Furthermore, increasing the trench wall angle further intensifies the backfill-trench wall interaction and the resulting removal mechanism, leading to a wider dispersal of backfill ejected from the trench.

- Pipeline interaction with the trench wall and backfill is critical in the pipeline's lateral behavior. At a fixed trench width, smaller trench wall angles lead to earlier interaction with the stiffer trench wall, reducing horizontal pipeline displacement. Similarly, smaller trench widths accelerate this interaction at a fixed trench wall angle.

- Case 2 (W=0m, α=35°), attributed to the ploughing method, demonstrated unique behavior. Immediate pipeline interaction with the stiff trench wall occurs due to the zero-width base, restricting horizontal displacement. However, the low uplift resistance of the backfill resulted in significant upward displacement. The larger deflection and bending stress experienced by the pipeline, in this case, led to higher overall stress levels in Case 2 compared to other configurations.

- An analysis of maximum plastic shear strain revealed a primary concentration within the backfill, near the pipeline, contact zones between the ice keel's chest and frontal mound, and the interface between the keel's base and the underlying soil.

- Case 1 (W=2.5m) exhibited a reduced upward displacement compared to cases with vertical wall angles. This intermediate position results in less trench wall interaction than Case 5 (W=2.0m), enabling more significant horizontal movement. However, a faster backfill removal in Case 1 (W=2.5m) than in Case 6 (W=3.0m) caused a swift backfill replacement with native soil above the pipeline, preventing excessive upward displacement.

- The trench's cross-sectional area directly influences the ice-soil reaction forces. A more pronounced decrease in these forces is observed as the trench wall angle or width increases.

These findings underscore the crucial role of trench geometry and trenching technique selection in pipeline design for ice gouging environments. Numerical modeling with advanced soil behavior modeling, like the CEL approach used in this study, empowers engineers to optimize trench design for enhanced pipeline safety and longevity under these extreme conditions.

Acknowledgments

The authors gratefully acknowledge the financial support of the "Wood" through establishing the Research Chair program in Arctic and Harsh Environment Engineering at the Memorial University of Newfoundland, the "Natural Science and Engineering Research Council of Canada (NSERC)" and the "Newfoundland Research and Development Corporation (RDC) (now IET) through "Collaborative Research and Developments Grants (CRD)". Special thanks are extended to Memorial University for providing excellent resources for conducting this research program.

References

ALA. (2001). Guidelines for the design of buried steel pipe. American Society of Civil Engineers.

ASCE. (1984). Guidelines for the Seismic Design of Oil and Gas Pipeline Systems. Amer Society of Civil Engineers.

Atangana Njock, P. G., Zheng, Q., Zhang, N., & Xu, Y.-S. (2020). Perspective Review on Subsea Jet Trenching Technology and Modeling. Journal of Marine Science and Engineering, 8(6), 460.

Bai, Y., & Bai, Q. (2005). Subsea pipelines and risers. Elsevier.

Biscontin, G., & Pestana, J. M. (2001). Influence of peripheral velocity on vane shear strength of an artificial clay. Geotechnical Testing Journal, 24(4).

Chaloulos, Y. K., Bouckovalas, G. D., & Karamitros, D. K. (2017). Trench effects on lateral py relations for pipelines embedded in stiff soils and rocks. Computers and Geotechnics, 83, 52–63.

Chaloulos, Y. K., Bouckovalas, G. D., Zervos, S. D., & Zampas, A. L. (2015). Lateral soil–pipeline interaction in sand backfill: effect of trench dimensions. Computers and Geotechnics, 69, 442–451.

Cheng, X., Huang, R., Xu, L., Ma, C., & Zhu, X. (2021). Parametric study on the trench designing for X80 buried steel pipeline crossing oblique-reverse fault. Soil Dynamics and Earthquake Engineering, 150, 106824.

CSA. (2015). CSA Z662-15: Oil and gas pipeline systems.

Dayal, U., & Allen, J. H. (1975). The effect of penetration rate on the strength of remolded clay and sand samples. Canadian Geotechnical Journal, 12(3), 336–348.

DNV GL. (2017). DNVGL-ST-F101, Submarine pipeline systems.

Einav, I., & Randolph, M. F. (2005). Combining upper bound and strain path methods for evaluating penetration resistance. International Journal for Numerical Methods in Engineering, 63(14), 1991–2016.

Ghorbanzadeh, A., Dong, X., & Shiri, H. (2023). The Response of Buried Pipelines to Ice Gouging in the Uniform and Trenched/backfilled Seabed. ISOPE International Ocean and Polar Engineering Conference, ISOPE-I.

Graham, J., Crooks, J. H. A., & Bell, A. L. (1983). Time effects on the stress-strain behaviour of natural soft clays. Géotechnique, 33(3), 327–340.

Hashemi, S., & Shiri, H. (2022). Numerical Modeling of Ice–Seabed Interaction in Clay by Incorporation of the Strain Rate and Strain-Softening Effects. Journal of Offshore Mechanics and Arctic Engineering, 144(4), 42101.

Jan De Nul Group. (2020). Starfish (Elevated Excavator). https://www.jandenul.com/fleet/trenchers

Jo, C. H., Lee, S. B., Shin, Y. S., Hong, S. G., & Min, K. H. (2002). Numerical and experimental study of offshore pipeline stability in trench. Journal of Waterway, Port, Coastal, and Ocean Engineering, 128(6), 258–270.

Jukes, P., Kenny, S., Panapitiya, U., Jafri, S., & Eltaher, A. (2011). Arctic and harsh environment pipeline trenching technologies and challenges. OTC Arctic Technology Conference.

Kianian, M., Esmaeilzadeh, M., & Shiri, H. (2018). Lateral Response of Trenched Pipelines to Large Deformations in Clay. In Offshore Technology Conference (p. D032S092R009). https://doi.org/10.4043/28842-MS

Lach, P. R. (1996). Centrifuge modelling of large soil deformation due to ice scour. Memorial University of Newfoundland. https://research.library.mun.ca/1194/

Nematzadeh, A., & Shiri, H. (2020). The influence of non-linear stress-strain behavior of dense sand on seabed response to ice gouging. Cold Regions Science and Technology, 170, 102929.

Neumann Dredging. (2024). Nu Enterprise cutter suction dredge. https://neumanndredging.com.au/dredging-equipment/nu-enterprise-cutter-suction-dredge

Paulin, M., Cocker, J., Humby, D., & Lanan, G. (2014). Trenching considerations for Arctic pipelines. International Conference on Offshore Mechanics and Arctic Engineering, 45462, V06AT04A005.

Peek, R., & Nobahar, A. (2012). Ice gouging over a buried pipeline: Superposition error of simple beam-and-spring models. International Journal of Geomechanics, 12(4), 508–516.

Phillips, R., Clark, J. I., & Kenny, S. (2005). PRISE studies on gouge forces and subgouge deformations. Proceedings of the International Conference on Port and Ocean Engineering Under Arctic Conditions.

Pike, K., & Kenny, S. (2016). Offshore pipelines and ice gouge geohazards: comparative performance assessment of decoupled structural and coupled continuum models. Canadian Geotechnical Journal, 53(11), 1866–1881.

PRCI. (2009). Guidelines for Constructing Natural Gas and Liquid Hydrocarbon Pipelines through Areas Prone to Landslide and Subsidence Hazards, Pipeline Research Council International.

Raie, M. S., & Tassoulas, J. L. (2009). Installation of torpedo anchors: numerical modeling. Journal of Geotechnical and Geoenvironmental Engineering, 135(12), 1805–1813.

Randolph, M. F. (2004). Characterization of soft sediments for offshore applications. Proc. ISC-2 on Geotechnical and Geophysical Site Characterization, 2004.

Schoonbeek, I. S. S., & Allersma, H. G. B. (2006). Centrifuge modelling of scouring ice keels in clay. In Proceedings, 8th International Conference on Physical Modelling in Geotechnics, ICPMG (pp. 1291-1296).

Shiri, H., & Hashemi, S. (2023). The Impact of Layering Seabed on its Response to Ice Gouging. In The 33rd International Ocean and Polar Engineering Conference (p. ISOPE-I-23-205).

Simulia, D. S. (2019). Abaqus 2019 documentation. Dassault Systemes Waltham, MA.

van Rhee, C. (2002). Numerical modelling of the flow and settling in a trailing suction hopper dredge. Proc., 11th Int. Symp. on Transport and Sedimentation of Solid Particles..

CHAPTER 6

Layered Seabed Effects on Buried Pipeline Response to Ice Gouging

Alireza Ghorbanzadeh, Xiaoyu Dong, Hodjat Shiri

Civil Engineering Department, Faculty of Engineering and Applied Science, Memorial University of Newfoundland, A1B 3X5, St. John's, NL, Canada.

This chapter is under review as a journal manuscript.

Abstract

In ice gouging analyses, the seabed is often simplified as a uniform material domain, overlooking the potential complexities inherent in layered seabed formations, which are widespread in numerous Arctic regions. This study investigates the pipeline response into the distinct seabed configurations, including layered soft over stiff clay, layered stiff over soft clay, and uniformly soft and uniformly stiff compositions, to ice gouging. This was achieved through comprehensive large deformation finite element (LDFE) analysis, employing a Coupled Eulerian Lagrangian (CEL) algorithm. Incorporation of the strain-rate dependency and strain-softening effects involved the development of a user-defined subroutine and incremental update of the undrained shear strength within the Abaqus software. The pipeline is explicitly incorporated into the model, allowing for a detailed investigation of its response to ice gouging phenomena within these layered seabed scenarios. This research demonstrates that simplifying a layered seabed into a uniform can be misleading. Such an approach can lead to significant errors, potentially overestimating or underestimating pipeline response to ice gouging. By incorporating these complexities, engineers can develop more optimized designs with enhanced safety margins in Arctic environments prone to ice gouging phenomena.

Keywords: ice gouging; ice-soil-pipeline interaction; numerical simulation; large deformation finite element analysis; layered seabed soil; pipeline response

6.1 Introduction

In Arctic and subarctic regions, the movement of floating icebergs poses a significant threat to subsea pipelines and structures. The scouring action of ice keels on the seabed, known as ice gouging, can lead to catastrophic damage or failure of pipelines. Protecting these vital pieces of infrastructure is a critical challenge for engineers and designers. Burial of pipelines has emerged as the most common and cost-effective approach to mitigate the risks associated with large subgouge soil deformations caused by ice gouging. However, determining the optimal trench depth to ensure pipeline safety while minimizing construction expenses remains a complex engineering problem (Nematzadeh & Shiri, 2020). Figure 6-1 depicts the seabed and the pipeline, highlighting the diverse mechanisms set in motion by the ice gouging phenomenon.

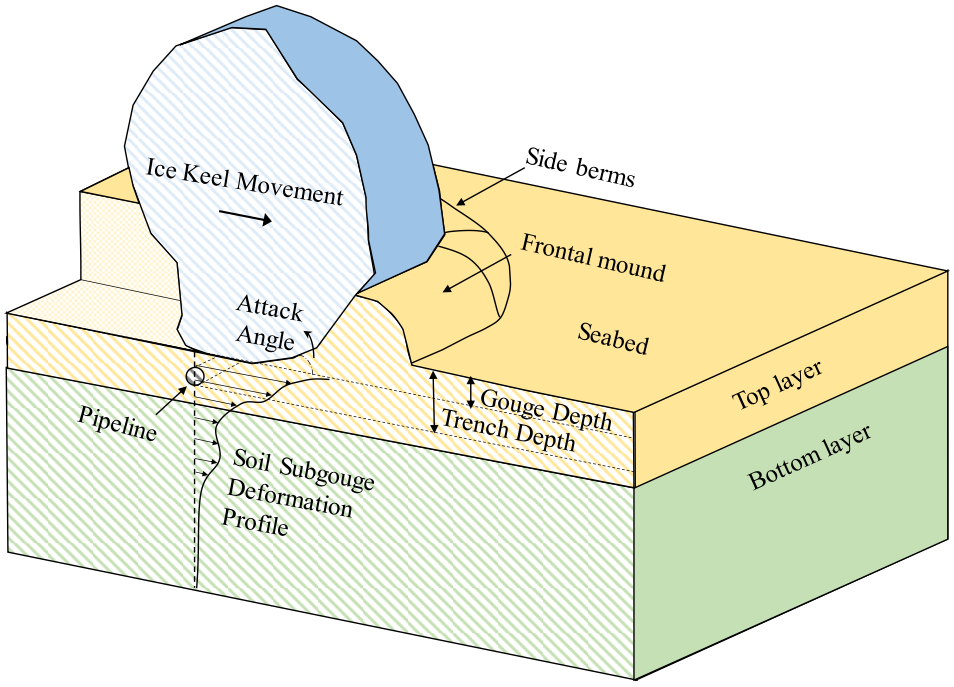

Figure 6-1. Schematic of ice gouging over a buried pipeline in a layered seabed (not to scale)

Layered seabed configurations, with their distinct strata of varying geotechnical properties, are a common feature in Arctic offshore regions where ice gouging is prevalent. Studies in areas like the Chukchi Sea (C-CORE, 2008; Winters & Lee, 1984), Alaskan Beaufort Shelf (C-CORE,

2008), and Russian Sakhalin (C-CORE, 1995) have documented the presence of these layered formations, often characterized by configurations such as soft over stiff clay or stiff over soft clay. While research on ice gouging has advanced over the years, encompassing the phenomenon's causes, mechanisms, and consequences (Liferov & Høyland, 2004; Phillips et al., 2005; Schoonbeek & Allersma, 2006; Been et al., 2008), a significant knowledge gap remains regarding the complex interaction between soil layers during gouging events. Current design codes (e.g., PRCI 2009; ALA 2005; ASCE 1984) based on earlier studies rarely account for this layering effect, often relying on simplified models that assume a uniform seabed. This assumption can be an oversimplification, potentially leading to inaccurate predictions of seabed response and pipeline behavior under ice gouging loads.

Despite this limitation, notable contributions have been made by Schoonbeek & Allersma (2006), Hashemi et al. (2022), Hashemi & Shiri (2022b, 2023), and Shiri & Hashemi (2023) to investigate the impact of layered seabeds on ice gouging. These studies have shown that the subgouge soil deformation resulting from ice gouging is significantly influenced by the strength characteristics of each soil layer and their interaction, ultimately affecting the failure mechanisms and reaction forces on the ice keel. While these researches greatly advanced the understanding of soil behavior in layered seabeds, there's a crucial gap in knowledge regarding the response of buried pipelines under these conditions. Previous studies primarily focused on free-field ice gouging, neglecting the ice-layered seabed-pipeline interaction.

Building upon previous research on ice gouging in layered seabeds, this study employs advanced numerical modeling techniques to investigate the response of buried pipelines under these conditions. Using a Coupled Eulerian-Lagrangian (CEL) algorithm within the Abaqus/Explicit

software, the complex interactions between an ice keel, layered seabed, and pipeline are simulated. To enhance the accuracy of soil behavior modeling, a VUSDFLD user subroutine, based on the Einav and Randolph (2005) equation, is incorporated to account for strain rate dependency and strain-softening effects. This numerical model has been rigorously validated against experimental data from Lach (1996).

This study demonstrates that simplifying a layered clay seabed into a uniform model can lead to inaccurate predictions of pipeline behavior, potentially jeopardizing structural integrity. Oversimplification by assuming a uniform soft or stiff seabed can result in overestimating pipeline trajectory in a "soft over stiff" configuration and underestimating deformation in a "stiff over soft" configuration. Furthermore, strategically burying the pipeline within a stiffer layer can significantly reduce displacement and stresses, even with minimal added depth. These findings offer valuable insights for enhancing pipeline risk assessments and refining engineering practices for Arctic pipelines.

6.2 Methodology

6.2.1 Model Configuration

The Coupled Eulerian-Lagrangian (CEL) method is a powerful numerical technique that combines Eulerian and Lagrangian frameworks to analyze large material deformations (Simulia, 2019). The Eulerian domain models fluid-like behavior on a fixed grid, while the Lagrangian domain tracks discrete elements within the material. By integrating both frameworks, CEL effectively simulates complex interactions in scenarios like ice gouging, where both material flow and structural response are crucial.

A three-dimensional Coupled Eulerian-Lagrangian (CEL) model, implemented in Abaqus/Explicit, was employed to simulate the ice-soil-pipeline interaction during ice gouging. The model, symmetrical about the gouge center plane, captures the complex dynamics of these events. The soil domain is represented using Eulerian, three-dimensional, eight-node, reduced integration brick elements and hourglass control (EC3D8R), with dimensions of 60 m in length, 25 m in half-width, and a depth of 17 m. An 8m wide ice keel was modeled as a rigid body using linear brick elements (C3D8R).

The soil domain is discretized into a structured mesh, with increased mesh density in the pipeline's proximity to ensure accurate representation. The boundaries are positioned sufficiently far from the pipeline to mitigate boundary effects on pipeline deformations and soil failure mechanisms. A surface layer of clay with a thickness of 3 meters was implemented above an underlying 12-meter layer of clay. These specific layer thicknesses were selected based on borehole data outlined in the works of Miller & Bruggers (1980) and Winters & Lee (1984), derived from observations in the Alaskan Beaufort Sea and the western Chukchi Sea. Furthermore, a void domain was incorporated above the seabed to accommodate surface deformations during the ice gouging process, as depicted in Figure 6-2. Following the Tresca criterion, the soil is modeled as an elastic-perfect plastic clay, with zero friction and dilation angles and a Poisson's ratio of 0.499. The Young's modulus remains constant at $400s_{ui}$ throughout the soil layer.

The pipeline, with an external diameter of 0.950 m and a wall thickness of 12.7 mm, is modeled using shell elements, employing a shell theory that incorporates shear deformations and features five integration points across the wall thickness. Following Peek and Nobahar (2012), the steel pipeline is characterized as an elastoplastic material. It possesses a Young's modulus of 205 GPa

and a Poisson's ratio of 0.3. Additionally, the pipeline model extends 5km beyond the discretized soil domain using beam elements restrained by Winkler springs.

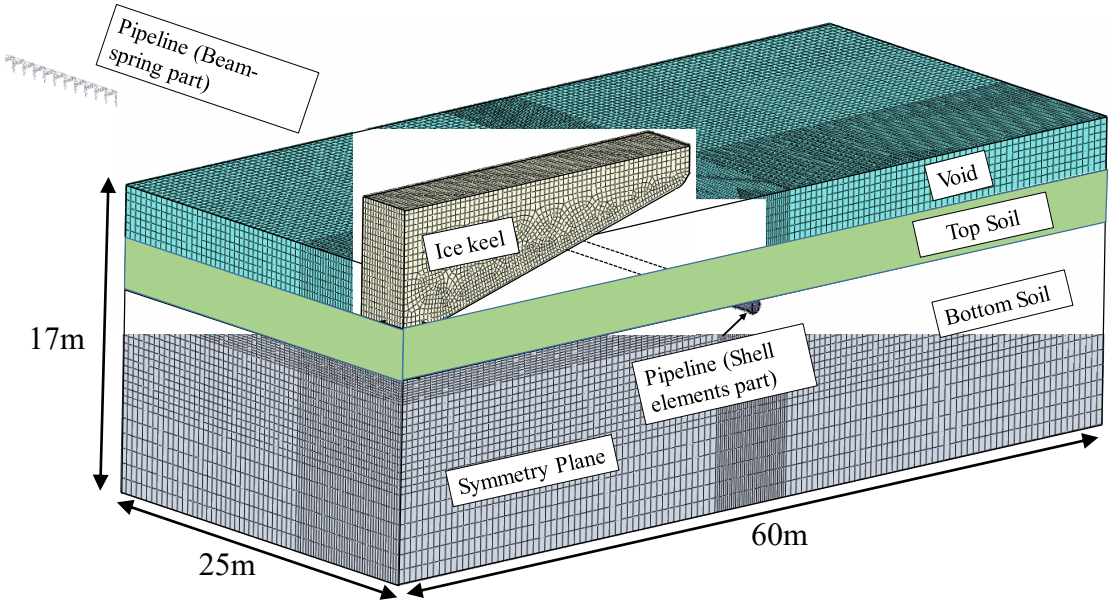

Figure 6-2. Finite element model configuration

The contact surface approach in Abaqus/Explicit simulates the interfaces between ice, soil, and pipeline. "Hard" behavior is applied for normal interaction, and the Coulomb friction model accounts for the frictional interface between the pipeline and soil and between the ice keel and soil. The friction coefficients are 0.3 and 1.0 for the soil-ice and soil-pipeline interfaces, respectively. The maximum permissible shear stress at the interface was constrained to be 0.5 times the measured in-situ undrained shear strength (s_{ui}) at the gouge depth, as Pike and Kenny (2016) recommended.

The analysis procedure comprises four steps, including the initiation of geostatic stress, lowering the ice keel to the intended gouge depth, applying an internal pressure of 12 MPa to the pipeline's shell elements, and applying a velocity boundary condition to move the ice keel horizontally. A velocity of 1 m/s for the iceberg movement was chosen based on established literature, as evidenced in studies such as those by Konuk et al. (2005) and Eskandari (2014). While lower

velocities of icebergs are frequently encountered in practical field settings, empirical data indicates that more than 80% of icebergs have speeds exceeding 0.2 m/s, as indicated by FitzMaurice et al. (2016). Moreover, Palmer et al. (1989) reported that, according to field observations of ice keel velocities, the gouging deformations in clayey soils tend to occur rapidly, often in undrained conditions. Hashemi & Shiri (2022a) stated that an ice keel velocity below one millimeter per second would lead to soil behavior transitioning into a drained or partially drained condition. In this study, it is presumed that the undrained condition governs the behavior.

6.2.2 Strain Softening and Shear Rate Effects

In the context of ice gouging analyses, Hashemi and Shiri (2022a) showed it is crucial to account for the influence of strain softening and shear rate dependency on the behavior of soil materials. To address this, a user subroutine, VUSDFLD, is implemented within the Abaqus software platform using the empirical Equation (6-1) proposed by Einav and Randolph (2005). This subroutine enabled the model to adjust material properties adaptively in response to variations in loading rates, ensuring a more accurate representation of soil behavior under dynamic conditions.

$$s_u = \left[1 + \mu \times \log_{10}\left(\frac{\max(|\dot{\gamma_{max}}|, \dot{\gamma_{ref}})}{\dot{\gamma_{ref}}}\right)\right] \times \left[\delta_{rem} + (1 - \delta_{rem})e^{-3\xi/\xi 95}\right] s_{ui} \qquad (6\text{-}1)$$

Where, s_{ui}, the undrained shear strength is updated at each time step according to ξ, the current accumulated absolute plastic shear strain, and $\dot{\gamma_{max}}$, the average rate of maximum shear strain from the previous time step. The reference shear strain rate ($\dot{\gamma_{ref}}$) and the increase rate of the shear strength per log cycle (μ) are considered constant. Additionally, the ratio of fully remolded to initial shear strength (δ_{rem}) and the value of accumulated absolute plastic shear strain resulting in a 95% reduction in the remolded shear strength ($\xi 95$) are also considered constant.

A value of 0.1 for the parameter μ was chosen, consistent with prior studies conducted by Dayal & Allen (1975), Graham et al. (1983), and Biscontin & Pestana (2001), all of which indicated a recommended range of 0.05 to 0.2. The reference shear strain rate ($\dot{\gamma_{ref}}$) was established at 0.024, aligning with the guidance provided by Raie & Tassoulas (2009). Additionally, the value of ξ_{95} for typical soft marine clays was determined to be 12, falling within the range of 10 to 25, as suggested by Randolph (2004) for soils exhibiting varying degrees of softening. The value of δ_{rem} is depending upon the soil sensitivity.

6.3 Validation of Numerical Model

A thorough comparison against the centrifuge test conducted by Lach (1996) is conducted to validate the accuracy of the numerical model. Lach's centrifuge tests are a widely recognized benchmark for studying ice-soil interaction in the context of ice gouging. Test 05 involved subjecting a scaled model of an ice keel to simulated free-field ice gouging conditions under controlled centrifugal acceleration.

The numerical simulation simulated the experimental setup from Test 05, including the geometric and material properties of the model. The boundary conditions and loading conditions also mirrored the centrifuge test. Horizontal soil subgouge displacement and vertical and horizontal ice keel-seabed reaction forces were compared with the data obtained from Lach's experiment and PRISE equation (Phillips et al., 2005). The findings from the horizontal subgouge displacement analysis underscore the significance of accounting for strain softening and strain rate effects. Figure 6-3 illustrates a notable inconsistency near the gouge depth without considering these effects, previously observed in studies neglecting them.

The model presented here also demonstrates higher agreement with experimental data than the PRISE empirical relationship. Figure 6-4 present a comparison of these forces from the current model with Lach's (1996) experimental data.

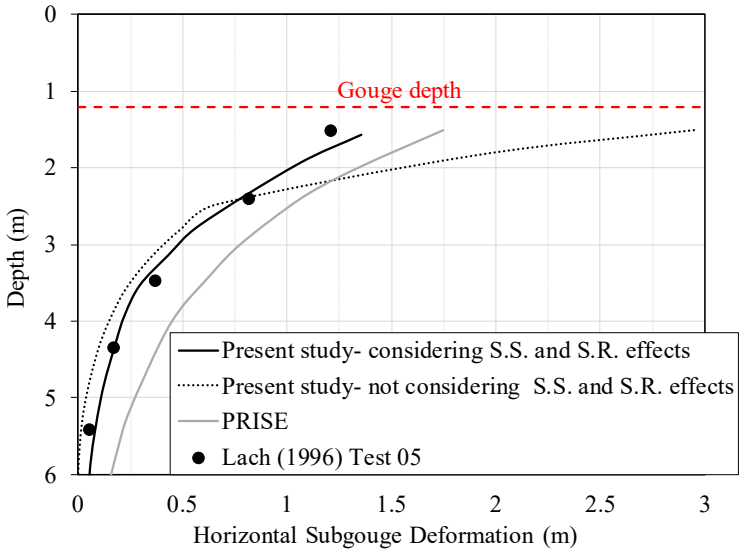

Figure 6-3. The comparison of the soil horizontal subgouge deformations

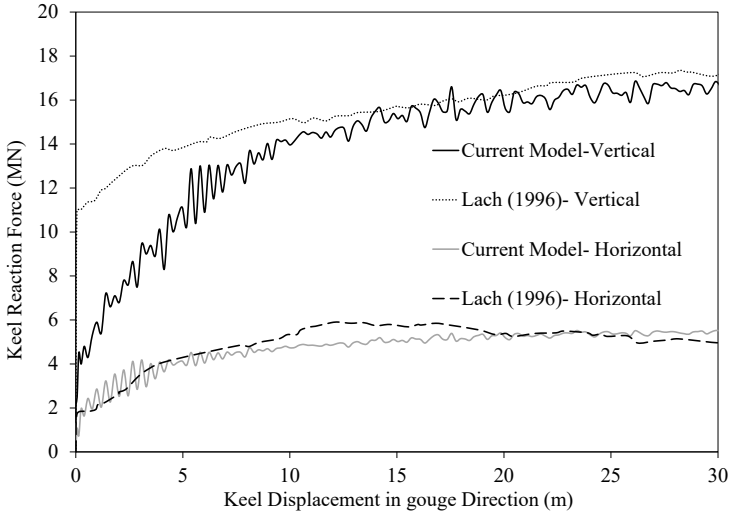

Figure 6-4. Comparison of ice keel-soil reaction forces

The numerical simulation results were validated against Lach's (1996) centrifuge test data, providing a robust basis for further analysis and interpretations presented in this study.

6.4 Failure Criteria for Subsea Buried Pipelines

The assessment of subsea buried pipelines under significant ground deformation requires the establishment of specific failure criteria. These criteria cover various modes of deformation and serve as essential guidelines for ensuring the structural integrity of the pipelines in the face of environmental challenges. The key criteria include:

Tensile Yielding Limit: The DNVGL-ST-F101 (DNV GL, 2017) standard specifies that during the design of buried steel gas pipelines, the maximum axial tensile strain allowed in the pipeline should not exceed 2.00%. This criterion is crucial in preventing the tensile failure of the pipeline material, especially in regions subjected to substantial ground deformation.

Critical Compressive Strain Limit: Pipeline buckling, a form of local collapse, may occur under compressive loading conditions induced by external forces such as ice gouging or soil pressure. To mitigate this risk, it is essential that the maximum compressive strain (ε_{max}) remains below the critical compressive strain value, calculated using established equations (6-2) and (6-3) specified in design codes such as CSA (2015).

$$\varepsilon_c^{crit} = 0.5\frac{t}{D} - 0.0025 + 3000\left(\frac{(p_i - p_e)D}{2Et}\right)^2 \qquad \text{for } \frac{(p_i - p_e)D}{2tf_y} < 0.4 \qquad (6\text{-}2)$$

$$\varepsilon_c^{crit} = 0.5\frac{t}{D} - 0.0025 + 3000\left(\frac{0.4f_y}{E}\right)^2 \qquad \text{for } \frac{(p_i - p_e)D}{2tf_y} \geq 0.4 \qquad (6\text{-}3)$$

where p_i and p_e are the maximum internal and external pressure, f_y is the effective specified yield strength, E is Young's modulus of elasticity, and t is the pipeline wall thickness.

Ovalization Failure Limit: Ovalization refers to a geometric distortion in the cross-sectional shape of a pipeline, transforming it from its original circular form into an elliptical or oblong shape. This

deformation can result from ice gouging events and may lead to increased stress concentrations and reduced stability. To safeguard against Ovalization failure, the degree of ovalization must remain below 3%, as stipulated by the submarine pipeline standard (DNV GL, 2017). DNV GL (2017) defined the ovalization parameter as equation (6-4).

$$f_0 = \frac{D_{max} - D_{min}}{D} \leq 0.03 \quad (6\text{-}4)$$

where D_{max} denotes the maximum outer diameter of the pipe, D_{min} denotes the minimum outer diameter of the pipe, and D denotes the nominal (intended) outer diameter of the pipe.

By defining failure limits, these criteria provide a comprehensive framework for assessing the structural integrity and ensuring the safe design of subsea pipelines subjected to significant ground deformation.

6.5 Numerical Study Plan

A study was conducted through 10 case studies (Case-1 to Case-10) to investigate the influence of the layered seabed on buried pipeline response to ice gouging. The ice gouging model examined crucial parameters such as gouging configuration, soil strength properties, and uniformity of soil. Table 6-1 summarizes the key parameters used in the proposed case studies.

Figure 6-5 depicts the soil in situ undrained shear strength profile applied in the present case studies incorporated from studies by Shiri and Hashemi (2023) and published reports for the Chukchi Sea (Winters and Lee, 1984) and Alaskan Beaufort Sea (Miller and Bruggers, 1980). These studies utilized field tests, including a combination of miniature vane, torvane, pocket penetrometer, and triaxial tests, to measure the undrained shear strength. Seabed soil unit weight is assumed to be 19.12 kN/m^3.

Table 6-1. Parametric study layout

Case No.	Burial Depth	Gouge Depth	Clearance depth	Soil profile
Case 1	3.475	2.5	0.5	Soft over Stiff
Case 2	3.475	2.5	0.5	Stiff over Soft
Case 3	3.475	2.5	0.5	Uniform Stiff
Case 4	3.475	2.5	0.5	Uniform Soft
Case 5	2.525	1.55	0.5	Soft over Stiff
Case 6	2.525	1.55	0.5	Stiff over Soft
Case 7	3.475	2	1	Soft over Stiff
Case 8	2.525	2	0.05	Soft over Stiff
Case 9	3.475	2	1	Stiff over Soft
Case 10	2.525	2	0.05	Stiff over Soft

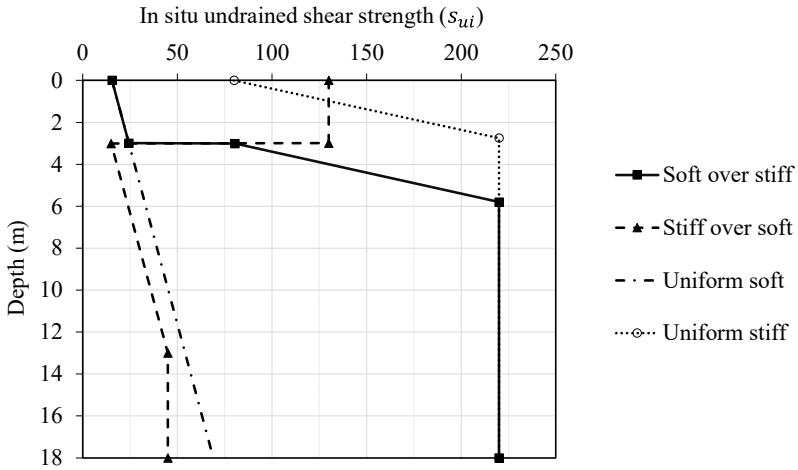

Figure 6-5. In situ undrained shear strength (s_{ui}) profile

Across all cases, a comparative analysis was conducted to examine the horizontal and vertical ice keel-soil reaction forces, equivalent plastic shear strains in the soil, pipeline displacement, equivalent Von Mises stress within the pipeline, as well as axial strains and ovalization experienced by the pipeline.

6.6 Results and Discussions

6.6.1 The Effect of Layered Relative to Uniform Seabed Strata

This study aims to quantify the impact of layered seabed strata on the response of buried pipelines subjected to ice gouging compared to uniform soil conditions. Four distinct cases (Cases 1-4) will

be analyzed, all maintaining constant pipe burial and gouge depths. In each case, the pipeline will be situated within the bottom layer. The effects of both "soft over stiff" and "stiff over soft" layering will be investigated, contrasting them with scenarios where the seabed is assumed to be uniformly stiff and uniformly soft. A schematic representation of these cases is presented in Figure 6-6, while the corresponding vertical and horizontal ice-soil reaction forces are detailed in Table 6-2.

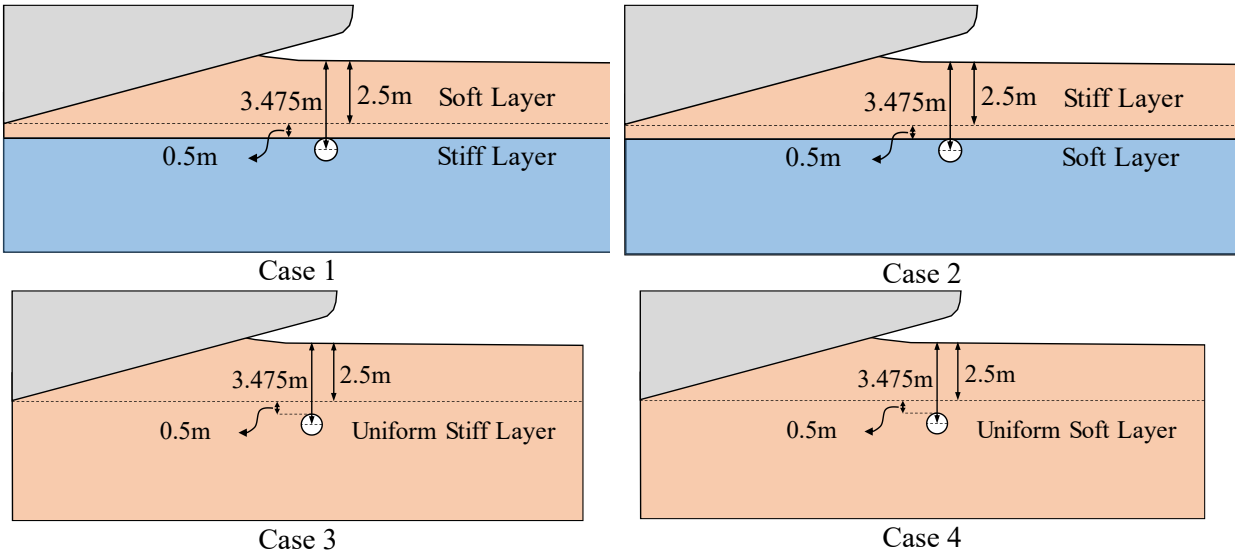

Figure 6-6. Schematics of configuration of cases 1-4

Table 6-2. Ice keel reaction forces

	Case 1 (soft/stiff)	Case 2 (stiff/soft)	Case 3 (uniform stiff)	Case 4 (uniform soft)
Horizontal ice keel reaction force (MN)	5.1	9.5	29.0	4.8
Vertical ice keel reaction force (MN)	20.5	37.7	128.5	19.9

The analysis reveals that for the "soft over stiff" configuration, where the gouge depth solely affects the top layer, the difference in ice-seabed reaction forces is minimal compared to the uniformly soft case. This suggests that for shallow gouges confined to the upper layer, assuming a uniform soft seabed may not introduce significant errors in ice keel reaction forces. However, the

results for other cases (stiff over soft, and both compared to uniform stiff) demonstrate that simplifying the seabed into a uniform material leads to discrepancies in ice-keel/seabed reaction forces.

6.6.1.1 Soil Displacement Mechanisms

Figure 6-7 illustrates the positioning of the soil, pipeline, ice, and tracer particles at the maximum pipe displacement. As Figure 6-7(a) and Hashemi et al. (2022) pointed out, deformations do not reach the stiff layer when the gouge depth is less than the soft layer thickness. The ice keel interacts solely with the soft layer, similar to a uniform soft seabed scenario. The interaction between the soft and stiff layers experiences direct shear, essentially decoupling them. The soft soil "slides" on the stiff layer, minimizing the contribution of the stiff layer's strength to resisting the ice gouging forces. Figure 6-7(b) illustrates a scenario where a stiff layer overlies a soft layer. The significant forces exerted by the ice cause the settlement of the soft layer. Consequently, the surrounding soil becomes predominantly composed of stiffer material when the ice crosses the pipe. Additionally, a wave-shaped profile of particles is observed, with the peak point of subgouge displacement located at a greater depth than uniform states within the soft layer.

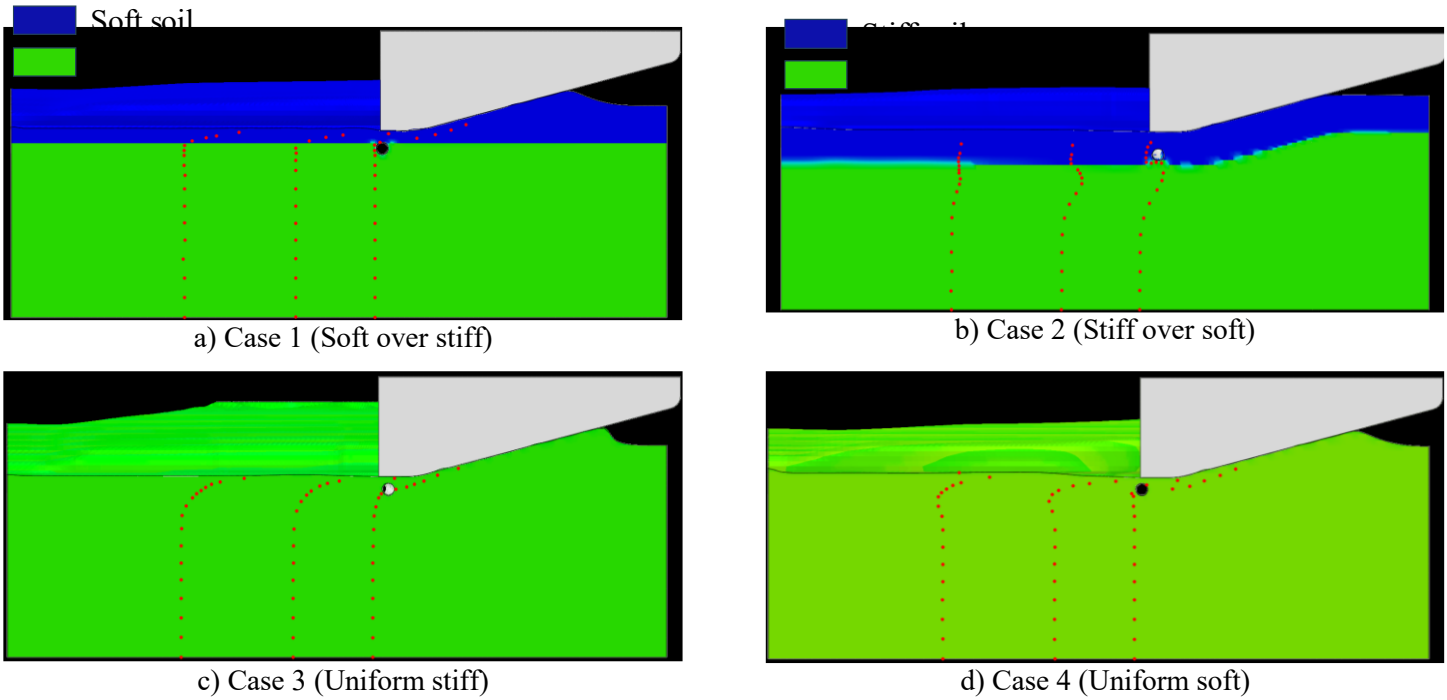

a) Case 1 (Soft over stiff)

b) Case 2 (Stiff over soft)

c) Case 3 (Uniform stiff)

d) Case 4 (Uniform soft)

Figure 6-7. The positioning of the soil, pipeline, ice, and tracer particles at the maximum pipe displacement

Figure 6-8 compares equivalent plastic shear strains (PEEQVAVG) alongside forming a frontal mound, side berm, and the interaction of soil layers in both uniform and layered seabed scenarios. The maximum plastic shear strain distribution exhibits similar patterns across uniform soft, stiff, and soft-over-stiff layered soil configurations during ice gouging. The figures reveal that the maximum plastic shear strain primarily concentrates in the contact zones between the keel chest and the frontal mound and between the keel base and the underlying soil layer for all three scenarios. However, Figure 6-8(b) sheds light on a crucial aspect of layered soil behavior. During gouging, the stiff layer becomes a compressed zone between the ice keel and the soft layer. This interaction leads to a significant transfer of plastic strain from the stiff layer to the underlying soft soil. The area surrounding the pipe also emerges as another zone of concentrated plastic shear strain.

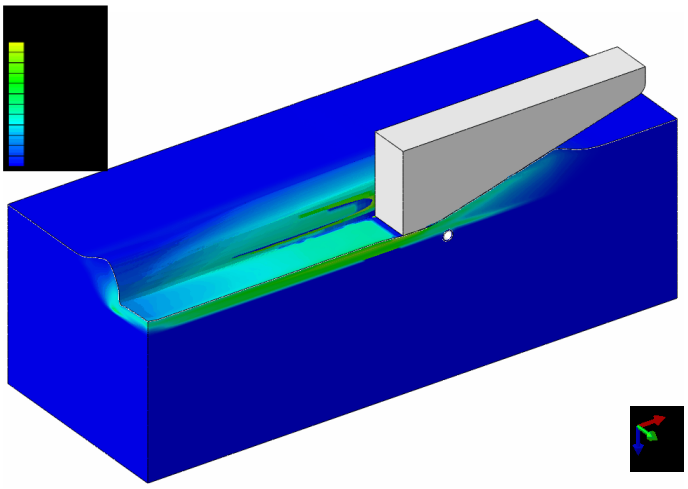

a) Case 1 (Soft over stiff)

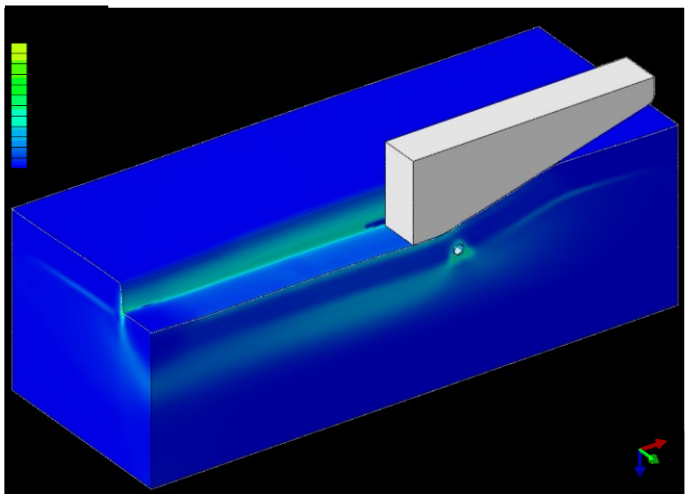

b) Case 2 (Stiff over soft)

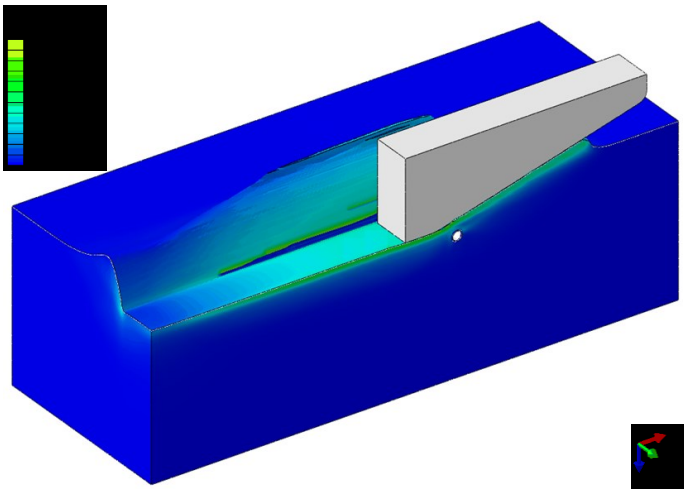

c) Case 3 (Uniform stiff)

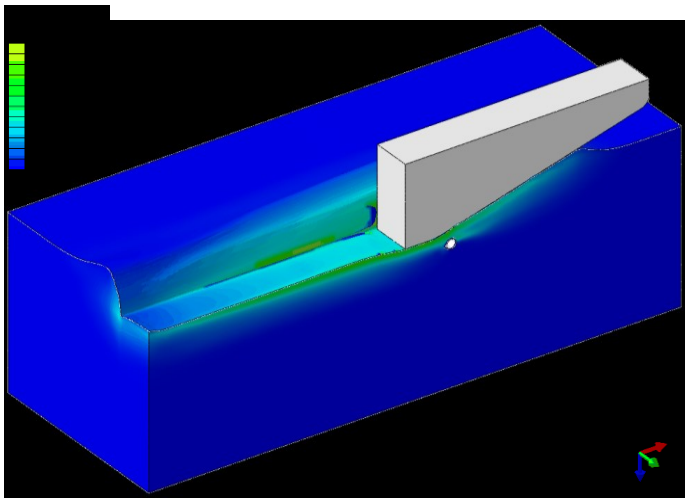

d) Case 4 (Uniform soft)

Figure 6-8. The effect of gouging in different layered soil strata on progressive plastic shear strain

These observations highlight the complex interaction between ice gouging and the soil layers, fundamentally influencing seabed failure mechanisms. This underscores the importance of considering layered seabed configurations to assess pipeline response and vulnerability in ice-prone environments accurately.

6.6.1.2 Pipeline Response

The typical pipeline trajectory during ice gouging in a uniform seabed involves upward and gouge-ward movement as the ice keel approaches, followed by partial elastic recovery to a rebound state.

However, layered seabed configurations can lead to variations in both vertical and horizontal displacements.

Figure 6-9 presents a comparative analysis of the pipeline's displacement path within the gouge centerline for various seabed configurations. Notably, Figures 6-9(a) and 6-9(b) demonstrate that assuming a uniform soft or stiff seabed instead of the actual "soft over stiff" layering leads to an overestimation of the pipeline's trajectory. Figure 6-9(a) illustrates that in a "soft clay over stiff clay" configuration, the upward vertical movement of the pipeline surpasses its horizontal movement as the ice approaches. This phenomenon can be attributed to the difference between the soft clay's low uplift resistance and the high horizontal passive resistance offered by the underlying stiff clay. This implies that the pipeline experiences less deformation in the more realistic "soft over stiff" scenario. Consequently, assuming uniform soil conditions could result in over-designing the pipeline for its intended service life. This observation aligns with the findings of Hashemi et al. (2022), who demonstrated that for gouge depths confined to the upper soil layer, the horizontal subgouge displacement in a "soft clay over stiff clay" configuration is less noticeable within the stiff clay layer compared to scenarios with uniformly soft or uniformly stiff soil profiles due to the truncated deformations in the bottom of the soft layer.

Conversely, Figure 6-9(b) highlights that neglecting the "stiff over soft" layering and adopting a uniform assumption (soft or stiff) underestimates the pipeline's deformation. This underestimation could translate to higher risks during the pipeline's operational lifespan. These findings support the observations of Hashemi and Shiri (2023), who reported that for gouge depths limited to the upper layer, a "stiff clay over soft clay" configuration induces a wave-like pattern in the horizontal subgouge displacement profile within the soft clay layer. This, in turn, leads to a greater magnitude of horizontal subgouge displacement compared to scenarios with uniformly soft or uniformly stiff

soil profiles. These findings underscore the crucial influence of soil layer interaction on sub-gouge soil deformation. By incorporating them, engineering practices can be refined to achieve enhanced safety and cost-efficiency in pipeline design against ice gouging events.

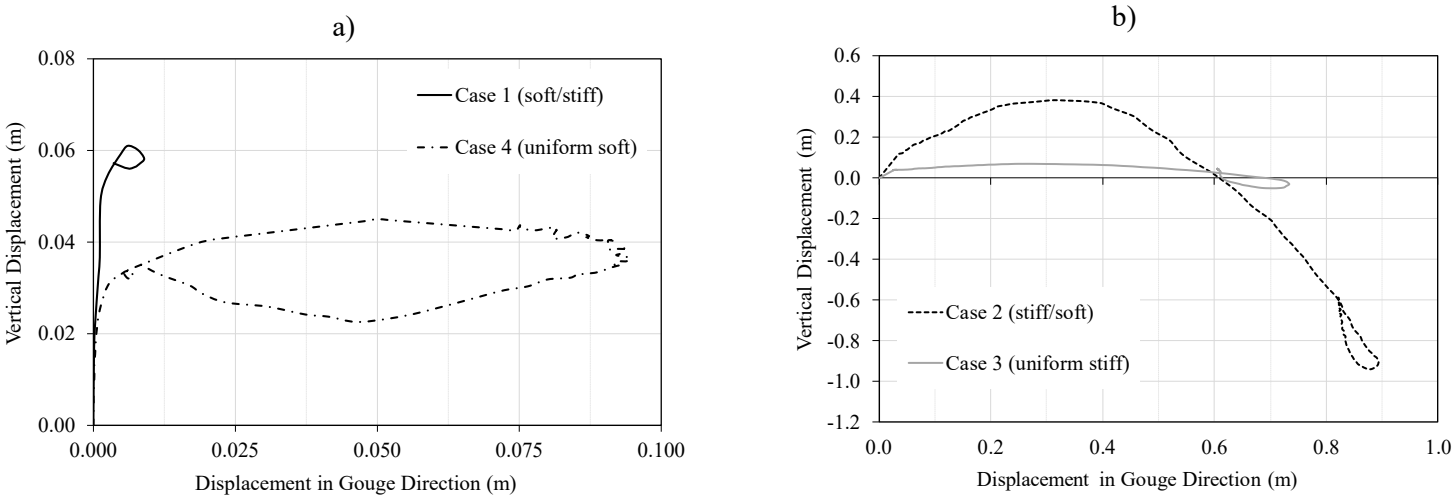

Figure 6-9. Pipeline trajectory in the vertical plane at gouge centerline

Figure 6-10 depicts the maximum displacement state of the pipeline along its longitudinal axis. The three components of this displacement are represented: horizontal (gouge direction), axial, and vertical. Figure 6-9(a) supports the observations of Hashemi et al. (2022, 2023), demonstrating that the horizontal displacement of the pipeline in the "soft over stiff clay" case is lower compared to the uniform soil scenarios. Conversely, the "stiff over soft clay" case experiences a more significant horizontal displacement than the uniform cases. Regarding axial displacement, the soft over stiff clay exhibits the lowest value. However, unlike the horizontal component, the uniform stiff clay exhibits a higher axial displacement than the other cases. Table 6-2 highlights a significant increase in ice-soil interaction forces when the ice keel encounters the stiff layer compared to the soft soil. This observation can be attributed to the higher resistance the higher shear strength material offers. Consequently, the increased forces acting on the pipe lead to larger

horizontal and axial displacements, as evidenced in Figures 6-10(a) and 6-10(b) for Cases 2 and 3.

The vertical displacement of the "stiff on soft clay" configuration, as shown in Figure 6-10(c), is significantly greater than in the other cases. This observation is consistent with Figure 6-9(a), which illustrates that the uplift resistance of the soft clay in the "uniform soft" and "soft over stiff clay" scenarios allows for substantial upward movement during the ice approach. Even when the ice overtops the pipe and exerts a downward force, these cases remain above their original buried level. Figure 6-11 presents the pipeline deflection and displacement vectors in a front view, corresponding to the state of maximum displacement.

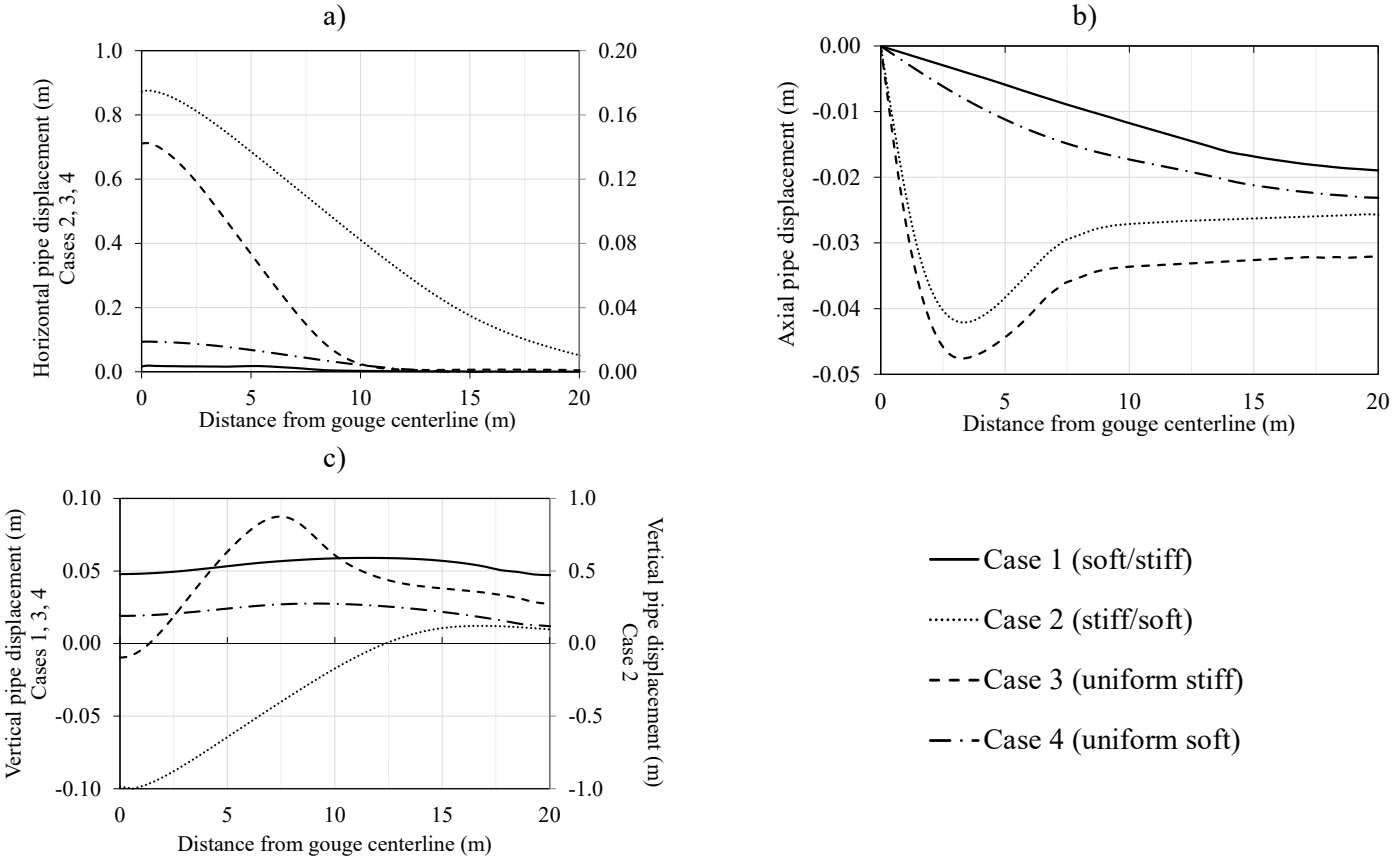

Figure 6-10. Pipeline displacement along the pipeline axis during the maximum displacement state, including (a) horizontal (gouge motion), (b) axial, and (c) vertical directions

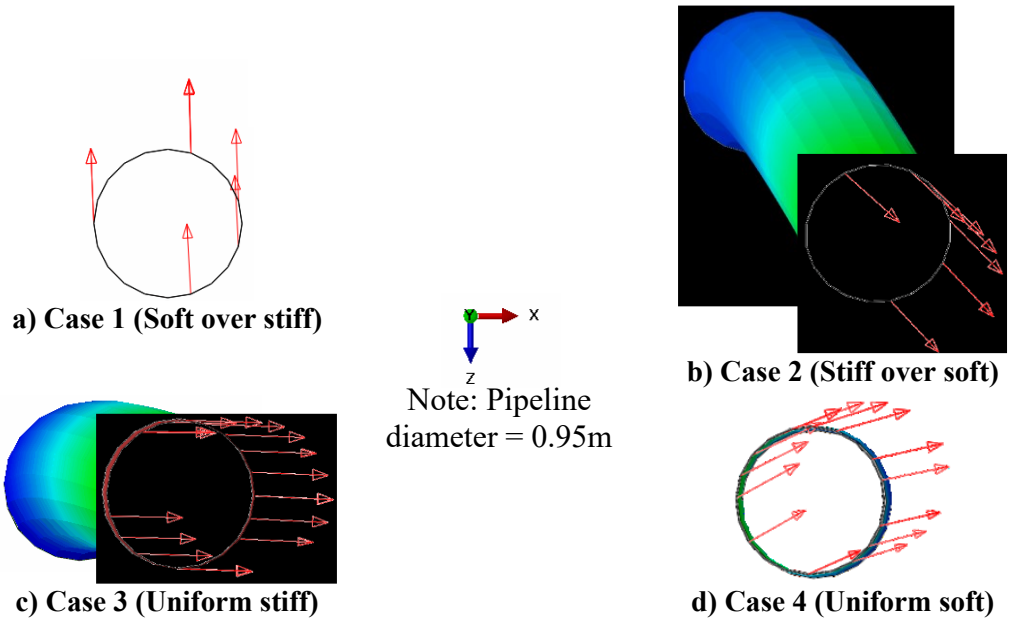

Figure 6-11. Pipeline deflection and displacement vectors at its Max. displacement state from the front view

The deformed shape and Von Mises stress contour of the pipeline under four different soil layered configurations have been presented in Figure 6-12. Figure 6-12 highlights the potential for errors in stress estimation when the soil medium is simplified to a uniform state. The 'soft over stiff' case exhibits the lowest stress values due to the interaction of soil layers observed in Figure 6-8(a). This interaction allows for a partial transfer of stress away from the pipe. In contrast, the 'stiff over soft' case (Figure 6-8(b)) experiences stress levels lower than the uniform stiff case but higher than the uniform soft case. The high stress in the uniform stiff scenario arises from the effect of the uniform stiff layer's high shear strength and the transfer of stresses from the ice directly to the pipe.

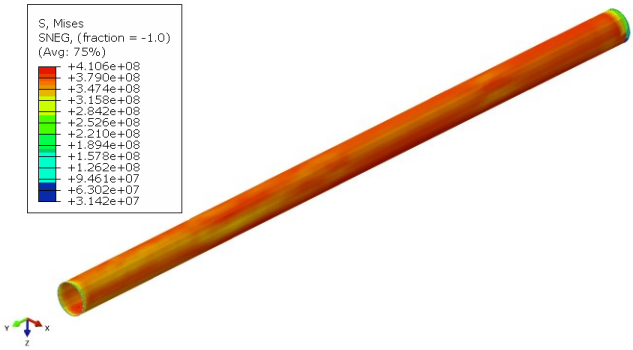

a) Case 1 (Soft over stiff)

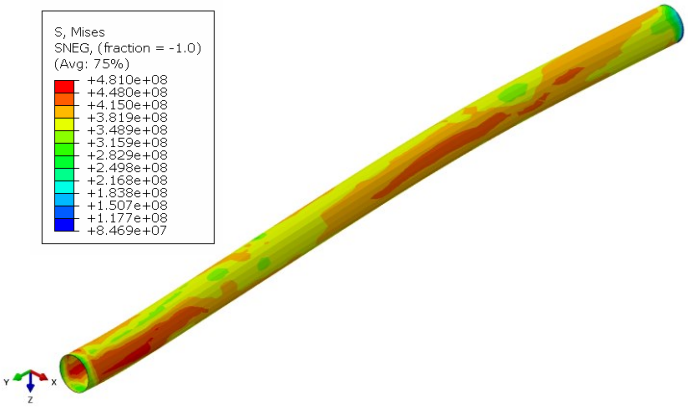

b) Case 2 (Stiff over soft)

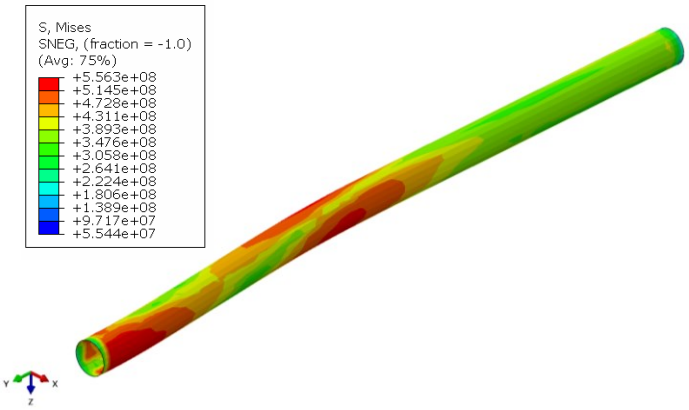

c) Case 3 (Uniform stiff)

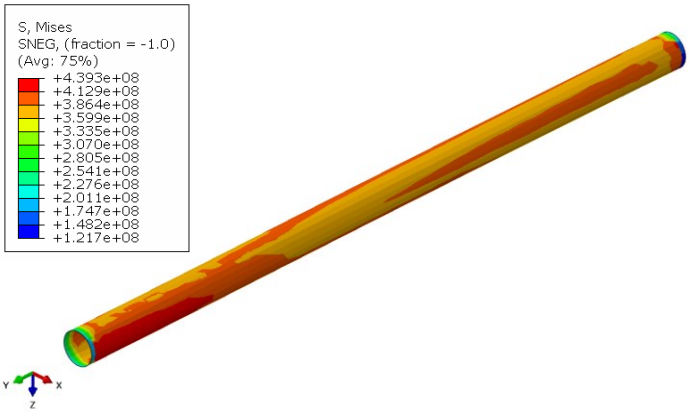

d) Case 4 (Uniform soft)

Figure 6-12. Stress distribution on deformed shapes of pipeline

Figures 6-13 and 6-14 illustrate the distribution of maximum axial strains induced in the pipeline along its longitudinal axis due to ice gouging loads. Ice gouging induces bending stresses in the central section of the pipeline, subjecting the leading surface to compression and the trailing surface to tension. Consistent with the axial displacement behavior, the "soft on stiff clay" configuration exhibits the lowest axial strain values. This result is a consequence of soil-layer interaction; the presence of the soft layer limits the transfer of stresses and strains from the gouging event to the underlying stiff layer. Additionally, the study indicates that assuming a uniform stiff layer when a layered profile is present might lead to overestimating the pipeline's compressive or tensile failure risk.

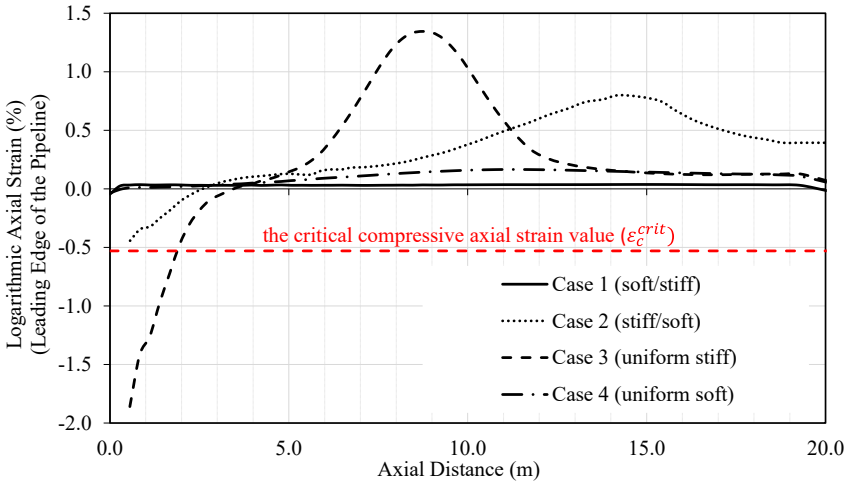

Figure 6-13. Logarithmic axial strain for the leading edge of the pipeline along the axis

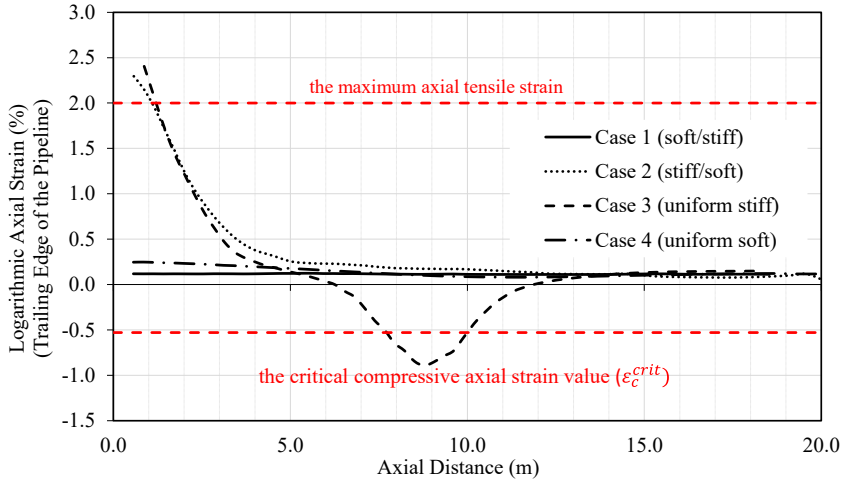

Figure 6-14. Logarithmic axial strain for the trailing edge of the pipeline along the axis

The study includes an analysis of pipeline ovalization. Pipe ovalization may occur due to a combination of factors. These include internal pressure and temperature acting during the initial stages of the analysis, as well as the external loading applied by the passing ice keel. Variations in the magnitude and distribution of strain along the pipeline circumference yield an irregular ovalization pattern. The way strain is spread out depends on the properties of the nearby soil. This becomes more complicated in the layered seabed and uneven media. Furthermore, the ice keel reaction forces play a pivotal role in determining the degree of ovalization, with higher forces leading to more pronounced ovalization, particularly evident in cases where stiff soil is on top of

the pipe. The study's findings align with the criteria employed for pipeline failure assessment, as illustrated in Figure 6-15.

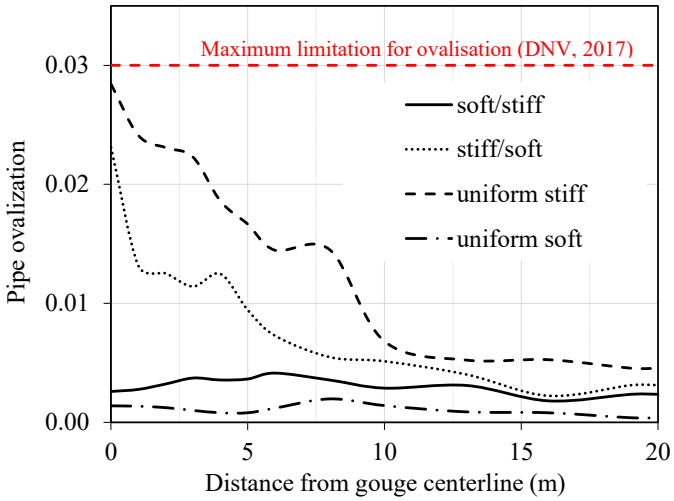

Figure 6-15. Pipeline ovalization along the pipe axis

Figures 6-13 to 6-15 highlight the critical importance of incorporating the non-uniformity of seabed soil characteristics into engineering design practices, particularly in relevant scenarios.

6.6.2 The Effect of Burying Pipeline into the Varied Soil Strength Layer with Constant Clearance Depth

In this section, the response of the pipe to the ice gouge in soil layers with different strengths and constant clearance depth is investigated. Cases 1, 5, 2, and 6 have been selected. In order to keep the clearance depth constant, the gouge depth is variable. In Figure 6-16, these 4 cases are shown schematically. In this section, it can be seen how the difference between burying the pipe in a soft or stiff layer affects the behavior of the pipe. Table 6-3 shows the horizontal and vertical ice keel reaction forces.

Table 6-3. Ice keel reaction forces

	Case 1 (soft/stiff buried in stiff)	Case 2 (stiff/soft buried in soft)	Case 5 (soft/stiff buried in soft)	Case 6 (stiff/soft buried in stiff)
Horizontal ice keel reaction force (MN)	5.1	9.5	2.75	6.7
Vertical ice keel reaction force (MN)	20.5	37.7	12.9	27.75

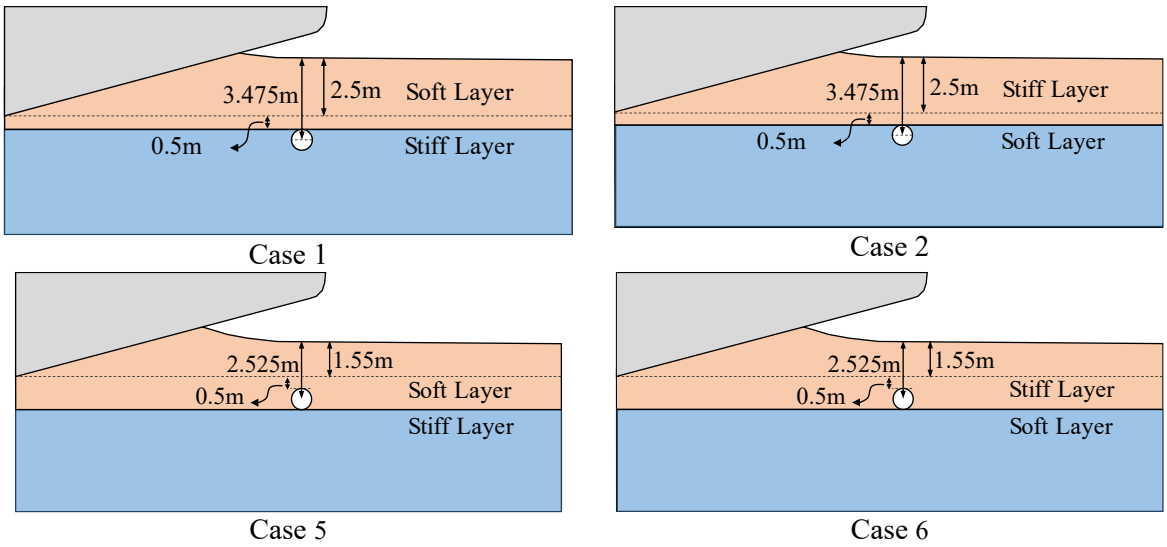

Figure 6-16. Schematics of configuration of cases 1, 2, 5, 6

Due to the expansion of the soil failure zone and its passive force, the reaction force is higher than the low ice depth at the higher depth of the gouge. Also, comparing cases with identical gouge depths reveals that the upper soil layer's shear strength significantly influences the ice-soil reaction forces.

6.6.2.1 Soil Displacement Mechanisms

Figure 6-17 illustrates that variations in pipe burial depth have a limited influence on the overall subgouge displacement mechanism. However, when the pipe is buried in soft soil, it experiences significant subgouge displacement due to the weak soil characteristics. Additionally, a comparison of Figures 6-17(d) and 6-17(b) reveals that burying the pipe at a greater depth corresponds to an

increase in the depth of the maximum subgouge displacement point. This phenomenon can be explained by the fact that the pipe acts as an obstacle to the natural flow of soil displacement during ice gouging and, consequently, a deeper maximum displacement point at greater burial depths.

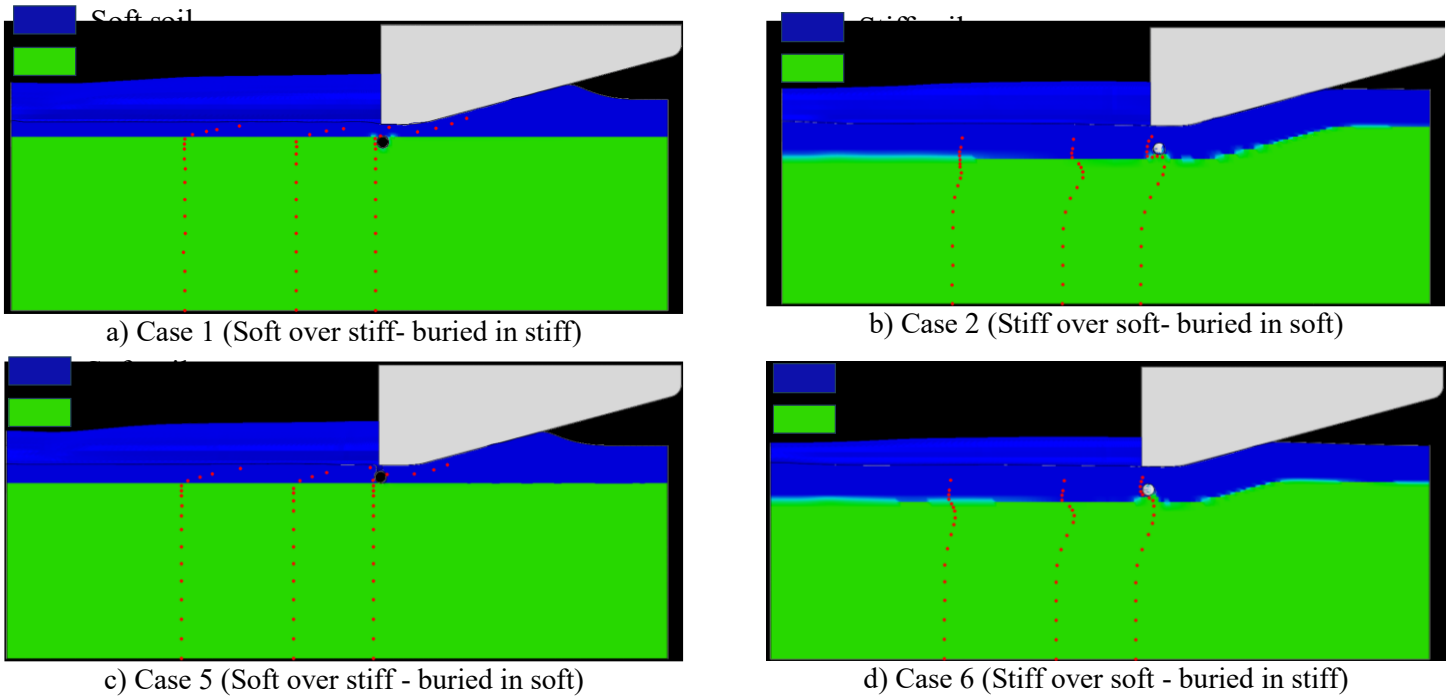

a) Case 1 (Soft over stiff- buried in stiff)

b) Case 2 (Stiff over soft- buried in soft)

c) Case 5 (Soft over stiff - buried in soft)

d) Case 6 (Stiff over soft - buried in stiff)

Figure 6-17. The positioning of the soil, pipeline, ice, and tracer particles at the maximum pipe displacement

Figure 6-18 illustrates the equivalent plastic shear strains (PEEQVAVG) in layered seabed scenarios. Figures 6-18(a) and (c) reveal a similar distribution pattern of maximum plastic shear strain for the 'soft over stiff layer' configuration during ice gouging.

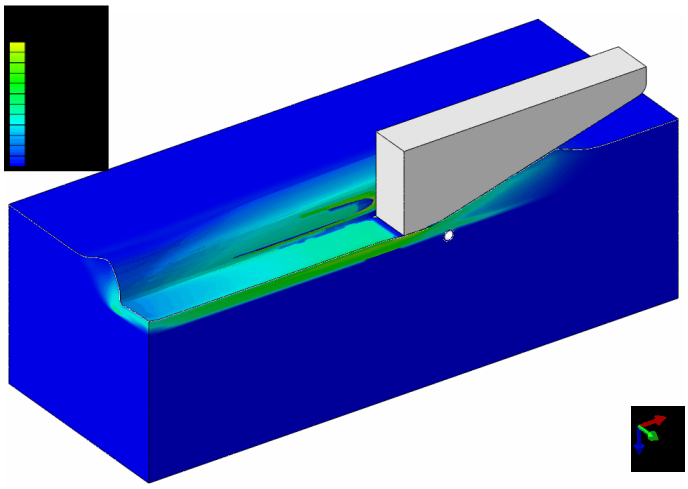

a) Case 1 (Soft over stiff- buried in stiff)

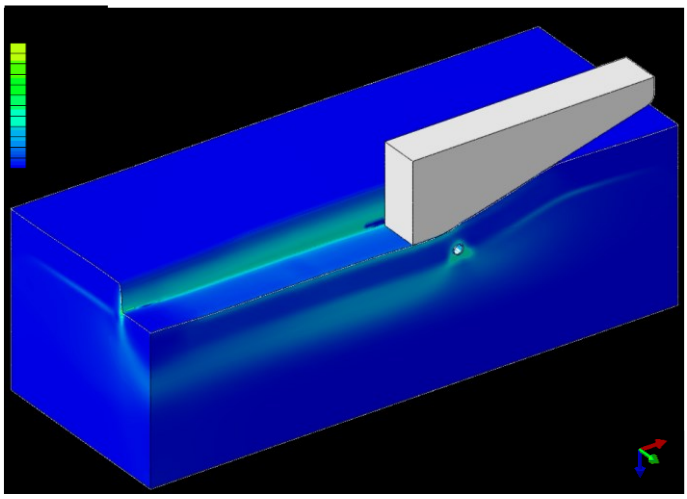

b) Case 2 (Stiff over soft- buried in soft)

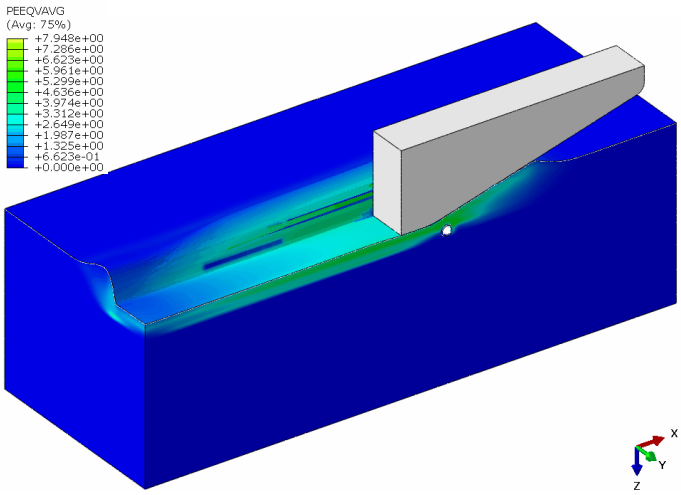

c) Case 5 (Soft over stiff - buried in soft)

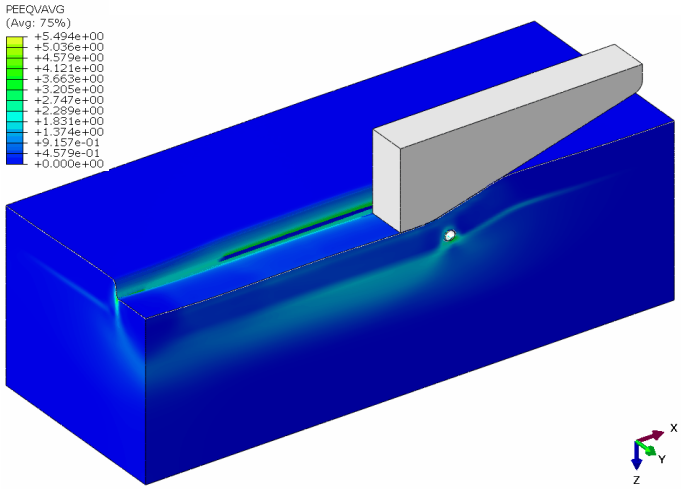

d) Case 6 (Stiff over soft - buried in stiff)

Figure 6-18. The effect of gouging in different layered soil strata on progressive plastic shear strain

As in previous observations, the strain concentrates primarily in the contact zones between the keel chest and the frontal mound, as well as the keel base and the underlying soft soil. A critical implication for pipeline safety is highlighted in these figures. When the pipeline resides within the soft soil layer (Figures 6-18(a) and (c)), it coincides with a zone of high equivalent plastic shear strain. This can pose a significant safety risk to the pipeline integrity. Figures 6-18(b) and (d) illustrate the phenomenon of strain transfer during the gouging process. The stiff layer acts as an intermediary, transferring considerable plastic strain to the underlying soft soil layer. This

observation emphasizes that even with increased burial depth (Figure 6-18(d)), the pipe remains susceptible to high levels of plastic shear strain within the soft soil.

6.6.2.2 Pipeline Response

Figure 6-19 compares the pipeline's trajectory along the gouge centerline for different seabed configurations and pipe burial depths. In the "soft over stiff clay" configuration, burial within the lower stiff layer results in substantial upward movement due to its high passive horizontal resistance and the low uplift resistance of the soft layer. Conversely, when the pipe is buried in the soft layer, low horizontal passive resistance and the stiff layer's high bearing resistance lead to a horizontal displacement exceeding three times the vertical displacement.

The "stiff over soft" profile exhibits a similar trend, but the horizontal displacement of the pipe buried in the soft layer exceeds twice as much as that in the stiff layer. These observations align with the findings of Hashemi et al. (2023), which emphasize that, in stratified soil, maximizing burial depth does not necessarily guarantee reduced displacement or enhanced pipeline safety.

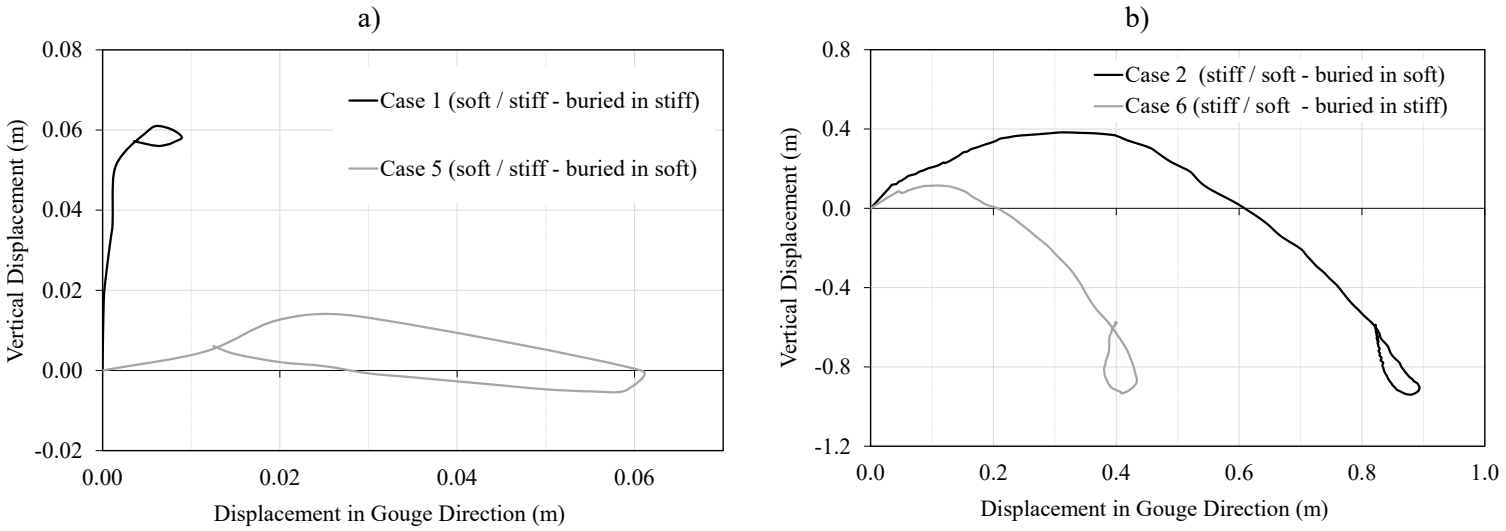

Figure 6-19. Pipeline trajectory in the vertical plane at gouge centerline

The pipeline maximum displacement along the longitudinal axis of the pipeline, including the horizontal (gouge direction), axial, and vertical directions, is illustrated in Figure 6-20. Figure 6-20(a), consistent with Figure 6-19, illustrates those cases where the pipe is buried within the soft layer and experience more significant horizontal displacement due to the low horizontal passive resistance of the soil. This observation is mirrored in the axial displacement, where the reduced axial resistance of the soft layer translates to lower frictional stress and, consequently, higher axial displacement for the pipe in these cases. The higher vertical displacement observed in Case 1 compared to Case 5 can be attributed to the same rationale stated in the previous section (high horizontal passive resistance of stiff clay and low uplift resistance of upper soft clay). Notably, the maximum vertical displacement in Cases 2 and 6 exhibits minimal variation. This can be ascribed to the high uplift resistance of the stiff soil, leading to similar pipe behavior in "stiff clay over soft clay" scenarios. Figure 6-21 depicts the pipeline deflection and displacement vectors in a front view, corresponding to the state of maximum displacement.

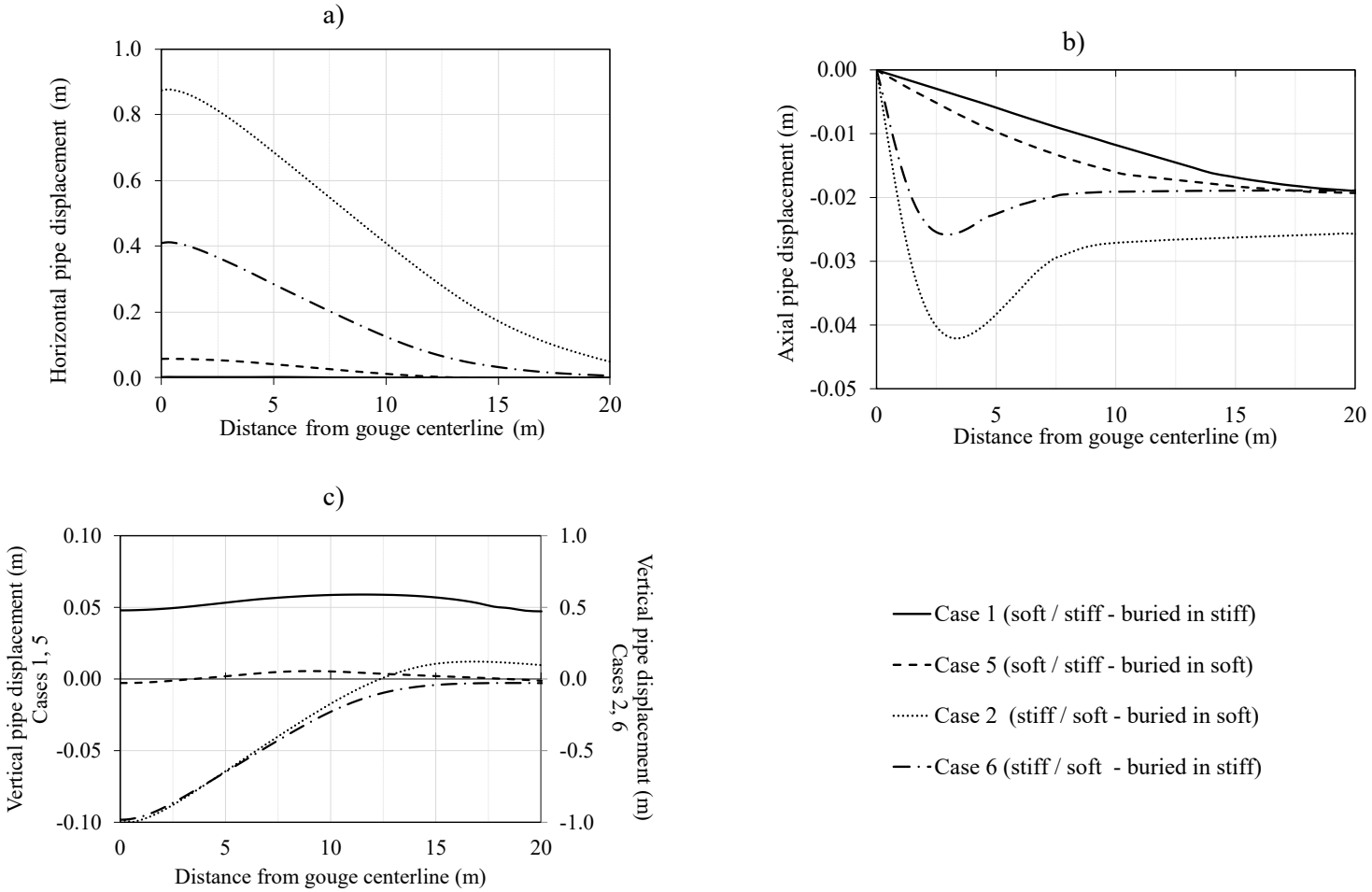

Figure 6-20. Pipeline displacement along the pipeline axis during the maximum displacement state, including (a) horizontal (gouge motion), (b) axial, and (c) vertical directions

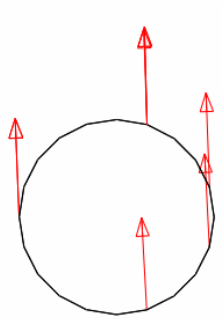

a) Case 1 (Soft over stiff- buried in stiff)

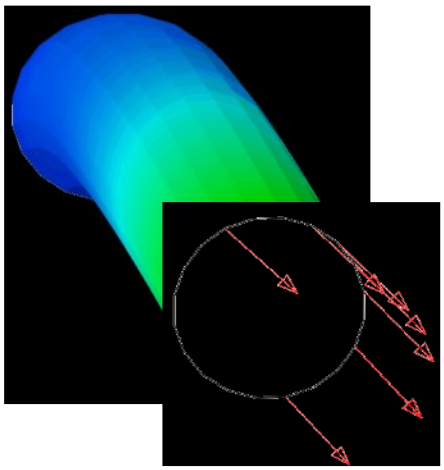

b) Case 2 (Stiff over soft- buried in soft)

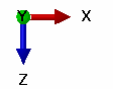

Note: Pipeline diameter = 0.95m

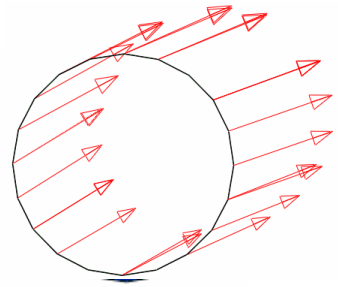

c) Case 5 (Soft over stiff - buried in soft)

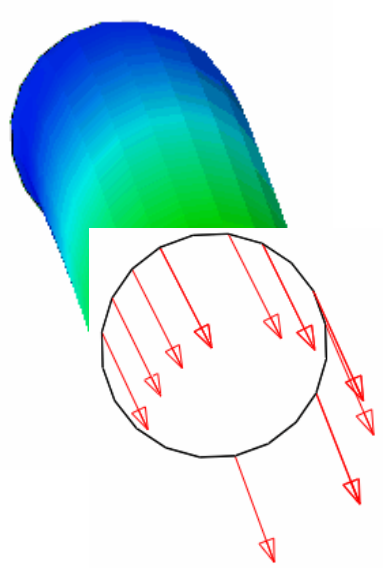

d) Case 6 (Stiff over soft - buried in stiff)

Figure 6-21. Pipeline deflection and displacement vectors at its maximum displacement state from the front view

Figure 6-22 presents the deformed shape and stress contour of the pipeline under four different soil-layered configurations. A comparison of "soft over stiff clay" scenarios reveals that burying the pipe within the lower stiff soil layer reduces the stresses acting on the pipe. This can be attributed to the reduced interfacial friction between the soft soil layer and the pipe. The weaker soil allows for a degree of relative movement between the pipe and the surrounding soil, thereby

mitigating the direct transfer of stresses from the ice gouging event. In contrast, the comparison of "stiff over soft clay" scenarios (Cases 2 and 6) demonstrates that burying the pipe in stiff soil increases stress tolerance at the pipe's centerline despite experiencing less deflection.

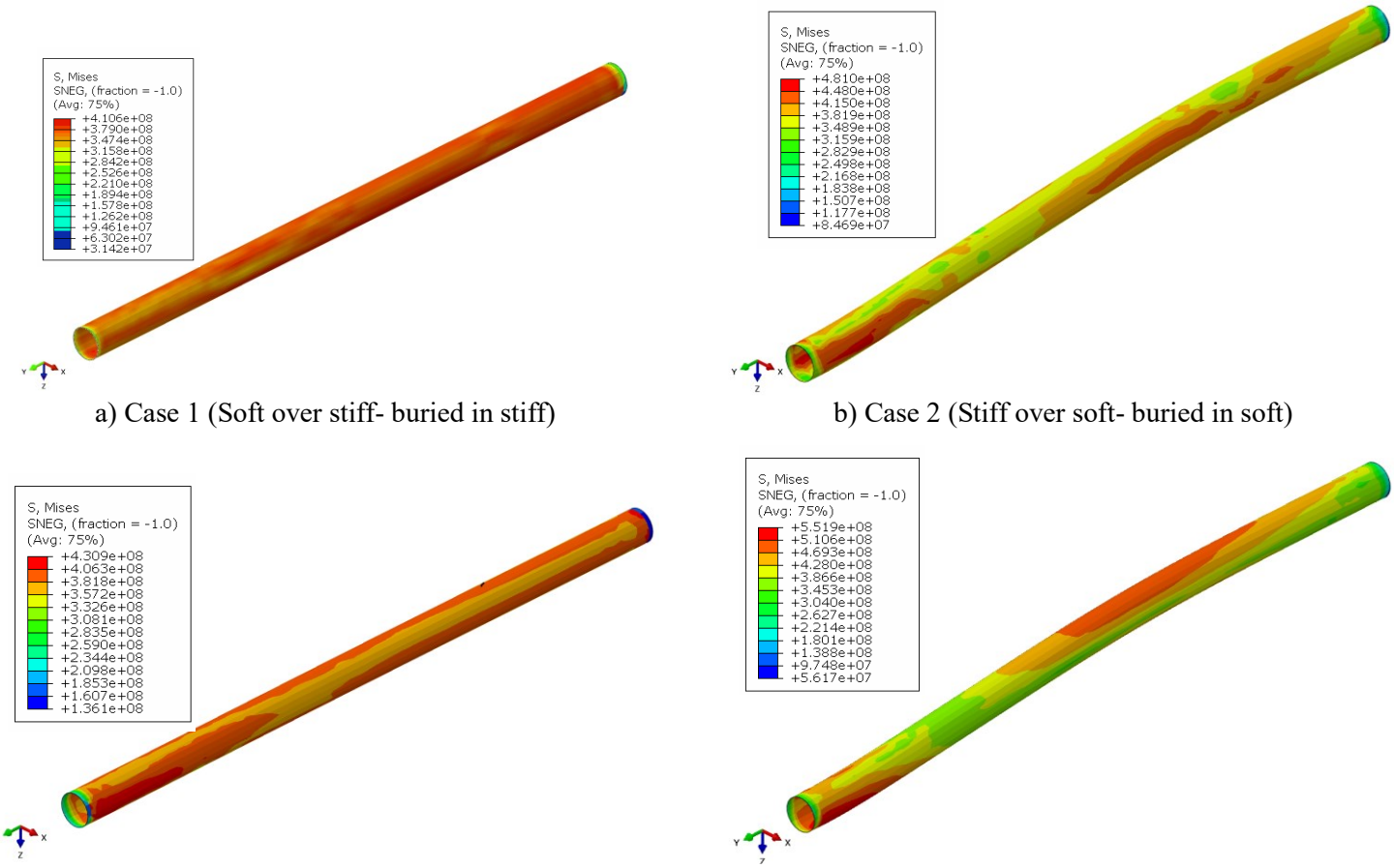

a) Case 1 (Soft over stiff- buried in stiff)

b) Case 2 (Stiff over soft- buried in soft)

c) Case 5 (Soft over stiff - buried in soft)

d) Case 6 (Stiff over soft - buried in stiff)

Figure 6-22. Stress distribution on deformed shapes of pipeline

Figures 6-23 and 6-24 depict the maximum axial strains experienced by the pipeline along its axis due to ice gouging loading. A comparative analysis reveals that placing the pipe in the stiff clay layer leads to a safer condition in terms of axial strain compared to other scenarios.

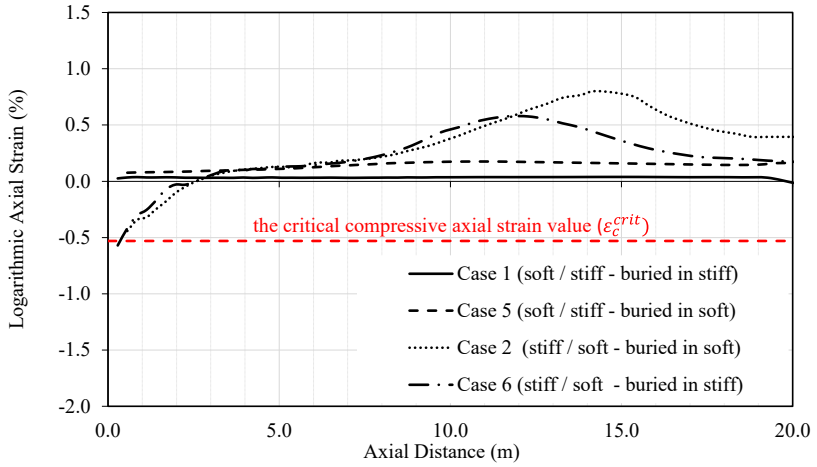

Figure 6-23. Logarithmic axial strain for the leading edge of the pipeline along the axis

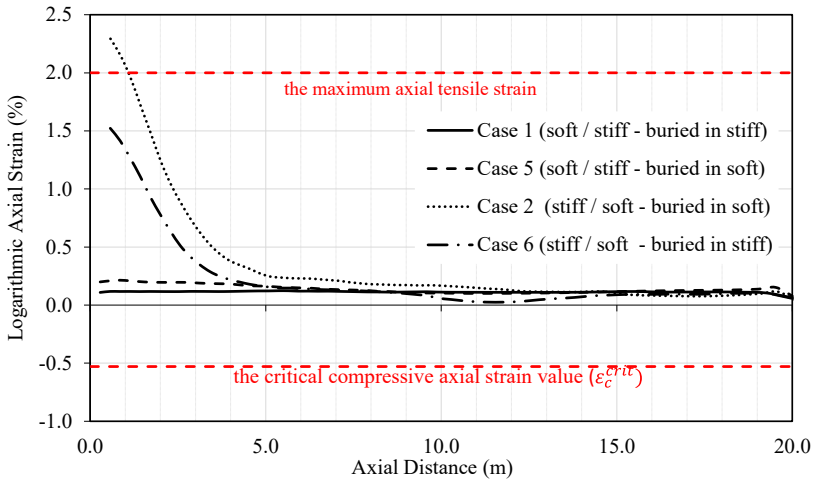

Figure 6-24. Logarithmic axial strain for the trailing edge of the pipeline along the axis

The ovalization results are demonstrated in Figure 6-25. Examining pipe ovalization in Case 1 versus Case 5 and Cases 2 versus 6 demonstrates slightly higher ovalization when the pipe is located in stiff clay. However, overall values in corresponding cases remain similar.

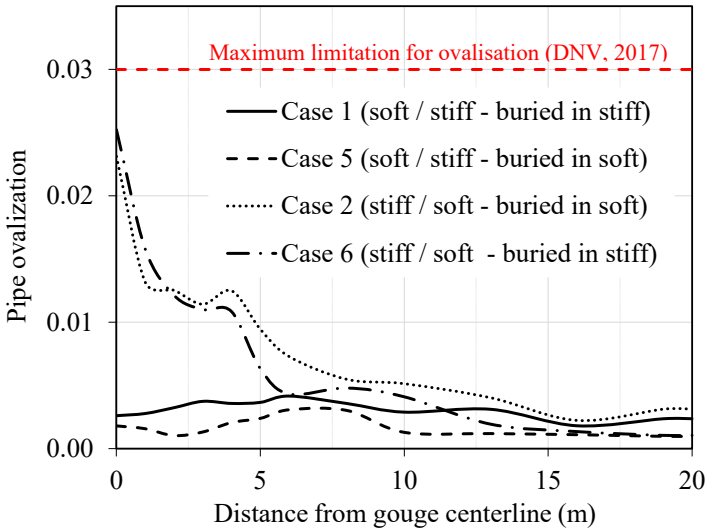

Figure 6-25. Pipeline ovalization along the pipe axis

These observations underscore the importance of considering soil layer interaction when evaluating pipeline integrity against ice gouging events using established criteria.

6.6.3 The Effect of Burying Pipeline into the Varied Soil Strength Layer with Constant Gouge Depth

This section investigates the influence of burial depth and layering on the pipeline's response to ice gouging while maintaining a constant gouge depth within a layered soil profile. Four distinct cases (Cases 7-10) are selected for analysis, with their configurations schematically presented in Figure 6-26. The corresponding horizontal and vertical ice keel reaction forces are detailed in Table 6-4.

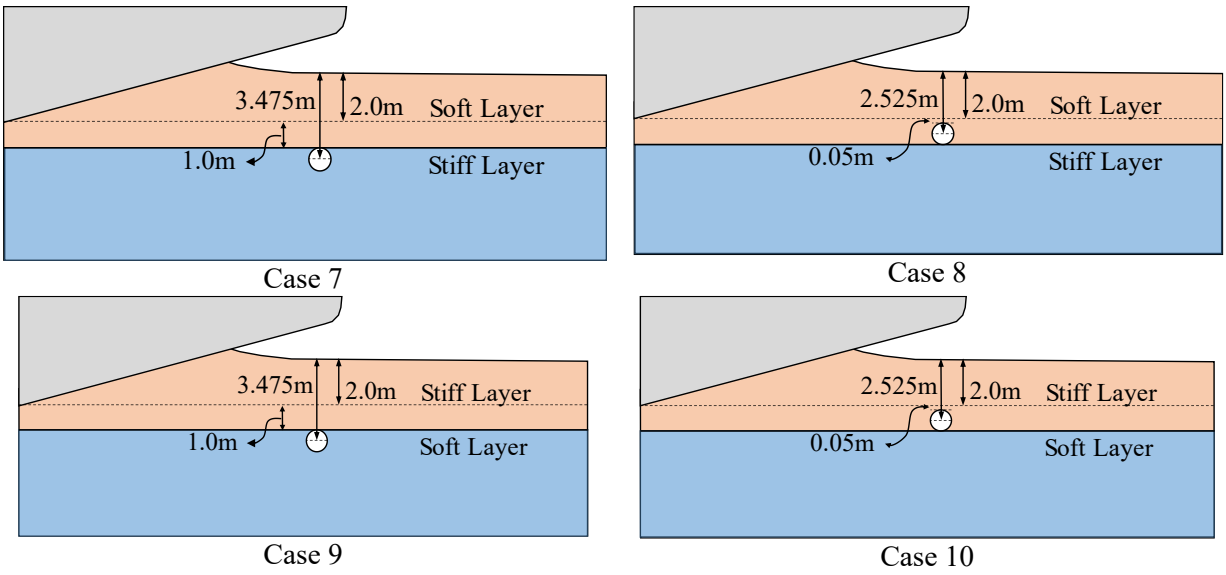

Figure 6-26. Schematics of configuration of cases 7-10

Table 6-4. Ice keel reaction forces

	Case 7 soft/stiff (buried in stiff)	Case 8 soft/stiff (buried in soft)	Case 9 stiff/soft (buried in soft)	Case 10 (stiff/soft buried in stiff)
Horizontal ice keel reaction force (MN)	3.5	3.6	7.6	7.5
Vertical ice keel reaction force (MN)	15.9	16.3	30.3	30.0

Analysis of the obtained forces reveals that the reaction force is unrelated to the pipe burial depth. Instead, the shear strength of the surrounding soil plays a crucial role in determining the magnitude of this force.

6.6.3.1 Soil Displacement Mechanisms

Figure 6-27 highlights the influence of burial depth and soil layering on pipe displacement. In the 'soft over stiff' configuration, a shallow pipe buried within the soft soil experiences significant horizontal displacement due to the large subgouge displacement of the soft layer. Conversely, burying the pipe below the interface of the two layers minimizes soil particle movement, resulting in a smaller horizontal pipe deflection. For the 'stiff over soft' configuration, a pipe buried closer

to the surface of the stiff layer experiences less subgouge displacement behind it. However, as the burial depth increases and approaches the peak of the subgouge displacement profile, the horizontal displacement of the pipe also increases.

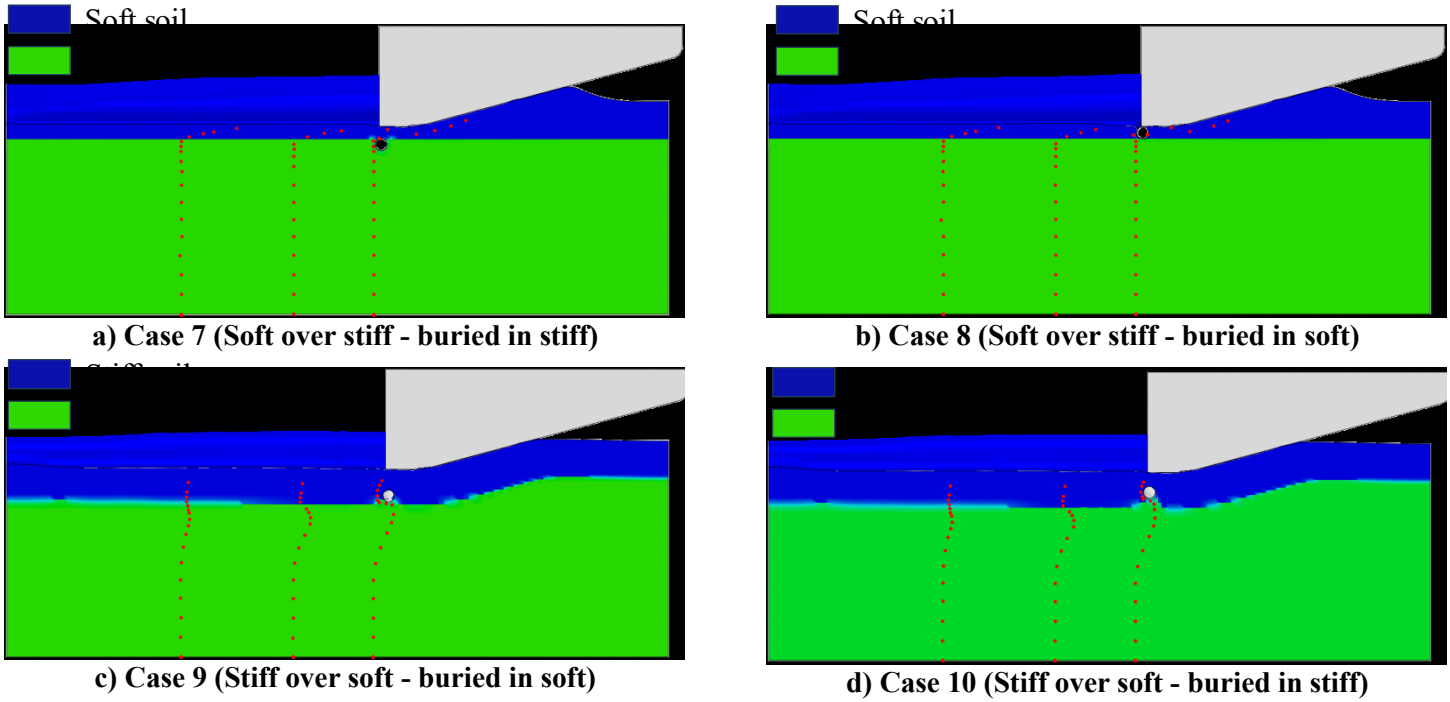

a) Case 7 (Soft over stiff - buried in stiff) **b) Case 8 (Soft over stiff - buried in soft)**

c) Case 9 (Stiff over soft - buried in soft) **d) Case 10 (Stiff over soft - buried in stiff)**

Figure 6-27. The positioning of the soil, pipeline, ice, and tracer particles at the maximum pipe displacement

Figure 6-28 compares equivalent plastic shear strains (PEEQVAVG) and resulting soil features. Figures 6-28(a) and (b) reveal a similar pattern of maximum plastic shear strain distribution for the 'soft over stiff' configuration during ice gouging. The strain concentrates primarily in the contact zones between the keel chest and the frontal mound, as well as the keel base and the underlying soft soil, aligning with previous observations.

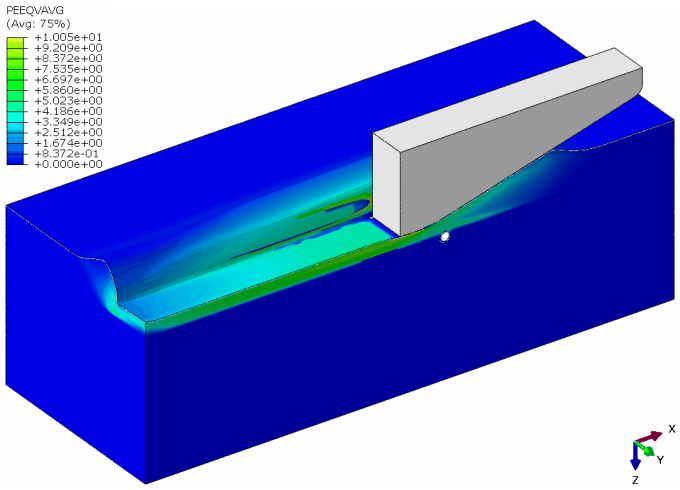

a) Case 7 (Soft over stiff - buried in stiff)

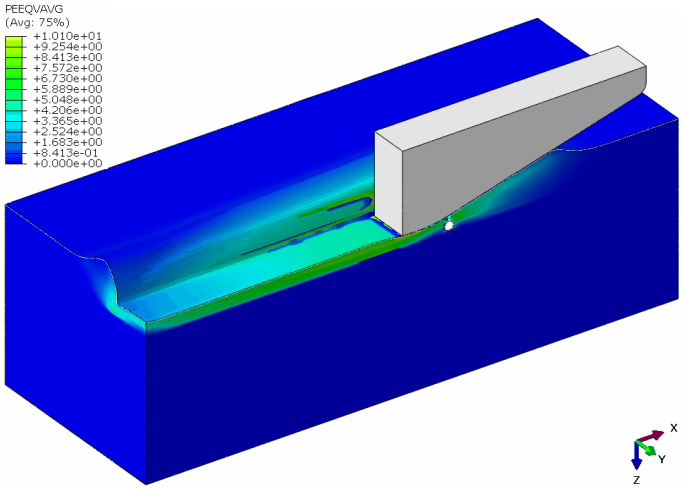

b) Case 8 (Soft over stiff - buried in soft)

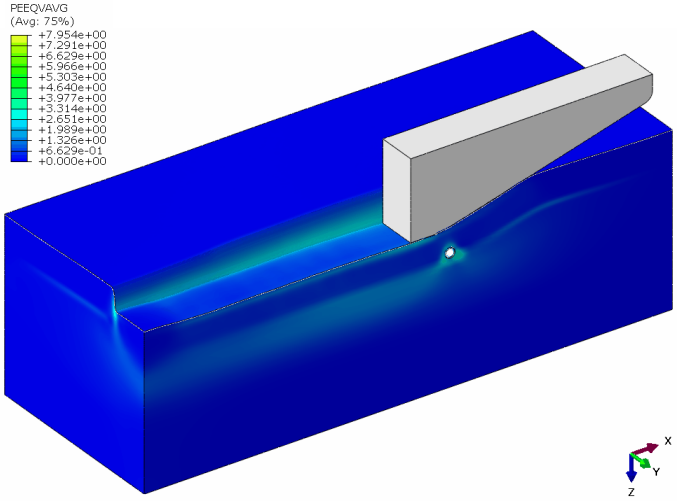

c) Case 9 (Stiff over soft - buried in soft)

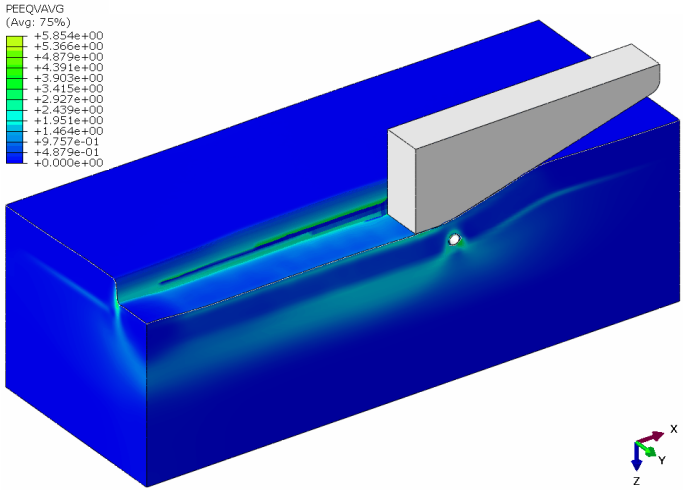

d) Case 10 (Stiff over soft - buried in stiff)

Figure 6-28. The effect of gouging in different layered soil strata on progressive plastic shear strain

The placement of the pipeline plays a crucial role in its safety. Figure 6-28(a) highlights a favorable scenario where burying the pipe directly beneath the interface, within the stiff layer, allows it to avoid the region of high equivalent plastic shear strain in the soft soil, potentially enhancing pipeline safety. However, Figures 6-28(c) and (d) reiterate the concept of strain transfer during gouging. It shows that even with increased burial depth within the stiff layer (Figure 6-28(d)), the pipe may still be exposed to high levels of plastic shear strain originating from the soft soil layer.

6.6.3.2 Pipeline Response

Figure 6-29 compares the pipelines' paths in the vertical plane along the centerline of the gouge. Figure 6-29 (a) illustrates that burying the pipe within the stiff soil layer significantly reduces the pipe's horizontal and overall displacement. This finding highlights the importance of considering soil layering, particularly in soft surface soils. By strategically placing the pipe within a stiffer layer, even with minimal additional depth, pipe displacement can be substantially reduced. Figure 6-29(b) demonstrates that contrary to common assumptions, increasing the burial depth up to 95 cm and placing the pipe within the soft layer while maintaining the same gouge depth can increase horizontal displacement with minimal impact on the overall displacement.

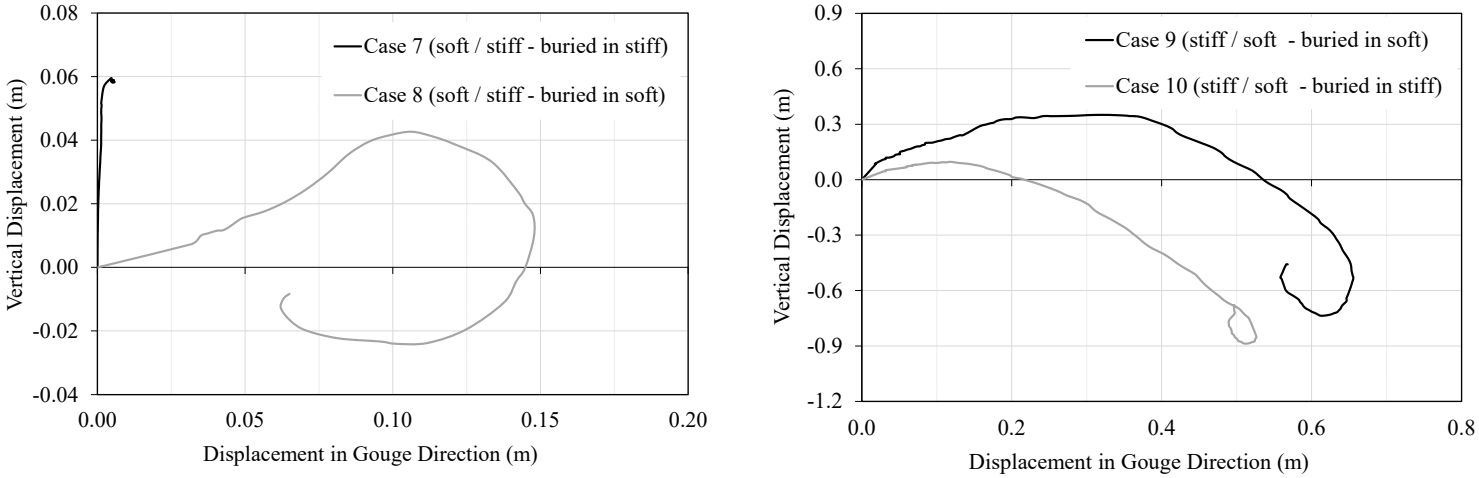

Figure 6-29. Pipeline trajectory in the vertical plane at gouge centerline

Figure 6-30 illustrates the maximum displacement along the longitudinal axis of the pipeline in three principal directions. Figure 6-30(a) demonstrates that burying the pipe within the stiff layer consistently results in lower horizontal displacement, regardless of the specific layering configuration. This observation can be attributed to soft soil's weak, passive lateral resistance, which cannot effectively restrain pipe movement even with increased clearance depth. Figure 6-30(b) highlights a significant reduction in axial displacement exceeding 40% for Case 7, where

the pipe is embedded within the stiff layer. Figure 6-30(c) visually confirms the stiff layer's effectiveness in preventing the pipe's downward movement in the soft clay over stiff clay configurations. Notably, even in the stiff soil on soft soil scenario, an increase in burial depth of 95 cm yielded a maximum displacement reduction of 9%. A frontal view of the pipeline's maximum deflection and displacement vectors is presented in Figure 6-31.

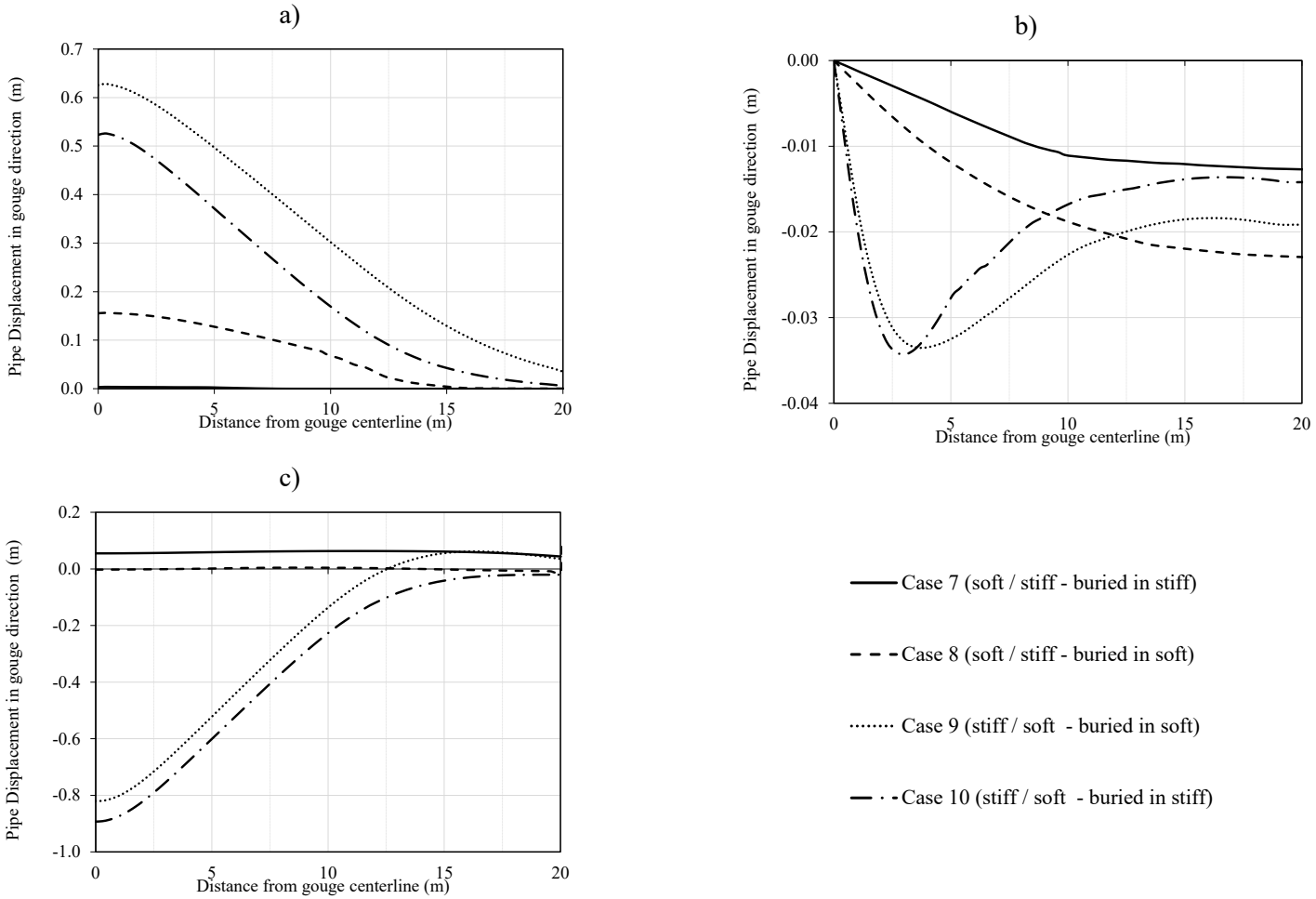

Figure 6-30. Pipeline displacement along the pipeline axis during the maximum displacement state, including (a) horizontal (gouge motion), (b) axial, and (c) vertical directions

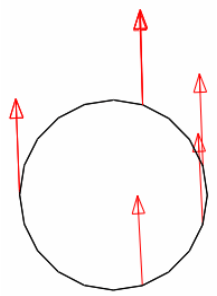

a) Case 7 (Soft over stiff - buried in stiff)

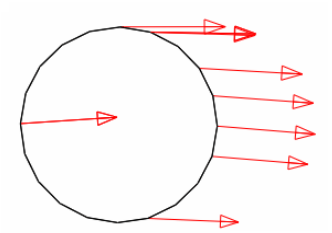

b) Case 8 (Soft over stiff - buried in soft)

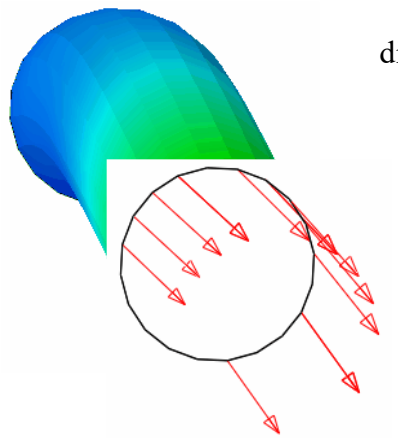

c) Case 9 (Stiff over soft - buried in soft)

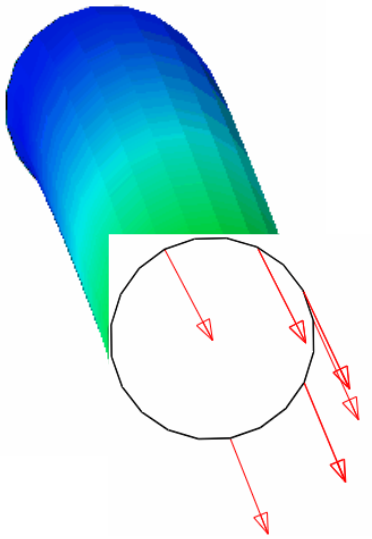

Note: Pipeline diameter = 0.95m

d) Case 9 (Stiff over soft - buried in stiff)

Figure 6-31. pipeline deflection and displacement vectors at its maximum displacement state from the front view.

Figure 6-32 underscores the interaction between the soft and stiff soil layers in stress distribution. When the pipe is buried within the stiff layer (owing to the reduced deflection observed in this configuration), it experiences lower stress levels. Conversely, examining the 'stiff over soft' cases reveals that increasing the pipe's burial depth does not significantly reduce stress. This observation suggests that simply increasing burial depth may not be an optimal mitigation strategy for ensuring pipeline integrity, and alternative measures should be considered in such scenarios.

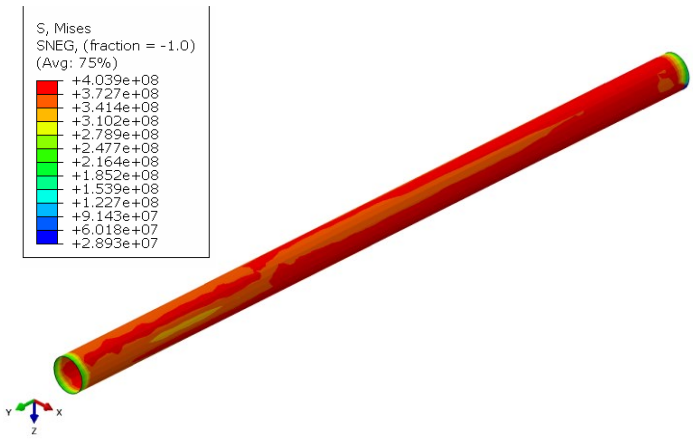

a) Case 7 (Soft over stiff- buried in stiff)

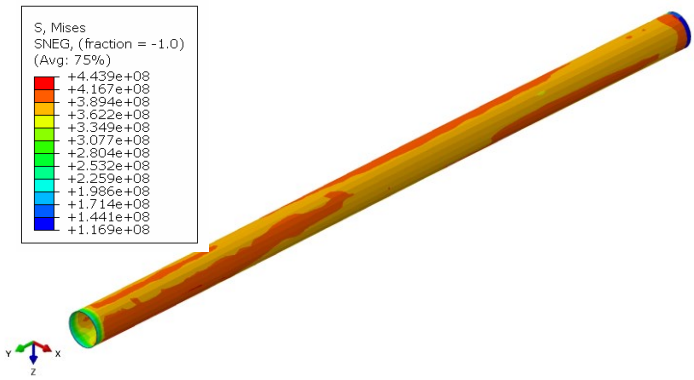

b) Case 8 (Soft over stiff - buried in soft)

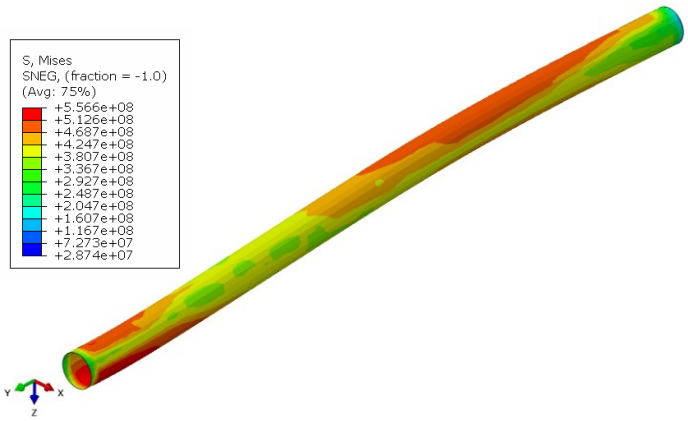

c) Case 9 (Stiff over soft - buried in soft)

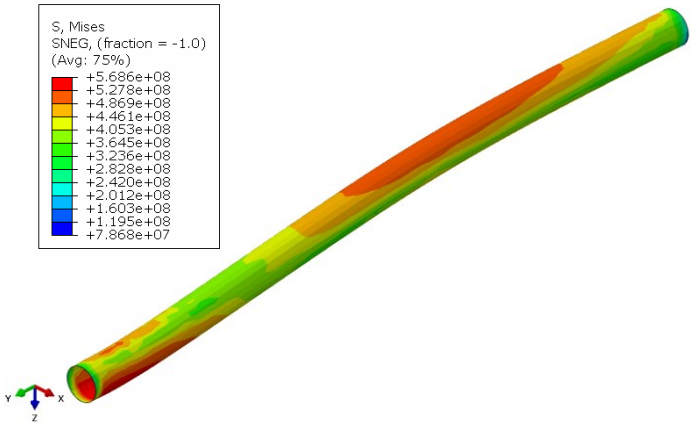

d) Case 10 (Stiff over soft - buried in stiff)

Figure 6-32. Stress distribution on deformed shapes of pipeline

Analysis of Figures 6-33 and 6-34 reveals minimal variation in axial strain for both the soft over stiff and stiff over soft configurations. This suggests that the burial in different strength layers has a limited influence on the axial strain experienced by the pipe.

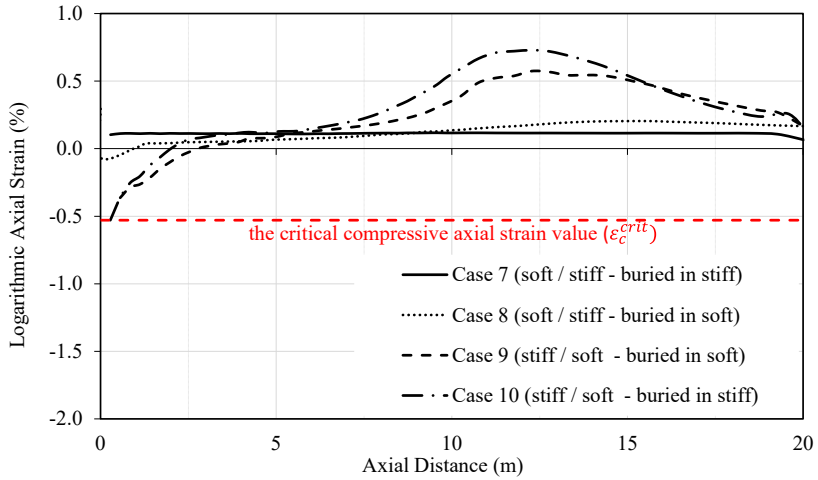

Figure 6-33. Logarithmic axial strain for the leading edge of the pipeline along the axis

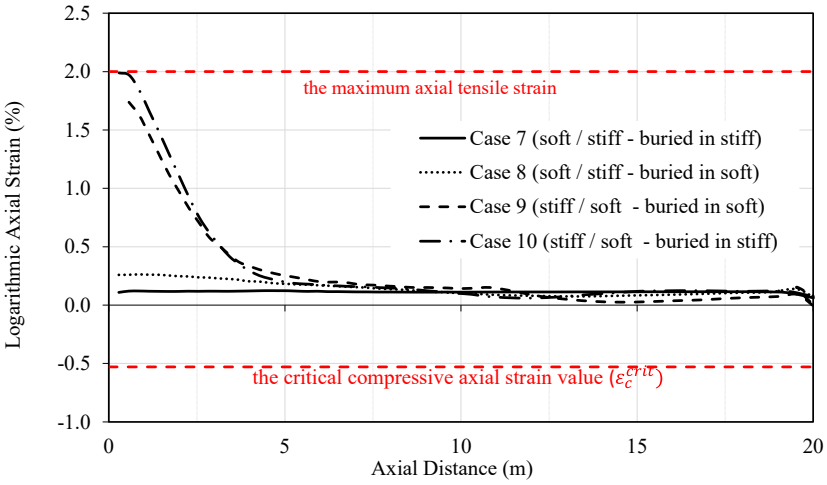

Figure 6-34. Logarithmic axial strain for the trailing edge of the pipeline along the axis

Figure 6-35 illustrates a comparable trend in ovalization across similar configurations. This observation suggests that the primary factor influencing pipe ovalization is the variation in the peripheral stresses acting upon it. Interestingly, the figure also reveals a slightly higher degree of ovalization in cases where the pipe is buried within stiff soil compared to soft soil. This phenomenon can be attributed to the increased stiffness of the surrounding soil, which may constrain the pipe's ability to deform freely.

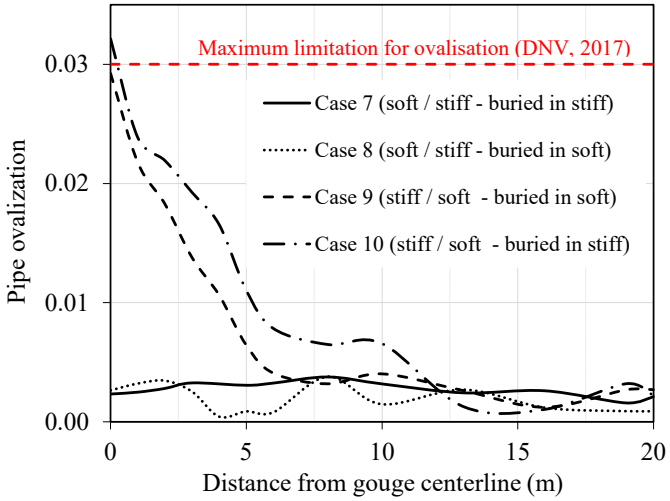

Figure 6-35. Pipeline ovalization along the pipe axis

In conclusion, the findings on pipeline displacement, Von Mises stresses, axial strain, and ovalization within layered seabed configurations highlight the need to strategically position pipelines for optimal performance under ice gouging loads, challenging conventional assumptions about the benefits of deeper burial.

6.7 Conclusions

This study investigates the ice-soil layers-pipeline interaction within layered seabed during ice gouging events, employing continuum finite element modeling (CEL). The model incorporated the Einav and Randolph (2005) relationship to account for strain softening and shear rate effects within the clay soil. Numerical simulations were conducted for various seabed, gouging, and pipeline configurations. The key findings of this investigation are summarized as follows:

- The shear resistance of the scoured soil significantly affects the ice reaction force, mainly when the depth of the gouge falls within the range of the upper layer. Simplifying the seabed to a uniform configuration can lead to substantial calculation errors, with variations

of up to 47% reduction or 240% increase in vertical ice reaction force observed when comparing soft over stiff clay scenarios to uniform seabed assumptions.

- Assumptions of the uniform soft or stiff seabed, instead of the actual "soft over stiff" layering, can lead to overestimating pipeline trajectory. Conversely, neglecting the "stiff over soft" layering and adopting uniform assumptions underestimates pipeline deformation. Also, uniform soil profiles can lead to overestimated or underestimated stress, potentially resulting in insufficient or excessive design measures.

- Uniform soil assumptions can lead to inaccurate predictions of axial strain values. The configuration of "soft on stiff clay" exhibits lower axial strain values than uniform soil cases, highlighting the role of soil-layer interaction in limiting stress and strain transfer between layers. Neglecting the non-uniformity of seabed soil characteristics can lead to overestimating the pipeline's compressive or tensile failure risk.

- Examining the effect of burying the pipeline into layers of varied soil strength reveals that placing the pipe in stiff clay leads to safer conditions in terms of axial strain, albeit with slightly higher ovalization compared to scenarios with the pipe in softer layers.

- Strategic burial depth and consideration of soil layering are crucial for mitigating pipeline displacement due to ice gouging. Placing the pipe within a stiffer layer can substantially reduce displacement and stresses, even with minimal additional depth in case of soft over stiff clay.

- Contrary to common assumptions, increasing burial depth within the soft layer may lead to increased horizontal displacement and stress in case of stiff over soft clay, underscoring the importance of detailed soil layer analysis in pipeline design and placement decisions.

Acknowledgments

The authors gratefully acknowledge the financial support of the "Wood" through establishing the Research Chair program in Arctic and Harsh Environment Engineering at the Memorial University of Newfoundland, the "Natural Science and Engineering Research Council of Canada (NSERC)" and the "Newfoundland Research and Development Corporation (RDC) (now IET) through "Collaborative Research and Developments Grants (CRD)". Special thanks are extended to Memorial University for providing excellent resources for conducting this research program.

References

ALA. (2001). Guidelines for the design of buried steel pipe. American Society of Civil Engineers.

ASCE. (1984). Guidelines for the Seismic Design of Oil and Gas Pipeline Systems. Amer Society of Civil Engineers.

Been, K., Sancio, R. B., Ahrabian, D., van Kesteren, W., Croasdale, K., & Palmer, A. (2008). Subscour displacement in clays from physical model tests. 2008 7th International Pipeline Conference, 239–245.

Biscontin, G., & Pestana, J. M. (2001). Influence of peripheral velocity on vane shear strength of an artificial clay. Geotechnical Testing Journal, 24(4).

C-CORE. (1995). Pressure Ridge Ice Scour Experiment, PRISE: Phase 3-Centrifuge Modelling of Ice Keel Scour: Draft Final Report.

C-CORE. (2008). Design Options for Offshore Pipelines in the US Beaufort and Chukchi Seas.

CSA. (2015). CSA Z662-15: Oil and gas pipeline systems.

Dayal, U., & Allen, J. H. (1975). The effect of penetration rate on the strength of remolded clay and sand samples. Canadian Geotechnical Journal, 12(3), 336–348.

DNV GL. (2017). DNVGL-ST-F101, Submarine pipeline systems.

Einav, I., & Randolph, M. F. (2005a). Combining upper bound and strain path methods for evaluating penetration resistance. International Journal for Numerical Methods in Engineering, 63(14), 1991–2016.

Einav, I., & Randolph, M. F. (2005b). Combining upper bound and strain path methods for evaluating penetration resistance. International Journal for Numerical Methods in Engineering, 63(14), 1991–2016.

Eskandari, F. (2014). Buried pipeline response to ice gouging. Memorial University of Newfoundland.

FitzMaurice, A., Straneo, F., Cenedese, C., & Andres, M. (2016). Effect of a sheared flow on iceberg motion and melting. Geophysical Research Letters, 43(24), 12–520.

Graham, J., Crooks, J. H. A., & Bell, A. L. (1983). Time effects on the stress-strain behaviour of natural soft clays. Géotechnique, 33(3), 327–340.

Hashemi, S., & Shiri, H. (2022a). Numerical Modeling of Ice–Seabed Interaction in Clay by Incorporation of the Strain Rate and Strain-Softening Effects. Journal of Offshore Mechanics and Arctic Engineering, 144(4), 42101.

Hashemi, S., & Shiri, H. (2022b). The response of layered seabed to ice gouging: Sand over clay. Ocean Engineering, 266, 113134. https://doi.org/https://doi.org/10.1016/j.oceaneng.2022.113134

Hashemi, S., & Shiri, H. (2023a). Numerical Modeling of Ice-seabed Interaction in Layered Soil: Stiff over Soft Clay. Canadian Geotechnical Journal. https://doi.org/10.1139/cgj-2022-0594

Hashemi, S., & Shiri, H. (2023b). Numerical Modeling of Ice-seabed Interaction in Layered Soil: Stiff over Soft Clay. Canadian Geotechnical Journal. https://doi.org/10.1139/cgj-2022-0594

Hashemi, S., Shiri, H., & Dong, X. (2022a). The influence of layered soil on ice-seabed interaction: Soft over stiff clay. Applied Ocean Research, 120, 103033.

Hashemi, S., Shiri, H., & Dong, X. (2022b). The influence of layered soil on ice-seabed interaction: Soft over stiff clay. Applied Ocean Research, 120, 103033.

Konuk, I., Yu, S., & Gracie, R. (2005). An ALE FEM model of ice scour. 11th International Conference of the International Association of Computer Models and Advances in Geomechanics, Turin, Italy.

Lach, P. R. (1996). Centrifuge modelling of large soil deformation due to ice scour. Memorial University of Newfoundland. https://research.library.mun.ca/1194/

Liferov, P., & Høyland, K. V. (2004). In-situ ice ridge scour tests: experimental set up and basic results. Cold Regions Science and Technology, 40(1–2), 97–110.

Miller, D. L., & Bruggers, D. E. (1980). Soil and permafrost conditions in the Alaskan Beaufort Sea. Offshore Technology Conference, OTC-3887.

Nematzadeh, A., & Shiri, H. (2020). The influence of non-linear stress-strain behavior of dense sand on seabed response to ice gouging. Cold Regions Science and Technology, 170, 102929.

Palmer, A., Konuk, I., Love, J., Been, K., & Comfort, G. (1989). Ice Scour Mechanics. A Research Paper Prepared for Canada Oil and Gas Lands Administration and Gulf Canada Resources Ltd.

Peek, R., & Nobahar, A. (2012). Ice gouging over a buried pipeline: Superposition error of simple beam-and-spring models. International Journal of Geomechanics, 12(4), 508–516.

Phillips, R., Clark, J. I., & Kenny, S. (2005a). PRISE studies on gouge forces and subgouge deformations. Proceedings of the International Conference on Port and Ocean Engineering Under Arctic Conditions.

Phillips, R., Clark, J. I., & Kenny, S. (2005b). PRISE studies on gouge forces and subgouge deformations. Proceedings of the International Conference on Port and Ocean Engineering Under Arctic Conditions.

Pike, K., & Kenny, S. (2016). Offshore pipelines and ice gouge geohazards: comparative performance assessment of decoupled structural and coupled continuum models. Canadian Geotechnical Journal, 53(11), 1866–1881.

Pipelines, A. T. C. on T. R. D. of B. (2014). Soil Parameters for Assessing Axial and Transverse Behavior of Restrained Pipelinesâ€" Part 2: Transverse Behavior. Pipelines 2014: From Underground to the Forefront of Innovation and Sustainability, 1849–1863.

PRCI. (2009). Guidelines for Constructing Natural Gas and Liquid Hydrocarbon Pipelines through Areas Prone to Landslide and Subsidence Hazards, Pipeline Research Council International.

Raie, M. S., & Tassoulas, J. L. (2009). Installation of torpedo anchors: numerical modeling. Journal of Geotechnical and Geoenvironmental Engineering, 135(12), 1805–1813.

Randolph, M. F. (2004). Characterization of soft sediments for offshore applications. Proc. ISC-2 on Geotechnical and Geophysical Site Characterization, 2004.

Schoonbeek, I. S. S., & Allersma, H. G. B. (2006). Centrifuge modelling of scouring ice keels in clay. Proceedings, 8th International Conference on Physical Modelling in Geotechnics, ICPMG, 1291–1296.

Shiri, H., & Hashemi, S. (2023a). The Impact of Layering Seabed on its Response to Ice Gouging. In The 33rd International Ocean and Polar Engineering Conference (p. ISOPE-I-23-205).

Shiri, H., & Hashemi, S. (2023b). The Impact of Layering Seabed on its Response to Ice Gouging. In The 33rd International Ocean and Polar Engineering Conference (p. ISOPE-I-23-205).

Simulia, D. S. (2019). Abaqus 2019 documentation. Dassault Systemes Waltham, MA.

Winters, W. J., & Lee, H. J. (1984). Geotechnical properties of samples from borings obtained in the Chukchi Sea, Alaska (Vol. 85, Issue 23). US Geological Survey.

CHAPTER 7

Conclusions and Recommendations

7.1 Conclusions

This study investigates the influence of seabed non-uniformities on seabed displacement mechanisms and pipeline response during ice gouging events, utilizing the Coupled Eulerian-Lagrangian (CEL) method within Abaqus/Explicit. The model results were compared with existing experimental and numerical studies to validate the model's accuracy. To account for the effects of strain rate and strain softening in native and backfill clay soils, a modified Mohr-Coulomb soil model incorporating the Einav and Randolph (2005) relationship was implemented through a user-defined subroutine (VUSDFLD). The research addressed knowledge gaps in the field by examining the effects of trenching and backfilling, backfill properties, trenching techniques and geometry, and layered seabeds on pipeline response.

Key findings include:

- This study demonstrated a unique mode of soil failure in trenched and backfilled seabeds during ice gouging. The pressure the ice keel exerts against the stiffer trench walls displaces softer backfill material outwards while native soil flows into the initial trench boundaries. This interaction between the backfill and trench wall triggers a "removal" mechanism, where backfill is expelled from the trench, particularly in scenarios with very soft backfill, high trench wall angles, and narrow

trench widths. The extent of this "removal" mechanism is influenced by backfill stiffness, configuration, and trench geometry.

- Maximum plastic shear strain concentrates in specific zones, including the backfill, pipeline contact points, and interfaces between the ice keel and soil layers.
- Ice-keel reaction forces can be amplified, reduced, or remain relatively unchanged compared to a uniform seabed, depending on backfill properties and trench geometry. Softer backfills, wider trenches, and steeper trench wall angles tend to decrease these forces.
- Very soft backfills can significantly amplify pipeline displacement, stresses, and susceptibility to buckling or ovalization due to pipeline-backfill-trench wall interaction, low shear strength, and the "removal" mechanism.
- Among clay backfills, those with an intermediate undrained shear strength ratio (backfill undrained shear strength divided by native soil undrained shear strength) offer the best overall performance in mitigating pipeline displacement, stresses, and susceptibility to buckling or ovalization. A value of 0.42 represents the optimal value for maximizing pipeline performance under the studied ice-loading conditions.
- Trench geometry plays a key role in lateral pipeline behavior. Steeper trench walls and wider trench bottoms delay interaction between pipeline and stiffer trench wall, allowing for larger lateral displacement. However, trench geometry does not significantly impact axial strain or ovalization in the pipeline.

- Simplifying layered seabeds to a uniform condition can lead to inaccurate predictions of soil displacement, pipeline trajectory, ice-keel reaction forces, and pipeline stresses, impacting the determination of appropriate safety margins in pipeline design.
- In the context of a soft-over-stiff layered seabed, the strategic placement of the pipeline directly beneath the interface of the two layers, within the stiffer soil, can significantly enhance its protection against ice gouging. Even with a minimal increase in burial depth, this positioning can reduce pipeline displacement by more than twofold and alleviate stresses on the pipeline. The mechanism behind this enhanced protection lies in the decoupling effect at the interface between the soft and stiff layers, where the soft soil tends to slide over the stiffer layer, minimizing the latter's contribution to resisting ice gouging forces. While construction costs may be higher in the stiffer zone, this strategic placement offers a considerable advantage in terms of increased safety and a reduced risk of pipeline failure, potentially outweighing the initial cost implications.
- Importantly, this study shows that simply increasing burial depth within a softer layer (in the case of stiff over soft clay) may sometimes be counterproductive and could potentially increase pipeline displacement and stress.

7.2 Recommendations for Future Studies

This comprehensive study offers valuable insights into the behavior of buried pipelines during ice gouging events in non-uniform seabeds. The findings open several avenues for future research:

- Investigate and resolve discrepancies between CEL predictions for vertical subgouge soil displacement and experimental laboratory results.
- Conduct experimental studies considering trenching/backfilling and layered seabed conditions to further validate observed failure mechanisms and develop analytical solutions.
- Adapt the existing framework for simulating ice gouging in cohesionless soils (e.g., sand), and Investigate coupled ice-soil-pipeline interaction scenarios considering trenching/backfilling and layered seabed conditions.
- Model partially and fully drained soil conditions to understand how ice gouging processes manifest at lower velocities where field observations exist. Incorporate both consolidation and rate effects into the constitutive soil models, and validate against experimental data.
- Incorporate pre-peak strain hardening and post-peak strain softening effects to improve the modeling of dense sand behavior, including sand particle crushing under ice keel contact.
- Integrate the effects of trenching and backfilling into the existing layered seabed models, allowing for comprehensive analysis of pipeline response in complex seabed environments.
- Develop analytical solutions for ice gouging in non-uniform seabeds. Refine existing beam-spring models used in decoupled analysis approaches to incorporate the findings of this research.

While this study provides valuable insights into the influence of pipeline-backfill-trench interaction on pipeline response to ice gouging, it is important to acknowledge its limitations. The CEL method, while powerful for simulating large deformations, has inherent weaknesses in accurately predicting vertical subgouge deformation. Additionally, the assumption of a rigid, steady-state ice keel may not fully capture the complexities of real-world ice gouging scenarios, where ice crushing and variations in keel shape and attack angle can significantly influence soil failure mechanisms and pipeline response. Furthermore, the idealized representation of the pipeline as a homogenous material neglects the potential impact of weak zones, such as weld zones, on pipeline integrity.

By pursuing these research directions, engineers and scientists can further develop robust and accurate modeling tools for pipeline design and risk assessment in the challenging Arctic offshore environment.

Bibliography

Abdalla, B., Jukes, P., Eltaher, A., & Duron, B. (2008). The technical challenges of designing oil and gas pipelines in the arctic. OCEANS 2008, 1–11.

Abdalla, B., Pike, K., Eltaher, A., Jukes, P., & Duron, B. (2009). Development and validation of a coupled Eulerian Lagrangian finite element ice scour model. International Conference on Offshore Mechanics and Arctic Engineering, 43451, 87–95.

ALA. (2001). Guidelines for the design of buried steel pipe. American Society of Civil Engineers.

Almirall, S. A. (2017). Ice Gouging in Sand and the Associated Rate Effects. University of Aberdeen.

ASCE. (1984). Guidelines for the Seismic Design of Oil and Gas Pipeline Systems. Amer Society of Civil Engineers.

Asgarihajifirouz, M., Dong, X., & Shiri, H. (2023). Assessment of the Response of Trenched–Backfilled Pipelines to Strike-Slip Faults: An Analytical Approach. Geosciences, 13(2), 47.

Aslkhalili, A., Shiri, H., & Zendehboudi, S. (2020). Probabilistic Assessment of Lateral Pipeline-Backfill-Trench Interaction. Reliability Assessment of Drag Embedment Anchors and Laterally Loaded Buried Pipelines, 96.

Aslkhalili, A., Shiri, H., & Zendehboudi, S. (2021). Probabilistic assessment of lateral pipeline–Backfill–Trench interaction. Journal of Pipeline Systems Engineering and Practice, 12(3), 4021034.

Atangana Njock, P. G., Zheng, Q., Zhang, N., & Xu, Y.-S. (2020). Perspective Review on Subsea Jet Trenching Technology and Modeling. Journal of Marine Science and Engineering, 8(6), 460.

Azimi, H., & Shiri, H. (2020a). Dimensionless groups of parameters governing the ice-seabed interaction process. Journal of Offshore Mechanics and Arctic Engineering, 142(5), 51601.

Azimi, H., & Shiri, H. (2020b). Ice-Seabed interaction analysis in sand using a gene expression programming-based approach. Applied Ocean Research, 98, 102120.

Azimi, H., & Shiri, H. (2021a). Assessment of ice-seabed interaction process in clay using extreme learning machine. International Journal of Offshore and Polar Engineering, 31(04), 411–420.

Azimi, H., & Shiri, H. (2021b). Evaluation of ice-seabed interaction mechanism in sand by using self-adaptive evolutionary extreme learning machine. Ocean Engineering, 239, 109795.

Azimi, H., & Shiri, H. (2021c). Sensitivity analysis of parameters influencing the ice–seabed interaction in sand by using extreme learning machine. Natural Hazards, 106(3), 2307–2335.

Azimi, H., & Shiri, H. (2021d). Modeling subgouge sand deformations by using multi-layer perceptron neural network. ISOPE International Ocean and Polar Engineering Conference, ISOPE-I.

Azimi, H., Mahdianpari, M., & Shiri, H. (2023). Determination of parameters affecting the estimation of iceberg draft. China Ocean Engineering, 37(1), 62–72.

Azimi, H., Shiri, H., & Mahdianpari, M. (2022a). Iceberg-seabed interaction evaluation in clay seabed using tree-based machine learning algorithms. Journal of Pipeline Science and Engineering, 2(4), 100075.

Azimi, H., Shiri, H., & Mahdianpari, M. (2022b). Simulation of Subgouge Sand Deformations Using Robust Machine Learning Algorithms. Offshore Technology Conference, D021S028R009.

Azimi, H., Shiri, H., & Mahdianpari, M. (2023a). Iceberg draft prediction using gradient boosting regression algorithm. Marine Systems & Ocean Technology, 18(3), 151–166.

Azimi, H., Shiri, H., & Mahdianpari, M. (2023b). Sensitivity analysis of parameters governing the iceberg draft through neural network-based models. Journal of Ocean Engineering and Marine Energy, 9(4), 587–602.

Azimi, H., Shiri, H., & Mahdianpari, M. (2023c). Evaluation of iceberg draft and iceberg-seabed interaction using random forest regression algorithm. ISOPE International Ocean and Polar Engineering Conference, ISOPE-I.

Azimi, H., Shiri, H., & Mahdianpari, M. (2024). Generalized Structure of the Group Method of Data Handling for Modeling Iceberg Drafts. Ocean Modelling, 102337.

Azimi, H., Shiri, H., & Malta, E. R. (2021). A non-tuned machine learning method to simulate ice-seabed interaction process in clay. Journal of Pipeline Science and Engineering, 1(4), 379–394.

Azimi, H., Shiri, H., & Zendehboudi, S. (2022). Ice-seabed interaction modeling in clay by using evolutionary design of generalized group method of data handling. Cold Regions Science and Technology, 193, 103426.

Bai, Y., & Bai, Q. (2005). Subsea pipelines and risers. Elsevier.

Banneyake, R., Hossain, M. K., Eltaher, A., Nguyen, T., & Jukes, P. (2011). Ice-soil-pipeline interactions using coupled eulerian-lagrangian (CEL) ice gouge simulations-extracts from ice pipe JIP. OTC Arctic Technology Conference.

Barker, A., & Timco, G. (2002). Laboratory experiments of ice scour processes: rigid ice indentor. Cold Regions Science and Technology, 35(3), 195–206.

Barker, A., & Timco, G. (2003). Laboratory experiments of ice scour processes: buoyant ice model. Cold Regions Science and Technology, 36(1–3), 103–114.

Barrette, P. D., & Timco, G. W. (2008). Ice scouring in a large flume: Test set-up and preliminary observations. SNAME International Conference and Exhibition on Performance of Ships and Structures in Ice, D041S015R001.

Barrette, P., Marquardt, J., & Timco, G. (2009). Test data from scour simulations with rigid indentors and real ice rubble. CHC-NRC Technical Report CHC-CTR-103.

Barrette, P. (2011). Offshore pipeline protection against seabed gouging by ice: An overview. Cold Regions Science and Technology, 69(1), 3-20.

Been, K., Sancio, R. B., Ahrabian, D., van Kesteren, W., Croasdale, K., & Palmer, A. (2008). Subscour displacement in clays from physical model tests. 2008 7th International Pipeline Conference, 239–245.

Biscontin, G., & Pestana, J. M. (2001). Influence of peripheral velocity on vane shear strength of an artificial clay. Geotechnical Testing Journal, 24(4).

C-CORE. (1995). Pressure Ridge Ice Scour Experiment, PRISE: Phase 3-Centrifuge Modelling of Ice Keel Scour: Draft Final Report.

C-CORE. (2008). Design Options for Offshore Pipelines in the US Beaufort and Chukchi Seas.

Chaloulos, Y. K., Bouckovalas, G. D., & Karamitros, D. K. (2017). Trench effects on lateral py relations for pipelines embedded in stiff soils and rocks. Computers and Geotechnics, 83, 52–63.

Chaloulos, Y. K., Bouckovalas, G. D., Zervos, S. D., & Zampas, A. L. (2015). Lateral soil–pipeline interaction in sand backfill: effect of trench dimensions. Computers and Geotechnics, 69, 442–451.

Chari, T. R. (1979). Geotechnical aspects of iceberg scours on ocean floors. Canadian Geotechnical Journal, 16(2), 379–390.

Chen, Xiangyu, Zhang, L., Chen, L., Li, X., & Liu, D. (2019). Slope stability analysis based on the Coupled Eulerian-Lagrangian finite element method. Bulletin of Engineering Geology and the Environment, 78(6), 4451–4463.

Chen, Xuejian, Li, D., Tang, X., & Liu, Y. (2021). A three-dimensional large-deformation random finite-element study of landslide runout considering spatially varying soil. Landslides, 18(9), 3149–3162.

Cheng, X., Huang, R., Xu, L., Ma, C., & Zhu, X. (2021). Parametric study on the trench designing for X80 buried steel pipeline crossing oblique-reverse fault. Soil Dynamics and Earthquake Engineering, 150, 106824.

CSA. (2015). CSA Z662-15: Oil and gas pipeline systems.

Dayal, U., & Allen, J. H. (1975). The effect of penetration rate on the strength of remolded clay and sand samples. Canadian Geotechnical Journal, 12(3), 336–348.

DNV GL. (2017). DNVGL-ST-F101, Submarine pipeline systems.

Dong, X., Malta, E. R., & Shiri, H. (2023). Deformation of trenched multilayer pipelines during large lateral displacement due to subsea geohazards. Ocean Engineering, 278, 114352.

Dong, X., Shiri, H., Zhang, W., & Randolph, M. F. (2021). The influence of pipeline-backfill-trench interaction on the lateral soil resistance: A numerical investigation. Computers and Geotechnics, 137, 104307.

Einav, I., & Randolph, M. F. (2005). Combining upper bound and strain path methods for evaluating penetration resistance. International Journal for Numerical Methods in Engineering, 63(14), 1991–2016.

El-Gebaly, S., Paulin, M., Lanan, G., & Cooper, P. (2012). Ice gouge interaction with buried pipelines assessment using advanced coupled Eulerian Lagrangian. OTC Arctic Technology Conference.

Eskandari, F, Phillips, R., & Hawlader, B. (2012). Finite element analyses of seabed response to ice keel gouging. Proceedings of the 65th Canadian Geotechnical Conference (GeoManitoba).

Eskandari, F. (2014). Buried pipeline response to ice gouging. Memorial University of Newfoundland.

Eskandari, Farzad, Phillips, R., & Hawlader, B. (2010). A State Parameter Modified Drucker-Prager Cap Model. Canadian Geotechnical Conference.

Eskandari, Farzad, Phillips, R., & Hawlader, B. (2011). Ice gouging analysis using NorSand critical state soil model. Proceedings of the Pan-Am CGS Geotechnical Conference, 2–6.

Eskandari, Farzad. (2014). Buried pipeline response to ice gouging. Memorial University of Newfoundland.

Esmaeilzadeh, M., & Shiri, H. (2019). Trench impact on lateral response of pipeline buried in sand. Experimental and Numerical Modeling of Lateral Pipeline-Trench Interaction Backfilled with Sand, 72.

Fadaifard, H., & Tassoulas, J. L. (2014). Numerical modeling of coupled seabed scour and pipe interaction. International Journal of Solids and Structures, 51(19–20), 3449–3460.

FitzMaurice, A., Straneo, F., Cenedese, C., & Andres, M. (2016). Effect of a sheared flow on iceberg motion and melting. Geophysical Research Letters, 43(24), 12–520.

Fredj, A., Comfort, G., & Dinovitzer, A. (2008). A case study of high pressure/high temperature pipeline for ice scour design using 3D continuum modeling. International Conference on Offshore Mechanics and Arctic Engineering, 48203, 563–572.

Gautier, D. L., Bird, K. J., Charpentier, R. R., Grantz, A., Houseknecht, D. W., Klett, T. R., Moore, T. E., Pitman, J. K., Schenk, C. J., & Schuenemeyer, J. H. (2009). Assessment of undiscovered oil and gas in the Arctic. Science, 324(5931), 1175–1179.

Ghorbanzadeh, A., Dong, X., & Shiri, H. (2023). The Response of Buried Pipelines to Ice Gouging in the Uniform and Trenched/backfilled Seabed. ISOPE International Ocean and Polar Engineering Conference, ISOPE-I.

Graham, J., Crooks, J. H. A., & Bell, A. L. (1983). Time effects on the stress-strain behaviour of natural soft clays. GÃ©otechnique, 33(3), 327–340.

Green, H. P., Reddy, A. S., & Chari, T. R. (1983). Iceberg scouring and pipeline burial depth. Proc., POAC–83, 7th Int. Conf. on Port and Oc. Engrg. under Arctic Conditions, 1, 280–288.

Hashemi, S., & Shiri, H. (2022a). Numerical Modeling of Ice–Seabed Interaction in Clay by Incorporation of the Strain Rate and Strain-Softening Effects. Journal of Offshore Mechanics and Arctic Engineering, 144(4), 42101.

Hashemi, S., & Shiri, H. (2022b). The response of layered seabed to ice gouging: Sand over clay. Ocean Engineering, 266, 113134. https://doi.org/https://doi.org/10.1016/j.oceaneng.2022.113134

Hashemi, S., & Shiri, H. (2023). Numerical Modeling of Ice-seabed Interaction in Layered Soil: Stiff over Soft Clay. Canadian Geotechnical Journal. https://doi.org/10.1139/cgj-2022-0594

Hashemi, S., & Shiri, H. (2023a). Numerical Modeling of Ice-seabed Interaction in Layered Soil: Stiff over Soft Clay. Canadian Geotechnical Journal. https://doi.org/10.1139/cgj-2022-0594

Hashemi, S., Shiri, H., & Dong, X. (2022a). The influence of layered soil on ice-seabed interaction: Soft over stiff clay. Applied Ocean Research, 120, 103033.

Hynes, F. (1996). Centrifuge modelling of ice scour in sand. Memorial University of Newfoundland.

Jan De Nul Group. (2020). Starfish (Elevated Excavator). https://www.jandenul.com/fleet/trenchers

Jo, C. H., Lee, S. B., Shin, Y. S., Hong, S. G., & Min, K. H. (2002). Numerical and experimental study of offshore pipeline stability in trench. Journal of Waterway, Port, Coastal, and Ocean Engineering, 128(6), 258–270.

Jukes, P., Kenny, S., Panapitiya, U., Jafri, S., & Eltaher, A. (2011). Arctic and harsh environment pipeline trenching technologies and challenges. OTC Arctic Technology Conference.

Kenny, S., Barrett, J., Phillips, R., & Popescu, R. (2007). Integrating geohazard demand and structural capacity modelling within a probabilistic design framework for offshore

arctic pipelines. The Seventeenth International Offshore and Polar Engineering Conference.

Kianian, M., Esmaeilzadeh, M., & Shiri, H. (2018). Lateral Response of Trenched Pipelines to Large Deformations in Clay. In Offshore Technology Conference (p. D032S092R009). https://doi.org/10.4043/28842-MS

Kianian, M., Esmaeilzadeh, M., & Shiri, H. (2021). The Effect of Backfilling Stiffness on the Lateral Response of Deeply Buried Pipelines: an Experimental Study. Journal of Marine Science and Application, 20(1), 21–33.

Kianian, Morteza, & Shiri, H. (2021a). Experimental study of trench effect on lateral failure mechanisms around the pipeline buried in clay. Journal of Pipeline Science and Engineering, 1(2), 198–211.

Kianian, Morteza, & Shiri, H. (2021b). The effect of backfilling stiffness on lateral response of the shallowly trenched-backfilled pipelines in clay. Marine Georesources & Geotechnology, 39(5), 610–622.

Kianian, Morteza, & Shiri, H. (2023). Large Deformation Analysis of Trenched Pipelines Under Lateral Displacements. Geotechnical and Geological Engineering, 41(4), 2537–2552.

Kianian, Morteza, Esmaeilzadeh, M., & Shiri, H. (2021). The Effect of Backfilling Stiffness on the Lateral Response of Deeply Buried Pipelines: an Experimental Study. Journal of Marine Science and Application, 20(1), 21–33.

Kioka, S. D., Kubouchi, A., & Saeki, H. (2003). Training and generalization of experimental values of ice scour event by a neural-network. ISOPE International Ocean and Polar Engineering Conference, ISOPE-I.

Kioka, S., Kubouchi, A., Ishikawa, R., & Saeki, H. (2004). Application of the mechanical model for ice scour to a field site and simulation method of scour depths. ISOPE International Ocean and Polar Engineering Conference, ISOPE-I.

Ko, J., Jeong, S., & Lee, J. K. (2016). Large deformation FE analysis of driven steel pipe piles with soil plugging. Computers and Geotechnics, 71, 82–97.

Konuk, I., Yu, S., & Fredj, A. (2006). Do Winkler models work: A case study for ice scour problem. International Conference on Offshore Mechanics and Arctic Engineering, 47497, 197–203.

Konuk, I., Yu, S., & Gracie, R. (2005). An ALE FEM model of ice scour. 11th International Conference of the International Association of Computer Models and Advances in Geomechanics, Turin, Italy.

Konuk, Ibrahim, & Gracie, R. (2004). A 3-dimensional Eulerian finite element model for ice scour. International Pipeline Conference, 41766, 1911–1918.

Konuk, Ibrahim, & Yu, S. (2007). A pipeline case study for ice scour design. International Conference on Offshore Mechanics and Arctic Engineering, 42711, 163–169.

Konuk, Ibrahim, Yu, S., & Fredj, A. (2006). Do Winkler models work: A case study for ice scour problem. International Conference on Offshore Mechanics and Arctic Engineering, 47497, 197–203.

Konuk, Ibrahim, Yu, S., & Gracie, R. (2005). A 3-Dimensional Continuum ALE Model for Ice Scour: Study of Trench Effects. International Conference on Offshore Mechanics and Arctic Engineering, 41960, 945–949.

Lach, P. R. (1996). Centrifuge modelling of large soil deformation due to ice scour. Memorial University of Newfoundland. https://research.library.mun.ca/1194/

Lele, S. P., Hamilton, J. M., Panico, M., & Arslan, H. (2011). Advanced continuum modeling to determine pipeline strain demand due to ice-gouging. The Twenty-First International Offshore and Polar Engineering Conference.

Liferov, P., & HÃ¸yland, K. V. (2004). In-situ ice ridge scour tests: experimental set up and basic results. Cold Regions Science and Technology, 40(1–2), 97–110.

Liferov, P., Nes, H., Asklund, J., Shkhinek, K., & Jilenkov, A. (2014). Ice gouging and its effect on pipelines. OTC Arctic Technology Conference, OTC-24605.

Liu, L., Bailey, E., Sarracino, R., Taylor, R., Power, C., & Stanbridge, C. (2015). Numerical simulation of ice ridge gouging. International Conference on Offshore Mechanics and Arctic Engineering, 56567, V008T07A022.

Miller, D. L., & Bruggers, D. E. (1980). Soil and permafrost conditions in the Alaskan Beaufort Sea. Offshore Technology Conference, OTC-3887.

Nagula, S. S., & Grabe, J. (2020). Coupled Eulerian Lagrangian based numerical modelling of vibro-compaction with model vibrator. Computers and Geotechnics, 123, 103545.

Nematzadeh, A, & Shiri, H. (2019a). Large deformation analysis of ice scour process in dense sand. 10th Congress on Numerical Methods in Engineering, At Guimaraes, Portugal.

Nematzadeh, A, & Shiri, H. (2019b). Self-correcting soil models for numerical simulation of strain rate dependent ice scour in sand.

Nematzadeh, A., & Shiri, H. (2020). The influence of non-linear stress-strain behavior of dense sand on seabed response to ice gouging. Cold Regions Science and Technology, 170, 102929.

Neumann Dredging. (n.d.). Nu Enterprise cutter suction dredge. https://neumanndredging.com.au/dredging-equipment/nu-enterprise-cutter-suction-dredge

Nobahar, A., Kenny, S., & Phillips, R. (2007). Buried pipelines subject to subgouge deformations. International Journal of Geomechanics, 7(3), 206–216.

Noh, W. F. (1963). CEL: A time-dependent, two-space-dimensional, coupled Eulerian-Lagrange code. Lawrence Radiation Lab., Univ. of California, Livermore.

Palmer, A. C., Konuk, I., Comfort, G., & Been, K. (1990). Ice gouging and the safety of marine pipelines. Offshore Technology Conference.

Palmer, A., Konuk, I., Love, J., Been, K., & Comfort, G. (1989). Ice Scour Mechanics. A Research Paper Prepared for Canada Oil and Gas Lands Administration and Gulf Canada Resources Ltd.

Panico, M., Lele, S. P., Hamilton, J. M., Arslan, H., & Cheng, W. (2012). Advanced ice gouging continuum models: comparison with centrifuge test results. ISOPE International Ocean and Polar Engineering Conference, ISOPE-I.

Paulin, M J. (1991). Preliminary results of physical model tests of ice scour. Memorial University of Newfoundland, Centre for Cold Ocean Resources Engineering.

Paulin, M. J. (1992). Physical model analysis of iceberg scour in dry and submerged sand. Memorial University of Newfoundland.

Paulin, M. J. (1998). An investigation into pipelines subjected to lateral soil loading. Memorial University of Newfoundland.

Paulin, M. J., Kenny, S. P., Palmer, A. C., Been, K., & Caines, J. V. M. (2008). Offshore Pipelines in Cold Regions-Environmental Loadings and Geotechnical Considerations. SNAME 8th International Conference and Exhibition on Performance of Ships and Structures in Ice.

Paulin, M., Cocker, J., Humby, D., & Lanan, G. (2014). Trenching considerations for Arctic pipelines. International Conference on Offshore Mechanics and Arctic Engineering, 45462, V06AT04A005.

Paulin, Michael J. (1992). Physical model analysis of iceberg scour in dry and submerged sand. Memorial University of Newfoundland.

Paulin, Michael J. (1998). An investigation into pipelines subjected to lateral soil loading. Memorial University of Newfoundland.

Peek, R, Been, K., Bouwman, V., Nobahar, A., Sancio, R., & Schalkwijk, R. V. (2013). Buried pipeline response to ice gouging on a clay seabed large scale tests and finite element analysis. 22nd International Conference on Port and Ocean Engineering under Arctic Conditions (POAC), 9–13.

Peek, R., & Nobahar, A. (2012). Ice gouging over a buried pipeline: Superposition error of simple beam-and-spring models. International Journal of Geomechanics, 12(4), 508–516.

Phillips, R, Barrett, J., & Al-Showaiter, A. (2010). Ice keel-seabed interaction: Numerical modeling validation. Offshore Technology Conference, 20696.

Phillips, R, Clark, J. I., & Kenny, S. (2005). PRISE studies on gouge forces and subgouge deformations. Proceedings of the International Conference on Port and Ocean Engineering Under Arctic Conditions.

Phillips, Ryan, Nobahar, A., & Zhou, J. (2004). Trench effects on pipe-soil interaction. International Pipeline Conference, 41766, 321–327.

Pike, K. P. (2016). Physical and numerical modelling of pipe/soil interaction events for large deformation geohazards. Memorial University of Newfoundland.

Pike, K. P., & Kenny, S. P. (2012). Advanced continuum modeling of the ice gouge process: Assessment of keel shape effect and geotechnical data. ISOPE International Ocean and Polar Engineering Conference, ISOPE-I.

Pike, K. P., & Kenny, S. P. (2012). Advanced continuum modeling of the ice gouge process: Assessment of keel shape effect and geotechnical data. ISOPE International Ocean and Polar Engineering Conference, ISOPE-I.

Pike, K., & Kenny, S. (2016). Offshore pipelines and ice gouge geohazards: comparative performance assessment of decoupled structural and coupled continuum models. Canadian Geotechnical Journal, 53(11), 1866–1881.

Pipelines, A. T. C. on T. R. D. of B. (2014). Soil Parameters for Assessing Axial and Transverse Behavior of Restrained PipelinesÃ¢â‚¬â€• Part 2: Transverse Behavior.

Pipelines 2014: From Underground to the Forefront of Innovation and Sustainability, 1849–1863.

Poorooshasb, F., Clark, J. I., & Woodworth-Lynas, C. M. (1989). Small scale modelling of iceberg scouring of the seabed.

PRCI. (2009). Guidelines for Constructing Natural Gas and Liquid Hydrocarbon Pipelines through Areas Prone to Landslide and Subsidence Hazards, Pipeline Research Council International.

Qiu, G., Henke, S., & Grabe, J. (2011). Application of a Coupled Eulerian–Lagrangian approach on geomechanical problems involving large deformations. Computers and Geotechnics, 38(1), 30–39.

Raie, M. S., & Tassoulas, J. L. (2009). Installation of torpedo anchors: numerical modeling. Journal of Geotechnical and Geoenvironmental Engineering, 135(12), 1805–1813.

Randolph, M. F. (2004). Characterization of soft sediments for offshore applications. Proc. ISC-2 on Geotechnical and Geophysical Site Characterization, 2004.

Rossiter, C., & Kenny, S. P. (2012). Assessment of ice-soil interactions: Continuum modeling in clays. The Twenty-Second International Offshore and Polar Engineering Conference.

Roy, K., Hawlader, B., Kenny, S., & Moore, I. (2018). Uplift failure mechanisms of pipes buried in dense sand. International Journal of Geomechanics, 18(8), 4018087.

Sancio, R., Been, K., & Lopez, J. (2011). Large scale indenter test program to measure sub gouge displacements. Proceedings of the International Conference on Port and Ocean Engineering Under Arctic Conditions, POAC11-096.

Sayed, M., & Timco, G. W. (2009). A numerical model of iceberg scour. Cold Regions Science and Technology, 55(1), 103–110.

Schoonbeek, I. S. S., & Allersma, H. G. B. (2006). Centrifuge modelling of scouring ice keels in clay. Proceedings, 8th International Conference on Physical Modelling in Geotechnics, ICPMG, 1291–1296.

Shin, M.-B., Park, D.-S., & Seo, Y. (2019). Comparative study of ice gouge simulation considering ice keel-seabed interactions. Journal of Ocean Engineering and Technology, 33(6), 556–563.

Shin, M.-B., Park, D.-S., Park, W.-J., & Seo, Y.-K. (2024). Behavioral analysis of seabed slope subjected to ice gouging. Cold Regions Science and Technology, 217, 104022.

Shiri, H., & Hashemi, S. (2023). The Impact of Layering Seabed on its Response to Ice Gouging. In The 33rd International Ocean and Polar Engineering Conference (p. ISOPE-I-23-205).

Simulia, D. S. (2019). Abaqus 2019 documentation. Dassault Systemes Waltham, MA.

Staubach, P., MachaÄ• ek, J., Skowronek, J., & Wichtmann, T. (2021). Vibratory pile driving in water-saturated sand: Back-analysis of model tests using a hydro-mechanically coupled CEL method. Soils and Foundations, 61(1), 144–159.

Stava, I., NystroÌ¸m, P. R., Vikse, N., Gudmestad, O. T., Liferov, P., & GroÌ¸nli, J. (2008). Small scale model tests of ice gouge in soft sandy silt. International Conference on Offshore Mechanics and Arctic Engineering, 48203, 891–900.

Tudorache, V.-P., & Antonescu, N.-N. (2020). Challenges of oil and gas exploration in the Arctic. J. Eng. Sci. Innov, 5, 273–286.

van Rhee, C. (2002). Numerical modelling of the flow and settling in a trailing suction hopper dredge. Proc., 11th Int. Symp. on Transport and Sedimentation of Solid Particles.

Vikse, N., Gudmestad, O. T., NystroÌ¸m, P. R., & Liferov, P. (2007). Small scale model tests on subgouge soil deformations. International Conference on Offshore Mechanics and Arctic Engineering, 42711, 157–162.

Winters, W. J., & Lee, H. J. (1984). Geotechnical properties of samples from borings obtained in the Chukchi Sea, Alaska (Vol. 85, Issue 23). US Geological Survey.

Woodworth-Lynes, C., Nixon, D., Phillips, R., & Palmer, A. (1996). Subgouge deformations and the security of Arctic marine pipelines. Offshore Technology Conference.

Yang, W. (2009). Physical modeling of subgouge deformations in sand. Memorial University of Newfoundland..

APPENDIX

APPENDIX A

The Response of Buried Pipelines to Ice Gouging in the Uniform and Trenched/backfilled Seabed

Alireza Ghorbanzadeh, Xiaoyu Dong, Hodjat Shiri

Civil Engineering Department, Faculty of Engineering and Applied Science, Memorial University of Newfoundland, A1B 3X5, St. John's, NL, Canada.

This paper was presented in the 33rd International Ocean and Polar Engineering Conference (ISOPE 2023), Ottawa, Canada, June 19-23.

Abstract

Ice gouging is a destructive incident to subsea pipelines in Arctic regions. Trenching and backfilling have been selected as the most efficient way to protect the pipeline. Studies indicate that remolded backfill materials with considerably less stiffness than native soil can significantly complicate soil failure mechanisms and pipe trajectories. In this paper, a numerical model was developed using coupled Eulerian-Lagrangian (CEL) method to investigate the influences of a backfilled trench on the seabed soil failure mechanism and the pipeline response with two model configurations. The study showed that the conventional simplification of assuming uniform seabed soil on trenched backfilled pipelines might misinterpret pipeline behavior and soil failure mechanisms.

Keywords: ice gouging; coupled Eulerian-Lagrangian (CEL); ice-soil-pipe interaction; arctic pipelines; backfill effect

A. 1 Introduction

Due to the depletion of older oil fields, the oil and gas industry is now paying more attention to new techniques and resources for oil extraction. The Arctic regions represent one of the unexplored hydrocarbon resources, with a high percentage of pristine resources (Gautier et al., 2009). However, some other obstacles and hazards could arise at various stages of exploitation in an ice environment, such as ice gouging (Abdalla et al., 2008). Water currents and winds in shallow areas cause ice gouging, which states the drifting of ice features like icebergs on the seabed. Pipelines are buried into the seabed as a practical and economical approach to protecting pipelines against ice gouging because ice keel-pipeline contact would be destructive to pipeline safety. Nonetheless, the ice gouge exerts multiple substantial stresses on the seabed, leading to soil failure mechanisms such major subgouge displacements, frontal mounds, and side berms (Figure A-1). As a result, the buried pipe will be impacted by the ice gouge and undergo a complicated path of lateral, vertical, and axial stresses and strains.

The most common source of backfilling is the excavated soil. Because of the drilling machine's contact with the excavated soil and mixing with the seawater, the soil is disturbed and has less shear strength.

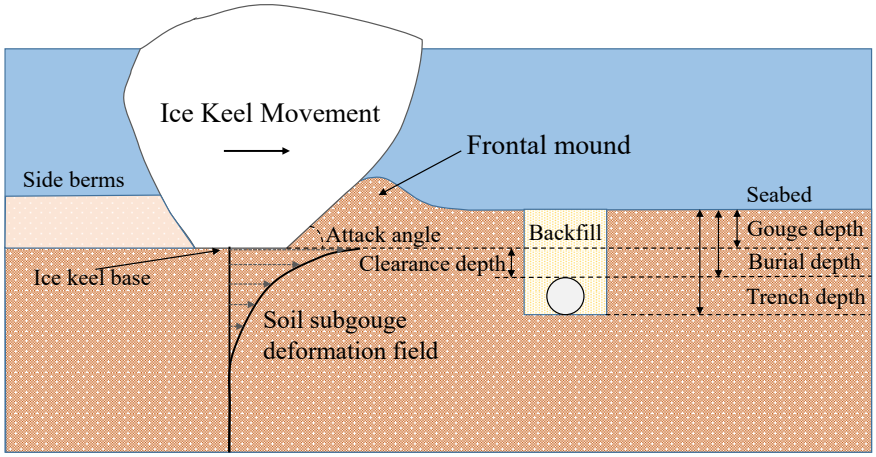

Figure A-1. The main components and soil failure mechanisms during an event of ice gouging

Several experimental and numerical models are available to comprehend the process of ice gouging. Numerical modeling is frequently used in this field due to the challenges associated with physical simulations of ice gouging under various boundary conditions, loading scenarios, or soil materials. Lagrangian modeling failed to simulate ice gouge because of several shortcomings, including mesh distortion and severe node displacement (Lach, 1996; Woodworth-Lynes et al., 1996). Researchers, therefore, used other techniques, including the Coupled Eulerian-Lagrangian (CEL) and the Arbitrary Lagrangian-Eulerian Method (ALE) ((Abdalla et al., 2009; Banneyake et al., 2011; Konuk et al., 2005; Konuk et al., 2005; Konuk & Yu, 2007; Pike & Kenny, 2016).

In this study, the movement of the ice keel traveling over a pipeline is simulated using the CEL method and Abaqus/Explicit. This approach allows for large deformations by modeling the soil environment using the Eulerian formulation. Two initial model configurations (shallowly buried and deeply buried pipelines) were conducted to examine the trenching/backfilling effect on the keel reaction forces, soil failure mechanisms, and the pipeline response. It was concluded that the proposed model is a primary yet robust tool

that may be utilized in the daily engineering practice of designing Arctic pipelines against ice gouge.

A. 2 Numerical Modeling

Framework

The Coupled Eulerian–Lagrangian (CEL) method was implemented in Abaqus/Explicit (Simulia, 2019) with explicit time integration. In this method, the soil can flow as an Eulerian material through the fixed mesh, causing the material boundary and the Eulerian volume fraction of the material in the meshes to change as time progresses. The Eulerian volume fraction (EVF) is a tool that represents the proportion of an element occupied by a specific material (which is the soil in this case). If an Eulerian element is filled with a material, its EVF is 1, whereas if the element is empty, its EVF is 0. Through a general contact based on a penalty contact method, soil interacts effectively with the ice keel and pipe (Lagrangian elements). This approach allows the soil to experience significant movement without mesh distortion, contact issues, or instability.

Finite Element Model

Soil domain meshed using Eulerian, three-dimensional, eight-node, reduced integration brick elements (EC3D8R) with the size being smaller close to the pipeline and larger as the distance from the pipeline increases. A mesh size of approximately 0.18 m is employed in the immediate proximity of the pipeline, whereas at the gouge depth, it is around 0.4 m, and it further increases to 1 m at the furthest points. In this study, the Eulerian medium dimensions and the initial location of the pipe were analyzed to reduce the computational time and optimize the numerical model without affecting the final results and raising the

boundary issues. For this purpose, soil subgouge displacements in the symmetry-plane section and along the pipe length, the ice keel reaction forces, the height of the frontal mound and side berms, and the boundaries effect on the final results were considered to ensure that the model reached steady-state conditions before going the pipe. The steady-state condition means when the reaction forces and frontal mound nearly remain constant with the ice keel's movement. The ice keel is modeled as a rigid indenter with a 15° attack angle from the horizontal (Fig. 2). Gouges have been demonstrated to retain a constant profile across long distances, according to (Blasco et al., 2011). As a result, the ice keel is considered to have a steady-state gouge condition and rigid translation (i.e., ignoring hydrostatic terms associated with a heave, pitch, and rotation).

The model is made half-symmetrically so that half the length of the pipe and ice are included in this model (the symmetry plane is at the gouge centerline). As a result, the boundary conditions at the middle cross-section of the pipe are assumed to be in accordance with the symmetry conditions. As boundary conditions, the velocity of soil particles perpendicular to the outer faces of the soil domain is not allowed.

The pipe is modeled using two parts: the continuum part discretized with shell elements (S4R in Abaqus) and the discontinuum part (Winkler-type method) meshed with structural elements (PIPE31H in Abaqus). The length of the continuum part of the pipe corresponds to the width of the Eulerian perimeter. Since the length of the pipe must be long enough to simulate the axial effect fully and to reduce the computation time, the pipe is extended after the Eulerian environment as a structural model. The length of the structural part is 5 km, which is connected to the continuum part of the pipe by a kinematic coupling constraint.

Finally, nonlinear springs in the discontinuum part are modeled with SPRINGA elements. The (PRCI, 2009) recommendations were used to establish the soil spring vertical and axial resistance curves. The equation presented by Phillips et al., (2004) generated the soil spring lateral resistance curve.

According to Pike & Kenny (2016), four steps constitute the coupled ice-soil-pipe interaction analysis. In the first step, the geostatic stress was applied in the soil domain in accordance with establishing the gravity load. Next, the ice keel is lowered to the specified gouge depth. Simultaneously, an internal pressure of 12 MPa was applied to the shell elements, while due to the internal software limitations (the effects of internal pressure are not transferred to the structural elements by the kinematic coupling constraint), an equivalent temperature change was subjected to the structural elements. In the third step, the temperature of both the structural and continuum pipe has increased by 50°. In the final step, the ice keel was horizontally moved over a large displacement domain with a velocity of 1m/s. Tracer particles are used to track subgouge displacements.

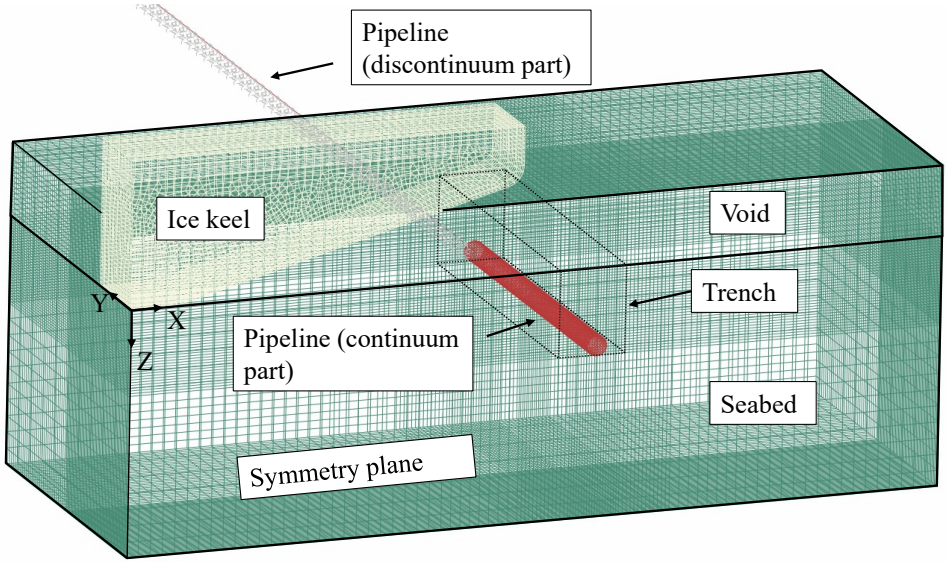

Figure A- 2. Isometric view of the CEL model configuration (dimensions and meshes)

Soil Properties and ice-soil-pipe interface behavior

In this study, the seabed soil was modeled as an elastic–perfectly plastic clay obeying the Tresca criterion in a total stress analysis (TSA). Since the ice gouge events are rapid, it can be assumed to be an undrained loading case; thus, the change in soil volume can be neglected. For this purpose, the soil Poisson's ratio was set at 0.499 (Pike & Kenny, 2016).

The study utilized a general contact algorithm to enforce contact between the Eulerian materials and the Lagrangian surfaces in the interaction between the ice keel surface and the soil. This algorithm was employed to compensate for discrepancies in mesh size and to prevent the Eulerian material from penetrating the Lagrangian surface (Simulia, 2019). A "hard" ice-soil interaction property was adopted for the normal interaction between the ice keel and the seabed soil, while an isotropic Coulomb friction formulation n was used for tangential behavior. The friction coefficient values of 0.3 and 1.0 were assigned to the ice keel-soil and pipe-soil interfaces, respectively, while a coefficient of 0.1 was set for the backfill interfaces. The surface polarity option has been used for the pipe-soil interface (outer pipe surface). The maximum shear stress at the interface was limited to half of the peak undrained shear strength.

Model Validation

Due to limitations in the process of physical modeling of ice gouging, the physical experimental study with a flexible buried pipe in clayey soils has not yet been published. For this reason, the Lach (1996) free-field centrifuge test and the PRISE empirical equation (Phillips et al., 2005) were selected for validation.

Lach (1996) conducted an experimental study to understand the effect of ice gouging on the seabed using a series of nine centrifuge model tests. Test 05 has been selected for validation in this study. The prototype ice keel gouge depth was 1.21m.

The soil properties were adapted from the experimental study by Lach (1996). The undrained shear strength (s_u) and overconsolidation ratio (OCR) profiles were reported in Lach (1996). Lach (1996) stated that undrained conditions are governing in an ice gouge event; therefore, a Poisson's ratio (v) of 0.499 was used for the seabed. Pike & Kenny (2016) presented a way to obtain varying elastic modulus with depth. Figure A-3 shows undrained shear strength and elastic modulus variation with depth (Pike & Kenny, 2016). The temperature is used as a dummy variable to define the linear variation of temperature with depth in Abaqus/CAE. Further details on the modeling procedures (e.g., material properties, boundary conditions) are discussed in Pike & Kenny (2016) and Hashemi & Shiri (2022).

Figure A-4 shows the horizontal soil subgouge displacement in the present study, the experimental test results, and the PRISE relationship. There is a significant difference in the subgouge displacement results immediately below the gouge depth, up to a depth almost equal to the gouge depth. This difference appeared in other studies of ice gouging using the CEL method (Abdalla et al., 2009; Hashemi & Shiri, 2022; Pike & Kenny, 2016). At greater depths, there is a closer convergence between the current model and experimental results than the PRISE equation. Also, Table A-1 shows the values of the ice keel reaction forces after reaching the steady-state condition in the current model and the Lach (1996) results. The agreement between the results shows that the current model is valid.

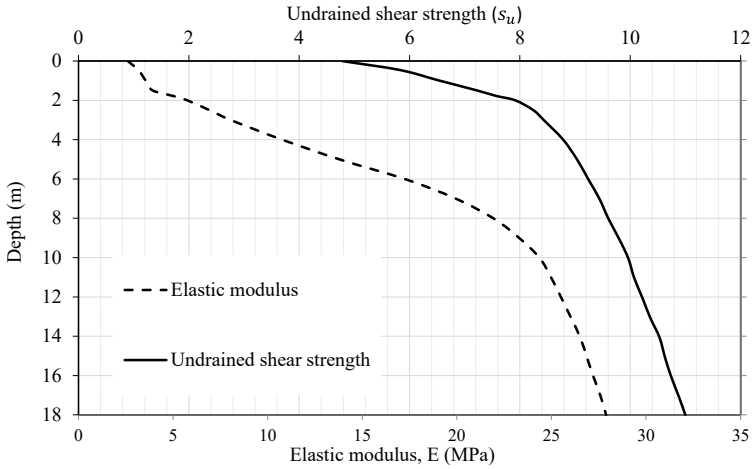

Figure A- 3. In-situ undrained shear strength (s_u) and Elastic modulus profiles extracted from the (Lach, 1996; Pike & Kenny, 2012)

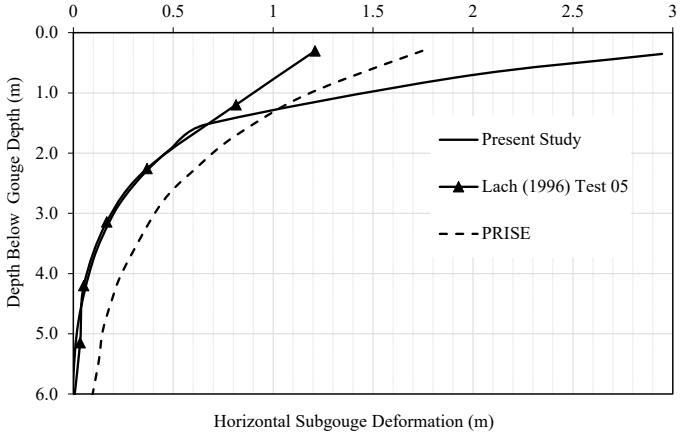

Figure A- 4. The comparison of the soil horizontal subgouge deformations

Table A- 1. The comparison of the vertical and horizontal ice keel-seabed reaction forces

	Horizontal Keel reaction Force (M.N.)	Vertical Keel reaction Force (M.N.)
Lach (1996) (Centrifuge test)	5.00	16.90
Present Study (CEL model)	4.95	15.50

A. 3 Model Configuration

The CEL method was used to model two alternative pipeline burial depth ratios that Paulin (1998) reported against ice gouge loading. Each geometry is simulated once with uniform seabed and once trenched and backfilled. The numerical analysis simulated the associated pipeline parameters, trench geometries, and soil properties from the centrifuge tests (T1P1 (Test 01, Pipeline 01) and T2P1 (Test 02, Pipeline 01) (Paulin, 1998). Test T1P1 (Case 1 in this study) represents the configuration of a shallowly buried pipeline, while model T2P1 (Case 3 in this study) depicts a deeply buried pipeline. The clearance depth (as defined in Fig. 1) was kept the same for all four cases. As the burial depth differs in cases 1&2 and cases 3&4, the gouge depths also differ. The pipe material properties are in conjunction with Peek & Nobahar (2012). The backfill soil consisted of the same material as the native soil but with a different stress history, resulting in undrained shear strength of around 3.3 ~ 3.5 kPa. Both a shallowly buried pipeline and a deeply buried pipeline were simulated in the models. The parameters of interest are given in Table A-2 (Case- 1~2 for T1P1, and Case- 3~4 for T2P1). In all case studies, the magnitude of horizontal and vertical reaction forces in the steady-state, soil tracer particles, and pipe deformations was extracted and compared.

The range of ice keel width reported in the literature is between 4 and 20 meters. For this work, an ice keel width of 8 meters was chosen based on the frequency of the using values. The typical range of ice keel attack angle is reported to be between 15 and 45 degrees, with 15 degrees being the most commonly reported value. Many studies have used a value of 1m/s for the ice keel velocity. For example Peek and Nobahar (2012) chose this value to be

large enough to reduce the computational effort with explicit time integration, yet small enough so that the steady-state behavior is still close to quasi-static. Also, Green et al. (1984) experiments showed that the speed of the model test had no effect on the forces measured during testing.

A brief view of the constant parameters are presented in Table A-3. The Eulerian medium dimensions for the shallowly buried models, 30 meters in length, 7 meters in depth, and 12 meters in width were chosen; while for the deeply buried cases, these values are 40, 12, and 20 meters, respectively.

Table A- 2. Parameters of interest in the present study plan

	Gouge Depth (m)	$s_{u(n)}$ (kPa)	$s_{u(b)}$ (kPa)	Trench Depth (m)	Trench base width (m)	Trench wall angle (degree)
Case 1	0.45	36.2	3.3	1.75	2.5	90
Case 2	0.45	36.2	N.A	1.75	N.A	N.A
Case 3	2.85	41.2	3.5	4.20	2.5	90
Case 4	2.85	41.2	N.A	4.20	N.A	N.A

Table A- 3. Constant Parameters in all case scenarios

		Parameter	Value
Pipe Specifications		Pipe Diameter (m)	0.950
		Pipe wall thickness (mm)	12.7
Soil properties	Native soil	Density (kg/m3)	1950.0
		Young's modulus (kPa)	16480
	Backfill soil	Density (kg/m3)	1875.0
		Young's modulus (kPa)	1400.0
Steel properties		Density (kg/m3)	7800
		Young's Modulus (GPa)	205
		Poisson ratio	0.3
		Expansion Coefficient	1.10E-05

A. 4 Results and Discussion

Shallowly Buried Pipeline (Case 1 and Case 2)

Examining the soil movement mechanisms in Case-1 and Case-2 shows a significant difference.

In Case 2 (uniform soil media), the soil failure mechanisms are more straightforward than in Case 1, including the frontal mound and side berms that have reached the steady-state condition before reaching the pipe. Figure A-5 shows plastic strain in the model while the ice keel moves through the native seabed soil toward the pipe. Tracer particles (red dots) depict the subgouge soil deformations. As the ice keel approaches the pipe, a shear band is formed on the rear side of the pipe, which causes the upward movement of the pipe before the ice reaches it (Figure A-5). The frontal mound is distorted since the pipe prevents the free soil subgouge displacement. The pipe reduces soil subgouge displacement around the pipe compared to areas further away. Finally, the frontal mound and side berms return to the steady-state condition after the ice keel passes over the pipe.

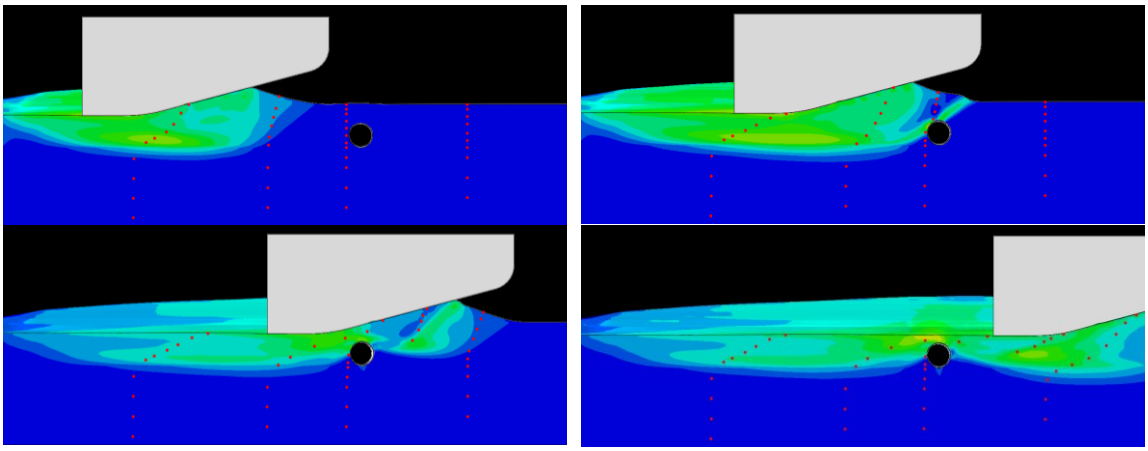

Figure A- 5. Plastic strain contours in the model while ice keel moves through the native seabed soil toward the pipe

In the case of the trenched/backfilled pipeline, along with the horizontal movement of the ice keel, the seabed soil is subjected to stresses and strains in different directions, including the horizontal subgouge displacements in the gouge direction. As the ice gets closer to the pipe, this horizontal stresses and strains cause the native soil to press against the trench wall. Due to the low shear strength, the backfill soil is squeezed by the trench walls and the native soil and moves upwards (Figure A-6). In such a way, in the ice gouge symmetry plane, most of the backfill soil is gradually removed from the trench, and the native soil takes its place. As a barrier, the lower half of the pipe prevents part of the backfill soil from exiting from the trench. Finally, the removed part of the backfill is spread on the sea surface mixed with the frontal mound and side berms (Figure A-7). This mechanism is formed along the pipe's length to the ice's width. As getting away from the ice keel gradually, more backfill remains in the trench.

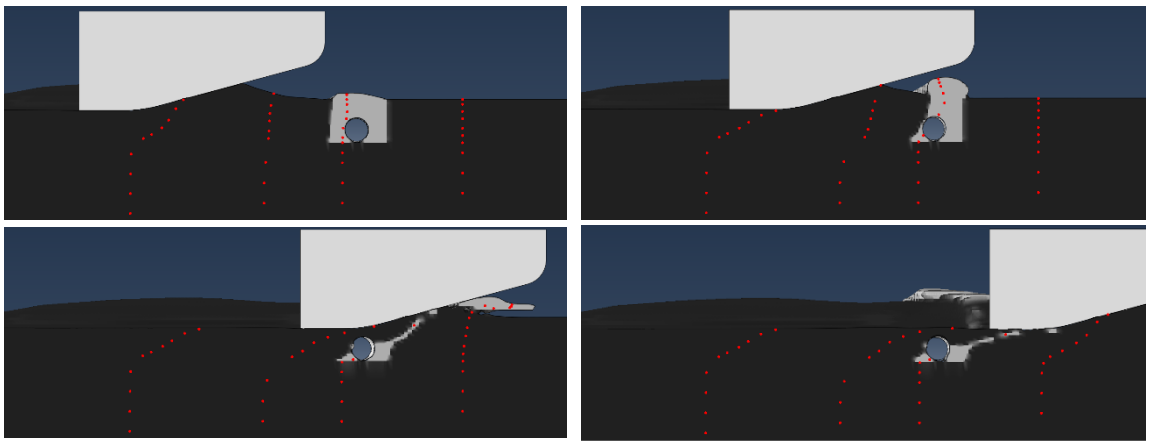

Figure A- 6. Backfill failure mechanism in an ice gouging event (shallowly buried pipe)

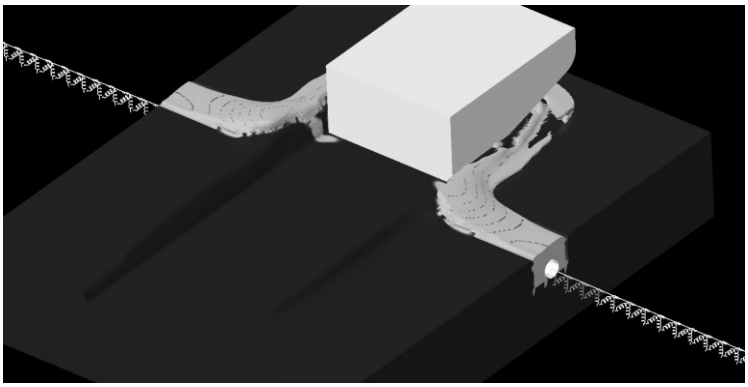

Figure A- 7. The state of the seabed after the ice keel passes through the trench

Figure A-8 shows the horizontal and vertical reaction forces obtained from the case studies. The ice keel reaction forces of the trenched model are not significantly different from the untrenched model. There is close convergence between the two cases until the ice keel approaches the trench. Due to the trench and backfill presence, a specific drop is formed in both horizontal and vertical reaction forces. After the ice keel passes over the pipe, these two graphs converge again.

Figure A-9 compares the pipe trajectory in the vertical plane at the gouge centerline in the case studies. The horizontal and vertical movement of the pipe in the mid-plane section takes a similar trend in both cases. As the ice keel moves toward the pipe, the pipe first deforms in the upward and gouge direction. When the ice reaches the pipe's top, the pipe's maximum displacement (Max. state) occurs. As the ice keel passes and moves away, some elastic displacement recovers, and the pipe remains stable in the rebound state. Figure A-9 indicates that the maximum horizontal displacement of the pipe in Case 1 is more than three times that of Case 2. This drastic difference is not only due to the lower value of the backfill soil's undrained shear strength and elastic modulus but also to the removal of the backfill material due to the movement of the walls.

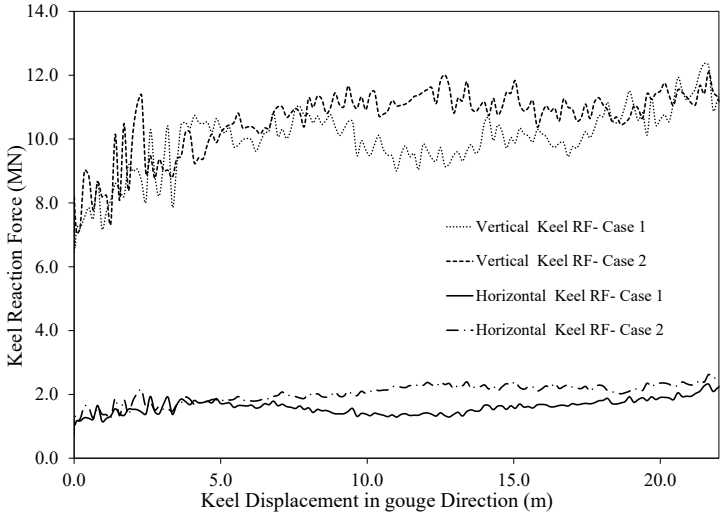

Figure A- 8. The vertical and horizontal components of ice keel reaction force (Case 1 and Case 2)

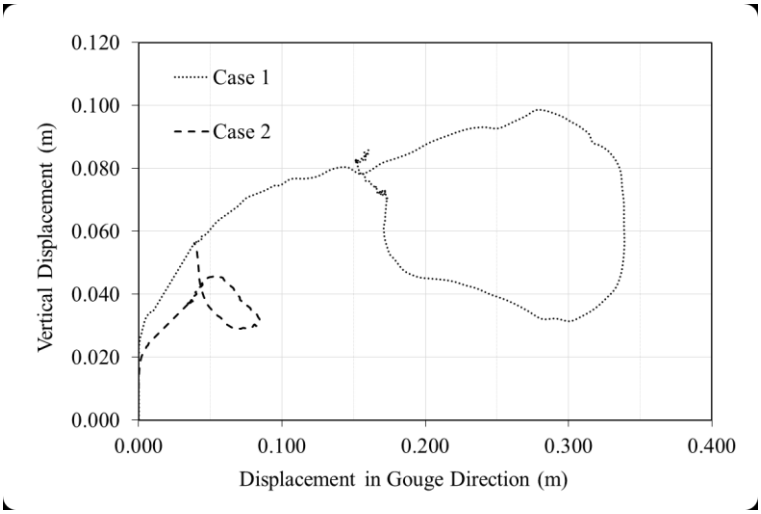

Figure A- 9. Pipe trajectory in the vertical plane at gouge centerline (Case 1 and Case 2)

Figure A-10 shows the numerical prediction of pipe displacement along the pipe axis in (a) horizontal (gouge motion), (b) transverse lateral, and (c) transverse vertical directions (present study with trench and un-trenched Pike's model). Predictably, pipe displacement in three directions (maximum and rebound states) is more than the trenched model. Figure A-11 demonstrates the maximum axial strain response, indicating the leading pipe face in

compression and the trailing pipe face in tension. The trend of the results is similar; however, axial strain in the trenched model is more critical than in the trenchless model.

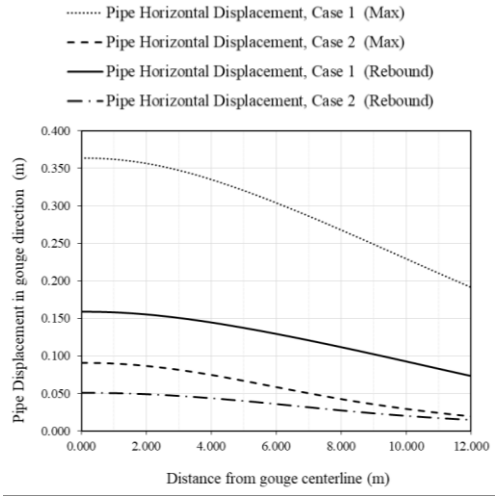

(a)

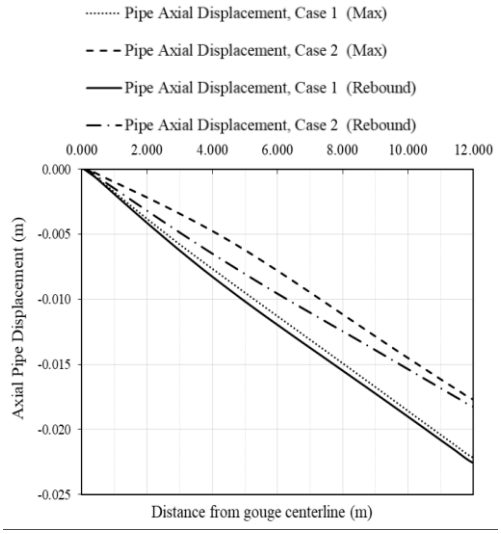

(b)

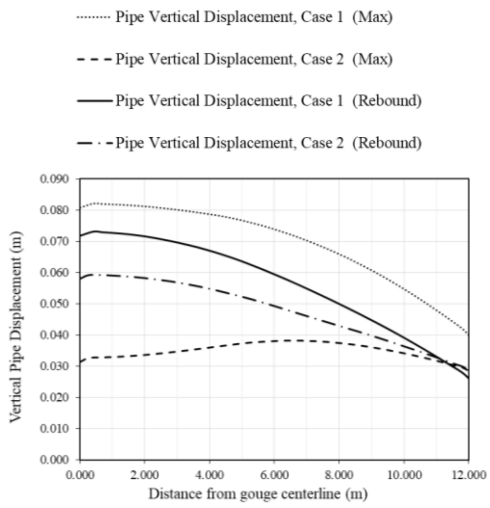

(c)

Figure A- 10. Pipe displacement along pipe axis in (a) horizontal (gouge motion), (b) transverse lateral, and (c) transverse vertical directions (Case 1 and Case 2)

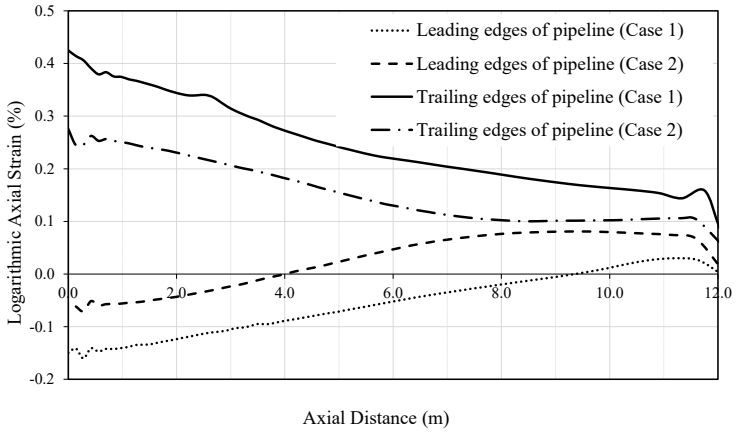

Figure A- 11. Distribution of logarithmic axial strain for the trailing and leading edges of the pipe (Case 1 and Case 2)

Deeply Buried Pipeline (Case 3 and Case 4)

The mechanism of the shear band formation and the backfill material removal from the trench is similar to Case 1~2. Figure A-12 shows the trench wall displacements and the backfill material squeezed by tracer particles.

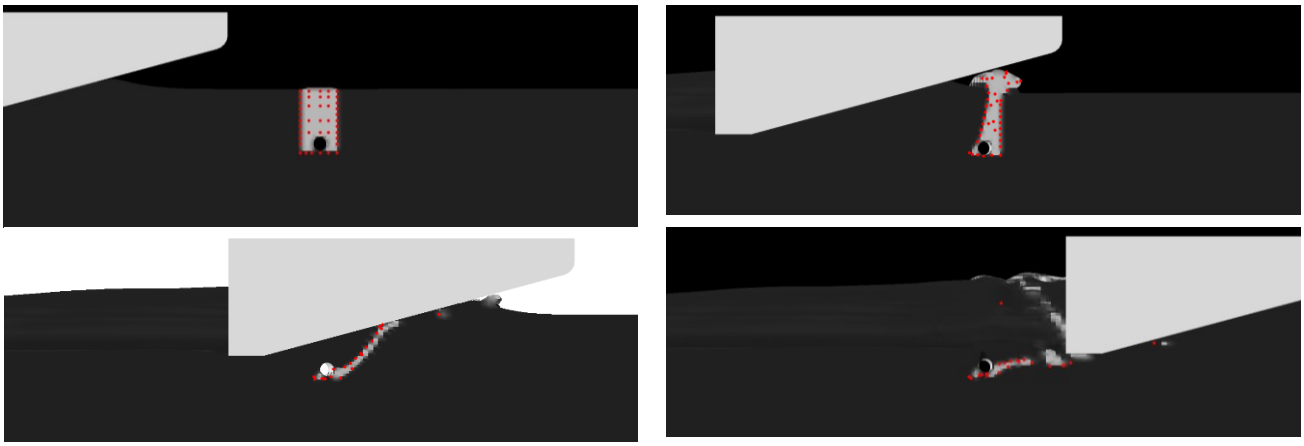

Figure A- 12. Backfill failure mechanism in an ice gouging event (deeply buried pipeline)

Figure A-13 shows the horizontal and vertical reaction forces obtained from the case studies. Similar to Figure A-8, two curves converge before and after the trench, and a drop is formed near the trench.

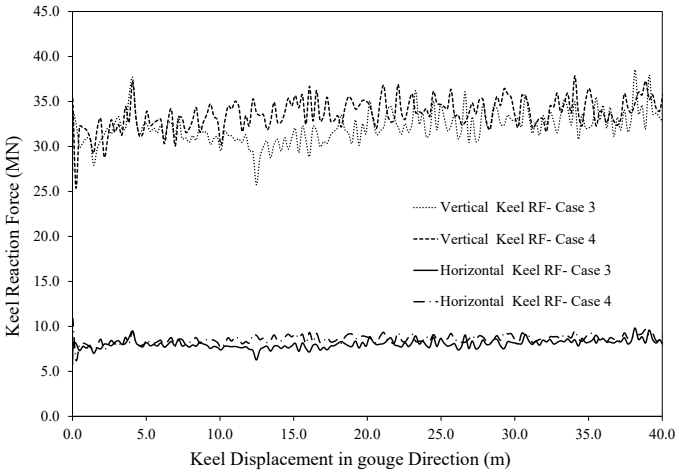

Figure A- 13. The vertical and horizontal components of ice keel reaction force (Case 3 and Case 4)

Figure A-14 compares the pipe trajectory in the vertical plane at the gouge centerline in the case studies. It can be seen in Fig. 12 that some of the backfill material penetrates beneath the pipe. It decreases the pipe bed's stiffness and even causes the pipe to have a negative displacement. Due to the greater gouge depth compared to Cases 1~2, the horizontal pipe displacement in the deeply buried ones is greater than in the shallowly buried ones.

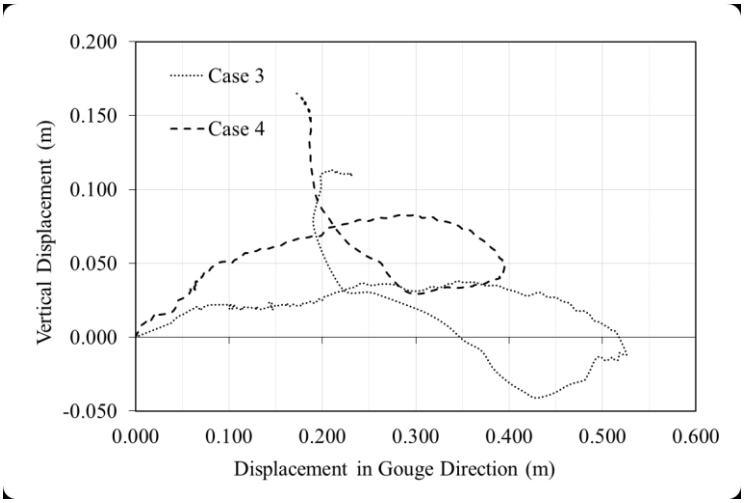

Figure A- 14. Pipe trajectory in the vertical plane at gouge centerline (Case 3 and Case 4)

Figure A-15 shows the numerical prediction of pipe displacement along the pipe axis in (a) horizontal (gouge motion), (b) transverse lateral, and (c) transverse vertical directions (present study with trench and un-trenched Pike and Kenny (2016) model). As expected, pipe displacement in three directions (maximum and rebound states) is more than the trenched model. Figure A-16 depicts that the greater maximum pipe axial strain in the trenched model makes the pipe more prone to structural integrity risks such as local buckling.

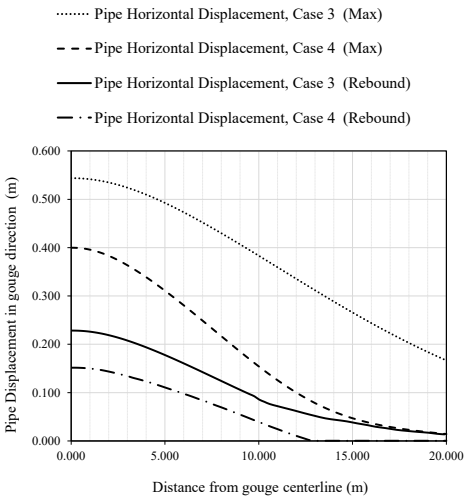

(a)

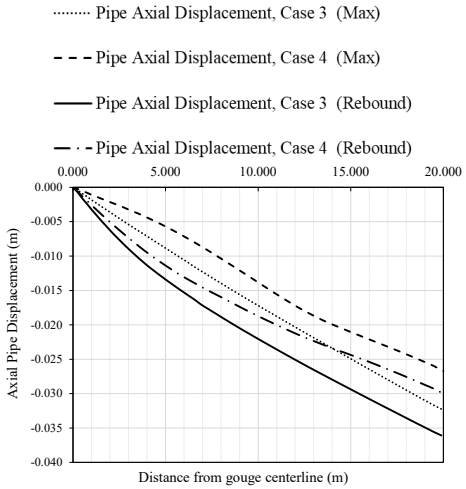

(b)

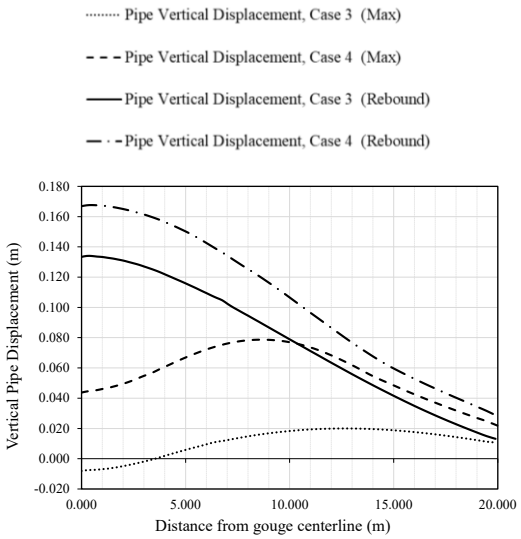

(c)

Figure A- 15. Pipe displacement along pipe axis in (a) horizontal (gouge motion), (b) transverse lateral, and (c) transverse vertical directions (Case 3 and Case 4)

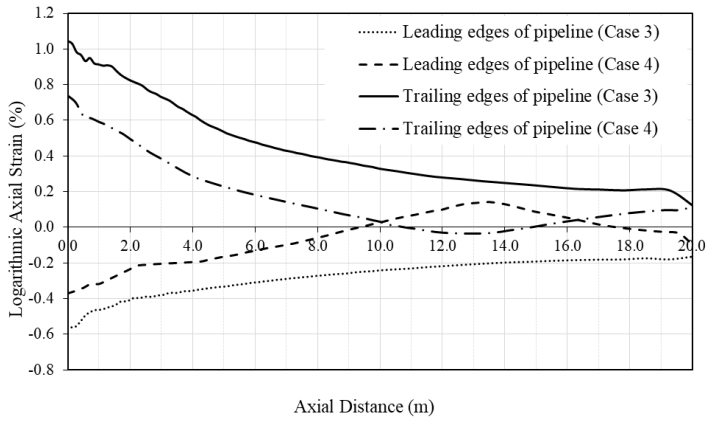

Figure A- 16. Distribution of logarithmic axial strain for the trailing and leading edges of the pipe (Case 3 and Case 4)

A. 5 Conclusion

This study has shown how to investigate the trench effects in the ice gouging process using continuous finite element modeling. The numerical model results of trenched/backfilled pipelines were shown to compare against the uniform seabed models. The divergence in results was mainly caused by the significantly lower backfill soil's elastic modulus and undrained shear strength. It was shown that backfilling results in a slight drop in ice keel/ seabed reaction forces.

However, it considerably influences the soil failure mechanisms around the pipe. The trench walls deflect as the native soil puts pressure on them. Consequently, the backfill soil in the gouge centerline section is squeezed and removed from the trench. This phenomenon increases pipe displacement and axial strain and increases the risk of local buckling in the pipe. As expected, trenching/backfilling was shown to affect soil and pipe behavior profoundly.

Acknowledgements

The authors gratefully acknowledge the financial support of the "Wood" through establishing Research Chair program in Arctic and Harsh Environment Engineering at the Memorial University of Newfoundland, the "Natural Science and Engineering Research Council of Canada (NSERC)" and the "Newfoundland Research and Development Corporation (RDC) (now IET) through "Collaborative Research and Developments Grants (CRD)". Special thanks are extended to Memorial University for providing excellent resources for conducting this research program.

References

Abdalla, B., Jukes, P., Eltaher, A., & Duron, B. (2008). The technical challenges of designing oil and gas pipelines in the arctic. OCEANS 2008, 1–11.

Abdalla, B., Pike, K., Eltaher, A., Jukes, P., & Duron, B. (2009). Development and validation of a coupled Eulerian Lagrangian finite element ice scour model. International Conference on Offshore Mechanics and Arctic Engineering, 43451, 87–95.

Banneyake, R., Hossain, M. K., Eltaher, A., Nguyen, T., & Jukes, P. (2011). Ice-soil-pipeline interactions using coupled Eulerian-Lagrangian (CEL) ice gouge simulations-extracts from ice pipe JIP. OTC Arctic Technology Conference.

Blasco, S., Carr, E., Campbell, P., & Shearer, J. (2011). Impact of environmental factors on the distribution of extreme scouring (gouging) events, Canadian Beaufort Shelf. Proceedings of the International Conference on Port and Ocean Engineering Under Arctic Conditions, POAC11-098.

Gautier, D. L., Bird, K. J., Charpentier, R. R., Grantz, A., Houseknecht, D. W., Klett, T. R., Moore, T. E., Pitman, J. K., Schenk, C. J., & Schuenemeyer, J. H. (2009). Assessment of undiscovered oil and gas in the Arctic. Science, 324(5931), 1175–1179.

Hashemi, S., & Shiri, H. (2022). Numerical Modeling of Ice–Seabed Interaction in Clay by Incorporation of the Strain Rate and Strain-Softening Effects. Journal of Offshore Mechanics and Arctic Engineering, 144(4), 42101.

Konuk, I, Yu, S., & Gracie, R. (2005). An ALE FEM model of ice scour. 11th International Conference of the International Association of Computer Models and Advances in Geomechanics, Turin, Italy.

Konuk, Ibrahim, & Yu, S. (2007). A pipeline case study for ice scour design. International Conference on Offshore Mechanics and Arctic Engineering, 42711, 163–169.

Konuk, Ibrahim, Yu, S., & Gracie, R. (2005). A 3-Dimensional Continuum ALE Model for Ice Scour: Study of Trench Effects. International Conference on Offshore Mechanics and Arctic Engineering, 41960, 945–949.

Lach, P. R. (1996). Centrifuge modelling of large soil deformation due to ice scour. Memorial University of Newfoundland. https://research.library.mun.ca/1194/

Phillips, R., Nobahar, A., & Zhou, J. (2004). Trench effects on pipe-soil interaction. International Pipeline Conference, 41766, 321–327.

Pike, K, & Kenny, S. (2012). Numerical pipe/soil interaction modelling: sensitivity study and extension to ice gouging. OTC Arctic Technology Conference.

Pike, Kenton, & Kenny, S. (2016). Offshore pipelines and ice gouge geohazards: comparative performance assessment of decoupled structural and coupled continuum models. Canadian Geotechnical Journal, 53(11), 1866–1881.

PRCI. (2009). Guidelines for Constructing Natural Gas and Liquid Hydrocarbon Pipelines through Areas Prone to Landslide and Subsidence Hazards, Pipeline Research Council International.

Simulia, D. S. (2019). Abaqus 2019 documentation. Dassault Systemes Waltham, MA.

Woodworth-Lynes, C., Nixon, D., Phillips, R., & Palmer, A. (1996). Subgouge deformations and the security of Arctic marine pipelines. Offshore Technology Conference.